

AD-756 860

STOL TRANSPORT THRUST REVERSER/
VECTURING PROGRAM. VOLUME I

John E. Petit, et al

Boeing Company

Prepared for:

Air Force Aero Propulsion Laboratory

February 1973

DISTRIBUTED BY:

NTIS

National Technical Information Service
U. S. DEPARTMENT OF COMMERCE
5285 Port Royal Road, Springfield Va. 22151

AFAPL-TR-72-108
Volume I

AD 756860



STOL TRANSPORT THRUST REVERSER/VECTORIZING PROGRAM

Volume I

John E. Petit
Michael B. Schelsky

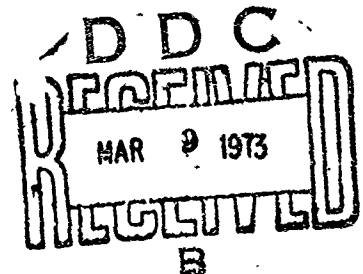
THE **BOEING** COMPANY

Technical Report AFAPL-TR-72-108, Volume I
February 1973

Reproduced by
NATIONAL TECHNICAL
INFORMATION SERVICE
U S Department of Commerce
Springfield, MA 01115

Approved for public release; distribution unlimited

Air Force Aero Propulsion Laboratory
Air Force Systems Command
Wright-Patterson Air Force Base, Ohio



NOTICE

When Government drawings, specifications, or other data are used for any purpose other than in connection with a definitely related Government procurement operation, the United States Government thereby incurs no responsibility nor any obligation whatsoever; and the fact that the government may have formulated, furnished, or in any way supplied the said drawings, specifications or other data, is not to be regarded by implication or otherwise as any manner licensing the holder or any other person or corporation, or conveying any rights or permission to manufacture, use, or sell any patented invention that may in any way be related thereto.

A. D. R. for	
White Section	<input checked="" type="checkbox"/>
Buff Section	<input type="checkbox"/>
Other	<input type="checkbox"/>
AVAILABILITY CODES	
1. 2. 3. 4. 5. 6. 7. 8. 9. 10. 11. 12. 13. 14. 15. 16. 17. 18. 19. 20. 21. 22. 23. 24. 25. 26. 27. 28. 29. 30. 31. 32. 33. 34. 35. 36. 37. 38. 39. 40. 41. 42. 43. 44. 45. 46. 47. 48. 49. 50. 51. 52. 53. 54. 55. 56. 57. 58. 59. 60. 61. 62. 63. 64. 65. 66. 67. 68. 69. 70. 71. 72. 73. 74. 75. 76. 77. 78. 79. 80. 81. 82. 83. 84. 85. 86. 87. 88. 89. 90. 91. 92. 93. 94. 95. 96. 97. 98. 99. 100.	

Copies of this report should not be returned unless return is required by security considerations, contractual obligations, or notice on a specific document.

Unclassified

Security Classification

DOCUMENT CONTROL DATA - R & D		
(Security classification of title, body of abstract and indexing information must be entered when the overall report is classified)		
1. ORIGINATING ACTIVITY (Corporate authority)		20. REPORT SECURITY CLASSIFICATION
The Boeing Company, Box 3999, Seattle, Washington 98124		<u>Unclassified</u>
3. REPORT TITLE		19. GROUP
STOL Transport Thrust Reverser/Vectoring Program, Volume I		
4. DESCRIPTIVE NOTES (Type of report and inclusives, dates)		
July 1971 - November 1972 Final Report Volume I		
5. AUTHOR (Last name, first name, middle initial, last name)		
John E. Petit and Michael B. Scholey		
6. REPORT DATE	7a. TOTAL NO. OF PAGES	7b. NO. OF REFS
December 1972	281	48
8a. CONTRACT OR GRANT NO.	9a. ORIGINATOR'S REPORT NUMBER(S)	
F33615-71-C-1850	None	
b. PROJECT NO.	9b. (OTHER REPORT NO(S)) (Any other numbers that may be assigned this report)	
643A	AFAPL-TR-72-109 Volume I	
c.		
d.		
10. DISTRIBUTION STATEMENT		
11. SUPPLEMENTARY NOTES		12. SPONSORING MILITARY ACTIVITY
[Details of illustrations in this document may be better studied on microfiche.]		Air Force Aero Propulsion Laboratory Wright-Patterson AFB, Ohio 45433
13. ABSTRACT		
<p>Existing data were reviewed for application to computer programs to predict TR/TV performance and evaluating TR/TV influence on the total airplane system. Three programs were developed: 1) Jet Trajectory and Spreading Program -- to predict the shape and trajectory of the TR/TV exhaust plume, 2) Reingestion Prediction Program -- to predict the onset of reingestion, and 3) TR and TV System Performance and effect of TR/TV operation on engine stability margin. Static tests were conducted to determine multibearing thrust vectoring nozzle performance and blocker door geometry effects on annular cascade thrust reverser performance. Results were incorporated in the TR and TV System Performance Program. The programs provide relatively simple design tools to evaluate TR/TV performance and to determine potential exhaustflow interference and reingestion data to STOL transport configurations is limited. Low speed wind tunnel testing is recommended to obtain this type of data.</p>		

I-u

DD FORM 1473
1 NOV 65

Unclassified

Security Classification

Unclassified

Security Classification

14

KEY WORDS

LINK A

LINK B

LINK C

ROLE

WT

ROLE

WT

ROLE

WT

Thrust Reverser

Thrust Vectoring

Nozzles

Turbine Engines

Transport Aircraft

I-4

Unclassified

Security Classification

STOL TRANSPORT THRUST REVERSER/VECTURING PROGRAM

VOLUME I

John E. Petit

Michael B. Scholey

This document has been approved for public
release, its distribution is unlimited.

FOREWORD

This report was prepared by Michael B. Scholey and John E. Petit of the Research and Engineering Division, Aerospace Group, The Boeing Company, Seattle, Washington. The work was conducted under USAF Contract F33615-71-C-1850, "STOL Transport Thrust Reverser/Vectoring Program," Project 643A "Tactical Airlift Technology," Task 63205F "Flight Vehicle Subsystem Concepts." The program was administered by the Air Force Aero Propulsion Laboratory, Wright-Patterson Air Force Base, Ohio with Captain J. W. Schuman and Mr. R. J. Krabal (AFAPL/TBP), as Project Engineers. Sub-contract support was provided by Pratt & Whitney Aircraft with H. Kozlowski as the Project Engineer.

This is the first of a two-volume final report submitted under the contract. Volume I covers work conducted during Part IA - Data Review and Analysis, from July 1971 through April 1972. Volume II covers work conducted during Part IB - Design and Part IC - Model Testing from July 1971 through October 1972. The final report was submitted to the Air Force in November 1972.

The authors acknowledge the following personnel for their assistance during the program: T. W. Wainwright, Airbreathing Propulsion; R. L. Wilson and L. J. Kimes, Propulsion Project; N. L. Prewitt, Boeing Computer Services Inc., and K. Ikeda and W. J. Stamm, Propulsion/Noise Laboratories. A special acknowledgement is due to M. E. Brazier, Chief, Propulsion Technology for his continuing interest and significant contributions to the program.

This technical report has been reviewed and is approved.



E. C. Simpson
Director, Turbine Engine Division
Air Force Aero Propulsion
Laboratory

TABLE OF CONTENTS

	Page
I. INTRODUCTION AND SUMMARY	1
II. PART IA - DATA REVIEW AND ANALYSIS	4
2.1 Task 1.1--Review and Correlate TR/TV Data	4
2.1.1 Cruise Nozzle Data Correlations	6
2.1.2 Thrust Reverser Data Correlations	23
2.1.3 Thrust Vectoring Nozzle Data Correlations	37
2.1.4 Casacde Lattice Loss Correlations	55
2.2 Task 1.2--Construct Computerized Analytical Models	69
2.2.1 Jet Trajectory and Spreading Program	70
2.2.2 Reingestion Prediction Program	96
2.2.3 TR and TV System Performance Program	134
2.3 Task 1.3--Plan and Conduct Supplemental Tests	144
2.3.1 Identification of Technology Voids	144
2.3.2 Supplemental Static Tests	145
III. CONCLUSIONS AND RECOMMENDATIONS	166
IV. COMPUTER PROGRAM USAGE	169
3.1 Jet Trajectory and Spreading Program Usage	169
3.2 Reingestion Prediction Program Usage	183
3.3 TR and TV System Performance Program Usage	187
APPENDIX I CHANG'S THEORY FOR THE ROLLUP OF A JET IN A CROSSFLOW	216
APPENDIX II PROGRAM SAMPLE CASES	222
REFERENCES	278

LIST OF ILLUSTRATIONS

<u>FIGURE</u>	<u>TITLE</u>	<u>PAGE</u>
1	Effect of Wall Angle on Velocity Coefficient for Conical Nozzles, $D_1/D_2 = 1.1$	9
2	Effect of Wall Angle on Velocity Coefficient for Conical Nozzles, $D_1/D_2 = 1.25$	10
3	Effect of Wall Angle on Velocity Coefficient for Conical Nozzles, $D_1/D_2 = 1.6$	11
4	Effect of Wall Angle on Velocity Coefficient for Conical Nozzles, $D_1/D_2 = 1.93$	12
5	Effect of Nozzle Offset on Velocity Coefficient Losses	13
6	Theoretical Velocity Coefficient Underexpansion Losses for Convergent Nozzles at Supercritical Pressure Ratios	14
7	Experimental Discharge Coefficient Curves for Convergent Conical Nozzles	15
8	Parametric Study of Conical Convergent Nozzles C_D Choke	16
9	Effect of Nozzle Offset on Annular Nozzle Velocity Coefficient Losses	18
10	Theoretical Discharge Coefficient Curves Using Bragg's Theory	19
11	Maximum Velocity Coefficient Correlation for Suppressor Nozzles	21
12	Clamshell Target Thrust Reverser Geometric Variables	24
13	Clamshell Target Thrust Reverser Geometric Variables	25
14	Effect of Setback Ratio on Static Reverser Efficiency, Clamshell Target Thrust Reverser	26
15	Effect of Door Length on Static Reverser Efficiency, Clamshell Target Thrust Reverser	27
16	Effect of Lip Height on Static Reverser Efficiency, Clamshell Target Thrust Reverser	28
17	Effect of Sweep Angle on Static Reverser Efficiency, Clamshell Target Thrust Reverser	29
18	Effect of Arc Angle on Static Reverser Efficiency, Clamshell Target Thrust Reverser	30

LIST OF ILLUSTRATIONS (Cont.)

<u>FIGURE</u>	<u>TITLE</u>	<u>PAGE</u>
19	Effect of Cone Angle on Static Reverser Efficiency, Clamshell Target Thrust Reverser	31
20	Effect of Bevel Angle on Static Reverser Efficiency, Clamshell Target Thrust Reverser	32
21	Effect of Setback Ratio on Airflow Match, Clamshell Target Thrust Reverser	34
22	Clamshell Target Thrust Reverser Baseline Performance	35
23	Effect of Blockage and Door Angle on Corrected Reverser Efficiency Annular Target Thrust Reverser	36
24	Effect of Door Setback on Airflow Match Annular Target Thrust Reverser	38
25	Discharge Coefficient Correlation Annular Target Thrust Reverser	39
26	Baseline Performance for Blocker-Deflector Thrust Reverser	40
27	Effect of Blocker Door Cone Angle on Blocker-Deflector Thrust Reverser Performance	41
28	Single Bearing Nozzle Nomenclature	43
29	Single Bearing Nozzle Thrust Component Relationships	44
30	Single Bearing Nozzle Performance	46
31	Spherical Eyeball Nozzle Performance	47
32	Lobstertail Nozzle Performance for 95 Degree Vector Angle	49
33	Effect of Vector Angle and Nozzle Pressure Ratio on Lobstertail Nozzle Performance	50
34	Effect of Deflection Angle on Flat Plate and Curved Deflector Performance	51
35	Effect of Nozzle Pressure Ratio and Deflection Angle on Curved Deflector Performance	52

LIST OF ILLUSTRATIONS (Cont.)

<u>FIGURE</u>	<u>TITLE</u>	<u>PAGE</u>
36	Effect of Flat Plate Length on Jet Deflection Angle	53
37	Mitre Bend Data, Contraction Coefficient Vs Setback Distance	54
38	Cascade Blade Nomenclature	56
39	Profile Losses for Reaction Blades at Zero Incidence	57
40	Profile Losses for Impulse Blades at Zero Incidence	58
41	Variation of Stalling Incidence and Flow Outlet Angle with Pitch/Chord Ratio	59
42	Variation of Stalling Incidence with Blade Inlet Angle and Flow Outlet Angle	60
43	Variation of Loss and Outlet Angle with Incidence	62
44	Variation of Flow Outlet Angle with Mach Number and Blade Trailing Edge Curvature	63
45	Variation of Relative Profile Loss with Mach Number and Trailing Edge Curvature	64
46	Effects of Reynolds Number on Profile Losses for Cascade Lattices	65
47	Effects of Reynolds Number on Flow Outlet Angle for Cascade Lattices	66
48	Correlation Relating Reaction and Momentum Thickness for Cascade Lattices	67
49	Form Factor Data for Cascade Lattices	68
50	STOL Transport Thrust Reverser Plume Side View	71
51	STOL Transport Thrust Reverser Plume Front View	72
52	STOL Transport Thrust Reverser Plume Plan View	73
53	Jet Trajectory and Spreading Program Diagram	74
54	Comparison of Jet Trajectory Equation with Data for $\alpha_o = 135$ Degrees	77

LIST OF ILLUSTRATIONS (Cont.)

<u>FIGURE</u>	<u>TITLE</u>	<u>PAGE</u>
55	Comparison of Jet Trajectory Equation with Data for $\alpha_o = 90$ degrees	78
56	Comparison of Jet Trajectory Equation with Data for $\alpha_o = 45$ Degrees	79
57	Jet Penetration Coefficient Data for Vizel and Mostiaskii's Trajectory Equation	80
58	Comparison of Two Dimensional Jet Trajectory Equation to Test Data for $\alpha_o = 135$ Degrees	81
59	Comparison of Two Dimensional Jet Trajectory Equation to Test Data for $\alpha_o = 90$ Degrees	82
60	Thickness Spreading Characteristics of a Round Jet Perpendicular to a Cross Flow	83
61	Computer Graphic Displays of Chang Cross Section for $V_{jo}/U_\infty = 8$	86
62	Jet Trajectory Photographs for $Re = 710$	87
63	Type = 1. Circular Jet Cross Section Geometry	90
64	Type = 2. Rectangular Jet Cross Section Geometry	92
65	Type = 3. Two Dimensional Jet Cross Section Geometry	94
66	Type = 4. Annular Jet Cross Section Geometry	97
67	Reingestion Prediction Program Diagram	100
68	Cross Flow Reingestion	101
69	Streamlines and Mach Contours for STOL Transport Inlet	103
70	Streamlines and Mach Contours for STOL Transport Inlet	105
71	Effect of Inlet Velocity Ratio on Pre-Entry Stagnation Streamtubes for a Representative STOL Transport Inlet	107
72	Inlet Streamtube Coordinate System	108
73	Jet Penetration Correlation Illustrating Data Scatter Due to Turbulent Fluctuations of Flow	110

LIST OF ILLUSTRATIONS (Cont.)

<u>FIGURE</u>	<u>TITLE</u>	<u>PAGE</u>
74	Crossflow Reingestion Results	111
75	Self Reingestion	113
76	Effect of Discharge Angle and Plate Length on the Reattachment of a Two Dimensional Incompressible Jet	114
77	Reattachment of a Three Dimensional Jet	115
78	Exhaust Flow Reattachment on SST Thrust Reverser	116
79	Near-Field Fountain Reingestion	118
80	Near-Field Fountain Flow Field Sketches	119
81	Far-Field Fountain Reingestion	122
82	Comparison of Flow Separation Data for 90° Jet Impingement	123
83	Abbott's Criterion for Predicting Far Field Fountain Flow Separation	124
84	Effect of Impingement Angle and Dynamic Pressure Ratio on Far Field Fountain Flow Separation	126
85	Dividing Streamline Comparison Between Theory and Experiment	127
86	Ground Plane Streamlines for 30° Jet Impingement Angle and Velocity Ratio $V_j/U_\infty = 1.0$	128
87	Ground Plane Streamlines for 30° Jet Impingement Angle and 45° Wind Direction	129
88	Ground Plane Streamlines for 30° Jet Impingement Angle and 90° Wind Direction	130
89	Effect of Wind Direction on Dividing Streamline Shape	131
90	Effect of Wind Direction on Dividing Streamline Shape	132
91	Effect of Velocity Ratio and Impingement Angle on Dividing Streamline Shapes	133
92	Height of Far Field Fountain Exhaust Cloud	135

LIST OF ILLUSTRATIONS (Cont.)

<u>FIGURE</u>	<u>TITLE</u>	<u>PAGE</u>
93	Position of Vortex and Separation Line Vs Corrected Dynamic Pressure Ratio	136
94	Far-Field Fountain Exhaust Cloud and Inlet Streamtube Intersections	137
95	TR and TV System Performance Program	138
96	Effect of Reverse Thrust on Airplane Drag During Ground Roll	140
97	Air Flow Match Curve Representing Reverser Deployment	142
98	Multibearing Vectoring Nozzle Model Installation	147
99	Effect of Duct Contraction Ratio on Vector Efficiency $\theta = 65^\circ$	148
100	Effect of Duct Contraction Ratio on Airflow Match $\theta = 65^\circ$	150
101	Effect of Duct Contraction Ratio at $P_T/P_\infty = 1.60$	152
102	Effect of Duct Turning Radius on Nozzle Vector Efficiency, $\theta = 65^\circ$	153
103	Effect of Duct Turning Radius on Nozzle Airflow Match, $\theta = 65^\circ$	154
104	Effect of Duct and Nozzle Length on Vector Efficiency, $\theta = 65^\circ$	157
105	Effect of Duct and Nozzle Length on Airflow Match, $\theta = 65^\circ$	158
106	Evaluation of Thrust Reverser Performance	159
107	Effect of Accelerating Duct Flow on Vector Efficiency	160
108	Effect of Accelerating Duct Flow on Airflow Match	161
109	Blocker Door Geometry Model Installation	163
110	Effect of Blocker Door Angle on Cascade Reverser Performance	164
111	Effect of Blocker Door Setback Distance on Cascade Reverser Performance	165

LIST OF ILLUSTRATIONS (Cont.)

<u>FIGURE</u>	<u>TITLE</u>	<u>PAGE</u>
112	Deck Arrangements for Programs TEM-356A, TEM-356B, and TEM-357 When Using a Symbolic	170
113	Deck Arrangements for Programs TEM-356A, TEM-356B, and TEM-357 When Using a Binary Deck	171
114	Data Card Arrangement for Several Cases, Program TEM-356A	173
115	Data Card Arrangement for TYPE = 1. Circular Jet	175
116	Data Card Arrangement for TYPE = 2. Rectangular Jet	177
117	Data Card Arrangement for TYPE = 3. Two Dimensional Jet	179
118	Data Card Arrangement for TYPE = 4. Annular Jet	182
119	Data Card Arrangement for Reingestion Prediction Program TEM-356B	185
120	Additional NAMELIST Data Cards for Reingestion Prediction Program TEM-356B	186
121	Data Card Arrangement for Several Cases, Program TEM-357	189
122	Data Card Arrangement for Conical Cruise Nozzles	191
123	Data Card Arrangement for Annular Cruise Nozzles	193
124	Data Card Arrangement for Irregular Shaped Cruise Nozzles	195
125	Data Card Arrangement for Target Thrust Reversers	199
126	Data Card Arrangement for Blocker Deflector and Blocker Cascade Thrust Reversers	201
127	Data Card Arrangement for Single Bearing Nozzles	203
128	Data Card Arrangement for Three Bearing Nozzles	205
129	Data Card Arrangement for Spherical Eyeball Nozzles	207
130	Data Card Arrangement for Lobstertail or Aft-Hood Deflector Nozzles	209
131	Data Card Arrangement for External Deflector Nozzles	211

LIST OF ILLUSTRATIONS (Cont.)

<u>FIGURE</u>	<u>TITLE</u>	<u>PAGE</u>
132	Data Card Arrangement for Cascade Loss Predictions	213
133	Data Card Arrangement for Engine Stability Margin Module	215

LIST OF NOMENCLATURE

a	longitudinal dimension of initial jet cross section
b	lateral dimension of initial jet cross section
C_D	nozzle discharge coefficient
C_V	nozzle velocity coefficient
C_{VS}	standard nozzle velocity coefficient
C_X	jet penetration coefficient
D	jet diameter, or distance between nozzles
d_o	jet initial diameter
D_{he}	equivalent hydraulic diameter
F	thrust force
H	boundary layer shape factor
m_2	momentum deficiency at cascade lattice trailing edge
NPR	nozzle pressure ratio
P_{TN}/P_{∞}	nozzle pressure ratio
q	dynamic pressure
R	cascade reaction, or radius
R_s	separation distance of far-field fountain dividing streamline
r_s	scatter radius
R_V	vortex distance from impingement point
t	jet thickness
t_o	jet initial thickness
U_{∞}	freestream velocity
V_{hilite}	inlet hilite velocity

LIST OF NOMENCLATURE (Concluded)

s	arc length along jet axis
w	jet width, or weight flow
x	body coordinate
X/D	ratio of setback distance to nozzle diameter
y	spanwise coordinate
γ_p	cascade pressure loss coefficient
z	vertical coordinate

Subscripts

a	annular coordinate system
f	forward thrust mode
j	jet
o	origin or initial
r	reverse thrust mode
∞	freestream conditions

Greek Symbols

α	angle of attack, azimuth angle, or cone angle
δ	jet thickness
δ^*	boundary layer displacement thickness
η_{RC}	corrected reverser efficiency
η_{Rg}	static reverser efficiency
η_{Vg}	vector efficiency
γ	angle of yaw
σ	cascade solidity, = C/S, or vector angle
θ	boundary layer momentum thickness, or vector angle
ξ	airflow match
Ω	flow turning angle
ν	skew angle of initial jet cross section

SECTION I

INTRODUCTION AND SUMMARY

An essential requirement of military STOL tactical transports planned for the 1980 time period will be to operate from airfields of 2500 feet or less. These aircraft will use thrust reversers as primary braking devices throughout the landing ground roll. Also, some STOL concepts will use thrust vectoring systems to help control the flightpath of the airplane and reduce take-off and landing speeds. Consequently, emphasis must be placed on designing efficient and reliable thrust reverser/vectoring systems to achieve the field length objective.

Commercial jet aircraft have used thrust reversers as secondary braking devices since the beginning of their operation. However, the complex problems caused by the interactions between reverser exhaust and aircraft flowfields have limited their usefulness. These problems include exhaust gas recirculation which can lead to engine surge, impingement of exhaust gases on the ground or adjacent aircraft surfaces, and engine mass flow matching. Also, the reverser flow can cause blanking out of aerodynamic control surfaces leading to a loss in aircraft directional stability and control, buoyancy effects that decrease the efficiency of the ground braking systems, and changes in airplane drag. All of these problems have been experienced during the development of existing commercial aircraft. However, the availability of long runways has made it unnecessary to completely resolve the interactions between the reverser and aircraft flowfields.

To avoid the limitations of existing systems on future STOL aircraft, attention must be given to the following technical areas:

- o TR/TV performance
- o Exhaust gas flowfield
- o Aerodynamic interference
- o Engine operation
- o TR/TV system design including weights and structures

The above considerations have significant influence on nacelle placement, thrust reverser and vectoring system geometry, and operating envelope.

The Boeing Company, with subcontract support from Pratt & Whitney Aircraft conducted an 18 month research program to study the above

technical areas. The program was administered by the Air Force Aero Propulsion Laboratory, Wright-Patterson Air Force Base, Ohio. Program objectives are:

1. To develop methods to predict thrust reverser and thrust vectoring system performance.
2. To establish design criteria for high efficiency, lightweight thrust reversers or thrust vectoring systems for STOL aircraft.

The program has three parts:

Part IA--Data Review and Analysis

Part IB--Design

Part IC--Model Testing

Part IA consists of three tasks:

Task 1.1 - Review and correlate TR/TV data

Task 1.2 - Construct computerized analytical models

Task 1.3 - Plan and conduct supplemental tests

During Task 1.1, existing data were reviewed for possible application to computer programs for thrust reverser and vectoring systems. Literature searches of DDC, NASA, and Boeing files resulted in approximately 160 references applicable to TR/TV systems. The results of the data review were used to develop data correlations for

- o Cruise nozzles
- o Thrust reversers
- o Thrust vectoring nozzles
- o Cascade lattices applicable to cascade TR and TV nozzles

Computer programs for predicting TR and TV nozzle performance and evaluating TR and TV influence on the total airplane system were developed during Task 1.2. Three programs were developed:

- 1) Jet Trajectory and Spreading Program -- to predict the shape and trajectory of the thrust reverser or vectoring nozzle exhaust plume.
- 2) Reingestion Prediction Program -- to predict the on-set of reingestion for arbitrary thrust reverser and airplane configurations as a function of geometry and flow conditions.
- 3) TR and TV System Performance Program -- consisting of four modules to predict:

- o TR and TV Internal Performance
- o Aerodynamic Performance
- o Reingestion
- o Engine Stability Margin

The TR and TV Internal Performance Module was assembled using the data correlations developed during Task 1.1. The Engine Stability Margin Module was developed by Pratt & Whitney Aircraft. Available reingestion and aerodynamic data for existing conventional take-off and landing aircraft were not applicable to the Reingestion and Aerodynamic Performance modules. A low speed wind tunnel test of STOL airplane TR and TV configurations is required to obtain the necessary data. However, logic was provided to allow easy incorporation of data into the modules as data become available.

Task 1.3 consisted of planning and conducting supplemental static test to fill data voids discovered in the open literature. Tests were conducted to determine:

- 1) Multibearing vectoring nozzle performance as a function of parametric geometry variations
- 2) Blocker door geometry effects on the performance of annular blocker/cascade thrust reversers

The results were incorporated into the Internal Performance Module of the TR and TV System Performance Program.

Detailed descriptions of the results of Part IA are provided in the following sections. Detailed results of Parts IB and IC are provided in Volume II.

SECTION II

PART IA - DATA REVIEW AND ANALYSIS

2.1 Task 1.1 Review and Correlate TR/TV Data

The objective of Task 1.1 was to review the existing literature for data pertinent to TR/TV systems and to correlate the data as a function of fundamental geometric and aerodynamic parameters. The data correlations are used to predict TR and TV nozzle performance. The first step of this task, a literature search, was made prior to start of the study contract. The literature search included the following sources of information.

- 1) Defense Documentation Center computerized literature search. This search was updated during Task 1.1
- 2) Computerized literature search of NASA reports
- 3) Boeing documents, STAR and TAB abstracts, technical journals (search performed by Boeing library personnel)
- 4) Foreign literature available through services of the Boeing International Corporation
- 5) Patent search

Approximately 160 reports found during the literature search were obtained and reviewed. Boeing was assisted in the literature review by the subcontractor, Pratt & Whitney Aircraft, who provided references and abstracts. Results were published as an Air Force Technical Report (Ref. 1). The data review document contains three types of information.

Bibliography Summary Chart

A typical bibliography summary chart for thrust reverser systems is shown in Table I. This chart summarizes information extracted from reports and cross references them by subject matter.

Report Abstracts

Abstracts were written for all reports reviewed. Abstracts describe contents of the report and provide an objective assessment of applicability and usefulness of the contents.

Table 1: TYPICAL BIBLIOGRAPHY SUMMARY
CHART FOR THRUST REVERSER
SYSTEMS

CHART FOR THRUST REVERSER SYSTEMS													
REFERENCE NUMBER	YEAR OF PUBLICATIONS	REVERSER CONCEPT	NATURE OF REPORT MATERIAL	TYPE OF TEST	TEST ARTICLE	SPECIFIC AREAS OF INVESTIGATION							
						INTERNAL PERFORMANCE	REVERSER EFFECTIVENESS	RE INGESTION	AERODYNAMIC INTERFERENCE	JET TRAJECTORY	FIELD LENGTH STUDIES	JET IMPINGEMENT	MECHANICAL DESIGN
1.1	1965	C, BD	E, A	S	C	X	X		X				
1.2	1970	T, BD, C	A	None	C, A/P	X							
1.3	1963	C, T	E	WT	C, A/P	X							
1.4	1966	C	E, A	B	C	X							
1.5	1958	BD, C	E	WT	C, A/P		X						
1.6	1966	C	E	WT	C, A/P		X						
1.7	1969	BD	E	WT	C, A/P		X						
1.8	1969	T	E	WT	C, A/P		X						
1.9	1958	C	E	WT	C, A/P	X							
1.10	1965	C	E	WT	C, A/P		X						
1.11	1967	C	E	WT	C, A/P		X						
1.12	1968	BD	E	WT	C, A/P		X						
1.13	1969	C	E	B	C	X							
1.14	1970	T	E	WT	C, A/P		X						
1.15	Up to Released	BD, T	A	None	C	X							
1.16	1962	BD, T	A	None	C	X							
1.17	1963	Any	A	None	C, A/P								
1.18	1963	Any	A	None	C, A/P								
1.19	1967	Any	A	None	C, A/P								
1.20	1962	Any	A	None	C, A/P								
1.21	1962	BD	E	FT	C, A/P								
1.22	1967	Any	A	None	C, A/P								
1.23	1963	C	E	FT	C, A/P								
1.24	1966	C	E	FT	C, A/P								
1.25	1966	C	E	FT	C, A/P								
1.26	1970	BD	E	S, WT, FT	C, A/P								
1.27	1968	T	E	S, WT	C, A/P								
1.28	1968	T	E	WT	C, A/P								
1.29	1968	T	E	FT	A/P								
1.30	1968	T	E	FT	A/P								
1.31	1968	T	E	FT	A/P								
1.32	1968	C	E	WT	C, A/P								

Data Review Charts

A sample data review chart is shown in Table II. This chart contains a sketch of the TR or TV configuration, summarizes the range of test variables, and lists the type of data contained in the report. Comments are included concerning the model, data quality, or usefulness of the data.

The second major objective of Task 1.1 was to formulate data correlations for thrust reverser and thrust vectoring systems as functions of fundamental geometric and aerodynamic parameters. Correlations were developed for the following types of TR/TV nozzles:

- 1) Cruise nozzles
 - a) Conical
 - b) Annular
 - c) Noncircular
- 2) Thrust reversers
 - a) Target (clamshell and annular)
 - b) Blocker deflector and blocker cascade
- 3) Thrust vectoring nozzles
 - a) Single bearing
 - b) Three bearing
 - c) Spherical eyeball
 - d) Lobstertail
 - e) External deflector
- 4) Cascade lattices applicable to cascade TR and TV nozzles

Data correlations for the above TR/TV nozzles are described in the following paragraphs.


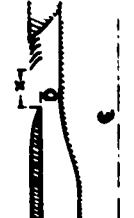


2.1.1 Cruise Nozzle Data Correlations

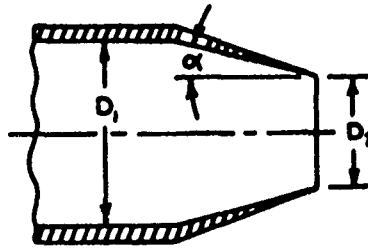
This section describes methods used to predict cruise nozzle performance in terms of velocity and discharge coefficients. Extensive parametric data for convergent conical nozzles are presented covering a wide range of wall angles and diameter ratios. Analytical results are also presented and compared to experimental data.

Conical Nozzle Velocity Coefficient

A sketch of a conical nozzle is shown on page 8.

Table II: TYPICAL THRUST REVERSER DATA
REVIEW CHART FOR CASCADE THRUST
REVERSERS

REFERENCE NUMBER	YEAR OF PUBLICATION	THRUST REVERSER CONCEPT	AIRPLANE MODEL	TYPE OF ENGINE	SCALE OF TEST	TYPE OF TEST	NUMBERS OF CONFIGURATIONS TESTED	SKETCH OF CONFIGURATION	TEST VARIABLES	TEST DATA	COMMENTS
1.1	1965	C C-5A	GE 1/6 FAC PWA JTF 14E/78	0.0658	S	4			$NPR = 1.4 \rightarrow 1.7$ $\sigma = 1.54$ $\lambda/D = 0.13$ 0.78 BLADE ENTRANCE ANGLE = 90° BLADE EXIT ANGLE = 40° , 50° NUMBER OF BLADES = 4, 5, 6 THIN REACTION BLADE PROFILE	F_r W_r	ANNULAR FAN NOZZLE CASCADE THRUST REVERSER
1.1	1965	C C-5A	GE 1/6 FAC PWA JTF 14E/78	0.0658	S	2			$NPR = 1.4 \rightarrow 1.7$ $\sigma = 1.54$ $\lambda/D = 0.0658$ 1.06 BLADE ENTRANCE ANGLE = 90° BLADE EXIT ANGLE = 40° NUMBER OF BLADES = 4, 6 THIN REACTION BLADE PROFILE	F_r W_r	ANNULAR FAN NOZZLE POST EXIT CASCADE THRUST REVERSER
1.1	1965	C C-5A	GE 1/6 FAC PWA JTF 14E/78	0.0658	S	4			$NPR = 1.4 \rightarrow 1.7$ $\sigma = 1.54$ $\lambda/D = 0.22$ 0.46 BLADE ENTRANCE ANGLE = 90° BLADE EXIT ANGLE = 40° NUMBER OF BLADES = 4, 5, 6 NUMBER OF TURNING VANE CONFIGURATIONS = 4 THIN REACTION BLADE PROFILE	F_r W_r	ANNULAR FAN NOZZLE CASCADE THRUST REVERSER WITH TURNING VANES
1.1	1965	C C-5A	GE 1/6 FAC PWA JTF 14E/78	0.0658	S	1			$NPR = 1.2 \rightarrow 1.6$ $\sigma = 1.54$ $\lambda/r = 0$ 0.25 BLADE ENTRANCE ANGLE = 90° BLADE EXIT ANGLE = 40° NUMBER OF BLADES = 3 THIN REACTION BLADE PROFILE	F_r W_r	ANNULAR PRIMARY NOZZLE CASCADE THRUST REVERSER



Results from a parametric test of 16 convergent conical nozzles (Ref. 2) are shown in Figures 1 to 4. The data show small but definite effects due to wall angle α and diameter ratio D_1/D_2 . These data are used in the Internal Performance Module 1² of the TR and TV System Performance Program. Penalties due to skin friction and underexpansion losses are charged separately, as shown in Figure 1. If the nozzle exit is offset from the nacelle centerline, which is typical of single bearing vectoring nozzle designs, then the ΔC_v penalty shown in Figure 5 is charged.

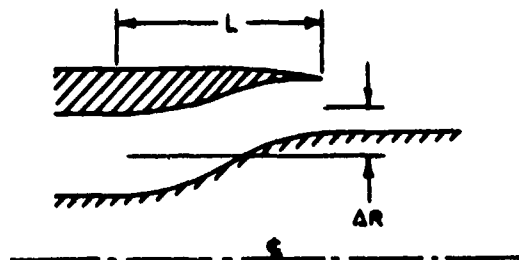
During preliminary design studies, the simplest method of predicting nozzle performance, termed a "Level 1" prediction, is adequate because the nozzle geometry is not well defined. The nozzle is charged with $\Delta C_v = 0.005$ for skin friction losses and offset losses from Figure 5. In addition, underexpansion losses are charged for supercritical pressure ratios as shown in Figure 6.

Conical Nozzle Discharge Coefficient

Experimental results for convergent nozzle discharge coefficients (Ref. 2) are shown in Figure 7. Note that wall angle, diameter ratio, and pressure ratio have significant effects on discharge coefficient. Experimentally determined choking pressure ratios are indicated on the curves by tick marks. A shaded band has been drawn bracketing the experimental points. The choked discharge coefficient levels are summarized in Figure 8 as a function of wall angle and diameter ratio.

Annular Nozzle Velocity Coefficient

A sketch of an annular nozzle is shown below.



$D_1/D_2 = 1.1$

CURVE α

— 5°

- - - 15°

- - - 30°

- - - 90°

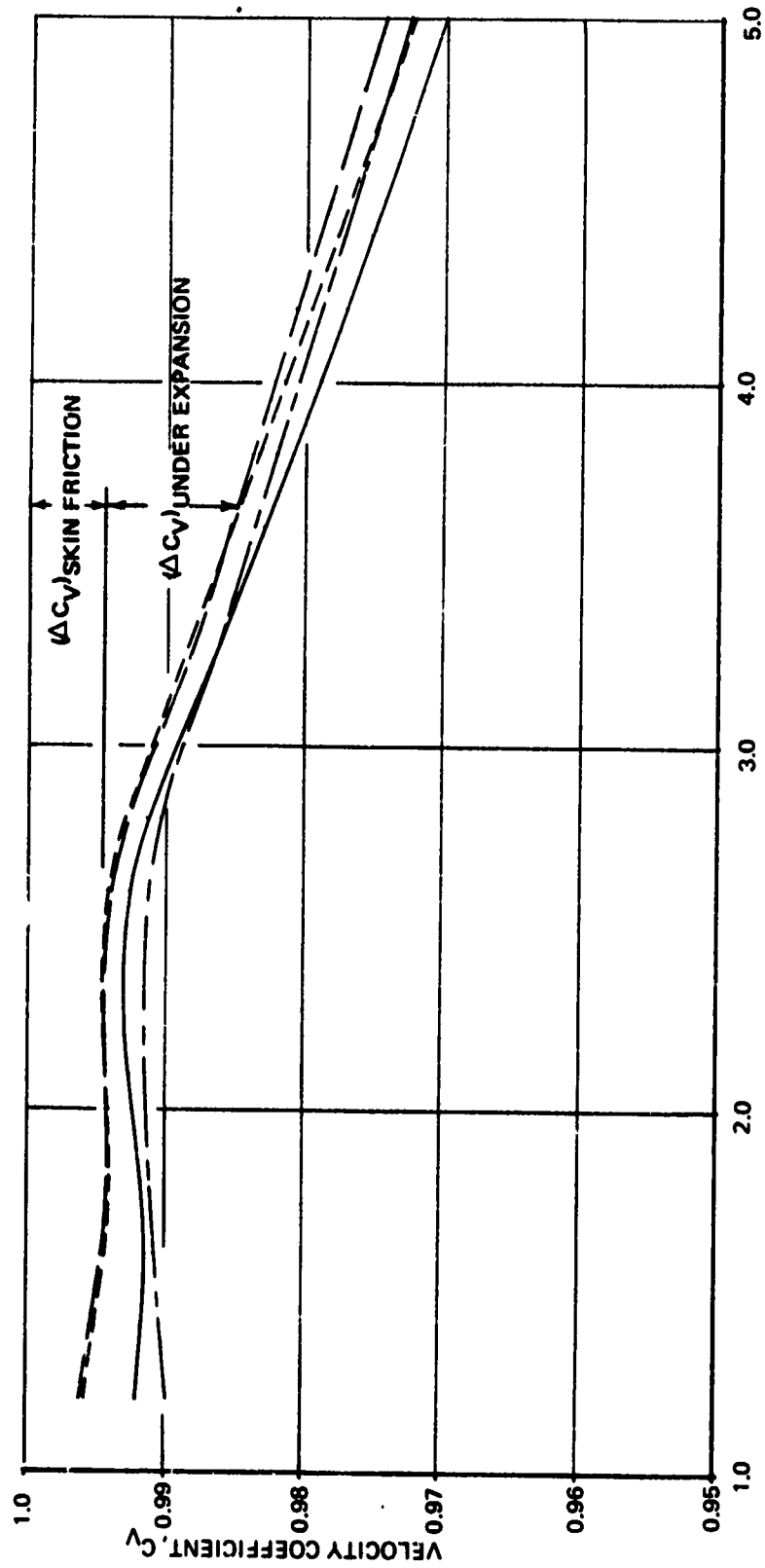
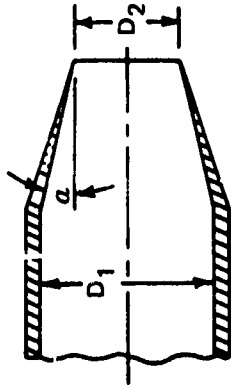


Figure 1: EFFECT OF WALL ANGLE ON VELOCITY COEFFICIENT FOR CONICAL NOZZLES, $D_1/D_2 = 1.1$

$D_1/D_2 = 1.25$

CURVE	α
—	5°
- - -	15°
- · - · -	30°
- - - - -	90°

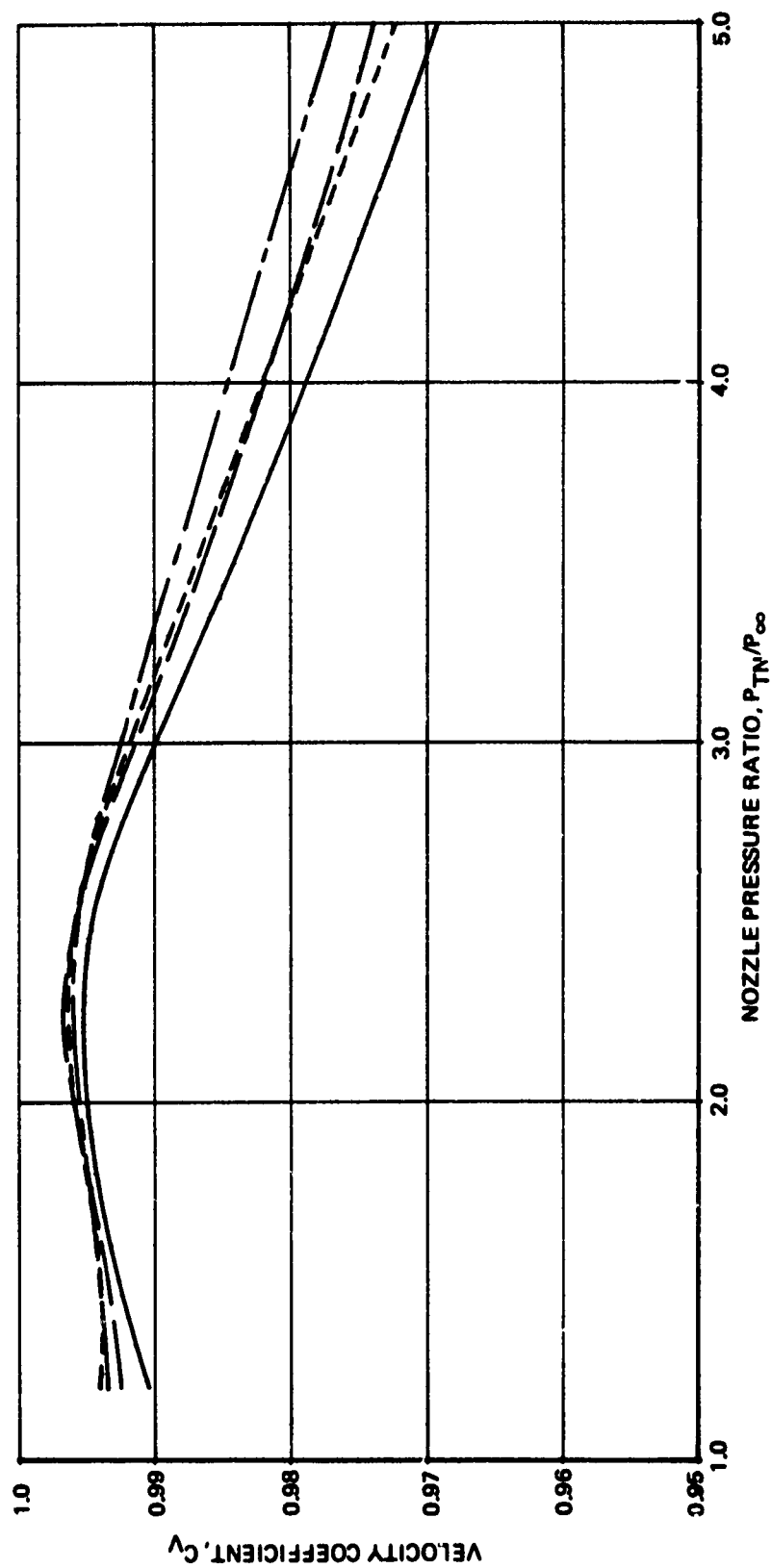
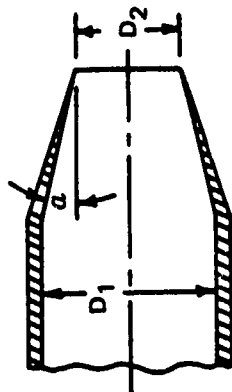


Figure 2: EFFECT OF WALL ANGLE ON VELOCITY COEFFICIENTS FOR CONICAL NOZZLES, $D_1/D_2 = 1.25$

$D_1/D_2 = 1.6$
 CURVE α
 — 5°
 - - 15°
 - - 30°
 - - 90°

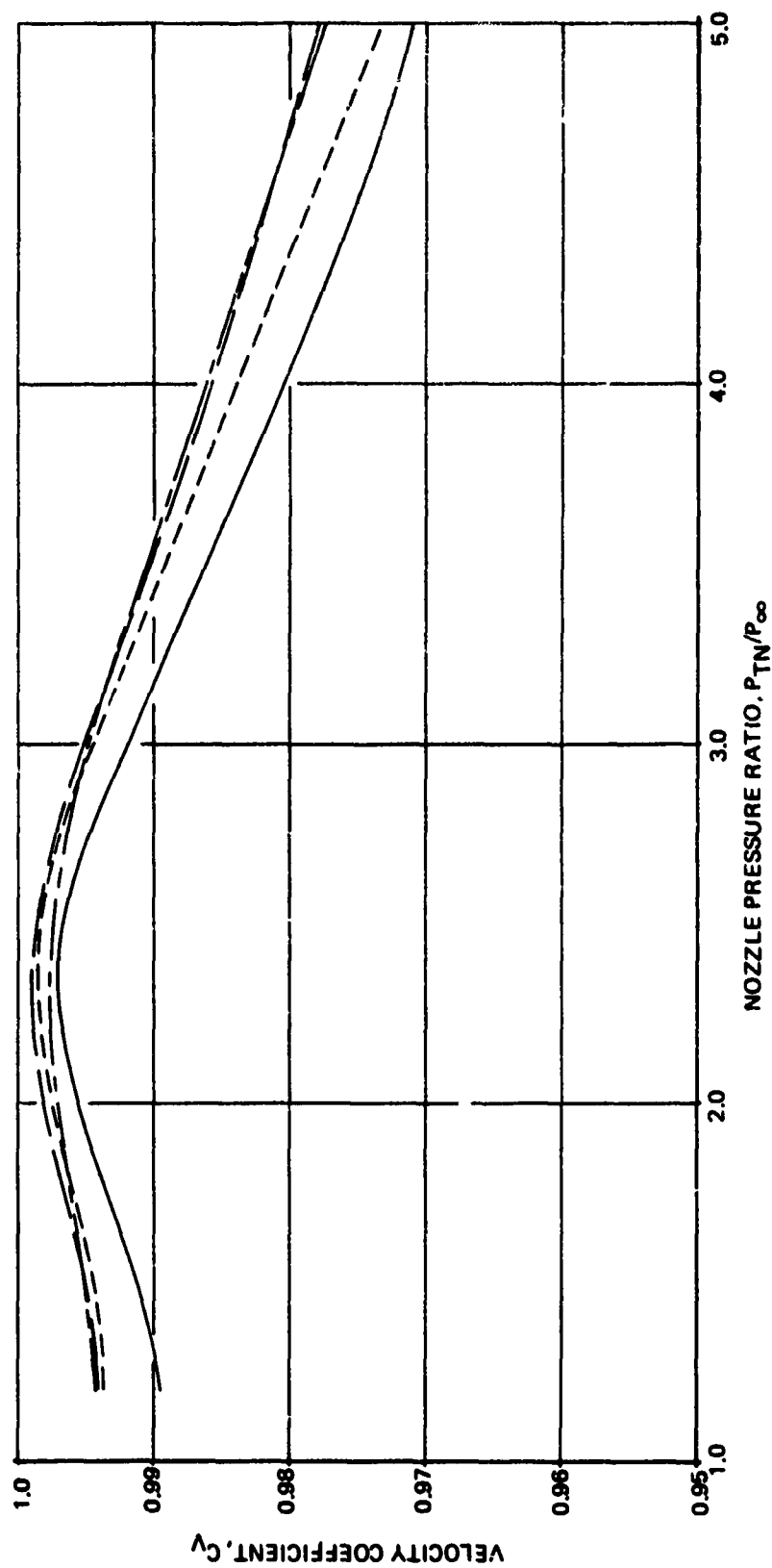
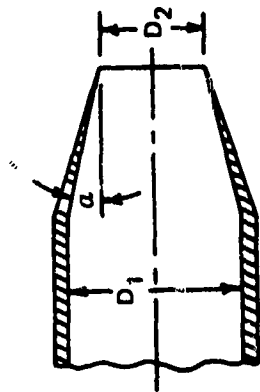
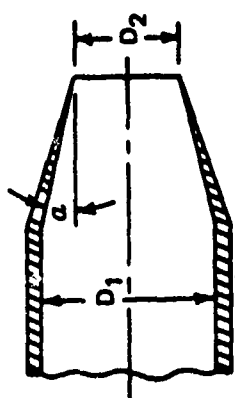


Figure 3: EFFECT OF WALL ANGLE ON VELOCITY
 COEFFICIENTS FOR CONICAL NOZZLES,
 $D_1/D_2 = 1.6$



$D_1/D_2 = 1.93$

CURVE α

— 5°

- - - 15°

- - - 30°

- - - 90°

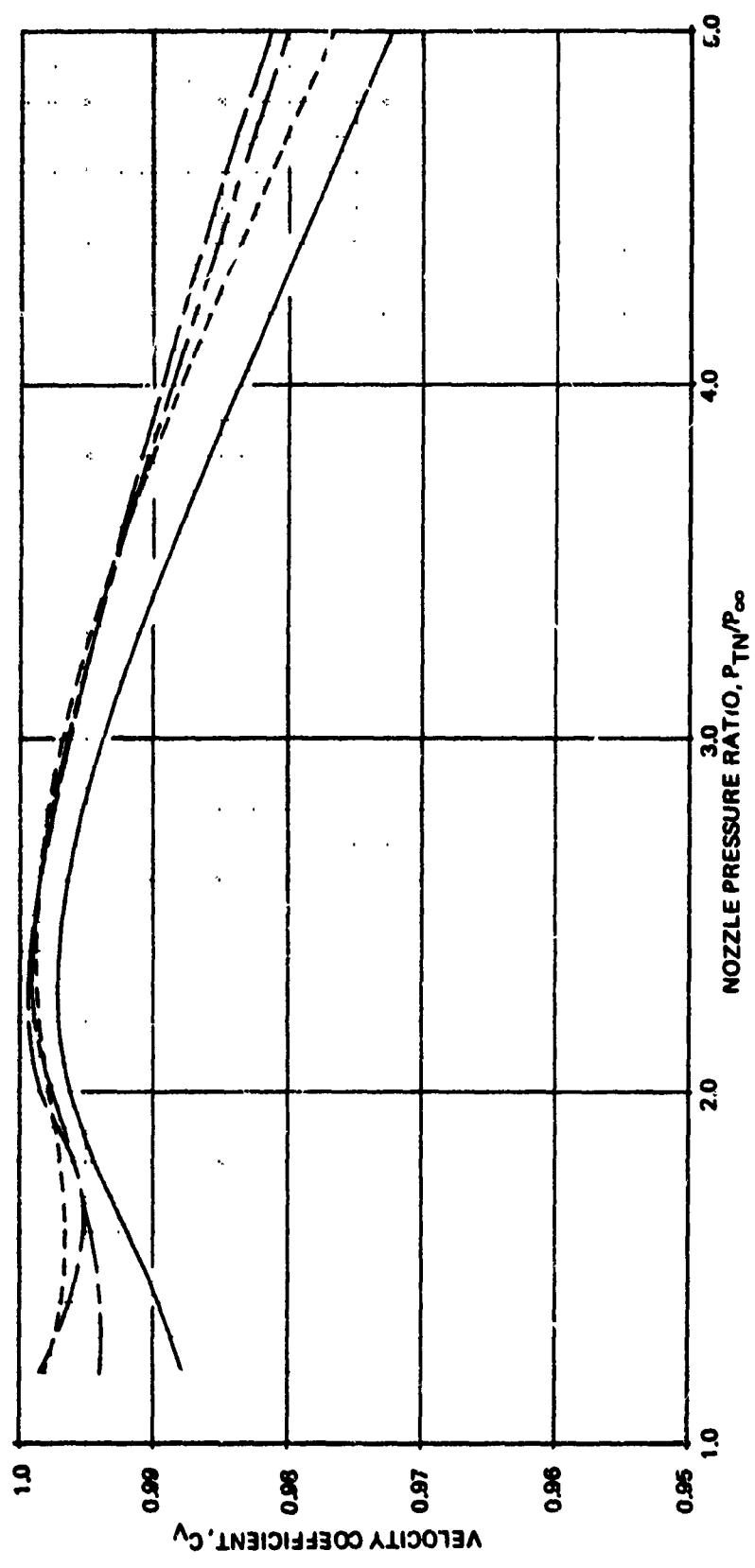


Figure 4: EFFECT OF WALL ANGLE ON VELOCITY COEFFICIENTS FOR CONICAL NOZZLES, $D_1/D_2 = 1.93$

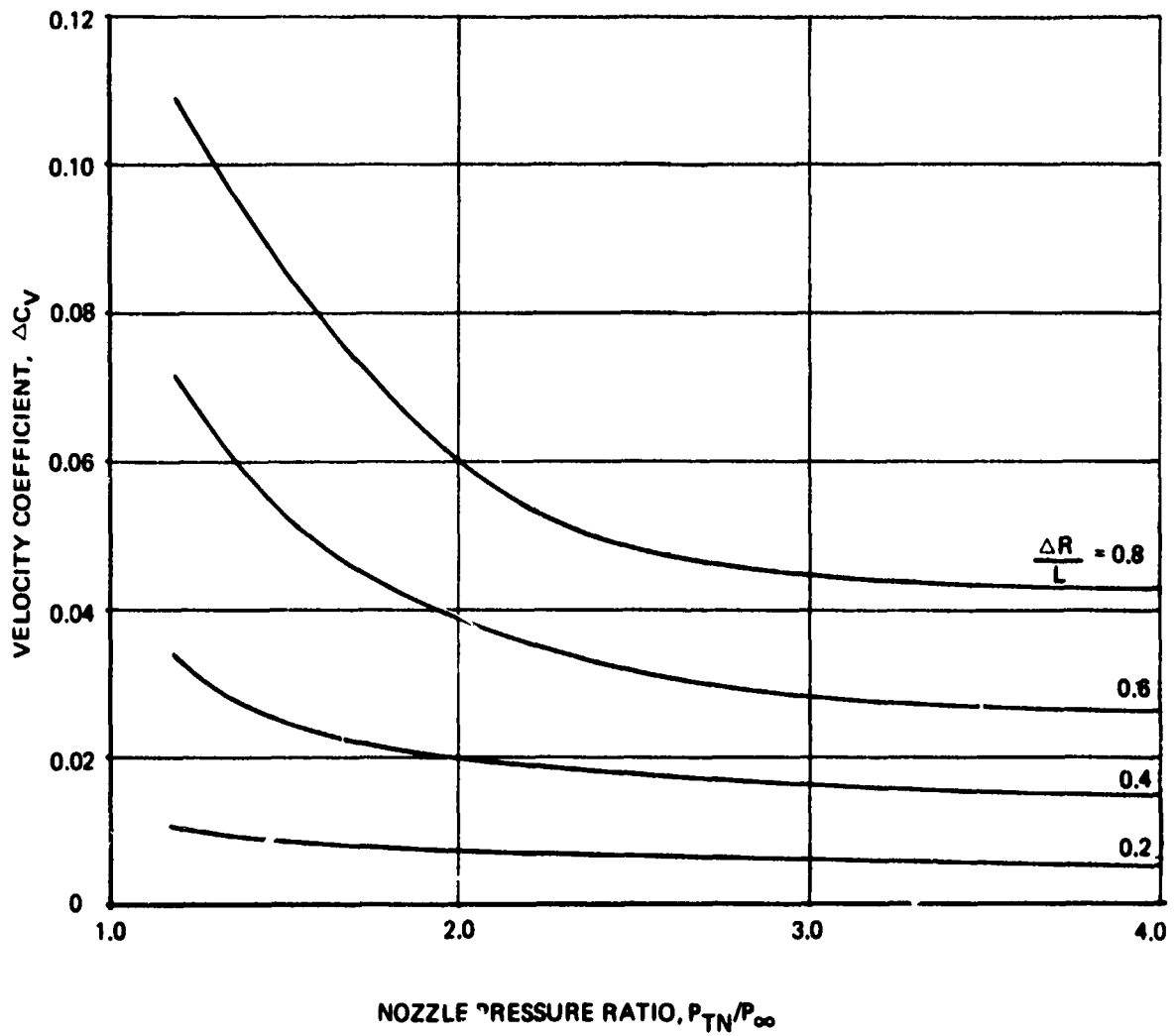
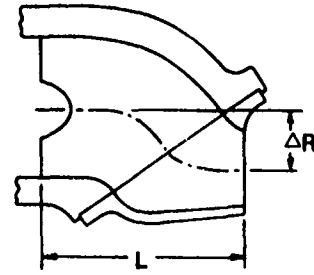


Figure 5: EFFECT OF NOZZLE OFFSET ON VELOCITY COEFFICIENT LOSSES

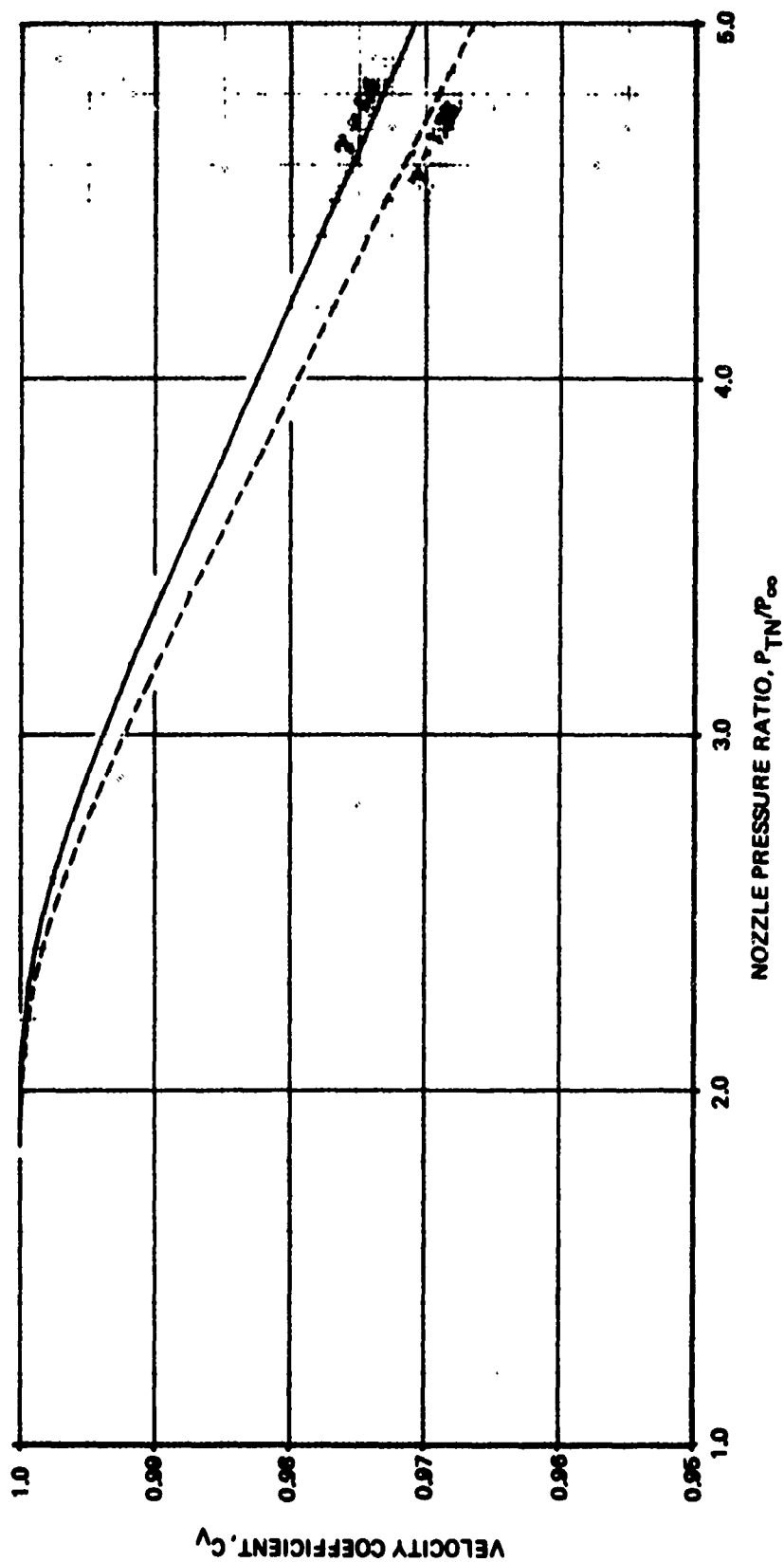


Figure 6: THEORETICAL VELOCITY COEFFICIENT
UNDER EXPANSION LOSSES FOR CONVERGENT
NOZZLES AT SUPERCRITICAL PRESSURE RATIOS

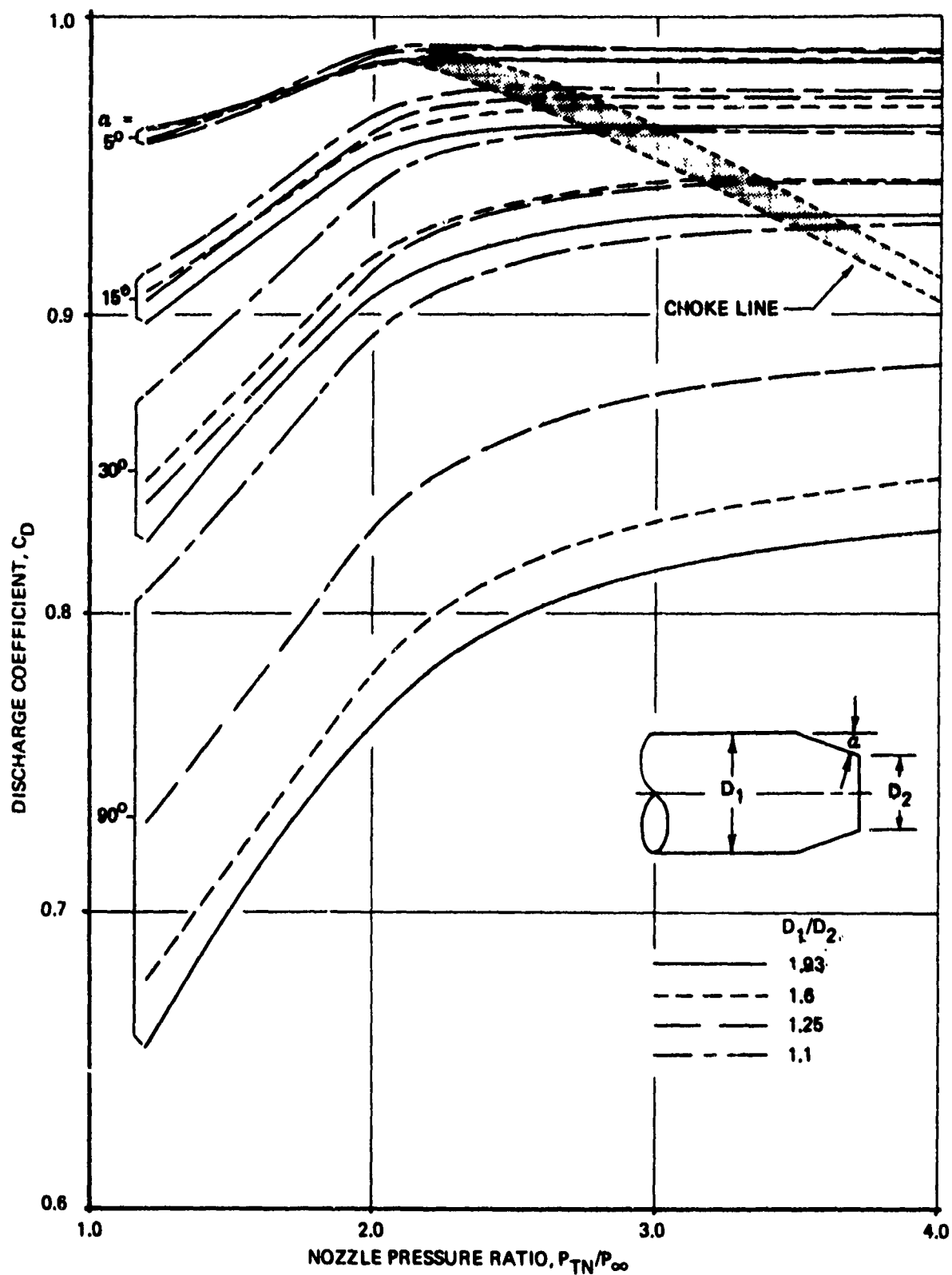


Figure 7: EXPERIMENTAL DISCHARGE COEFFICIENT CURVES FOR CONVERGENT CONICAL NOZZLES

NOTE: CONICAL CONVERGENT NOZZLES
CHOKE AT PRESSURE RATIOS HIGHER
THAN CRITICAL. CONSEQUENTLY C_D CHOKE
DOES NOT APPLY AT CRITICAL P_T/P_∞

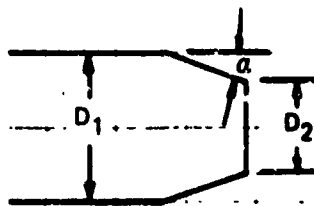
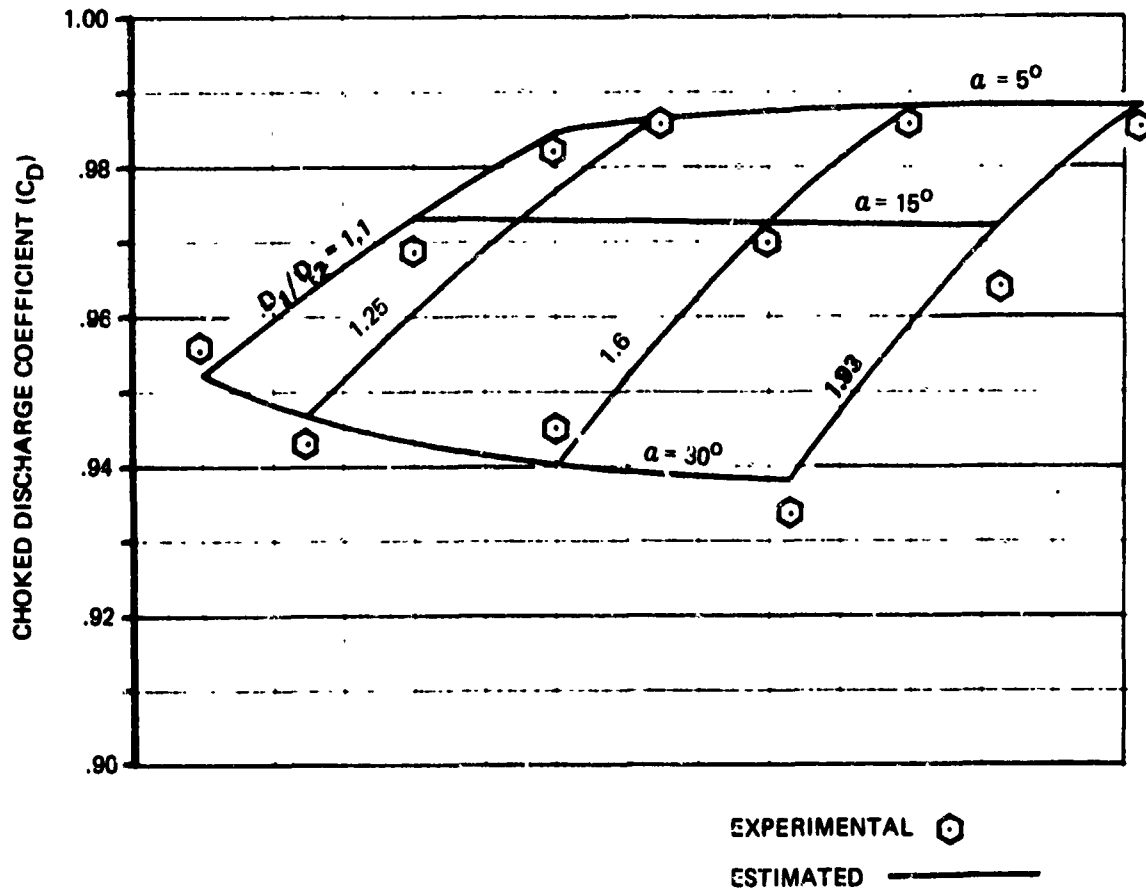


Figure 8: PARAMETRIC STUDY OF CONICAL CONVERGENT
NOZZLES - C_D CHOKE

Test results are used to predict the ΔC_y penalty of annular nozzles relative to conical nozzles. Results from Boeing tests of JT3D and C-5A fan nozzles are shown in Figure 9. The conical nozzle C_y data are charged with this additional increment to predict annular nozzle performance.

Annular Nozzle Discharge Coefficient

Review of the literature did not produce a usable set of data for annular nozzle discharge coefficients. However, a combination of conical nozzle data and theory was developed that is adequate. Boundary layer theory is used to determine discharge coefficient assuming only viscous losses, i.e., no vena contracta or three-dimensional flow effects. For a conical nozzle,

$$C_{D\text{conical nozzle}} = 1 - \frac{2\delta^*}{R} \quad (1)$$

where R is the nozzle exit radius and δ^* is the boundary layer displacement thickness at the nozzle exit. For an annular nozzle,

$$C_{D\text{annular nozzle}} = 1 - \frac{2\delta^*}{R_o - R_i} \quad (2)$$

where R_o and R_i are the annular nozzle inner and outer radii. Assuming that the conical and annular nozzles have the same length, area, exit Mach number, and Reynolds number

$$\delta_{\text{conical}}^* = \delta_{\text{annular}}^* \quad (3)$$

Eliminating δ^* between Equations 1 and 2 and solving for $C_{D\text{annular}}$ gives

$$C_{D\text{annular}} = 1 - \frac{\sqrt{R_o^2 - R_i^2}}{R_o - R_i} (1 - C_{D\text{conical}}) \quad (4)$$

The term $C_{D\text{conical}}$ is obtained from the conical nozzle data at choked flow conditions, Figure 8. Equation 4 is used to calculate $C_{D\text{annular}}$ at choked conditions.

In order to predict C_D at subcritical pressure ratios, the analytical method of Bragg (Ref. 3) is used. Bragg's analytical discharge coefficient curves are shown in Figure 10. Bragg's results are erroneous for pressure ratios greater than choke. Consequently, the curves were corrected by making C_D constant above the choked pressure ratio. The choking line was taken from Figure 7. A good check of the accuracy of Bragg's theory is made by overlaying Figures 7 and 10.

Bragg's theory does not permit the discharge coefficient to be calculated for a particular nozzle geometry. It predicts how the discharge coefficient of a nozzle, known under choked flow conditions will vary for subcritical pressure ratios. To use Bragg's method, the choked discharge coefficient is located on

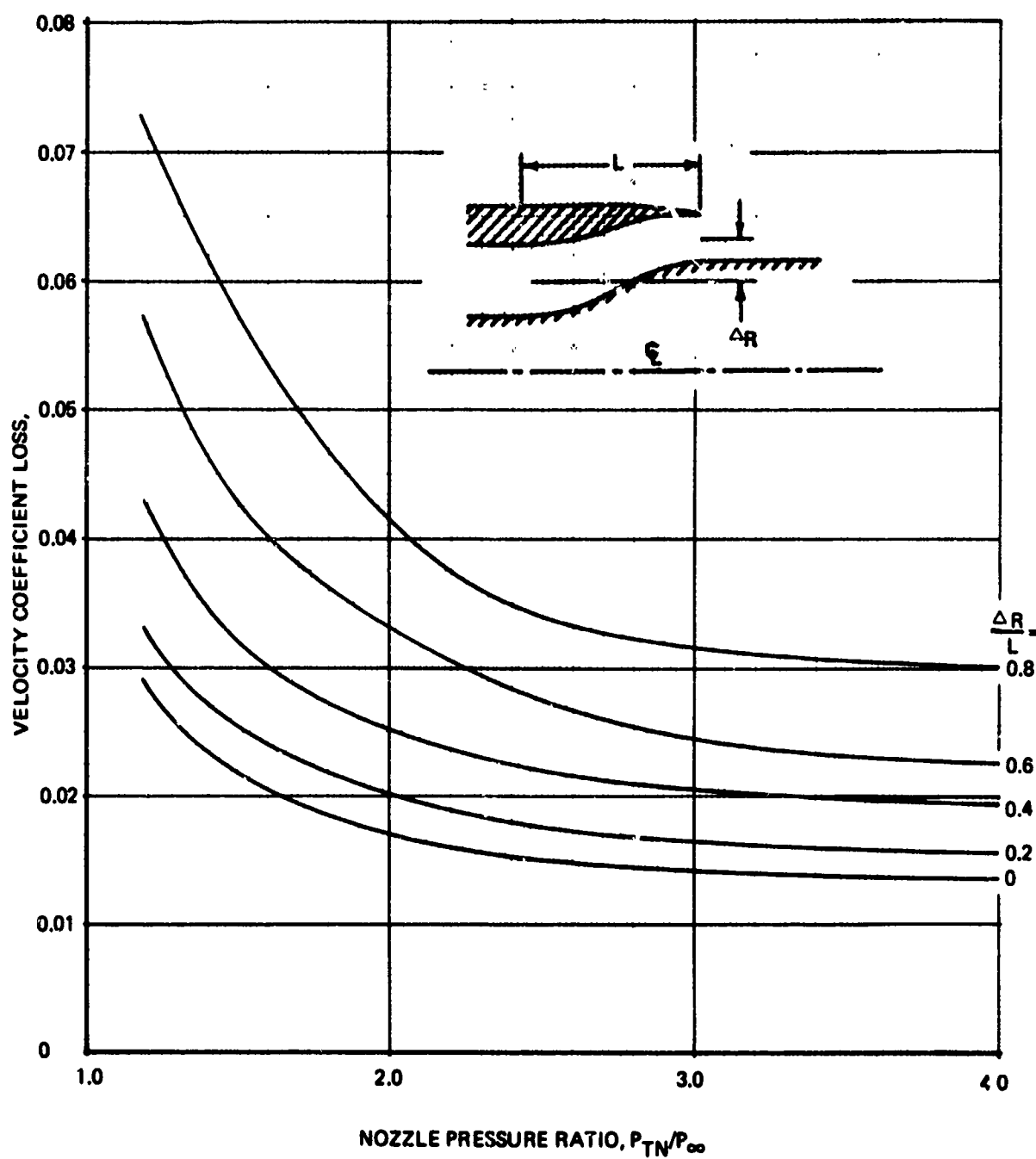


Figure 9: EFFECT OF NOZZLE OFFSET ON ANNULAR NOZZLE VELOCITY COEFFICIENT LOSSES

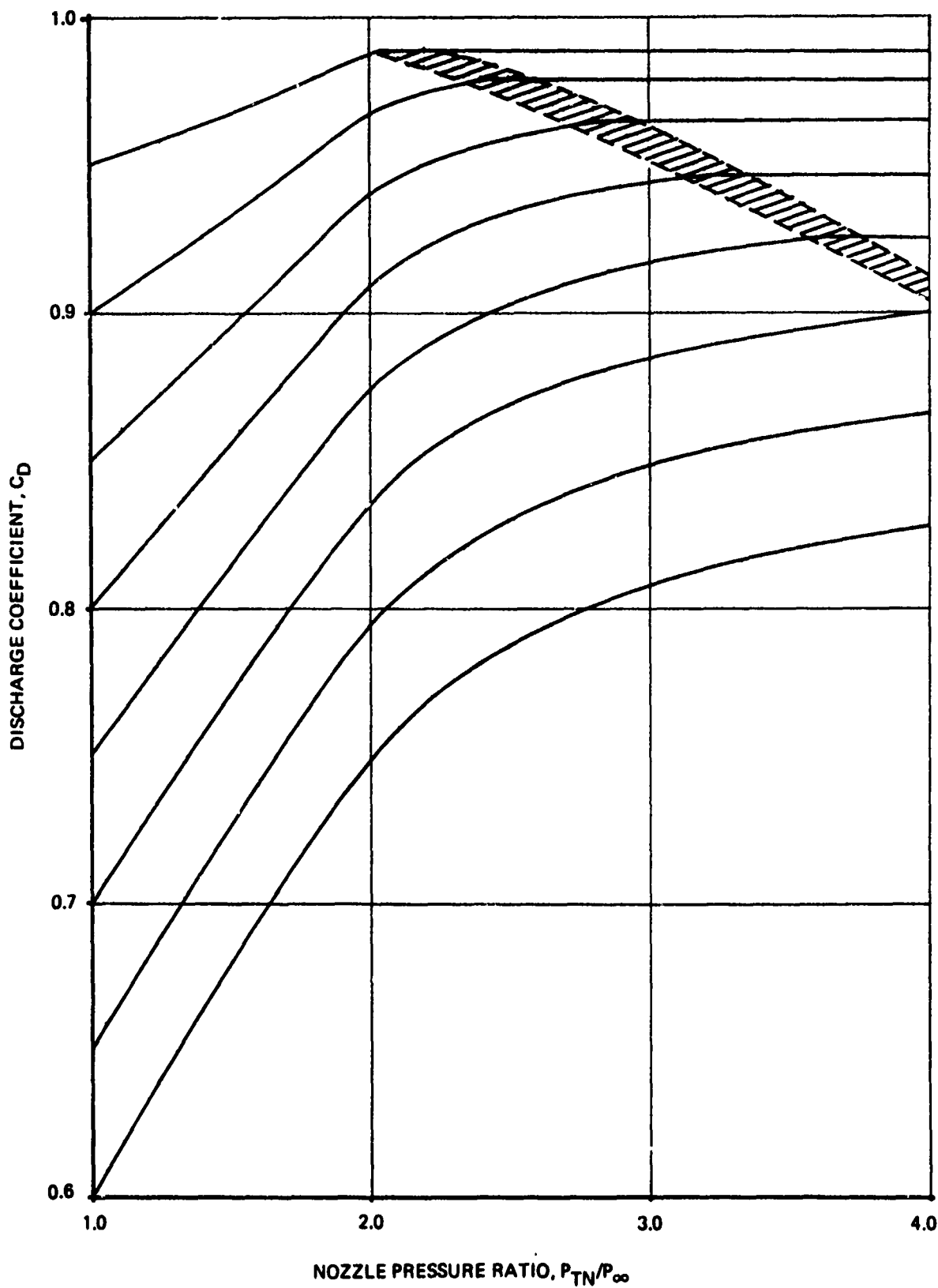
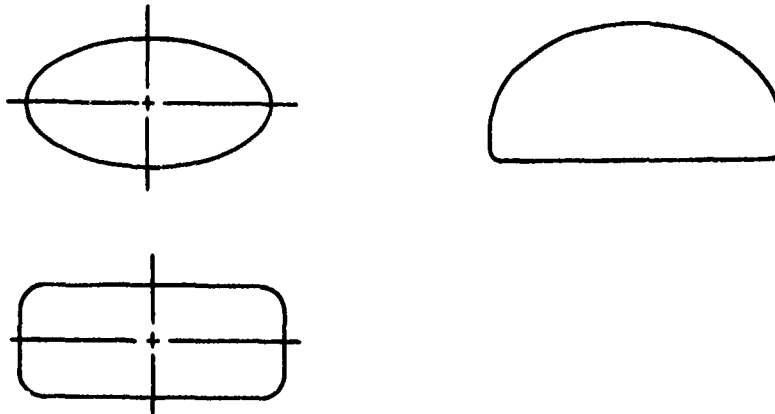


Figure 10: THEORETICAL DISCHARGE COEFFICIENT CURVES
USING BRAGG'S THEORY

the right side of Figure 10. The curve is followed back to the left by fairing in the best fit at the choke line.

Noncircular Nozzle Velocity Coefficient

Noncircular nozzles have rectangular, D-shaped, or elliptical shaped cross sections as shown in the sketches below.



The prediction method for noncircular nozzles employs an equivalent hydraulic diameter correlation developed to predict the maximum velocity coefficient of suppressor nozzles, as shown in Figure 11 from Ref. 4. If the losses are assumed to be caused predominantly by skin friction losses in the boundary layer, the maximum velocity coefficient of circular convergent nozzle is given by

$$(C_{v_{max}})_{\text{circular}} = 1 - \frac{4\theta}{D} \quad (5)$$

where D is the diameter and θ is boundary layer momentum thickness at the nozzle exit. The maximum velocity coefficient occurs at a pressure ratio such that the convergent nozzle is choked but does not exhibit any underexpansion loss. This typically occurs at a nozzle pressure ratio of about 2.2. By dimensional analysis, it can be shown that for noncircular nozzles,

$$(C_{v_{max}})_{\text{noncircular}} = 1 - \left(\frac{1 - C_{vs}}{\sqrt{D_{he}}} \right) \quad (6)$$

where C_{vs} is the maximum velocity coefficient of a standard convergent nozzle, and D_{he} is the equivalent hydraulic diameter

$$D_{he} = \frac{\sqrt{4\pi \text{ area}}}{\text{perimeter}} \quad (7)$$

REF. 4

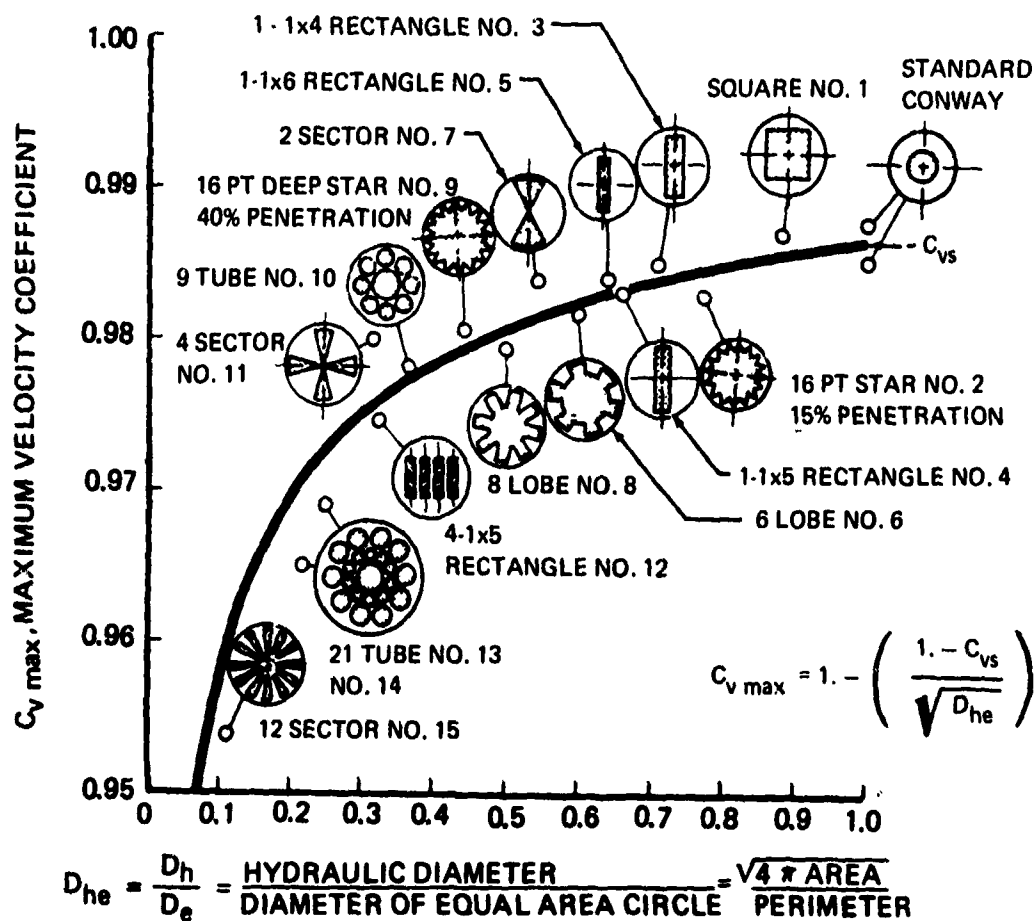


Figure 11: MAXIMUM VELOCITY COEFFICIENT CORRELATION FOR SUPPRESSOR NOZZLES

The percent loss in velocity coefficient relative to the standard nozzle is given by

$$\frac{\Delta C_v}{C_{vs}} = 1 - \frac{(C_{vmax})_{noncircular}}{C_{vs}} \quad (8)$$

To apply the equivalent hydraulic diameter correlation to a noncircular nozzle, the parametric velocity coefficient data shown in Figures 1 to 4 are used to obtain the nozzle skin friction loss ΔC_v . The increase in skin friction loss due to increased wetted area of the noncircular nozzle is given by

$$\Delta C_v \text{ wetted area increase} = \left(1 - \frac{(C_{vmax})_{noncircular}}{C_{vs}}\right) (1 - \Delta C_v \text{ skin friction}) \quad (9)$$

Noncircular Nozzle Discharge Coefficient

Boundary layer theory is employed to predict discharge coefficient penalties. Assuming only skin friction losses,

$$C_{v \text{ skin friction}} = 1 - \frac{4\theta}{D} \quad (10)$$

$$C_{D \text{ skin friction}} = 1 - \frac{4\delta^*}{D} \quad (11)$$

Combining Equations 10 and 11 gives

$$\Delta C_{D \text{ skin friction}} = H \Delta C_{v \text{ skin friction}} \quad (12)$$

where $H = \delta^*/\theta$ is boundary layer shape factor. For a turbulent, flatplate boundary layer with $M_\infty = 1$, a good value for $H = 1.7$. The discharge coefficient penalty due to wetted area increase is given by

$$\Delta C_{D \text{ wetted area increase}} = H \Delta C_{v \text{ wetted area increase}} \quad (13)$$

The maximum discharge coefficient is given by

$$C_{Dmax} = C_{Dchoke} - \Delta C_{D \text{ wetted area increase}} \quad (14)$$

where $C_{D \text{ choke}}$ is obtained from the conical nozzle choked discharge coefficient data, Figure 8. Discharge coefficient is predicted at lower pressure ratios using Bragg's theoretical curves with C_{Dmax} from Equation 14 as the choked discharge coefficient value.

2.1.2 Thrust Reverser Data Correlations

This section describes data correlations developed for several types of thrust reverser systems. Boeing was assisted in formulating the data correlations by Pratt & Whitney Aircraft who provided data for annular target and blow-in door ejector thrust reversers.

Clamshell Target Thrust Reverser

A clamshell target thrust reverser is shown in Figure 12. Clamshell target reversers are used on the 737, DC-9, and C-141 airplanes. An experimental study of geometric variables influencing the static performance of clamshell target reversers is presented in Ref. 5. The geometric variables are defined in Figure 13. Table III summarizes the range, nominal value, and the figure number showing the effect of each geometric variable on corrected static reverser efficiency.

Table III: SUMMARY OF CLAMSHELL TARGET THRUST REVERSER
GEOMETRIC VARIABLES

Geometric Variable	Definition	Nominal Test Value	Range	Figure
X/D	Setback ratio	0.94	0.81 → 0.94	14
L/D	Door length ratio	1.0	0.90 → 1.20	15
\overline{LH}/D	Average lip height ratio	0.106	0.0545 → 0.121	16
λ	Sweep angle, degrees	10	0 → 15	17
θ	Arc angle, degrees	140	120 → 180	18
α	Cone angle, degrees	10	0 → 10	19
β	Bevel angle, degrees	0	0 → 40	20

In addition to the geometric variables, nozzle pressure ratio was varied from 1.2 to 1.98. Data were taken for corrected static reverser efficiency, η_{RC} and airflow match, \bar{F} . In functional form,

$$\eta_{RC} = f\left(\frac{P_{TN}}{P_0}, \frac{X}{D}, \frac{L}{D}, \frac{\overline{LH}}{D}, \lambda, \theta, \alpha, \beta\right) \quad (15)$$

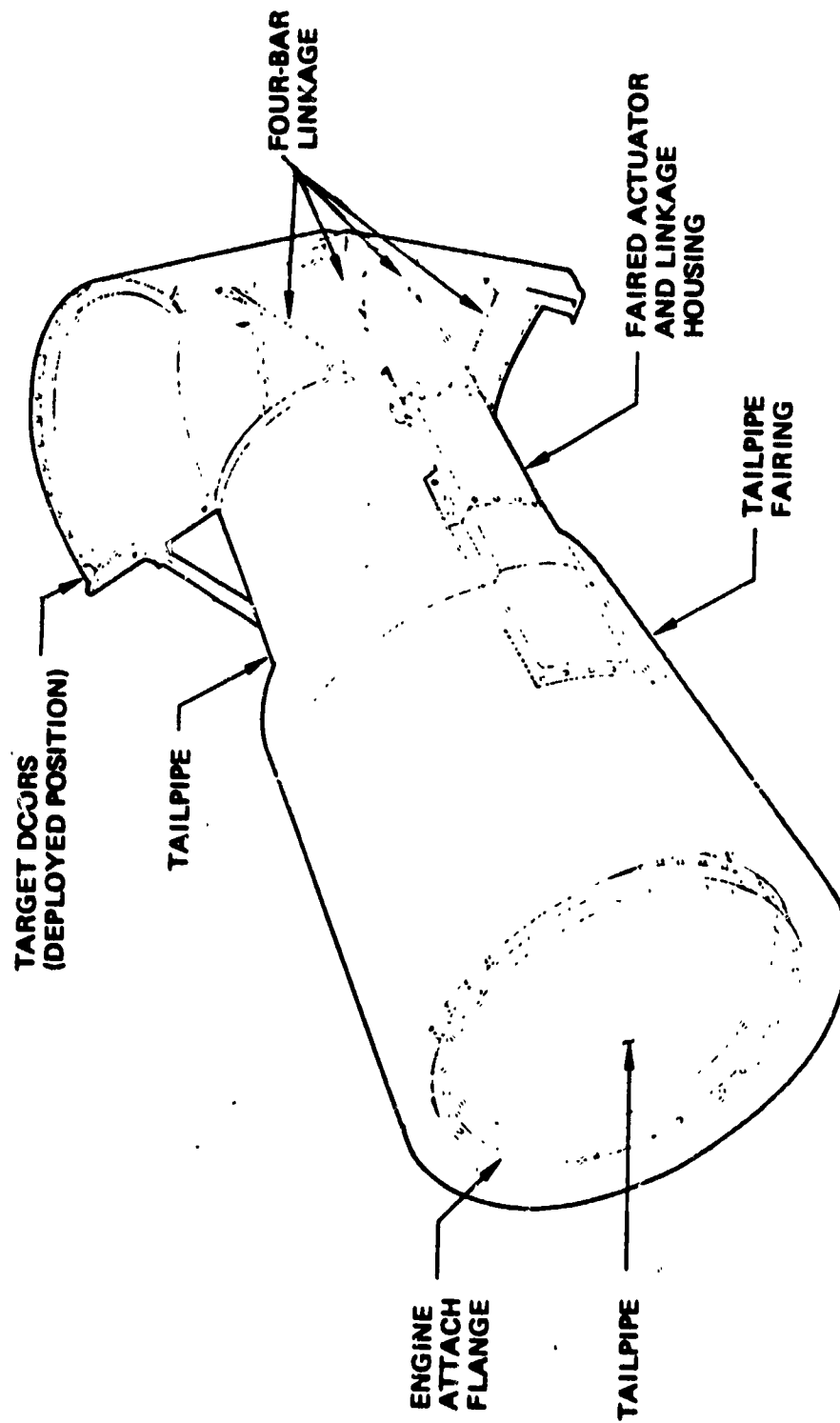
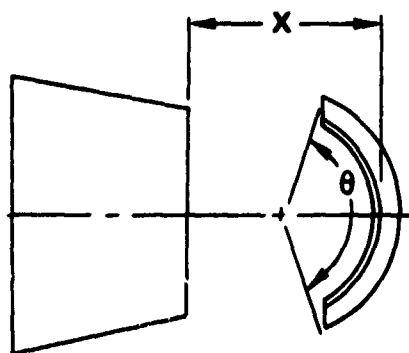
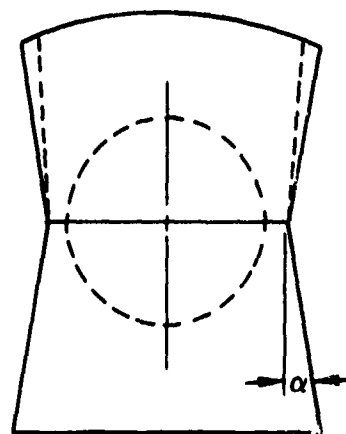
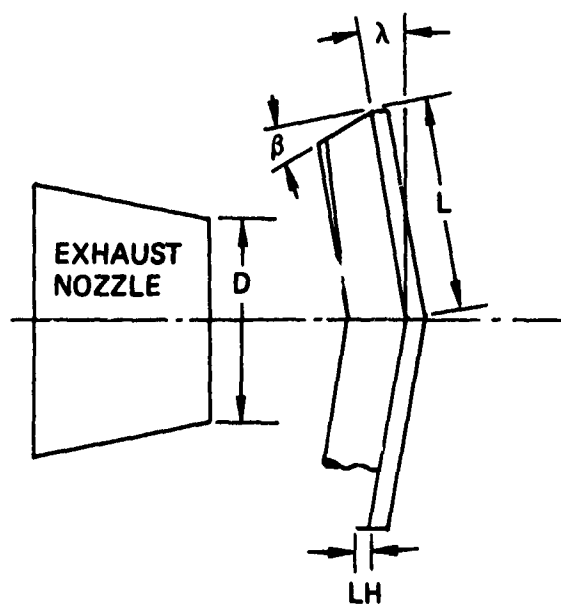


Figure 12: CLAMSHELL TARGET THRUST REVERSER
SCHEMATIC



DESIGN PARAMETERS

SET BACK = X
 DOOR LENGTH = L
 LIP HEIGHT = LH
 SWEEP ANGLE = λ
 ARC ANGLE = θ
 CONE ANGLE = α
 BEVEL ANGLE = β

**Figure 13: CLAMSHELL TARGET THRUST REVERSER
GEOMETRIC VARIABLES**

DOOR LENGTH RATIO = $L/D = 0.95$
 AVERAGE LIP HEIGHT = $LH/D = 0.106$
 SWEEP ANGLE = $\lambda = 10^\circ$
 ARC ANGLE = $\theta = 140^\circ$
 CONE ANGLE = $\alpha = 10^\circ$
 BEVEL ANGLE = $\beta = 0^\circ$
 NO SIDE FENCES

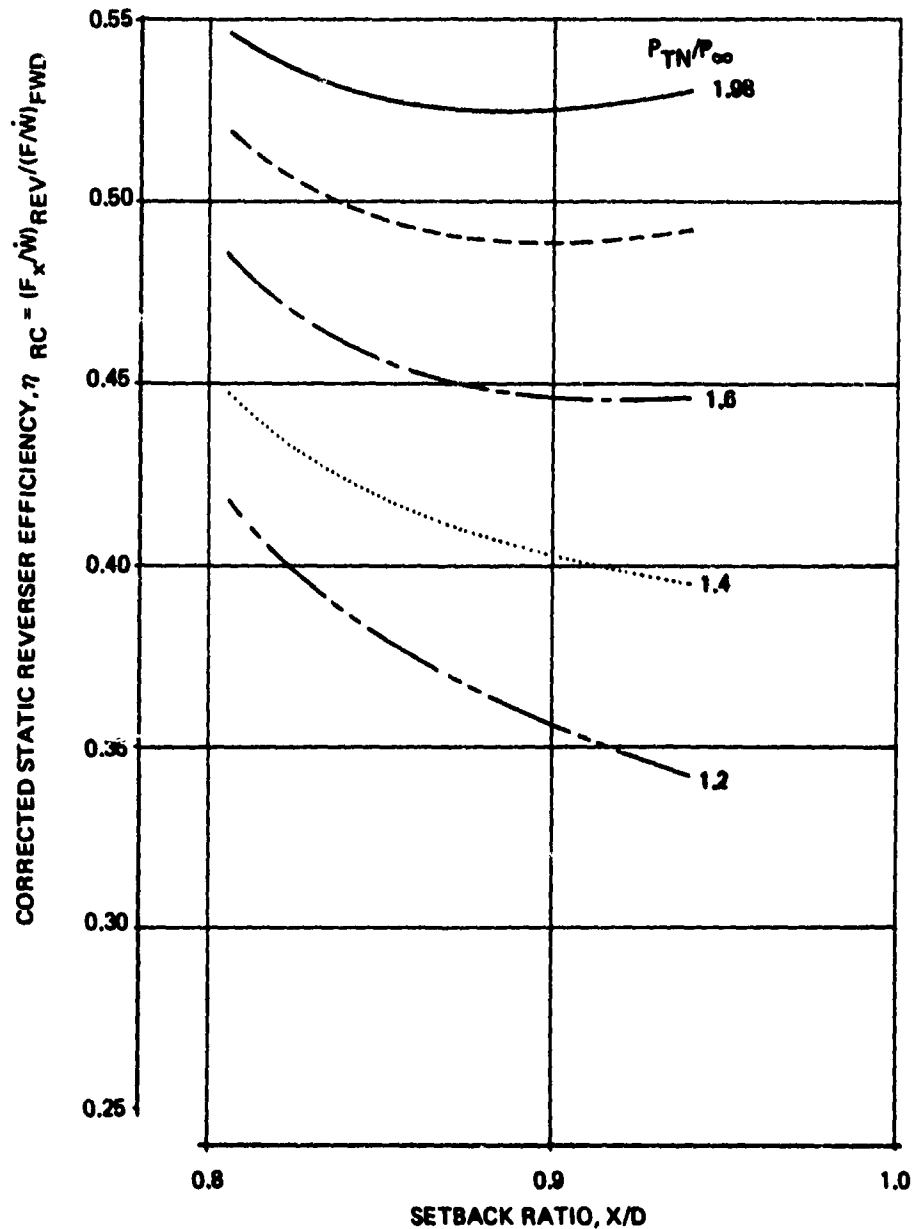
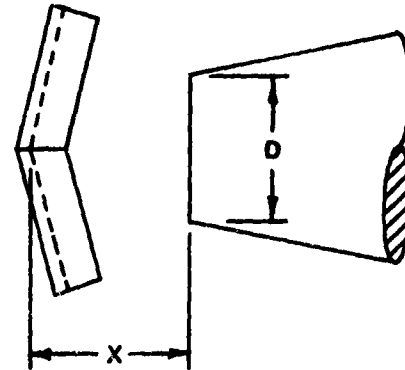


Figure 14: EFFECT OF SETBACK RATIO ON STATIC REVERSER EFFICIENCY, CLAMSHELL TARGET THRUST REVERSER

SETBACK RATIO = $X/D = 0.94$
 AVERAGE LIP HEIGHT = $LH/D = 0.106$
 SWEEP ANGLE = $\lambda = 10^\circ$
 ARC ANGLE = $\theta = 140^\circ$
 CONE ANGLE = $\alpha = 10^\circ$
 BEVEL ANGLE = $\beta = 0^\circ$
 NO SIDE FENCES

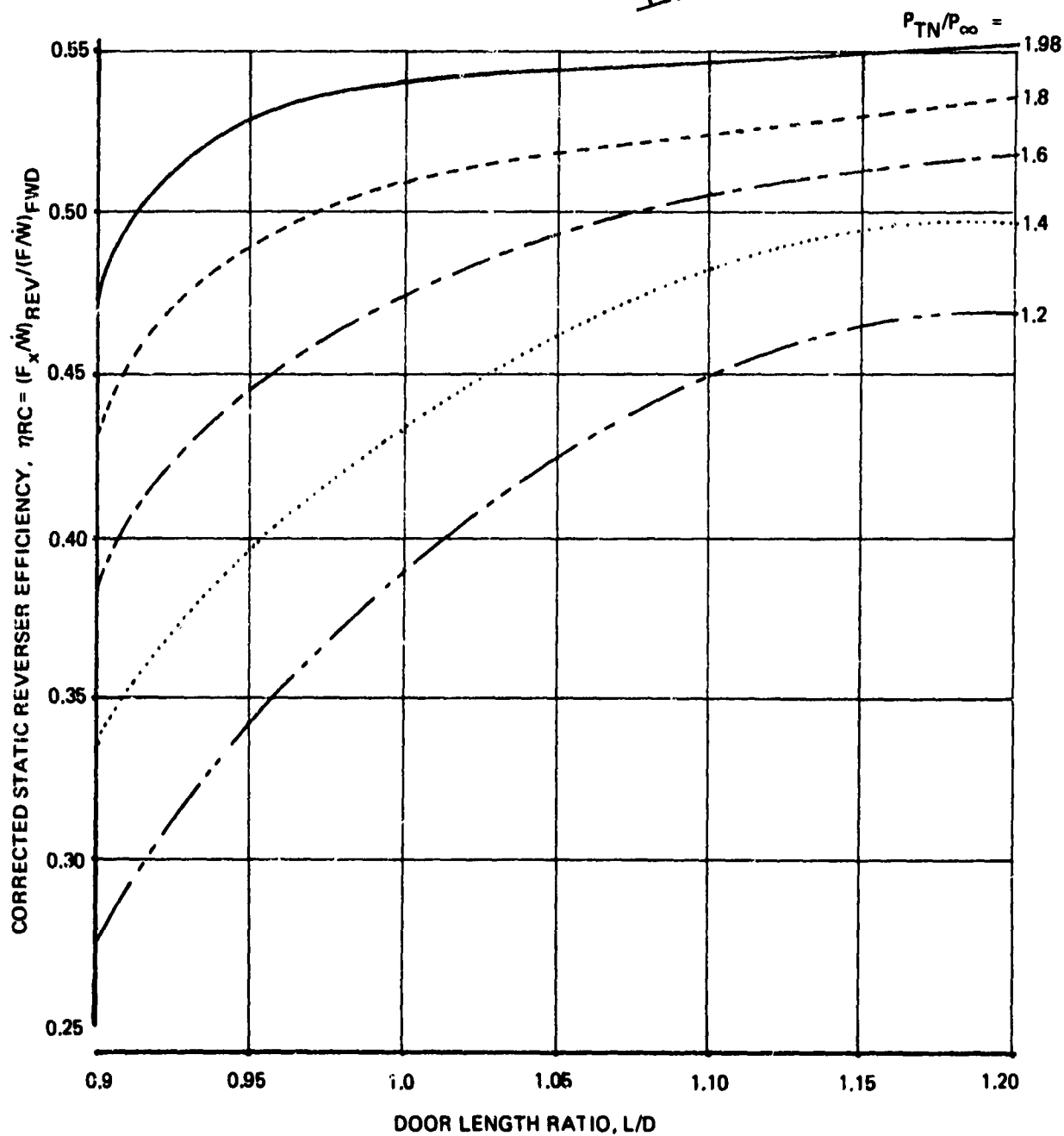
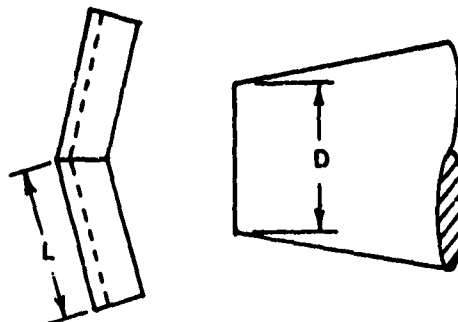


Figure 15: EFFECT OF DOOR LENGTH ON STATIC
 REVERSER EFFICIENCY, CLAMSHELL
 TARGET THRUST REVERSER

SETBACK RATIO = $X/D = 0.94$
 DOOR LENGTH RATIO = $L/D = 1.06$
 SWEEP ANGLE = $\lambda = 9.5^\circ$
 ARC ANGLE = $\theta = 137^\circ$
 CONE ANGLE = $\alpha = 10^\circ$
 BEVEL ANGLE = $\beta = 0^\circ$
 NO SIDE FENCES

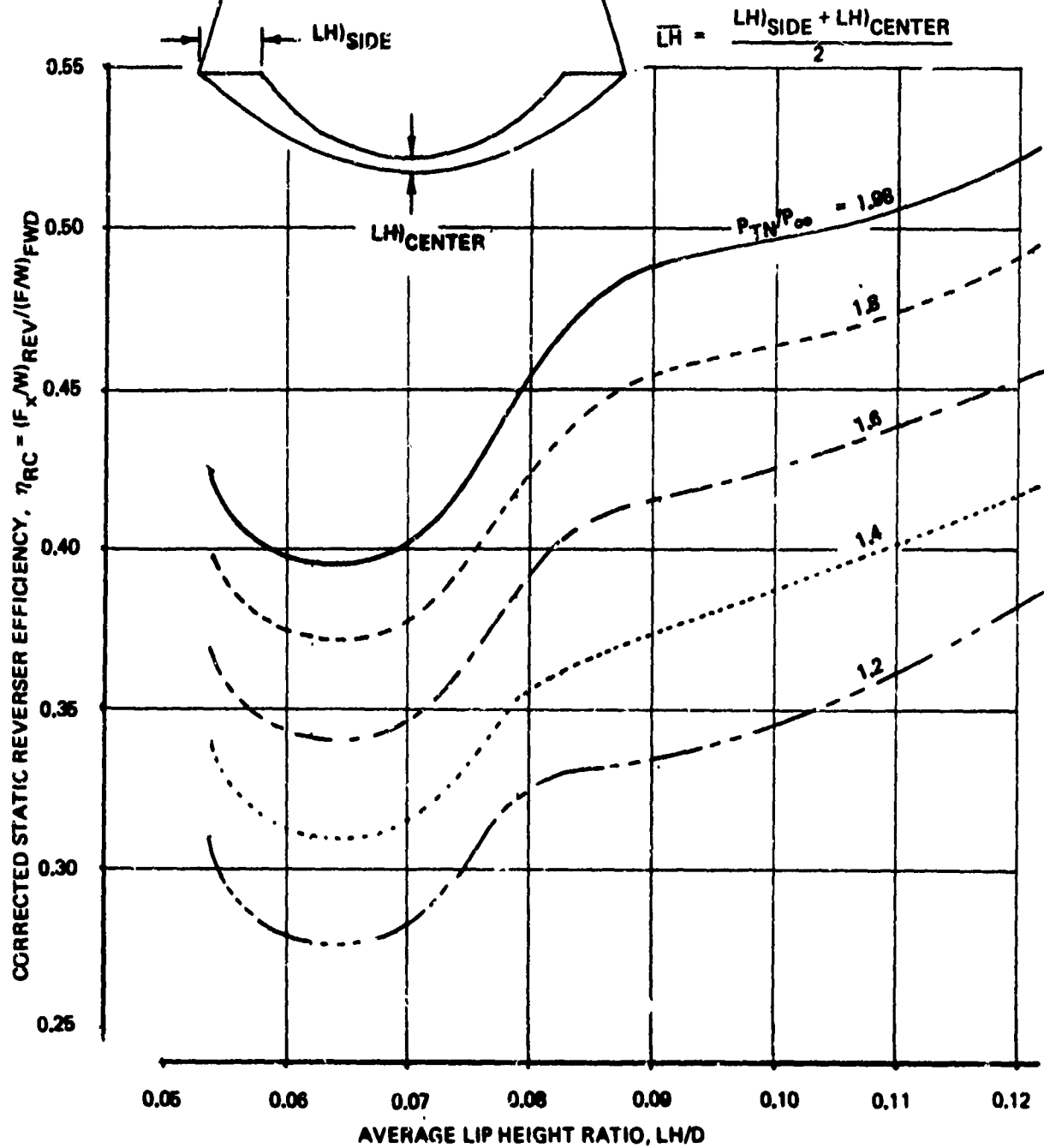


Figure 16: EFFECT OF LIP HEIGHT ON STATIC REVERSER
 EFFICIENCY, CLAMSHELL TARGET THRUST
 REVERSER

SETBACK RATIO = $X/D = 0.94$
 DOOR LENGTH RATIO = $L/D = 1.0$
 AVERAGE LIP HEIGHT = $\overline{LH}/D = 0.106$
 ARC ANGLE = $\theta = 140^\circ$
 CONE ANGLE = $\alpha = 10^\circ$
 BEVEL ANGLE = $\beta = 0^\circ$
 NO SIDE FENCES

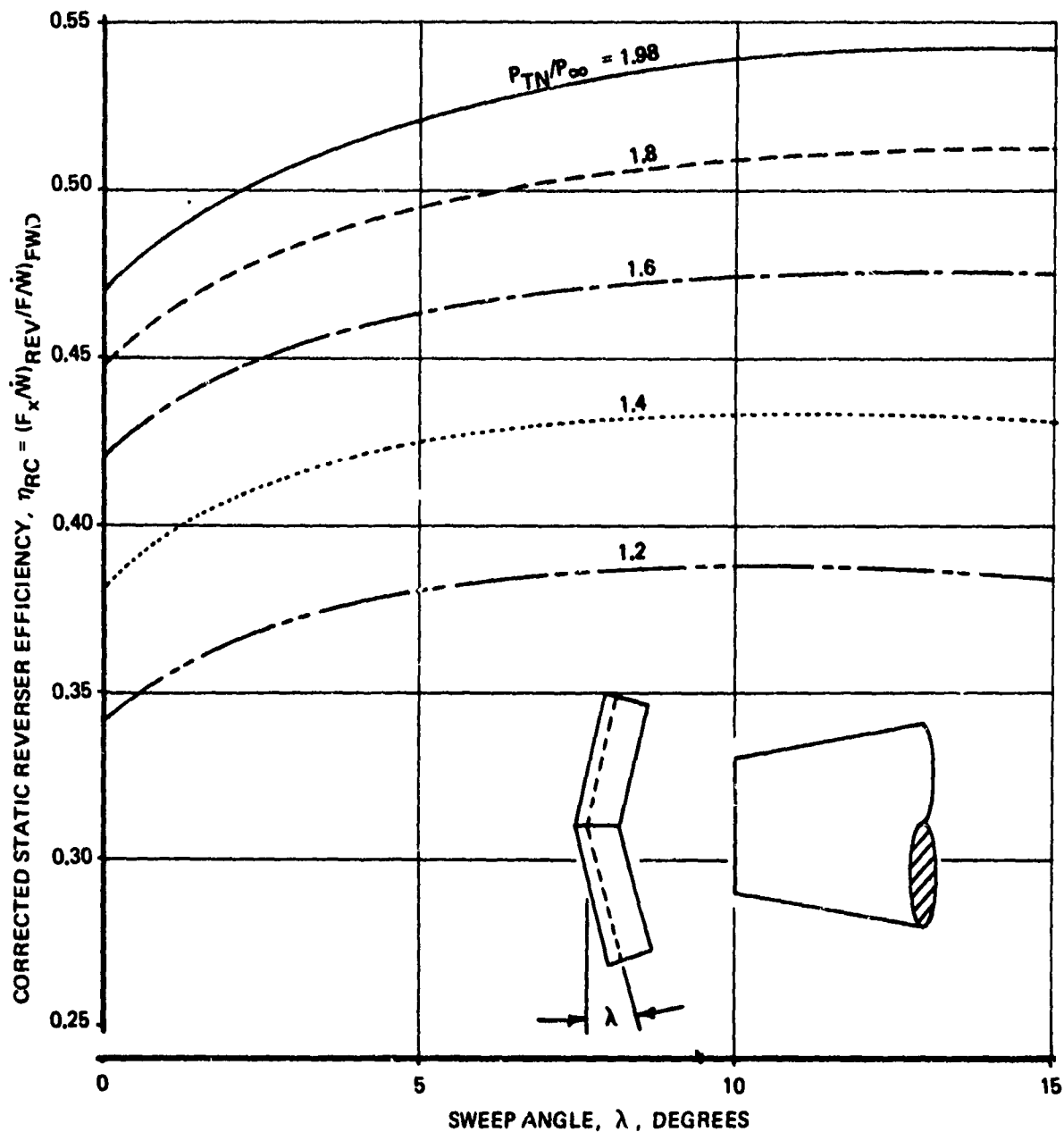


Figure 17: EFFECT OF SWEEP ANGLE ON STATIC REVERSER EFFICIENCY, CLAMSHELL TARGET THRUST REVERSER

SETBACK RATIO = $X/D = 0.94$
 DOOR LENGTH RATIO = $L/D = 1.0$
 AVERAGE LIP HEIGHT = $LH/D = 0.106$
 SWEEP ANGLE = $\lambda = 10^\circ$
 CONE ANGLE = $\alpha = 10^\circ$
 BEVEL ANGLE = $\beta = 0^\circ$
 NO SIDE FENCES

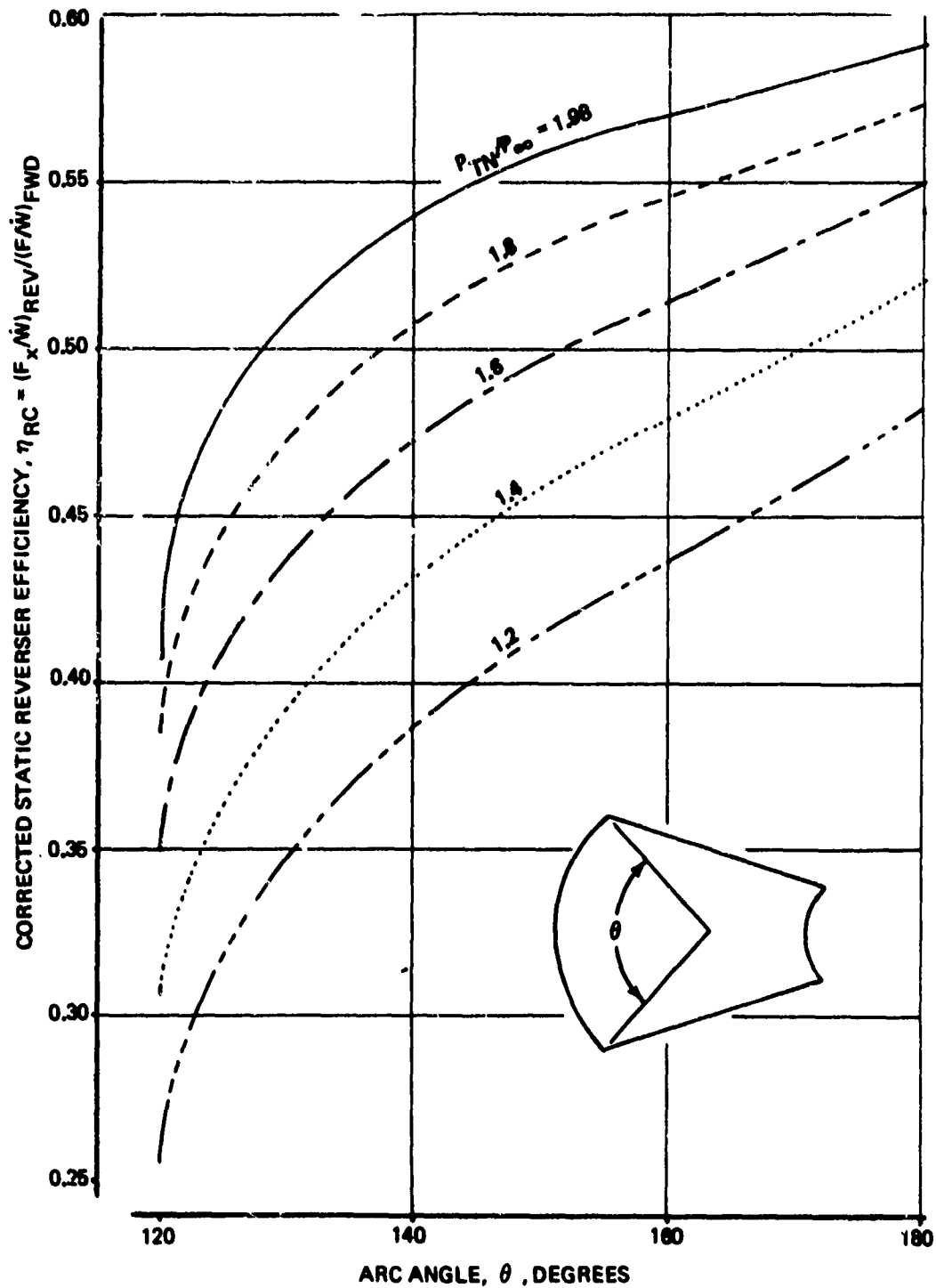


Figure 18: EFFECT OF ARC ANGLE ON STATIC REVERSER
 EFFICIENCY, CLAMSHELL TARGET THRUST
 REVERSER

SETBACK RATIO = $X/D = 0.84$
 DOOR LENGTH RATIO = $L/D = 1.0$
 AVERAGE LIP HEIGHT = $LH/D = 0.106$
 SWEEP ANGLE = $\lambda = 10^\circ$
 ARC ANGLE = $\theta = 140^\circ$
 BEVEL ANGLE = $\beta = 0^\circ$
 NO SIDE FENCES

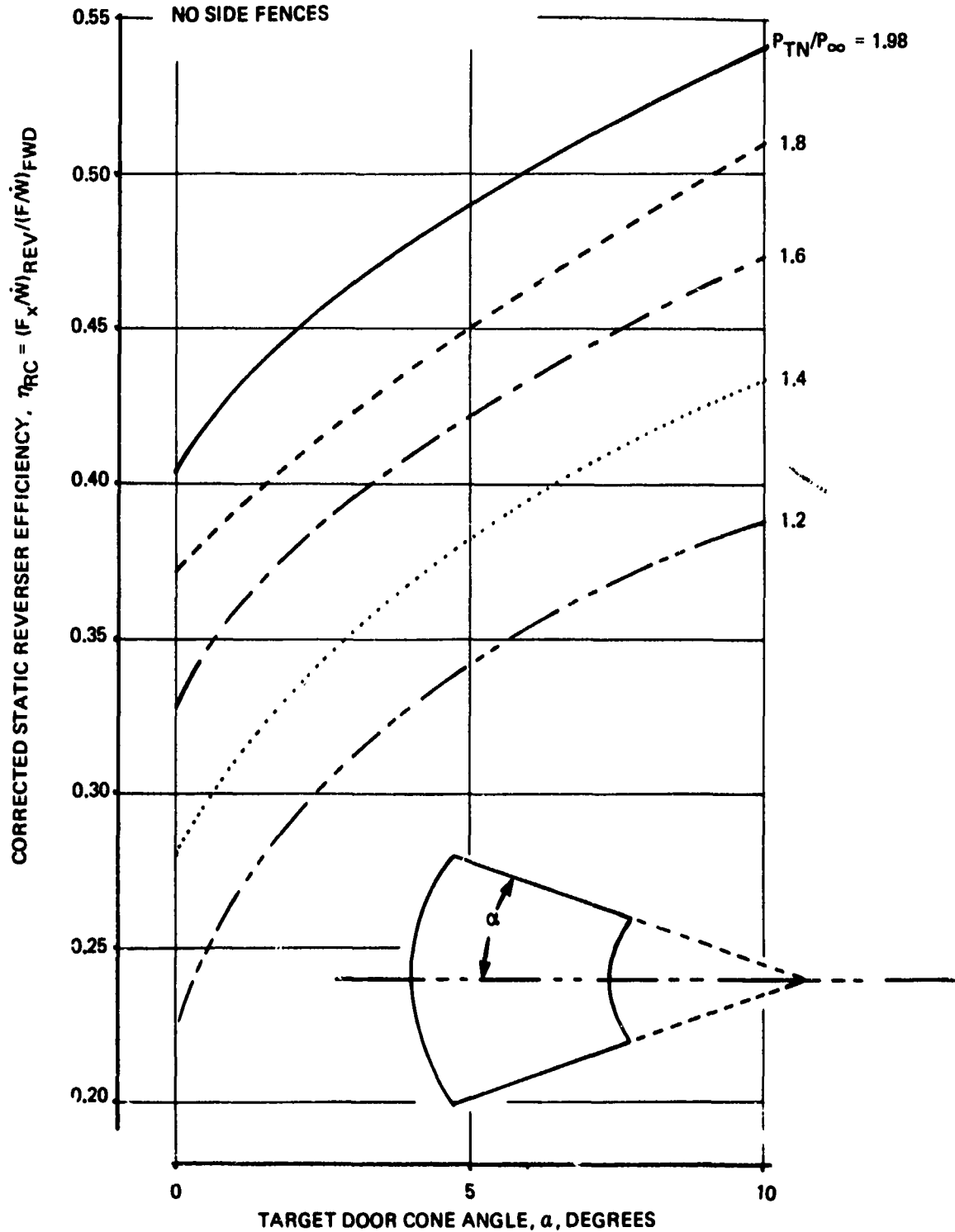


Figure 19: EFFECT OF CONE ANGLE ON STATIC THRUST
 REVERSER EFFICIENCY, CLAMSHELL TARGET
 THRUST REVERSER

SETBACK RATIO = $X/D = 0.94$
 DOOR LENGTH RATIO = $L/D = 1.0$
 AVERAGE LIP HEIGHT = $LH/D = 0.108$
 SWEEP ANGLE = $\lambda = 10^\circ$
 ARC ANGLE = $\theta = 140^\circ$
 CONE ANGLE = $\alpha = 10^\circ$
 NO SIDE FENCES

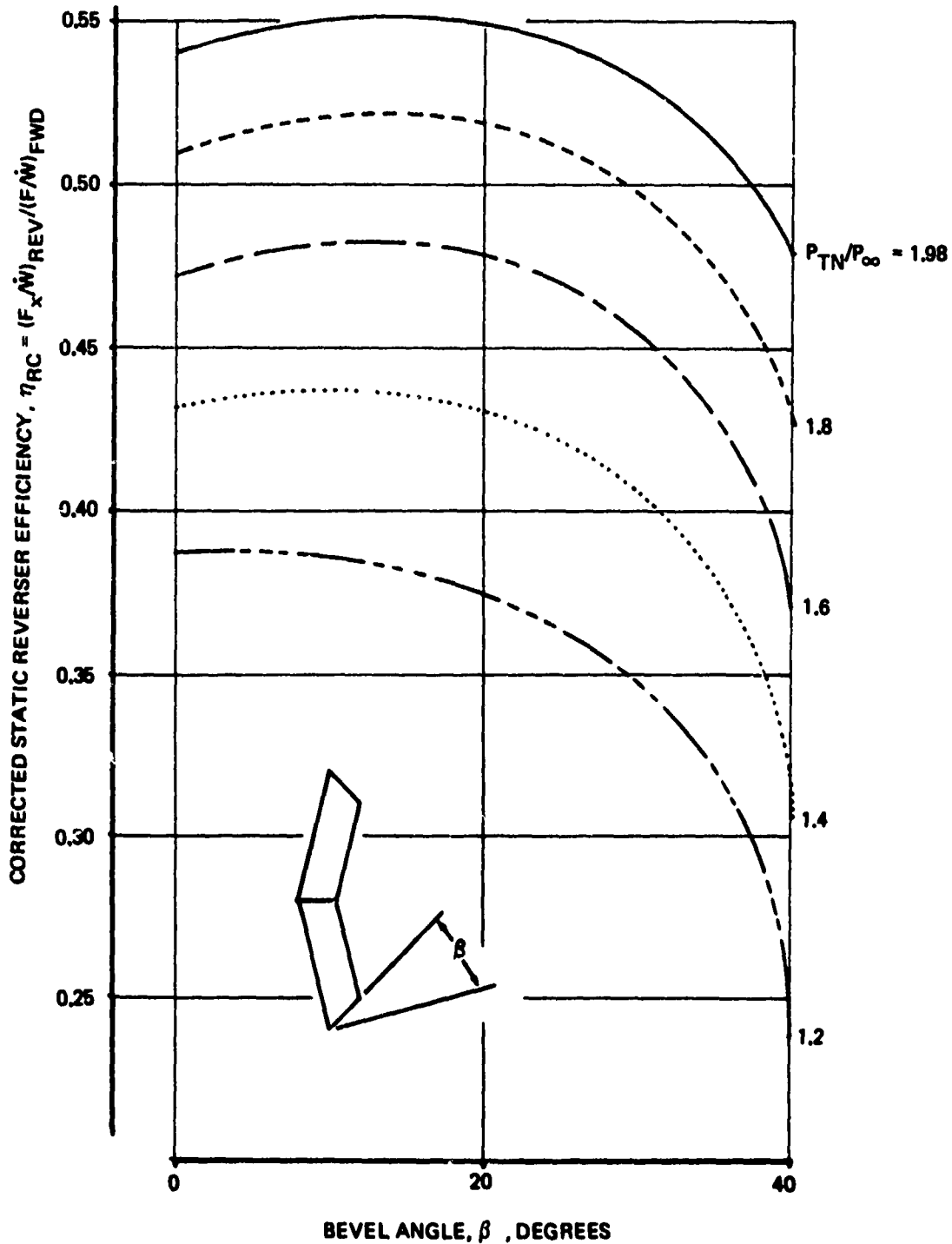


Figure 20: EFFECT OF BEVEL ANGLE ON STATIC REVERSER EFFICIENCY, CLAMSHELL TARGET THRUST REVERSER

Nozzle pressure ratio and setback distance X/D were the only variables that significantly affected airflow match.

$$\bar{I} = f\left(\frac{P_{TN}}{P_{\infty}}, \frac{X}{D}\right) \quad (16)$$

Effects of setback distance on airflow match are shown in Figure 21. The baseline corrected reverser efficiency and airflow match curves are shown in Figure 22. The procedure used to predict η_{RC} and \bar{I} for an arbitrary clamshell geometry is to assume that effects of the variables in Equation 15 are independent. This assumption is necessary because the test did not include all possible combinations of parameters. The equations for corrected reverser efficiency and airflow match then become:

$$\eta_{RC} = (\eta_{RC})_{BASELINE} + (\Delta\eta_{RC})_{X/D} + (\Delta\eta_{RC})_{L/D} + (\Delta\eta_{RC})_{LH/D} + (\Delta\eta_{RC})_{\lambda} + (\Delta\eta_{RC})_{\theta} + (\Delta\eta_{RC})_{\alpha} + (\Delta\eta_{RC})_{\beta} \quad (17)$$

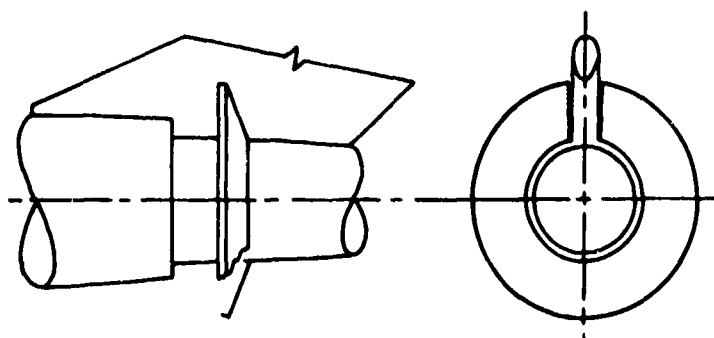
$$\bar{I} = \bar{I}_{BASELINE} + (\Delta\bar{I})_{X/D} \quad (18)$$

where the incremental terms are found by subtracting the baseline values from Figures 14 to 21, e.g.

$$(\Delta\eta_{RC})_{X/D} = (\eta_{RC})_{X/D \text{ FIG. 14}} - (\eta_{RC})_{BASELINE \text{ FIG. 22}} \quad (19)$$

Annular Target Thrust Reverser

A sketch of an annular target thrust reverser is shown below.



Several excellent data sources exist for annular reversers (Ref. 6, 7 & 3). A correlation for corrected reverser efficiency that summarizes the data sources is shown in Figure 23. The correlating parameter for η_{RC} is blockage angle minus door angle, $\phi - \theta$, as identified in Figure 23. As $\phi - \theta$ increases, η_{RC} approaches the limiting value of $\cos \theta$. The parameter

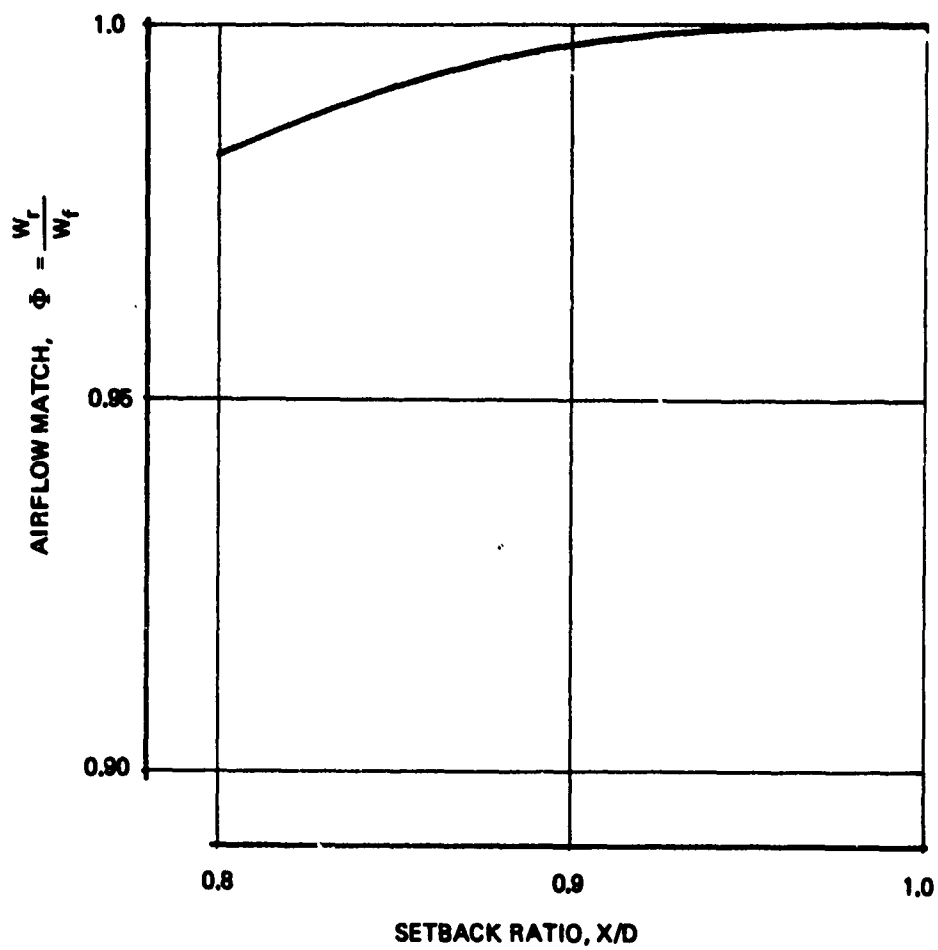
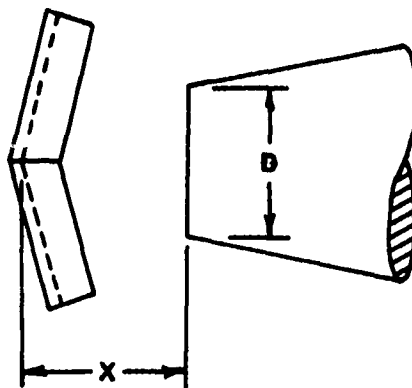
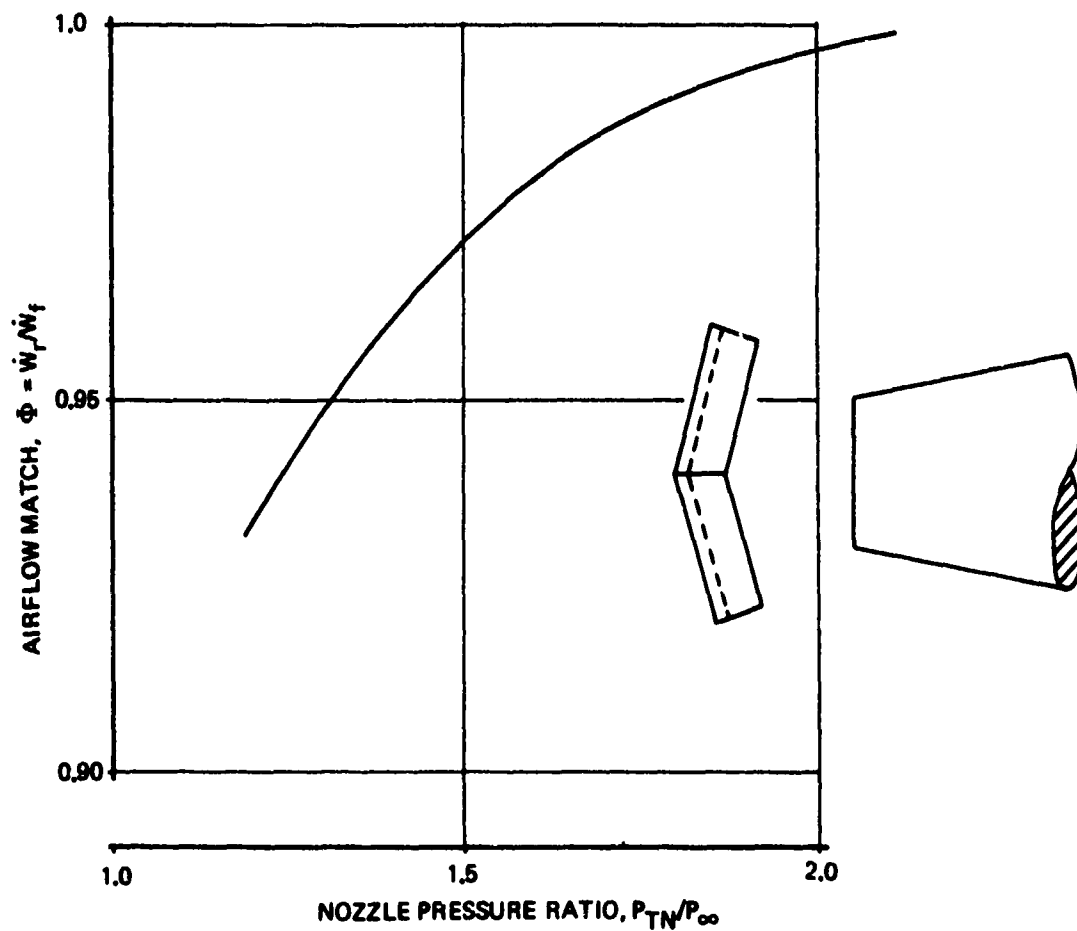
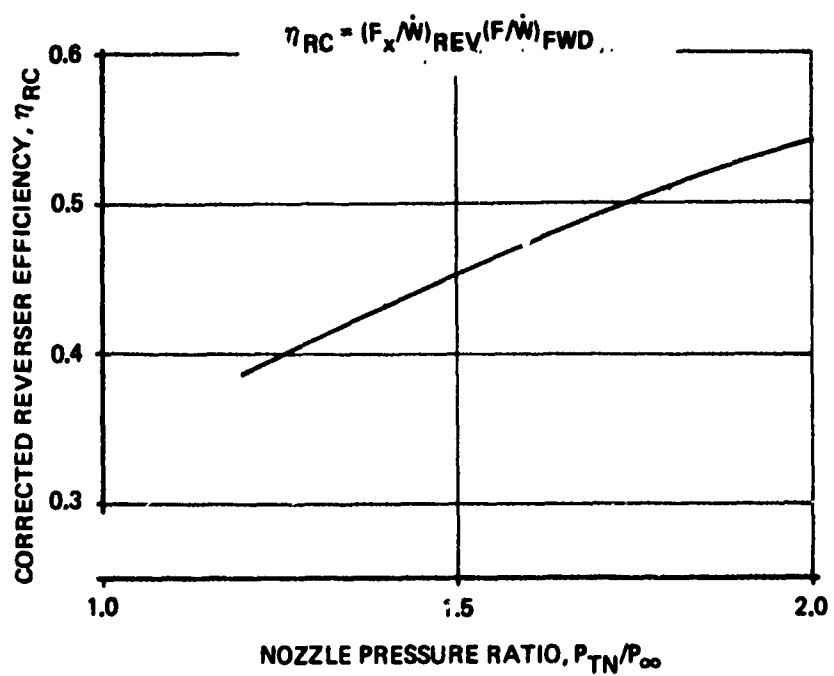


Figure 21: EFFECT OF SETBACK RATIO ON AIRFLOW MATCH, CLAMSHELL TARGET THRUST REVERSER



**Figure 22: CLAMSHELL TARGET THRUST REVERSER
BASELINE PERFORMANCE**

SYMBOL	P_{TN}/P_{∞}	θ	X/H	L/H	C/H	DATA SOURCE
—○—	1.4, 1.7	40°	1.10 → 1.77	0.7 → 1.65	0.71 → 1.22	REF 6
---□---	1.74	45°	2.21 → 4.14	2.9 → 5.23	2.03 → 2.93	REF 8
---◇---	1.74	50.3°	2.39 → 4.33	3.37 → 5.40	1.85 → 3.32	REF 8
---△---	1.74	54.8°	2.51 → 5.43	3.53 → 5.40	2.06 → 3.63	REF 8

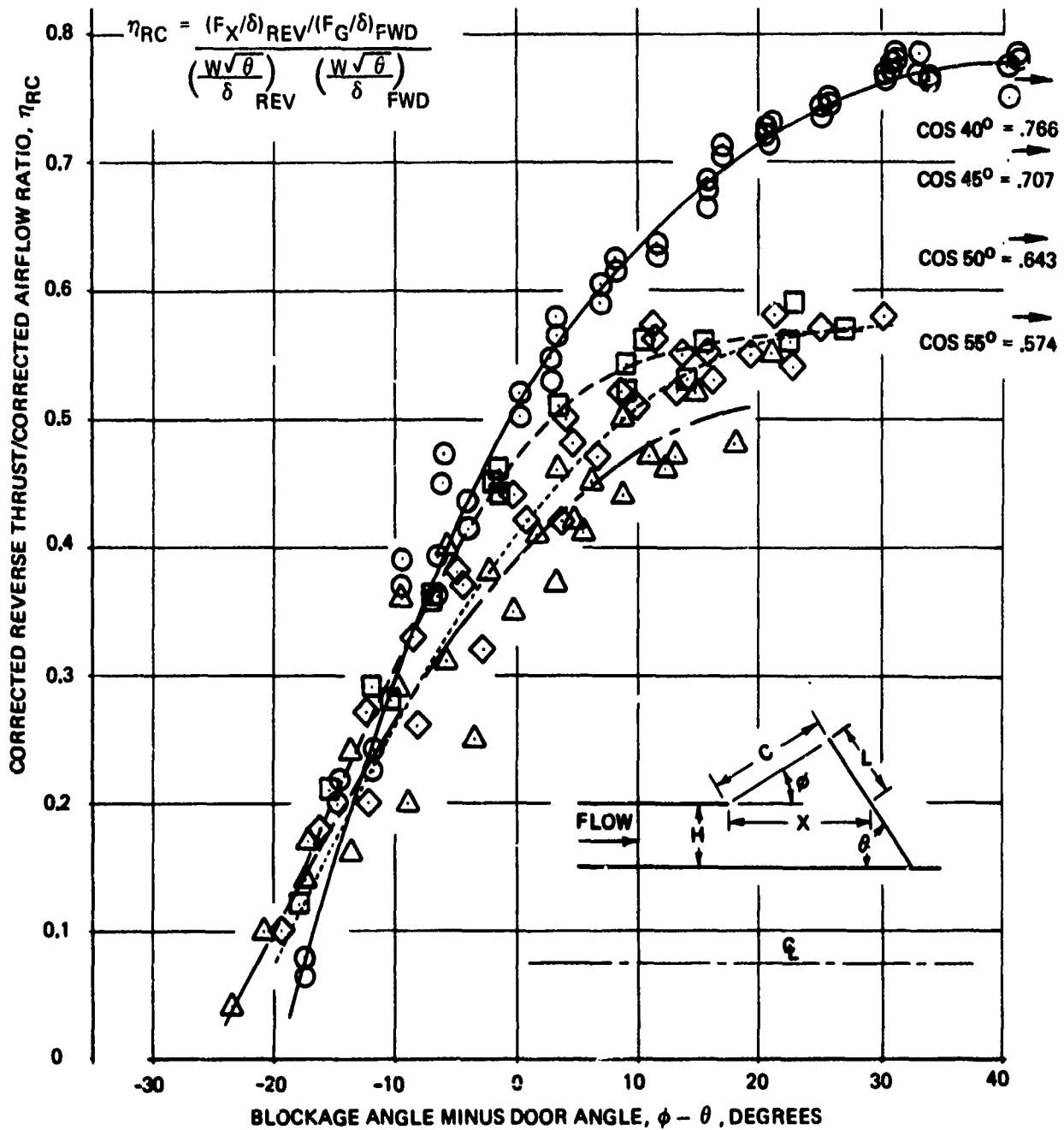


Figure 23: EFFECT OF BLOCKAGE AND DOOR ANGLE
 ON CORRECTED REVERSER EFFICIENCY
 ANNULAR TARGET THRUST REVERSER

$\phi-\theta$ was found to improve the ability to correlate annular TR data.

The airflow match data are correlated as a function of throat gap over annulus height in Figure 24. The Boeing 707 and Pratt & Whitney Aircraft data are for a postexit annular target reverser. Because the controlling area for a postexit reverser is the cruise nozzle area, the limiting value for airflow match \bar{I} equals 1.0. On the other hand, the Boeing C-5A proposal data are for a pre-exit annular blocker deflector reverser. The controlling area in the TR mode is larger than the cruise nozzle area so \bar{I} is greater than 1.0. The equation for airflow match is

$$\bar{I} = \frac{\dot{w}_r}{\dot{w}_f} = \frac{C_{Dr}}{C_{Df}} \frac{A_r}{A_f} \quad (20)$$

where \dot{w} is mass flow rate, C_D is discharge coefficient, A is exit area and subscripts r and f refer to reverser and forward thrust modes, respectively. Equation (20) was used to calculate discharge coefficient ratio from the Boeing C-5A airflow match data. The resulting data correlation curve for discharge coefficient ratio is shown in Figure 25.

Blocker Deflector Thrust Reverser

Data correlations were developed for two types of blocker deflector reversers, a blocker with cascade deflectors, and a blocker reverser with deflector doors. Cascade blocker deflector thrust reversers are used on the 707, 747, DC-10, and L-1011 airplanes. Blocker reversers with deflector doors are used on the 727 and F-11A airplanes.

The cascade blocker deflector shown in Figure 109 on page 163 was tested during the Task 1.3 supplemental static test and the results are discussed in Section 2.3. Baseline performance of the blocker reverser with deflector doors is presented in Figure 26 from Ref. 9. The effects of blocker door cone angle on reverser efficiency and airflow match are displayed in Figure 27.

2.1.3 Thrust Vectoring Nozzle Data Correlations

This section describes data correlations developed for several types of thrust vectoring nozzles. Boeing was assisted in this task by Pratt & Whitney Aircraft, who provided data for single-jet and spherical eyeball vectoring nozzles.

SYMBOL	P_{TN}/P_{∞}	θ	X/H	L/H	DATA SOURCE
●	1.7	40°	1.10 → 1.77	0.7 → 1.65	REF. 6
○	1.4	40°	1.10 → 1.77	0.7 → 1.65	REF. 6
◇	1.5	30°, 40°, 50°	1.02 → 4.09	0.89 → 2.70	REF. 8
□	1.74	45°, 50.3°, 54.8°	2.21 → 4.43	2.9 → 5.40	REF. 7

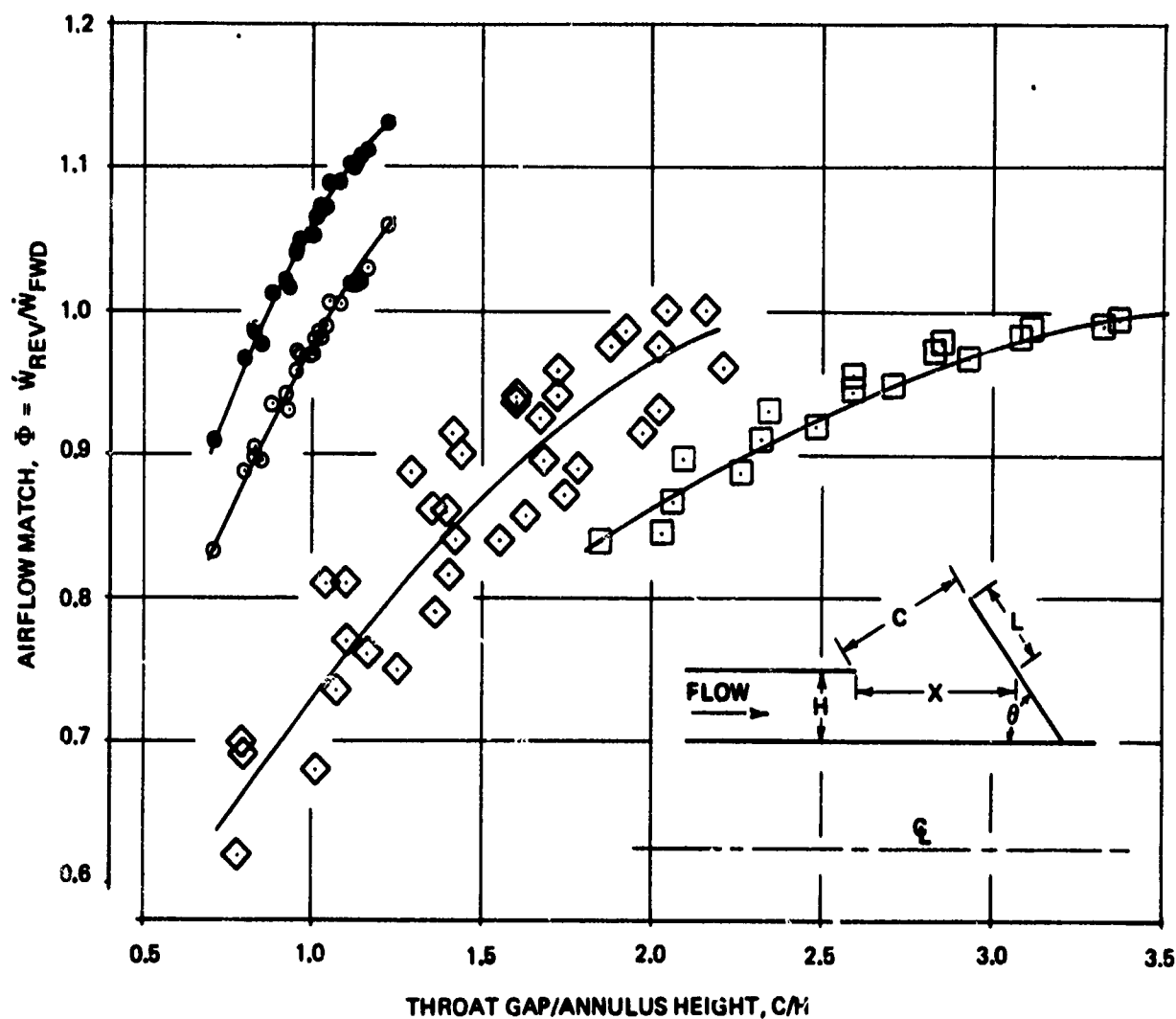


Figure 24: EFFECT OF DOOR SETBACK ON AIRFLOW MATCH ANNULAR TARGET THRUST REVERSER

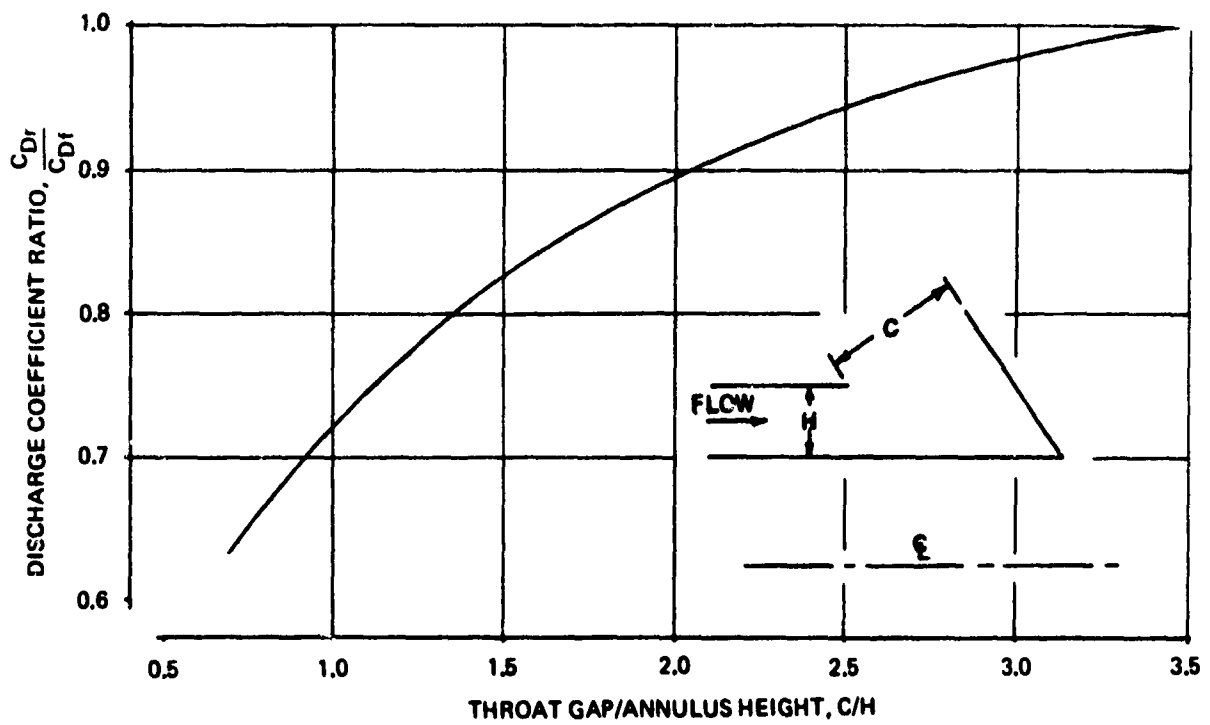


Figure 25: DISCHARGE COEFFICIENT CORRELATION
ANNULAR TARGET THRUST REVERSER

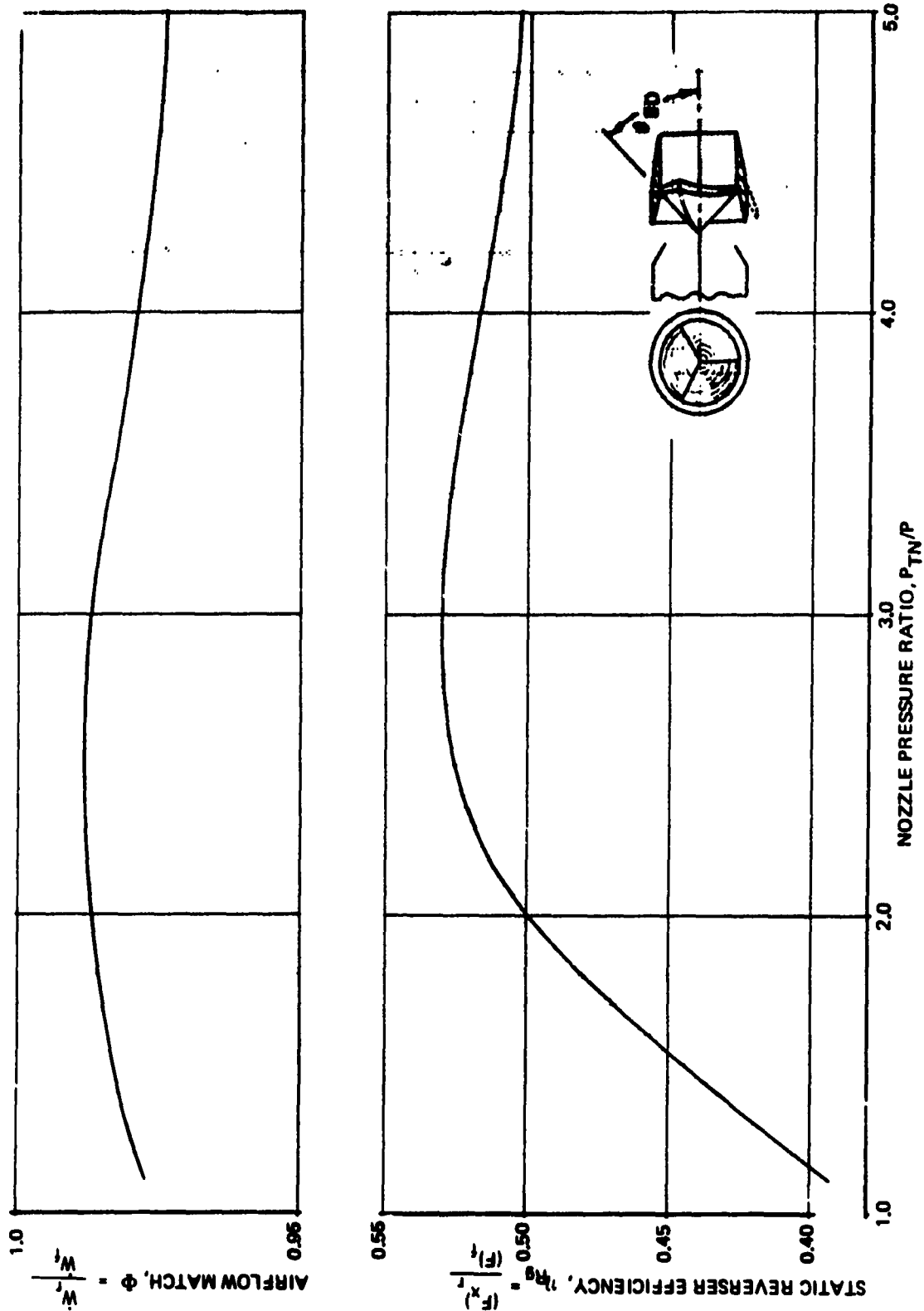


Figure 26: BASELINE PERFORMANCE FOR BLOCKER-DEFLECTOR THRUST REVERSER

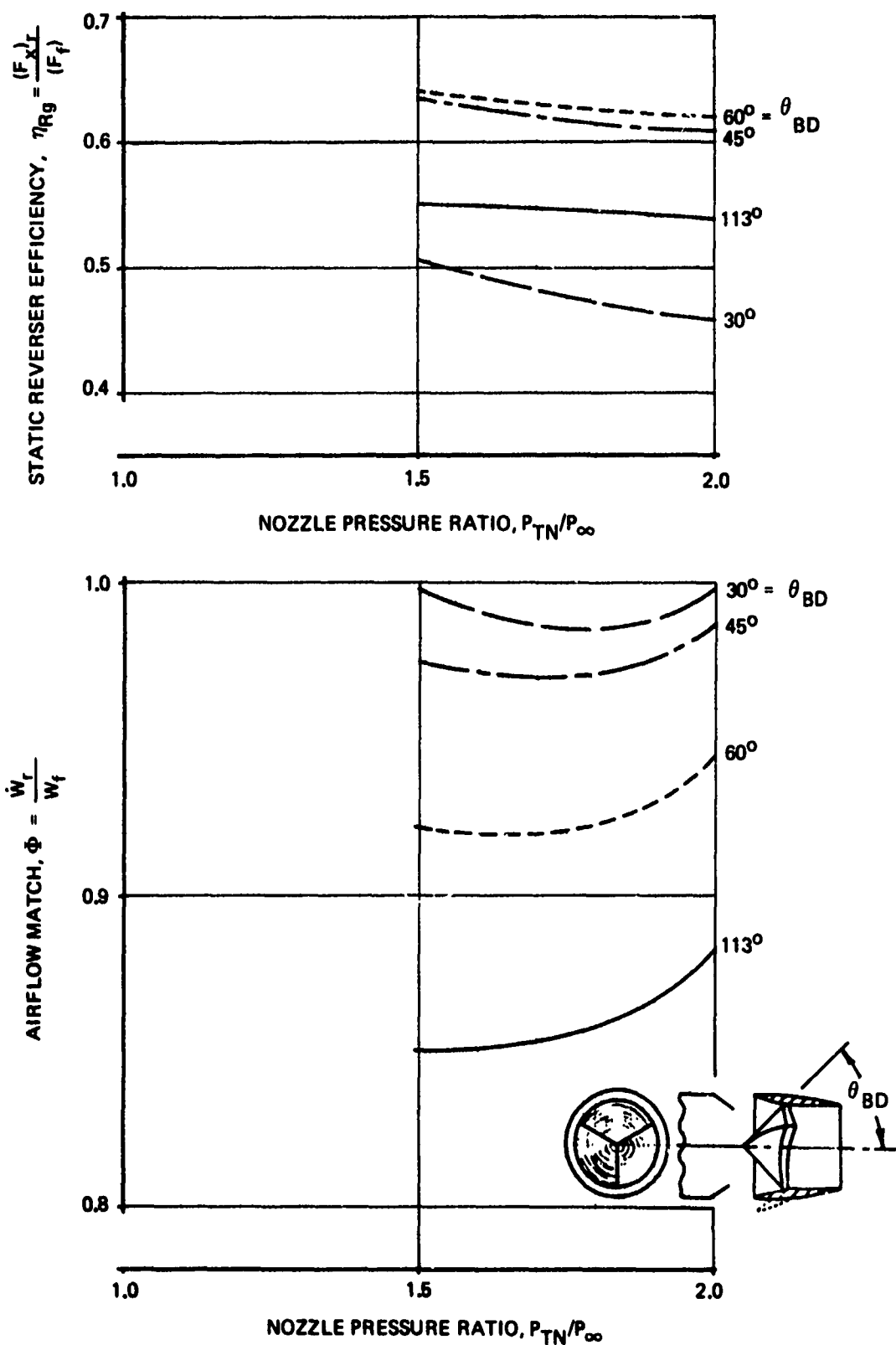
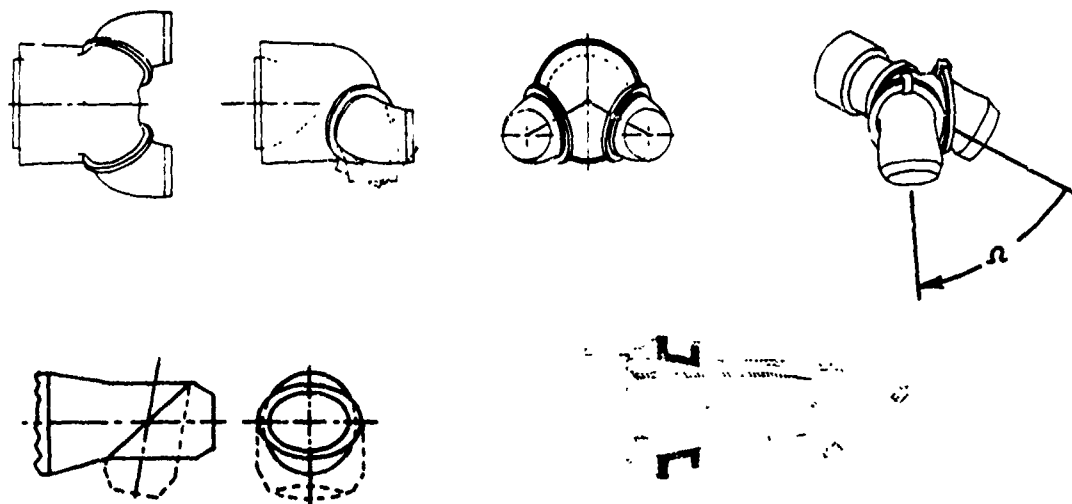


Figure 27: EFFECT OF BLOCKER DOOR CONE ANGLE ON BLOCKER-DEFLECTOR THRUST REVERSER PERFORMANCE

Single-Bearing Nozzle

Sketches of single-bearing nozzles are shown below.



Considerable geometric flexibility is possible by varying the nozzle offset, bearing plane angle, and bearing duct angle. Single-bearing nozzles frequently are designed in symmetric pairs to minimize asymmetric engine side loads. Theoretical thrust components for a single-bearing nozzle or half of a dual swiveling single-bearing nozzle are given by

$$F_x/F_r = 1 - \sin^2 \beta (1 - \cos \phi) \quad (21)$$

$$F_y/F_r = \sin \alpha \sin \beta \cos \beta (1 - \cos \phi) - \cos \alpha \sin \beta \sin \phi \quad (22)$$

$$F_z/F_r = -\cos \alpha \sin \beta \cos \beta (1 - \cos \phi) - \sin \alpha \sin \beta \sin \phi \quad (23)$$

where the resultant force F_r is given by

$$F_r = (F_x^2 + F_y^2 + F_z^2)^{1/2} \quad (24)$$

The (x, y, z) coordinate system and angles α , β , and ϕ are defined in Figure 28. Theoretical thrust components for a nozzle with bearing plane and duct angles of 45 and 56 degrees are given in Figure 29. The theoretical flow turning angle is given by

$$\Omega = \cos^{-1} \left(\frac{F_x}{F_r} \right) \quad (25)$$

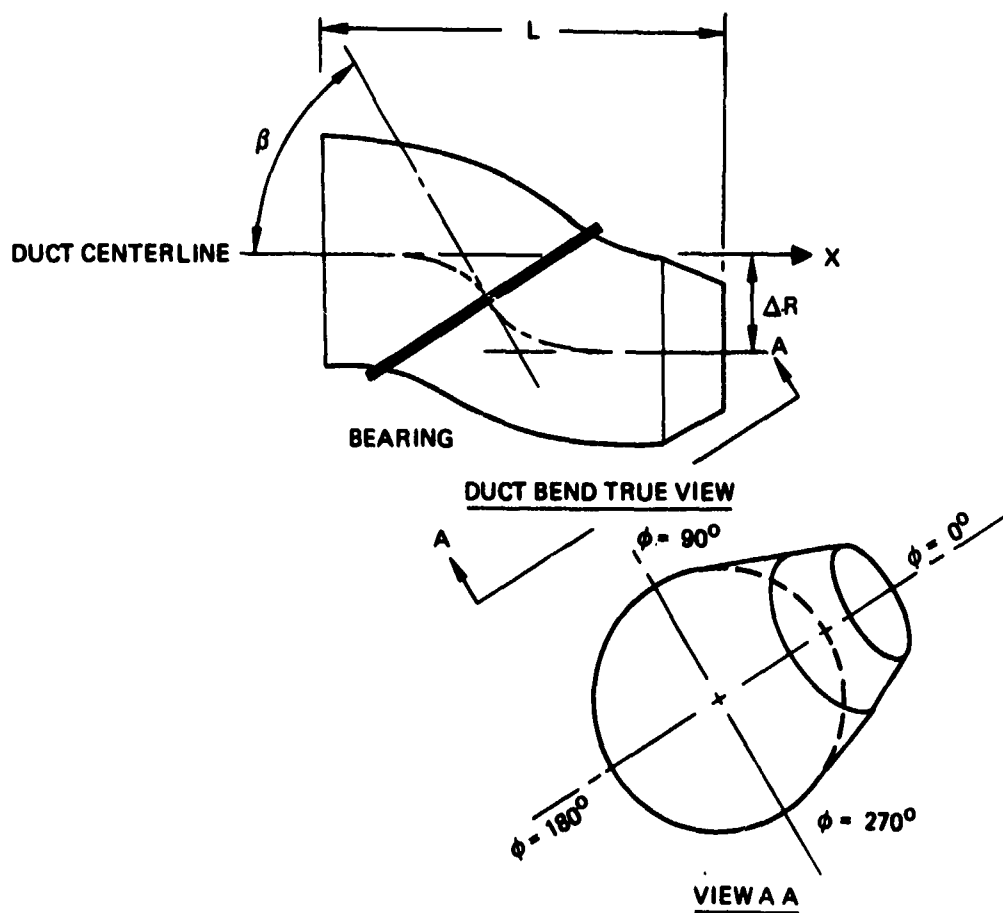
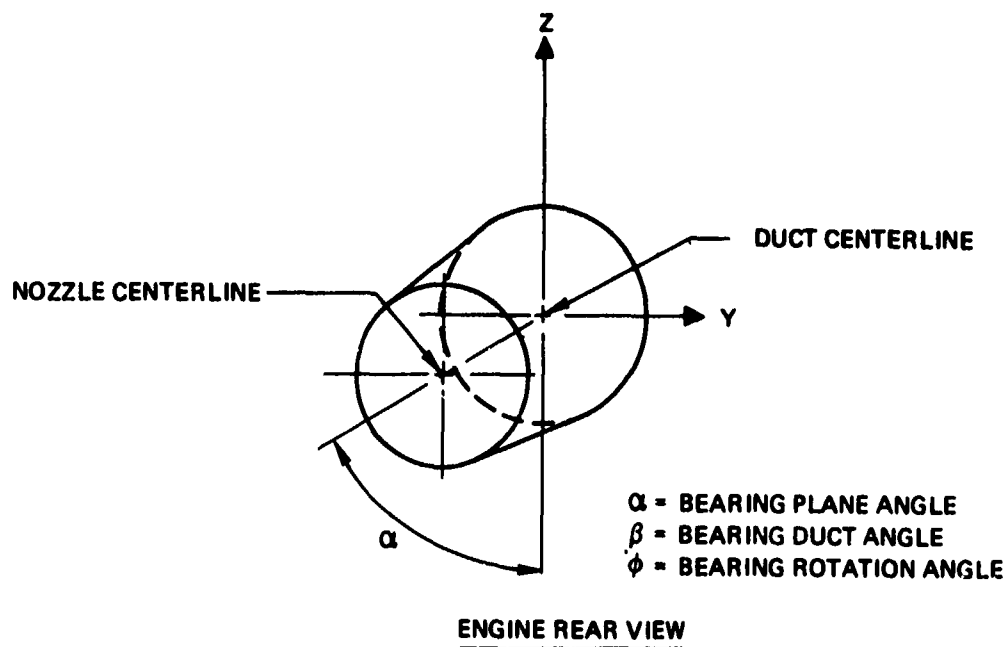


Figure 28: SINGLE BEARING NOZZLE NOMENCLATURE

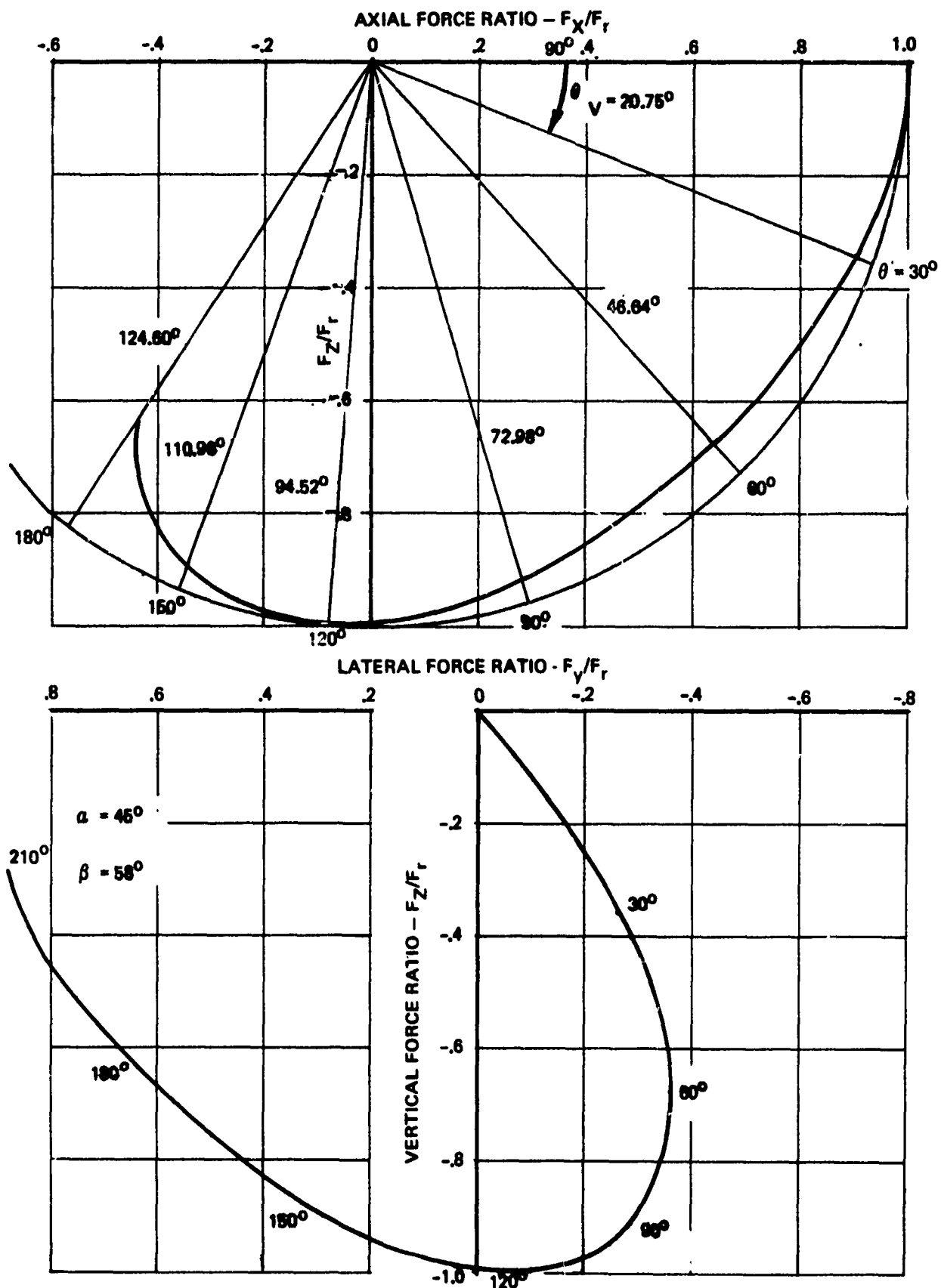


Figure 29: SINGLE BEARING SWIVEL NOZZLE THRUST COMPONENT RELATIONSHIPS

Vector angle is given by the following equation

$$\sigma = \tan^{-1} \left(\frac{F_{\theta}/F_r}{F_x/F_r} \right) \quad (26)$$

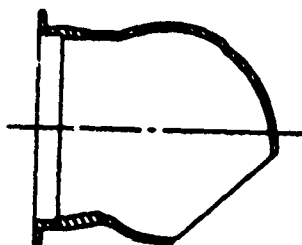
Several data sources exist for single-bearing nozzle performance (Ref. 8, 10, and 11). As shown in Figure 30, the various data sources agree fairly well considering the geometric differences between test configurations. Consequently, data supplied by Pratt & Whitney Aircraft was selected for use in the Internal Performance Module.

Three-Bearing Nozzle

Data measured during the Task 1.3 supplemental static tests are used to predict three-bearing nozzle performance. The data are discussed in Section 2.3.

Spherical Eyeball Nozzle

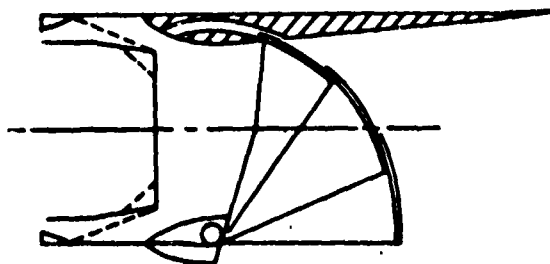
A sketch of a spherical eyeball nozzle is shown below.



Velocity and discharge coefficient performance is shown in Figure 31 from Ref. 8 and 11.

Lobstertail Nozzle

A lobstertail (also known as aft hood deflector) sketch is shown below.



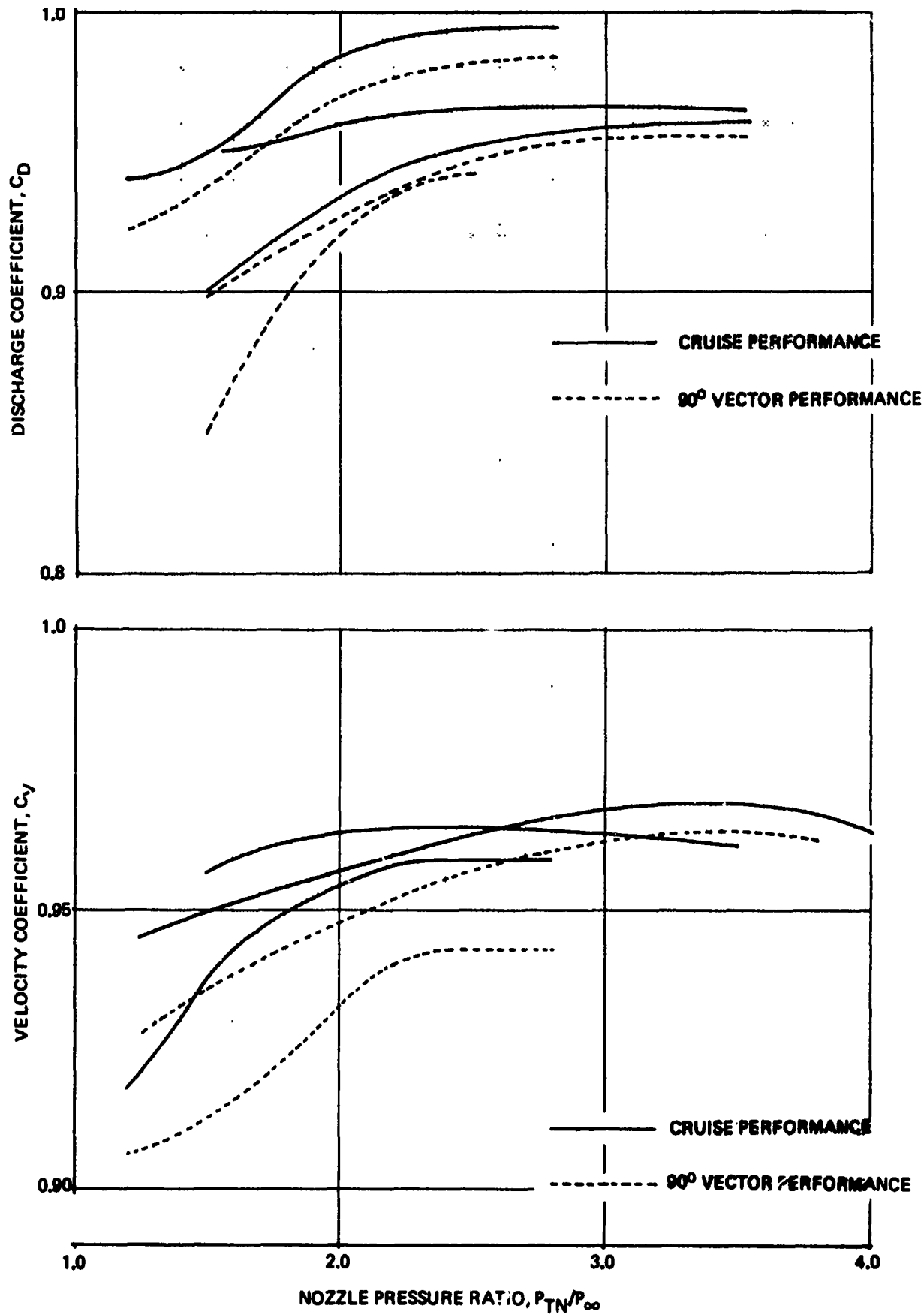


Figure 30: SINGLE BEARING NOZZLE PERFORMANCE

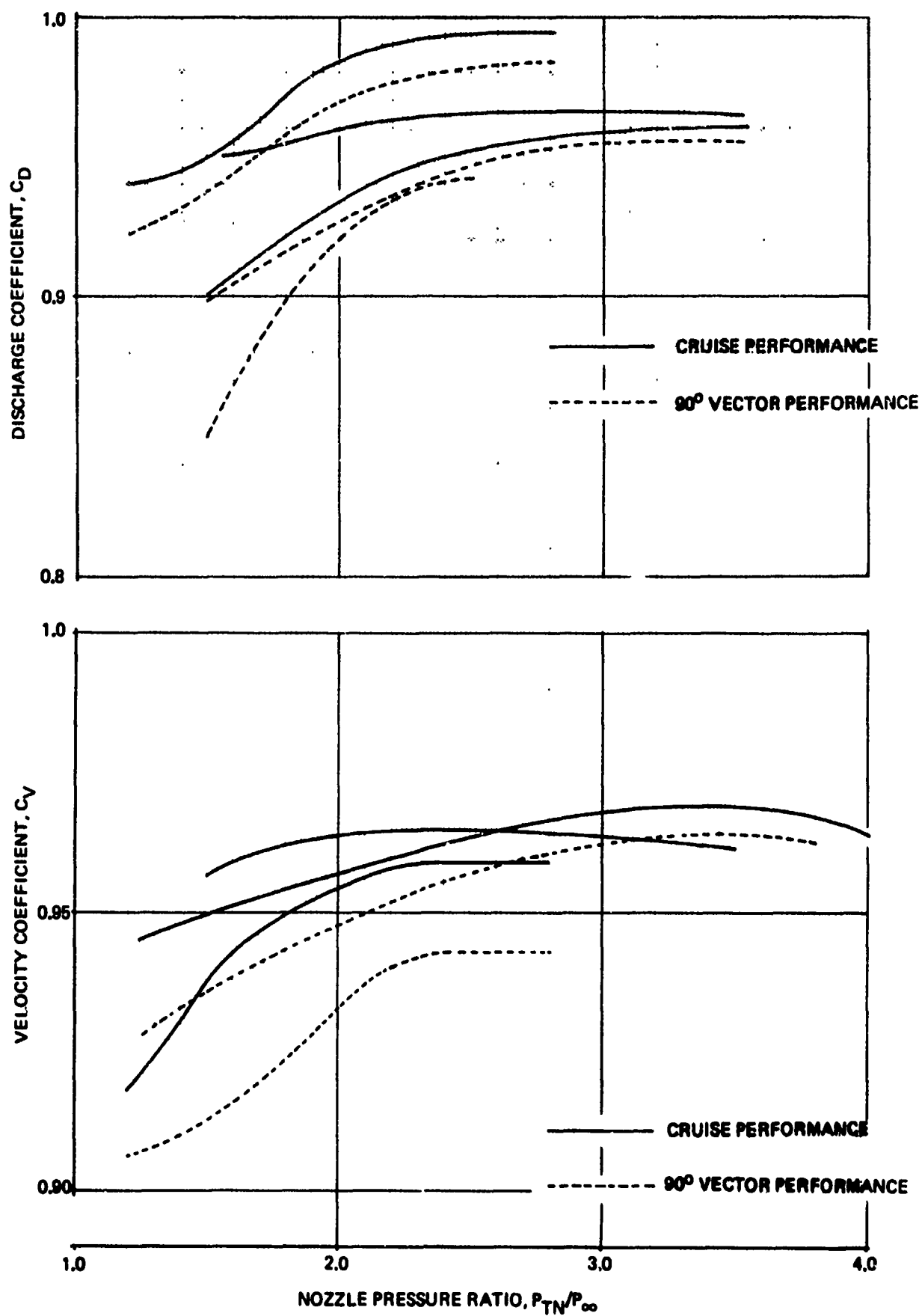


Figure 30: SINGLE BEARING NOZZLE PERFORMANCE

DATA: REF 8 AND 11

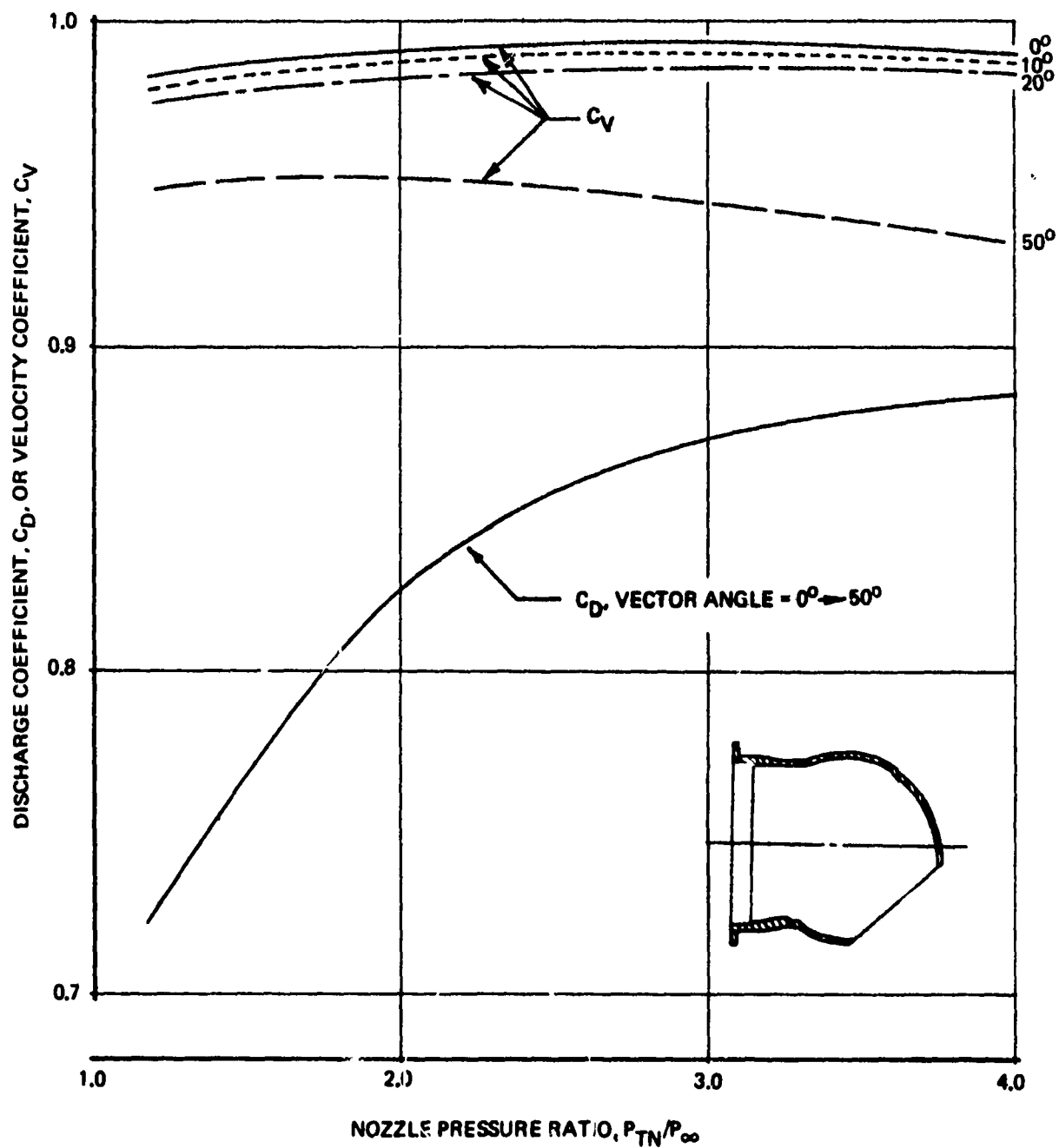
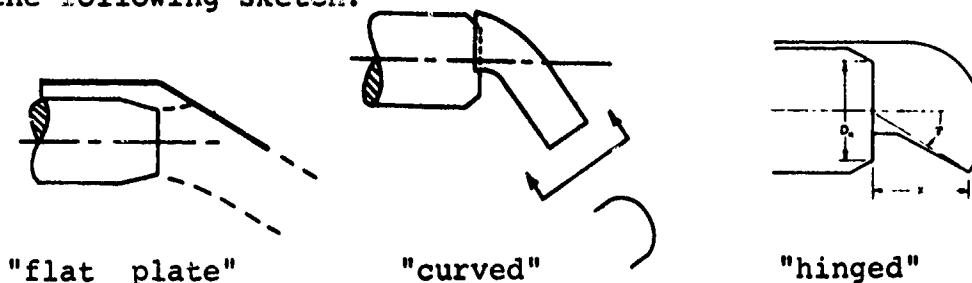


Figure 31: SPHERICAL EYEBALL NOZZLE PERFORMANCE

Velocity and discharge coefficient performance for 95-degree vector angle is shown in Figure 32 from Ref. 8. Effects of vector angle and nozzle pressure ratio on C_V and C_D are given in Figure 33. The cruise nozzle C_V and C_D are estimated to be 0.995 and 0.98, respectively at choked conditions. Bragg's theoretical discharge coefficient curves are used for C_D at intermediate vector angles.

External Deflector Nozzle

External deflector nozzles employ a flat plate or curved surface downstream of the nozzle exit to deflect the flow, as depicted in the following sketch.



Variables include nozzle pressure ratio, deflection angle Θ , setback ratio X/D , and door length ratio L/D . The effect of deflection angle on C_V and choked C_D for flat plate and curved deflectors is shown in Figure 34 for nozzle pressure ratio $P_{TN}/P_\infty = 2.0$. Choked discharge coefficient is used with Bragg's theoretical curves to give C_D at subcritical pressure ratios. The effect of pressure ratio on C_V at 70° deflection angle is shown in Figure 35.

Existing data were found inadequate to predict effects of setback and door length ratio. Theoretical results showing the effect of door length ratio on deflection angle are shown in Figure 36 from Ref. 13. Theoretical contraction ratios for mitre bends (Ref. 14) were used to calculate the effect of setback ratio on nozzle airflow match as shown in Figure 37. The theory predicts a lower airflow match than indicated by test data, probably due to spillage around the sides of the plate for the test model. Spillage is not possible for the two-dimensional, incompressible potential flow model.

During Part 1C of this program, a hinged external deflector was tested statically to determine its performance both as a thrust reverser and as a vectoring nozzle. Data correlations were developed showing the effects of setback ratio on airflow match and vectoring efficiency. The test results and data correlations are discussed in Volume II.

DATA: REF 8

$\theta = 95^\circ$

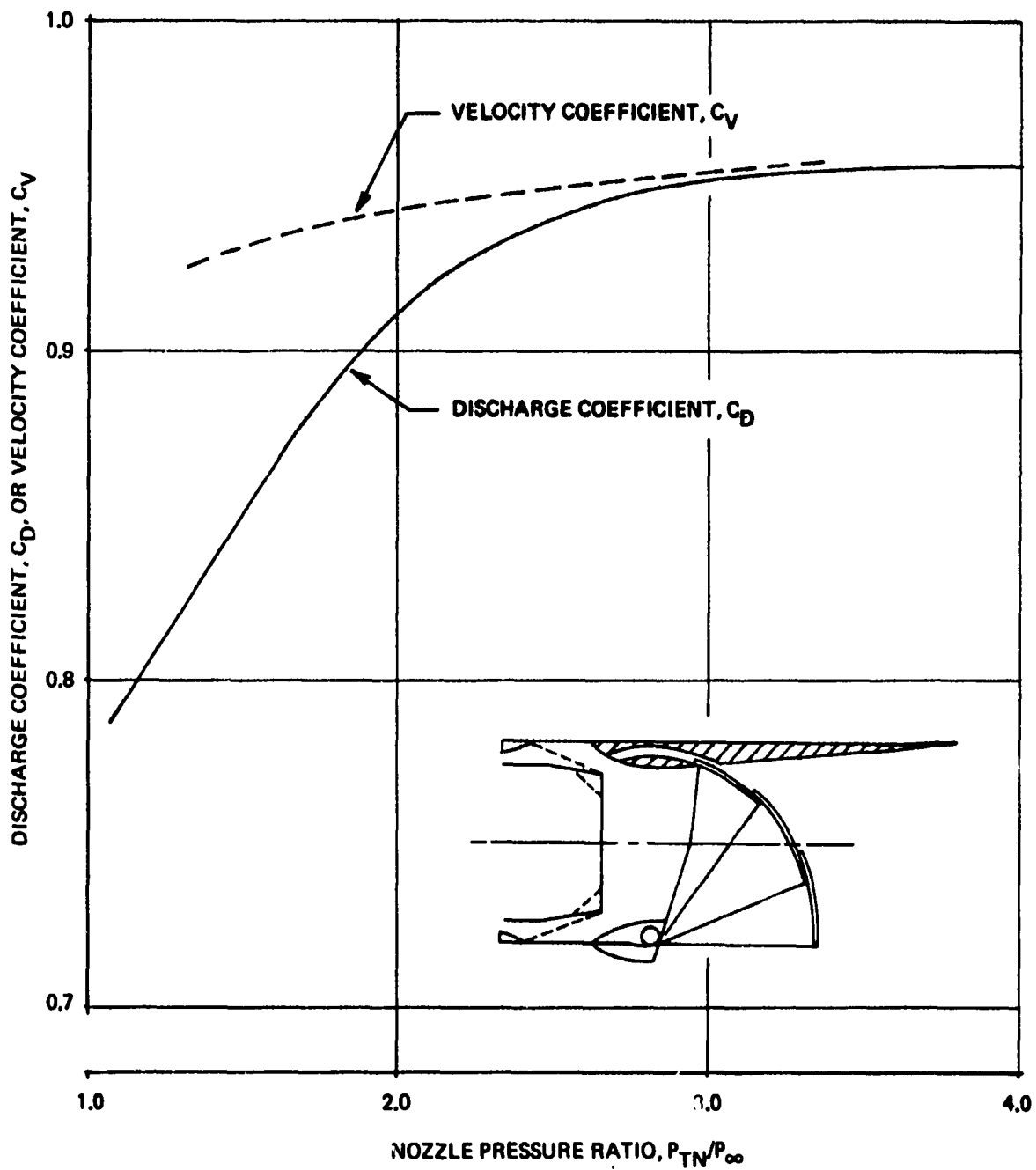


Figure 32: LOBSTERTAIL NOZZLE PERFORMANCE FOR 95 DEGREE VECTOR ANGLE

DATA: REF 8

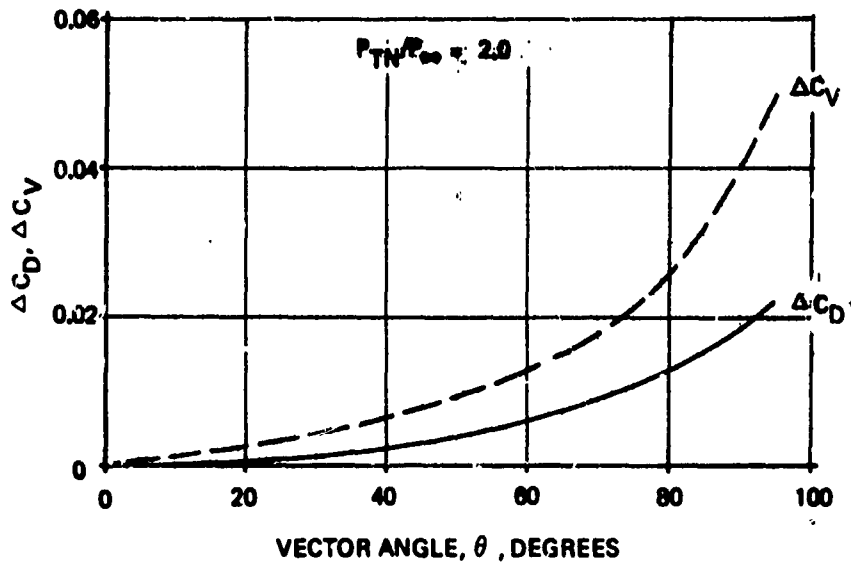
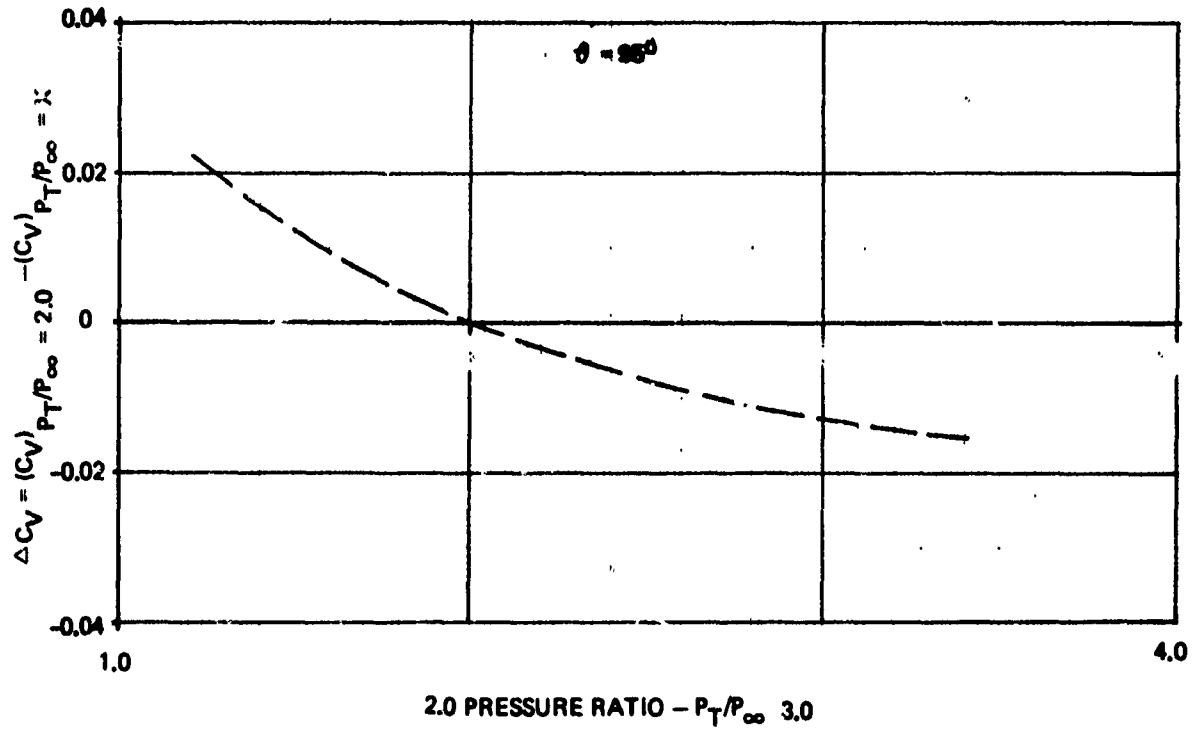


Figure 33: EFFECT OF VECTOR ANGLE AND NOZZLE PRESSURE RATIO ON LOBSTERTAIL NOZZLE PERFORMANCE

DATA: REF 12

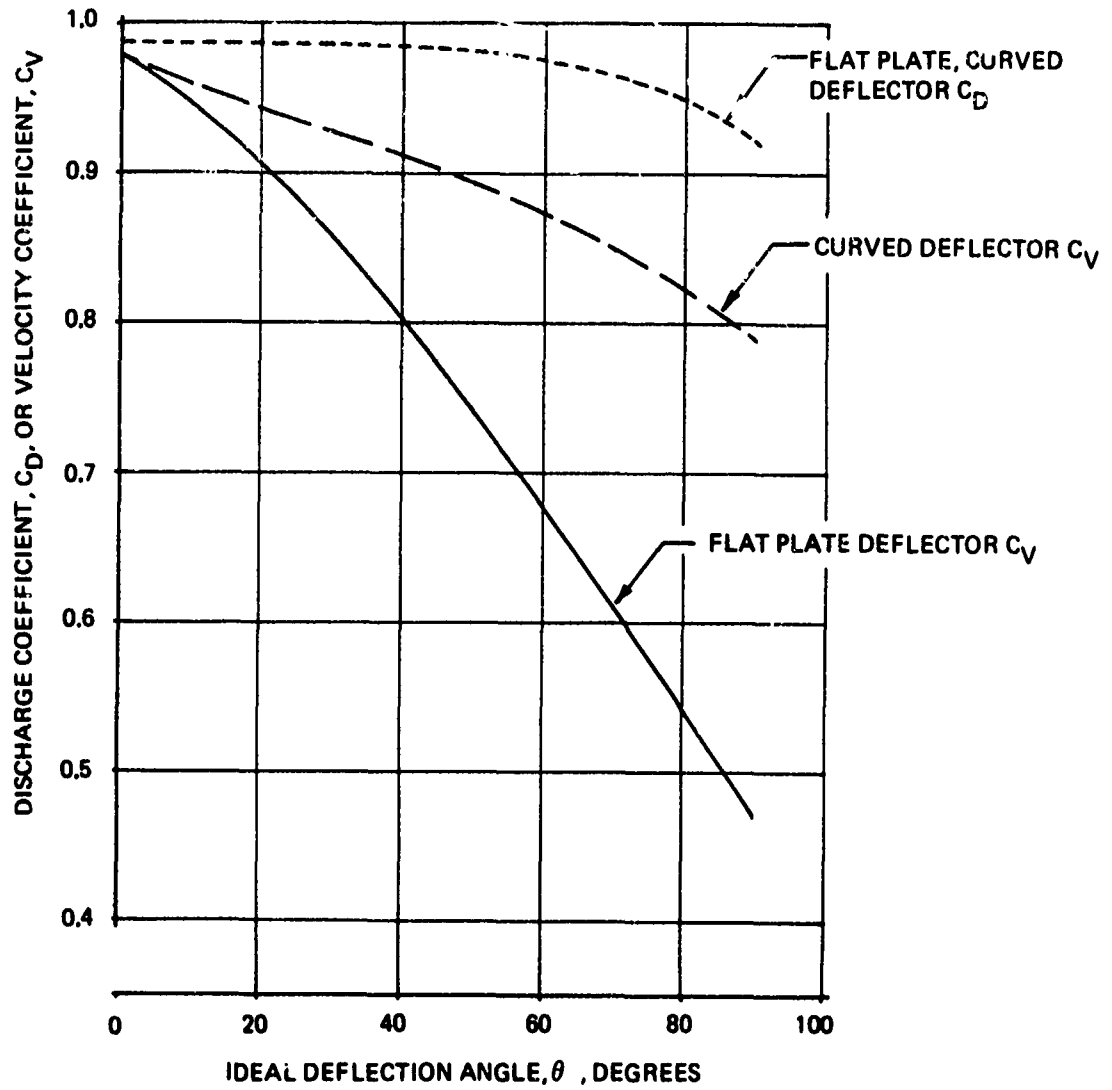


Figure 34: EFFECT OF DEFLECTION ANGLE ON FLAT PLATE AND CURVED DEFLECTOR PERFORMANCE

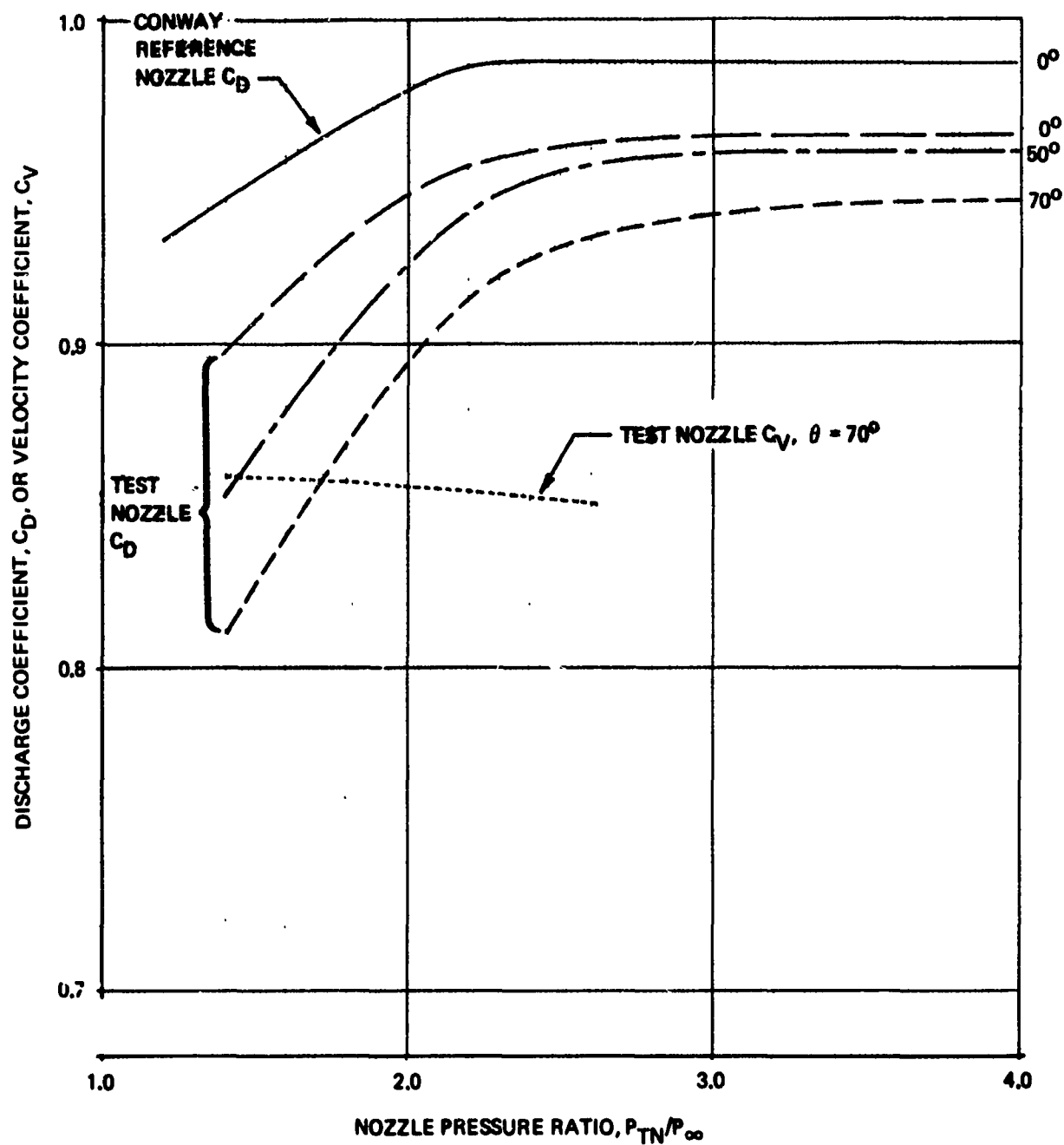


Figure 35: EFFECT OF NOZZLE PRESSURE RATIO AND DEFLECTION ANGLE ON CURVED DEFLECTOR PERFORMANCE

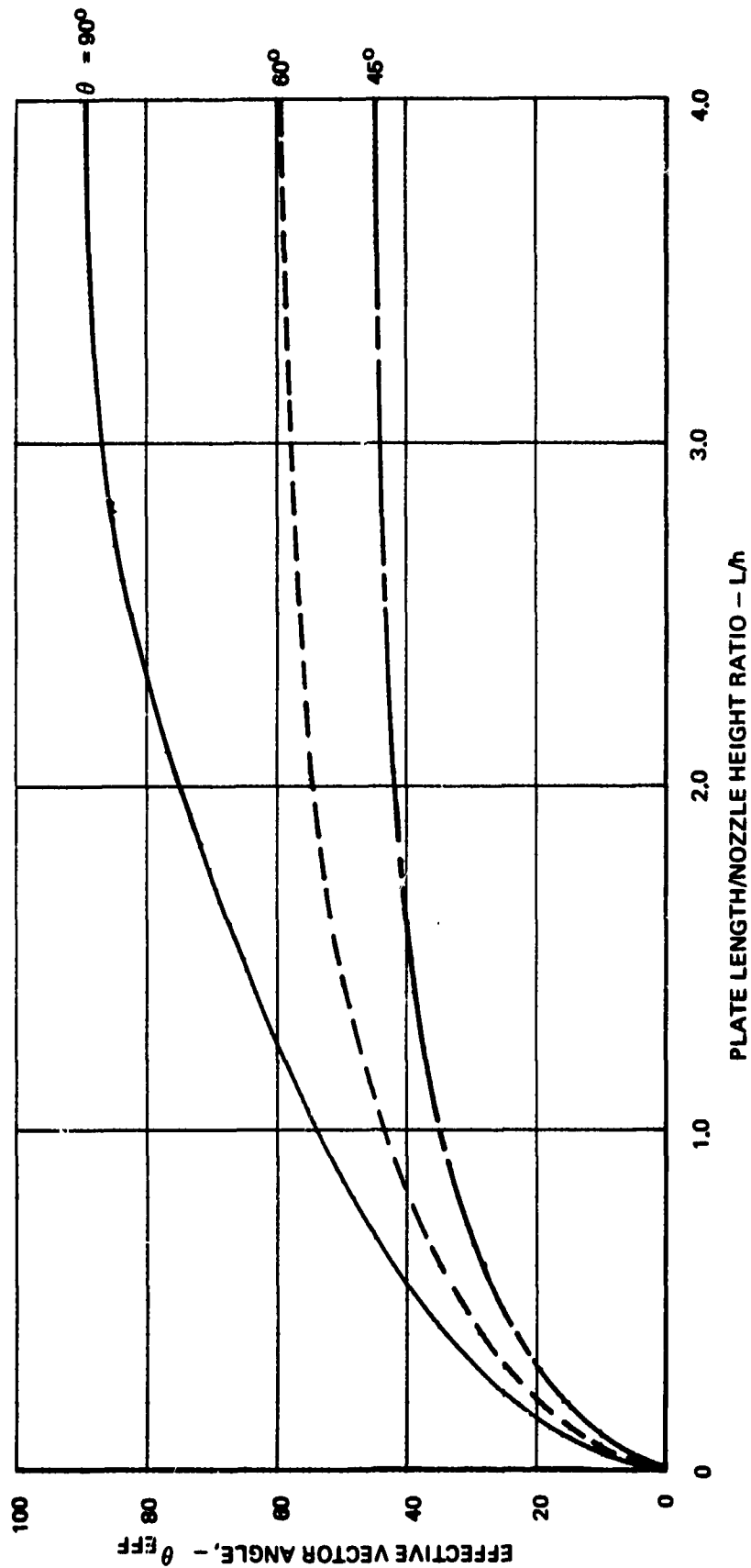
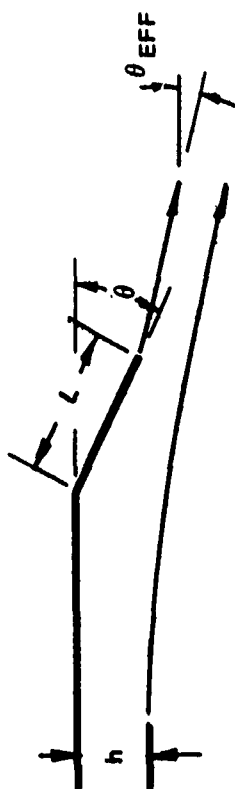


Figure 36: EFFECT OF FLAT PLATE LENGTH ON JET DEFLECTION ANGLE

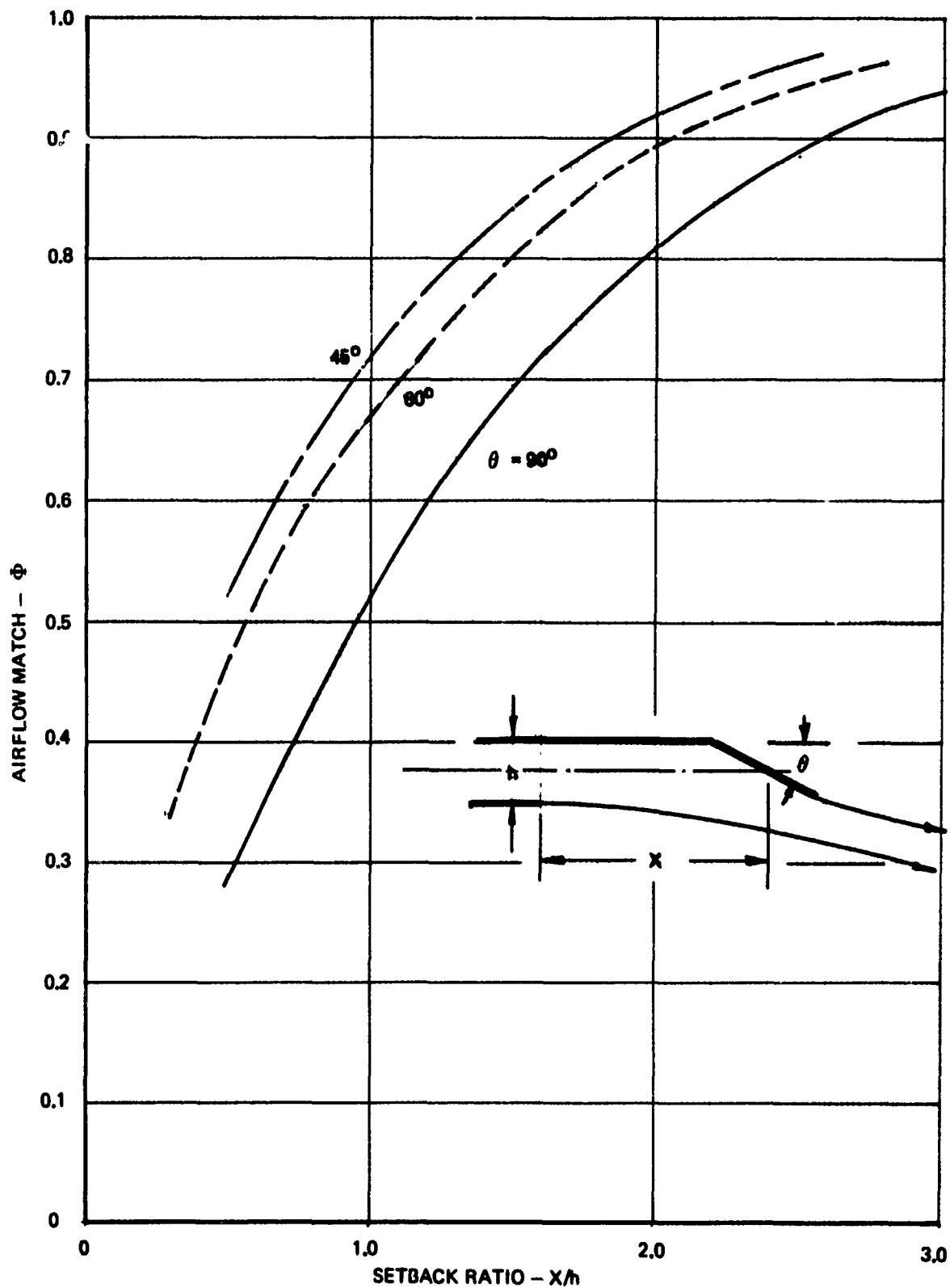


Figure 37: MITRE BEND DATA, CONTRACTION COEFFICIENT VS SETBACK DISTANCE

2.1.4 Cascade Lattice Loss Correlation

Correlations were employed to predict losses across TR or TV cascade lattices in terms of velocity and discharge coefficients. The prediction method employs pressure loss data of Ainley and Mathieson (Ref. 15) and a momentum thickness correlation developed by Stewart (Ref. 16). Ainley and Mathieson's data are used to obtain total pressure loss, exit Mach number and exit flow angle. The entrance and exit flow properties are used to calculate reaction across the blade row. Reaction is used in Stewart's correlation for trailing edge momentum thickness. Velocity and discharge coefficients are readily determined from boundary layer momentum and displacement thicknesses.

A commonly used system for defining the geometry of a blade row and the flow angles relative to a blade row is illustrated in Figure 38. Flow inlet angle α_1 is a required input for the analysis. For thrust reverser lattices, α_1 may vary from 0 degrees to 90 degrees along the blade row. Consequently, a logical range of values should be used when analyzing a particular design. Also, note that the values of flow outlet angle α_2 are numerically negative in Figure 38. For thrust reverser lattices, discharge angle θ_r is related to α_2 by the following equation.

$$\theta_r = 90^\circ + \alpha_2 \quad (27)$$

A family of profile loss curves are shown in Figure 39 for reaction blades at low Mach number ($M < 0.5$), high Reynolds number ($Re = 2 \times 10^5$), and zero incidence. Profile losses are presented in terms of pressure loss coefficient, Y_p .

$$Y_p = \frac{\text{loss of total pressure}}{\left[\begin{array}{c} \text{total pressure} \\ \text{at blade outlet} \end{array} \right] - \left[\begin{array}{c} \text{static pressure} \\ \text{at blade outlet} \end{array} \right]} \quad (28)$$

A family of curves for profile losses of impulse blades is shown in Figure 40. Profile losses of blades intermediate between reaction and impulse blades are interpolated by the following equation:

$$Y_p = \left(\frac{t/c}{0.2} \right) \left\{ Y_p(\beta_1=0) + \left(\frac{\beta_1}{\alpha_2} \right)^2 \left[Y_p(\beta_1=-\alpha_2) - Y_p(\beta_1=0) \right] \right\} \quad (29)$$

In order to find the variation of profile loss with incidence angle, it is necessary to find the stalling incidence (i_s), defined as the incidence at which the profile loss is twice the minimum loss. The variation of stalling incidence and flow outlet angle with pitch to chord ratio is shown in Figure 41. The effects of blade inlet angle and flow outlet angle on stalling incidence are shown in Figure 42. The stalling incidence found from Figures 41 and 42 is used to find the relative profile loss

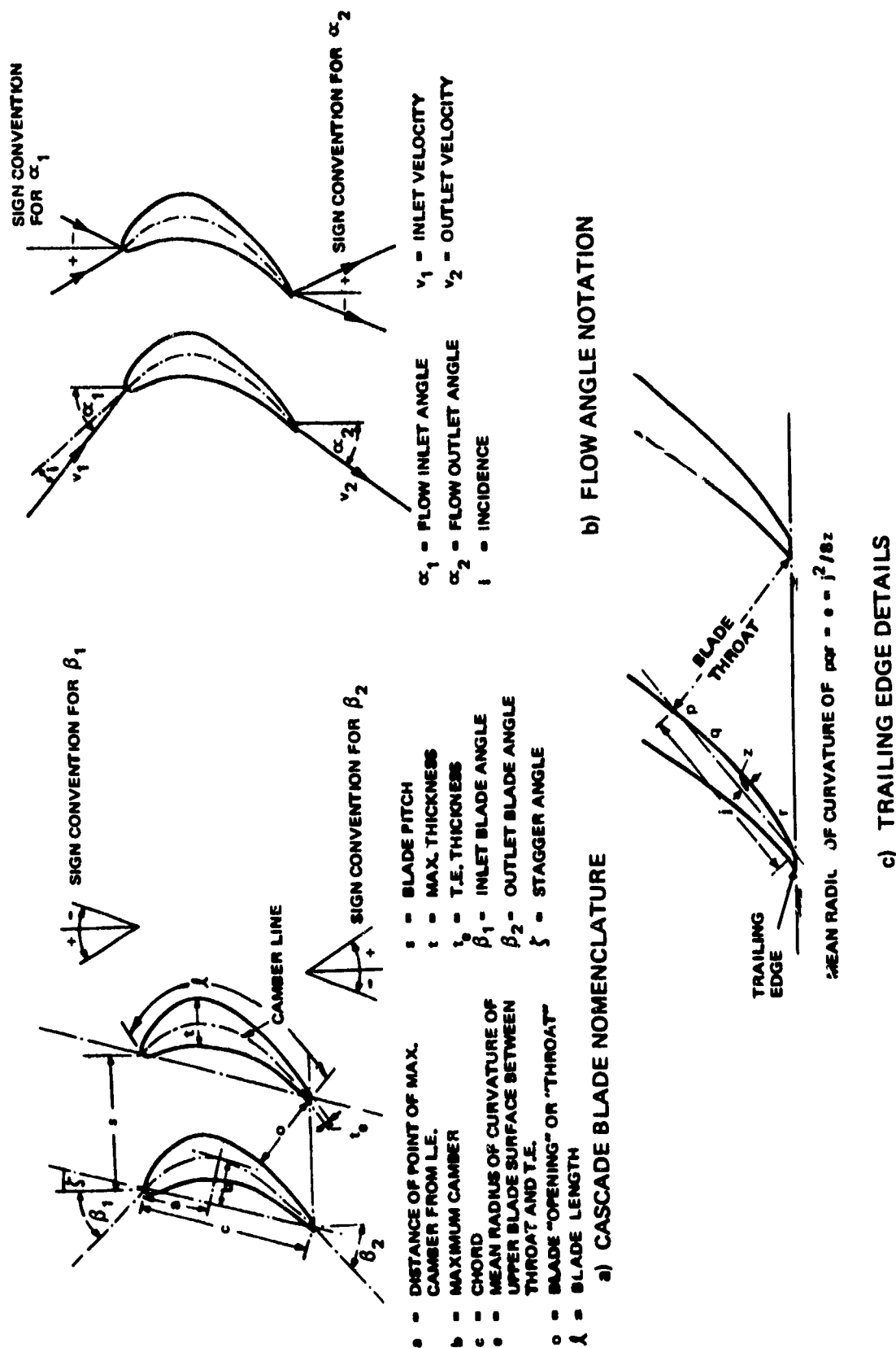


Figure 38: CASCADE BLADE NOMENCLATURE

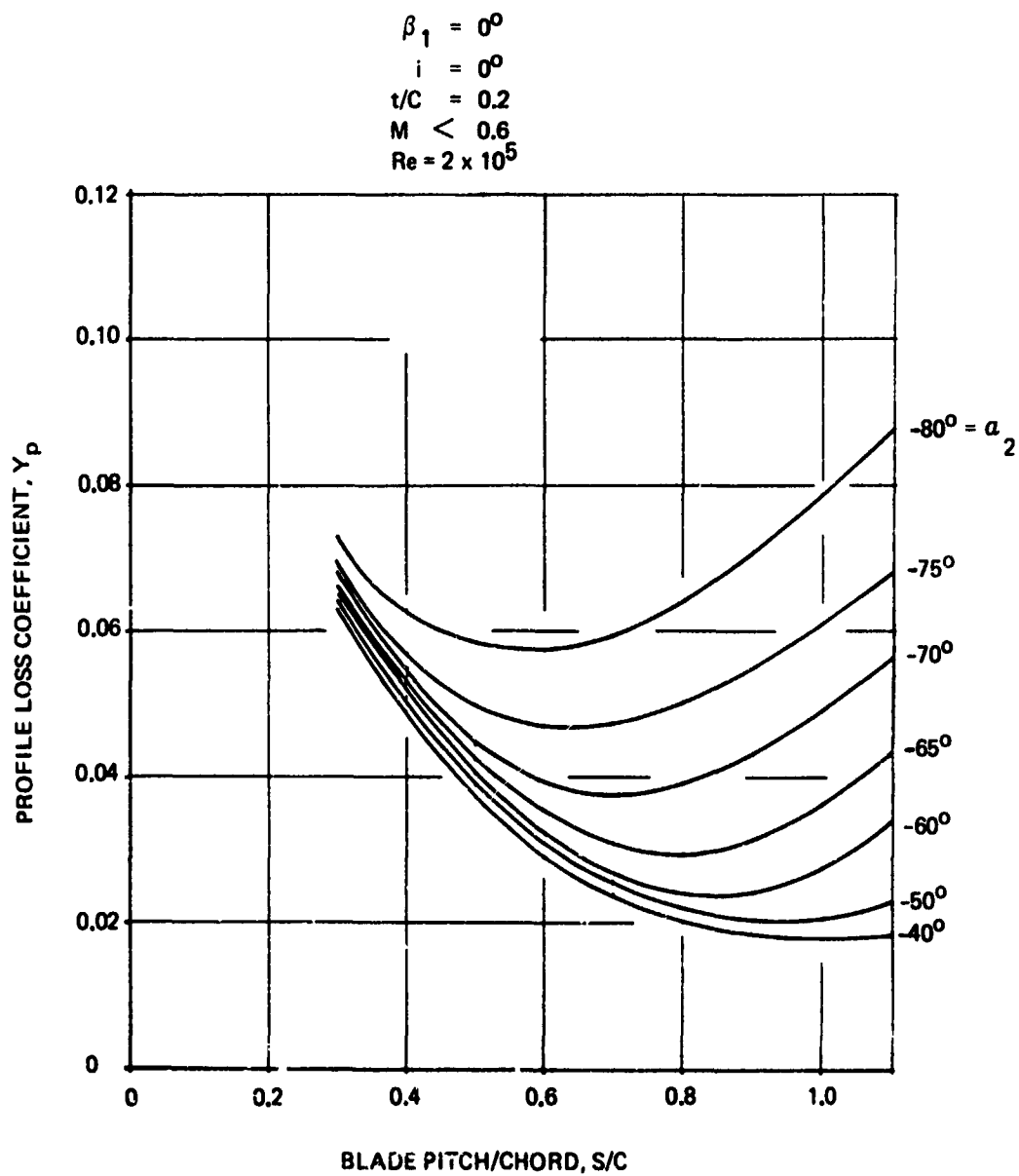


Figure 39: PROFILE LOSSES FOR REACTION BLADES AT ZERO INCIDENCE

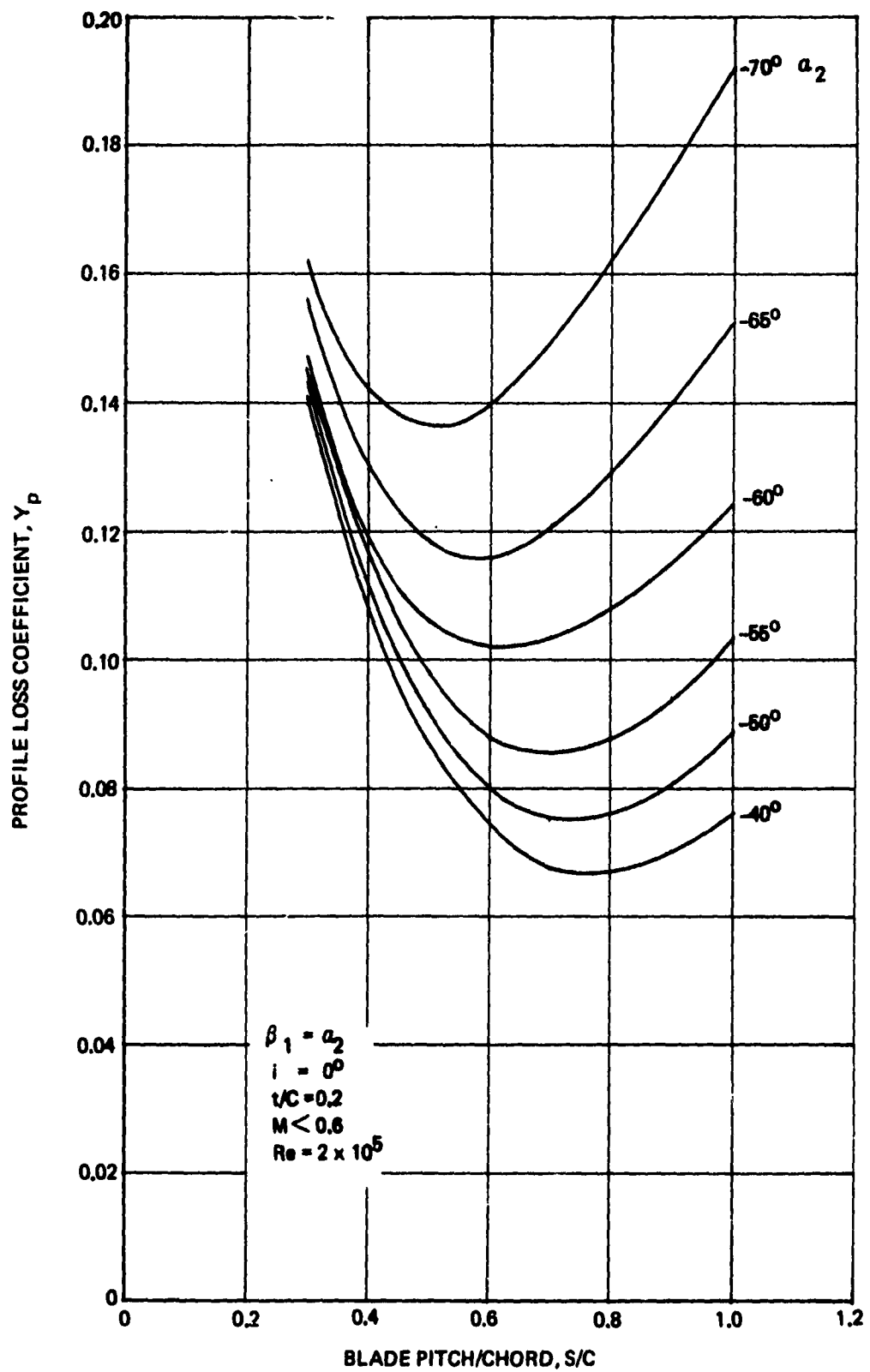


Figure 40: PROFILE LOSSES FOR IMPULSE BLADES AT ZERO INCIDENCE

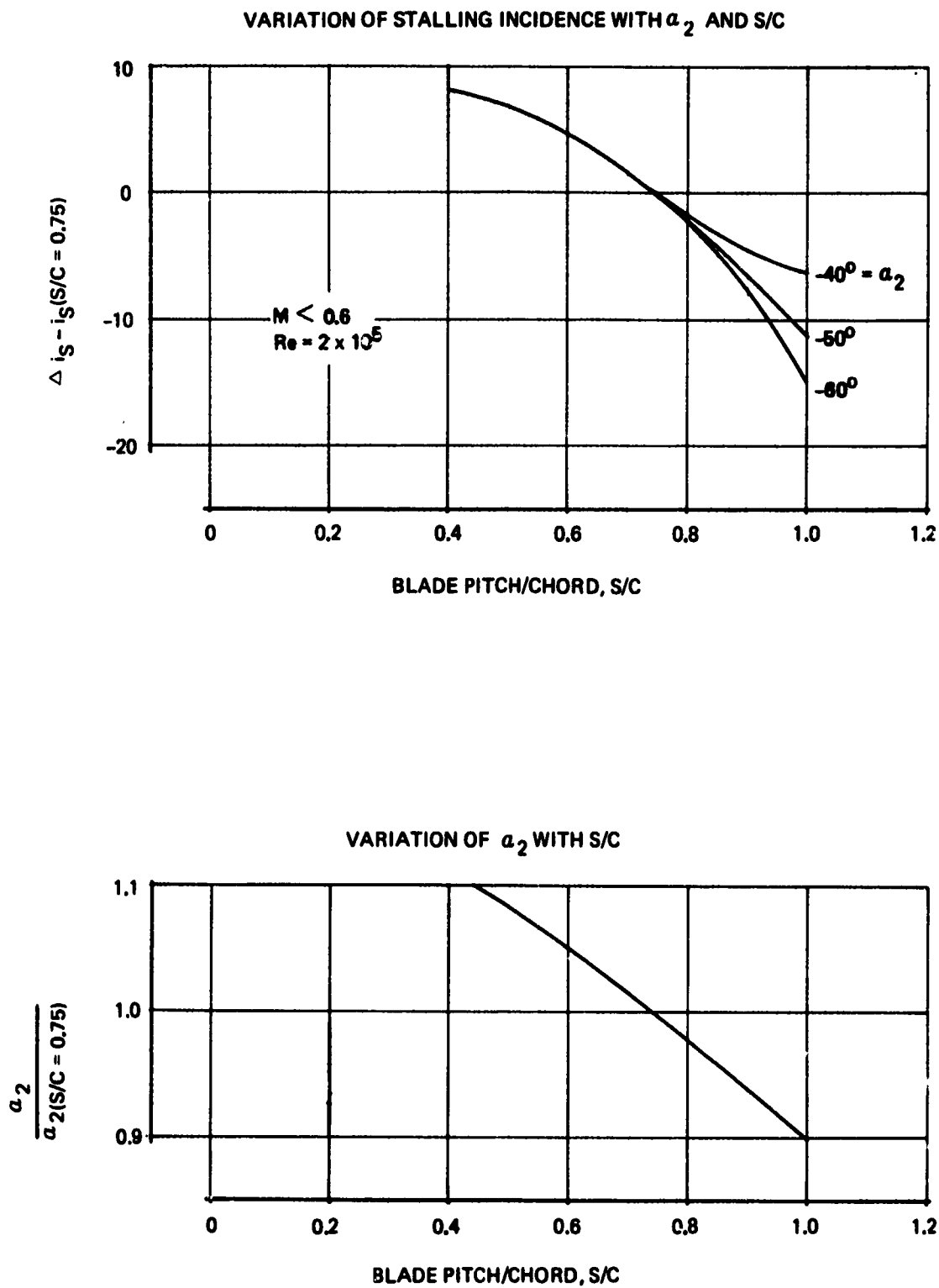


Figure 41: VARIATION OF STALLING INCIDENCE AND FLOW OUTLET ANGLE WITH PITCH/CHORD RATIO

$M < 0.6$
 $Re = 2 \times 10^5$

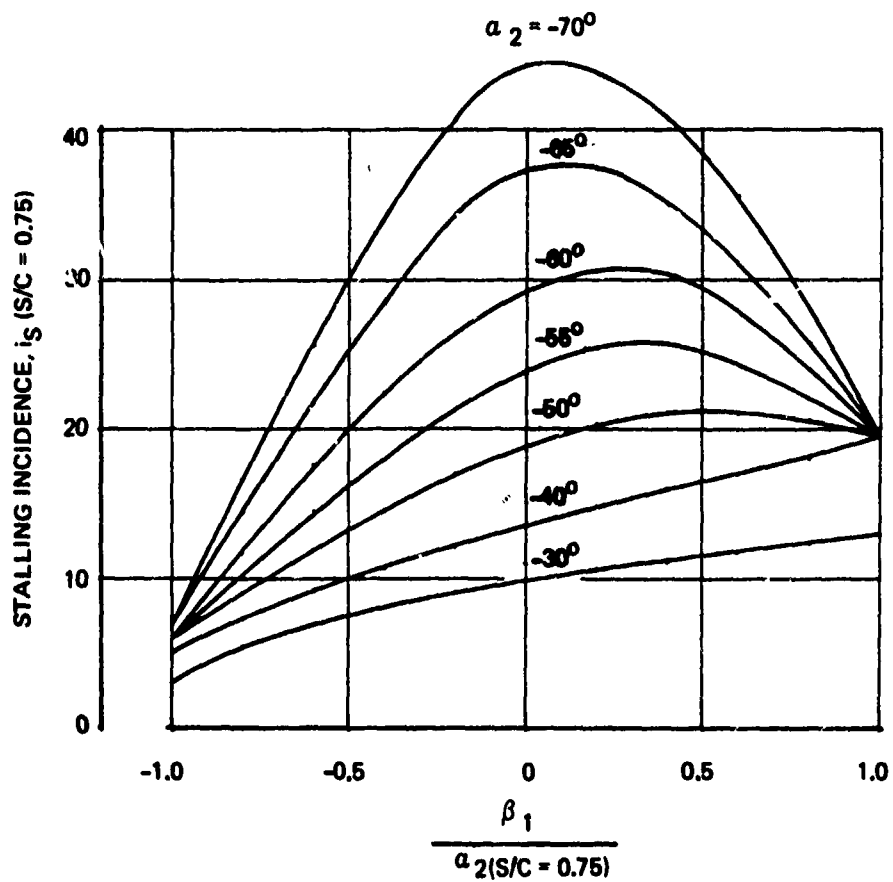


Figure 42: VARIATION OF STALLING INCIDENCE WITH BLADE INLET ANGLE AND FLOW OUTLET ANGLE

and change in flow outlet angle from Figure 43. For positive incidence angles, the flow outlet angle decreases with increasing losses. Effects of exit Mach number M_2 are shown in Figures 44 and 45. Flow outlet angle is obtained from Figure 44a for exit Mach number $M_2 < 0.5$ and Figure 44b for $M_2 = 1.0$. Linear interpolation is used for intermediate Mach numbers. The effect of exit Mach number and blade trailing edge curvature on relative blade profile loss is given in Figure 45.

Effects of Reynolds number are shown in Figures 46 and 47. Profile losses and flow outlet angle decrease as Reynolds number increases.

Entrance and exit flow properties (Figures 39 to 47) are used to calculate reaction across the blade row:

$$R = 1 - \frac{V_1}{V_2} \quad (30)$$

where V_1 and V_2 are entrance and exit velocity. A correlation between reaction and trailing edge momentum thickness was established by Stewart (Ref. 19) as shown in Figure 48. The following equation corrects for Reynolds number effects.

$$\frac{\theta_r}{l} = \left(\frac{\theta_r}{l} \right)_b \left[\frac{Re}{Re_b} \right]^{-1/5} \quad (31)$$

where $(\theta_r/l)_b$ is obtained from Figure 48 and baseline $Re_b = 300,000$. The fraction of momentum loss based on actual weight flow is given by the following equation for a two-dimensional cascade.

$$m_{2,20} = \frac{\left(\frac{\theta_r}{l} \right) \left(\frac{l}{c} \right) \left(\frac{\sigma}{\cos \alpha_1} \right)}{1 - \frac{t_e + \delta_r}{\cos \alpha_1}} \quad (32)$$

where total boundary layer displacement thickness at the blade trailing edge δ_r is related to momentum thickness θ_r by the equation

$$H = \frac{\delta_r}{\theta_r} \quad (33)$$

Data and theory for form factor H are shown in Figure 49. The term $m_{2,20}$ considers the blades to have infinite length. In a cascade, however, there are end walls and stiffeners that also have boundary layer losses that are appreciable. Losses on these surfaces are assumed equal to the average loss occurring on the blade surfaces. Therefore, the factor to correct for end walls is given by the area ratio

$$\frac{A_{30}}{A_{20}} = \frac{A_{blade} + A_{wall}}{A_{blade}} = 1 + \frac{A_{wall}}{A_{blade}} \quad (34)$$

VARIATION OF RELATIVE PROFILE
LOSS WITH RELATIVE INCIDENCE

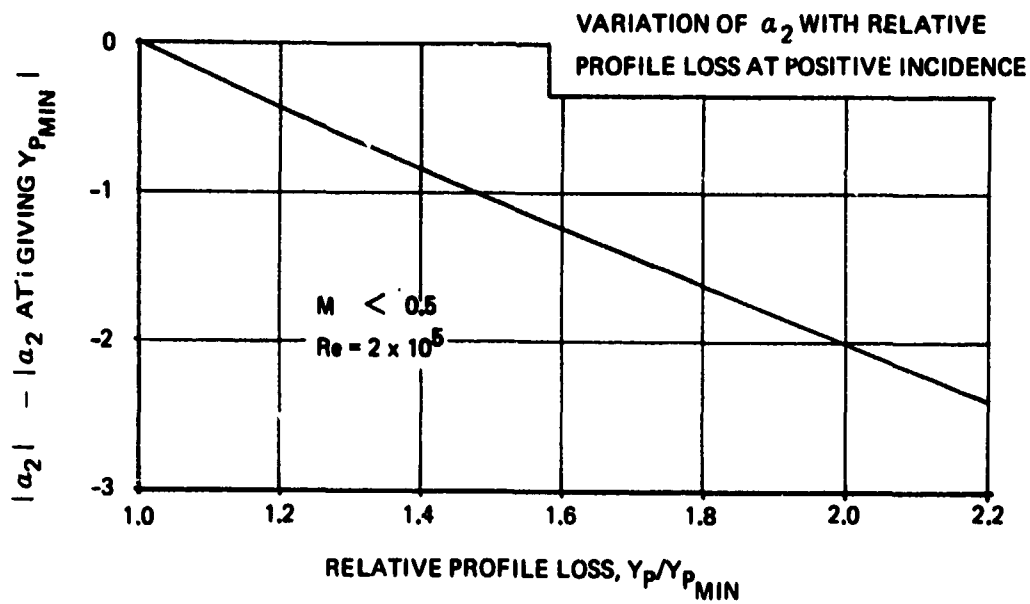
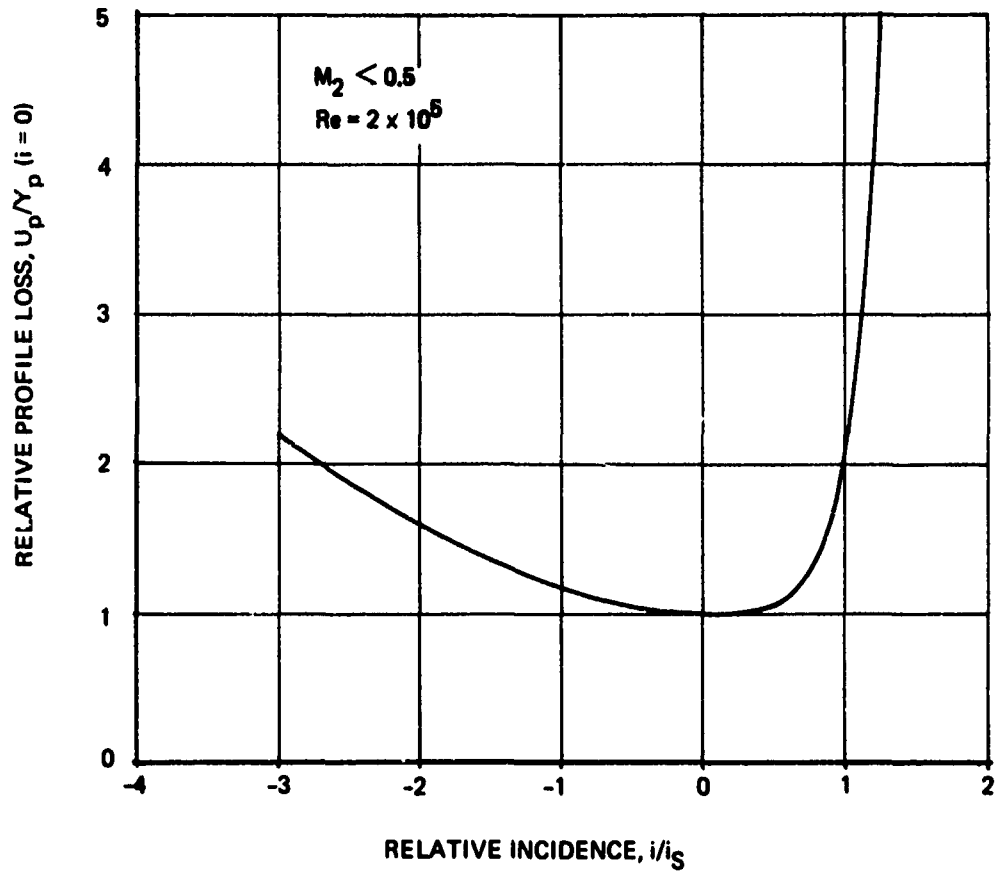
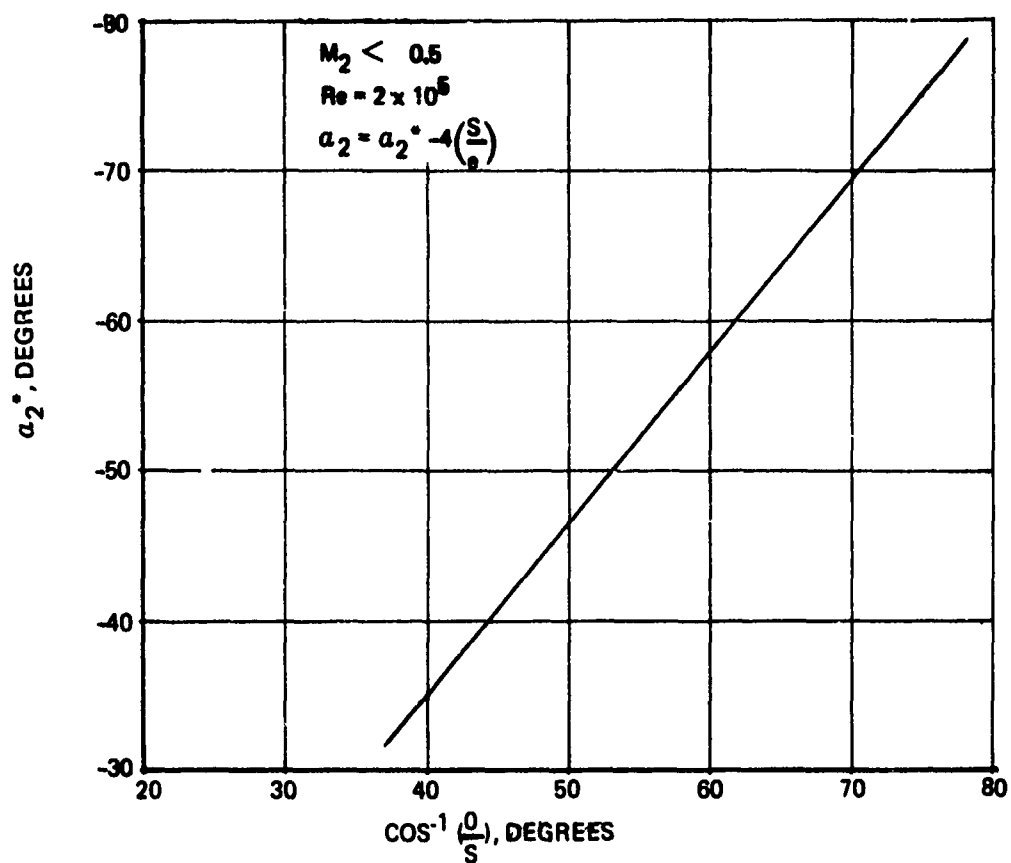
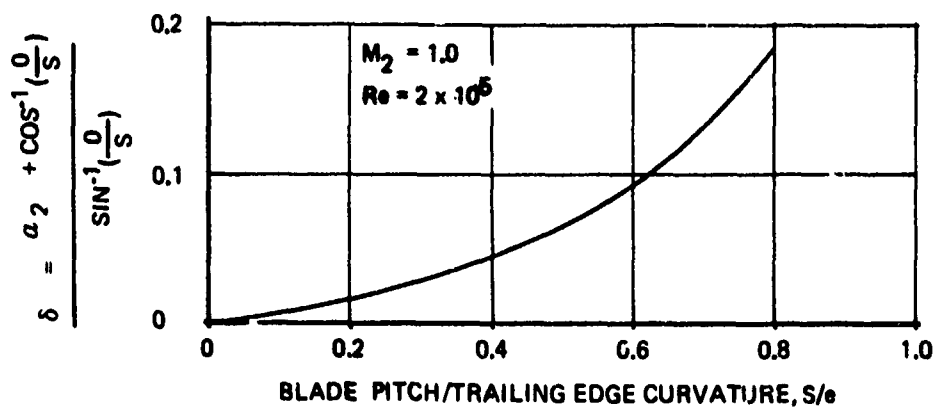


Figure 43: VARIATION OF LOSS AND OUTLET ANGLE WITH INCIDENCE



a) FLOW OUTLET ANGLE WHEN $M_2 < 0.5$



b) FLOW OUTLET ANGLE WHEN $M_2 = 1.0$

Figure 44: VARIATION OF FLOW OUTLET ANGLE WITH MACH NUMBER AND BLADE TRAILING EDGE CURVATURE

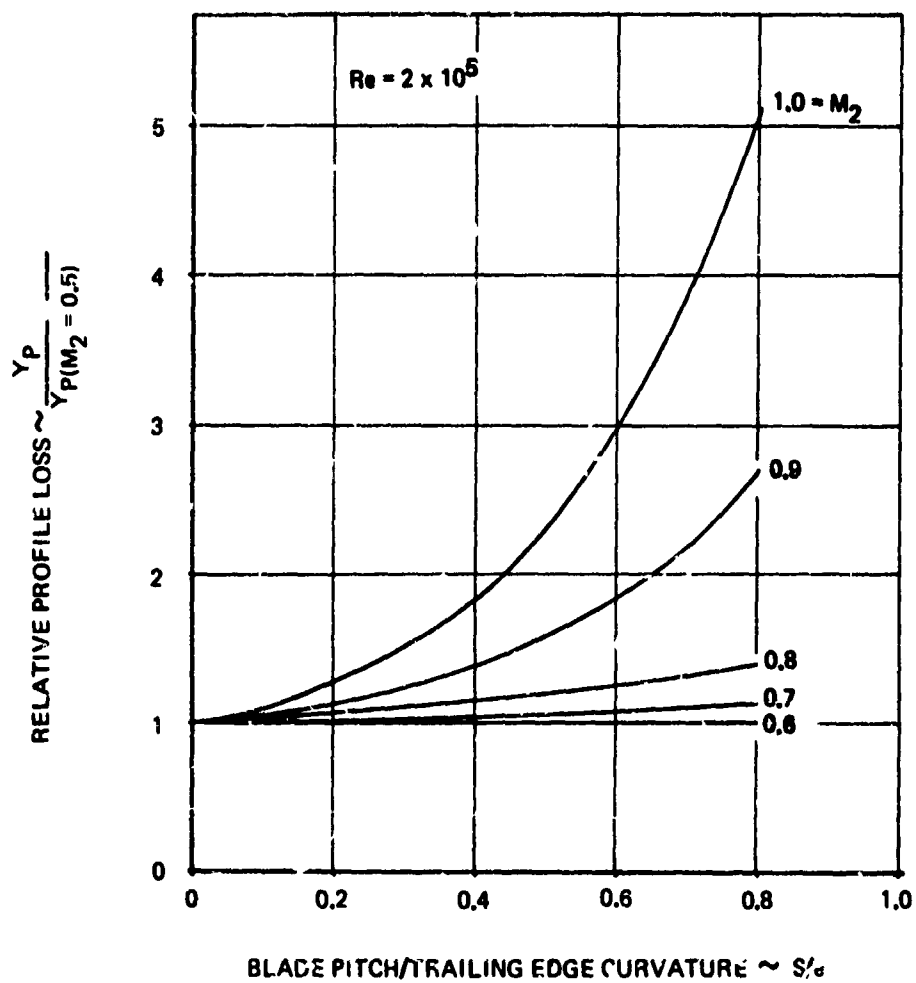


Figure 45: VARIATION OF RELATIVE PROFILE LOSS WITH MACH NUMBER AND TRAILING EDGE CURVATURE

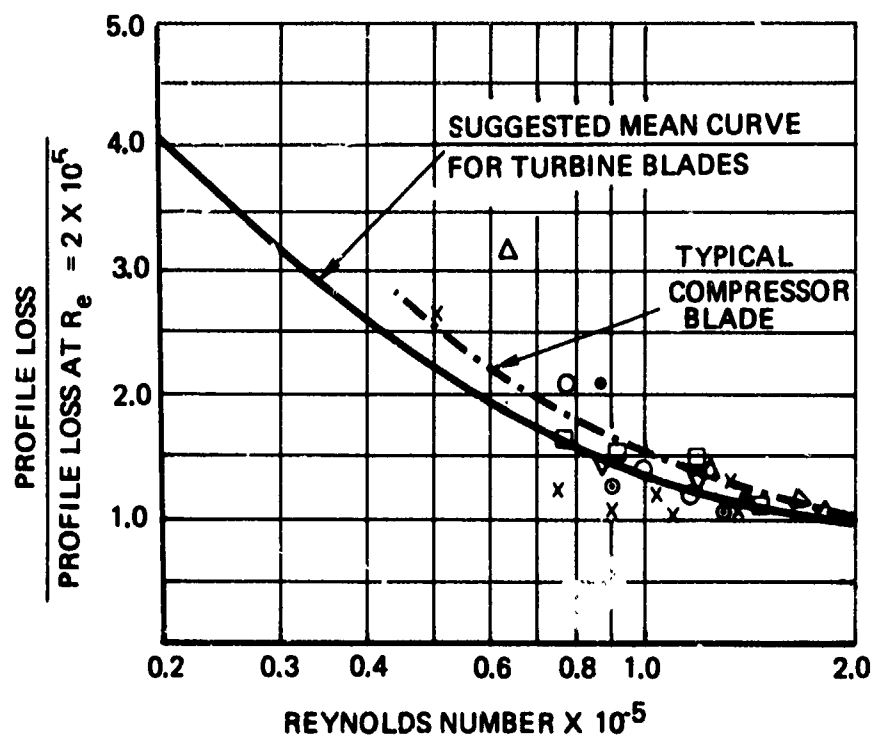
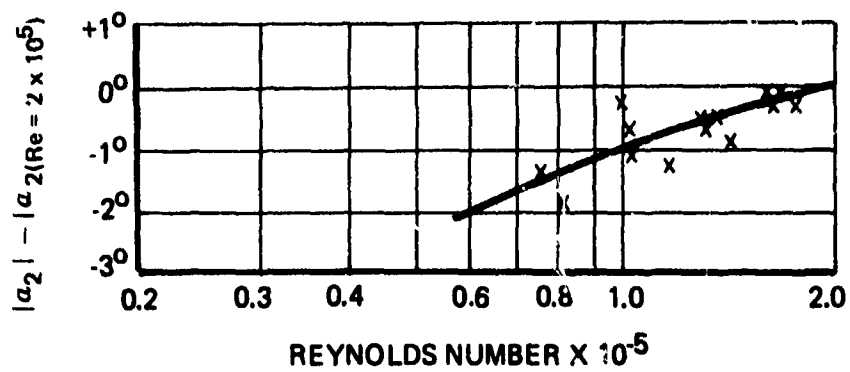
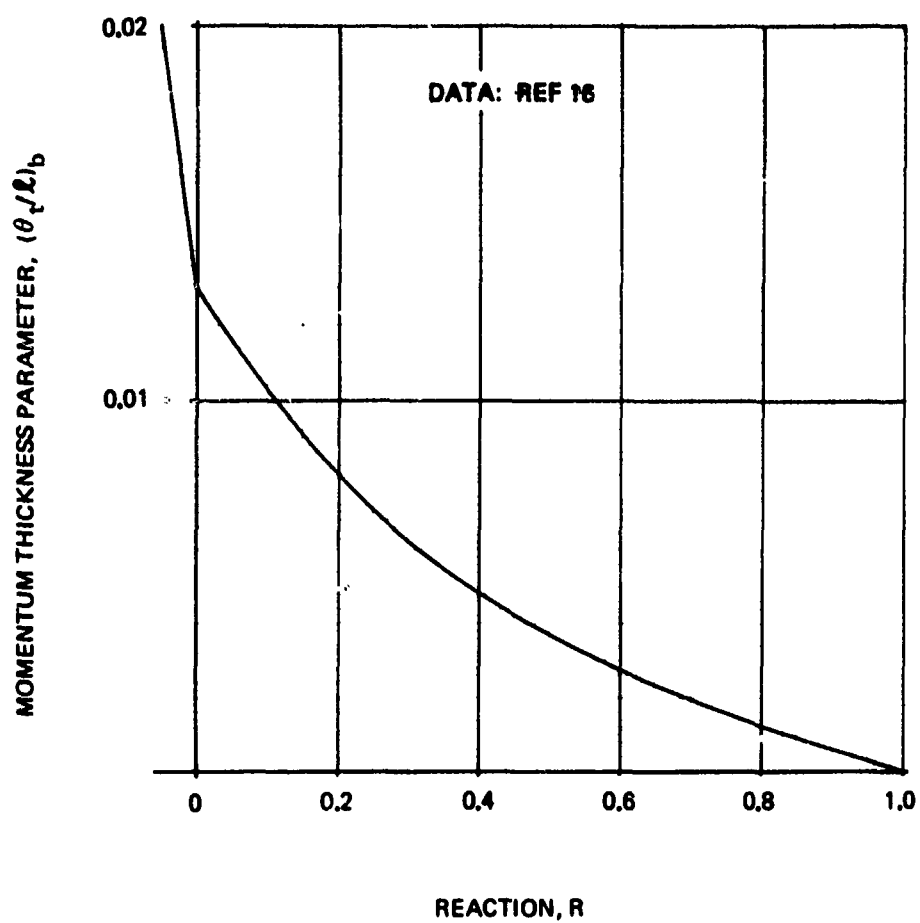


Figure 46: EFFECTS OF REYNOLDS NUMBER ON PROFILE LOSSES FOR CASCADE LATTICES



**Figure 47: EFFECTS OF REYNOLDS NUMBER ON FLOW
OUTLET ANGLE FOR CASCADE LATTICES**



**Figure 48: CORRELATION RELATING REACTION AND
MOMENTUM THICKNESS FOR CASCADE LATTICES**

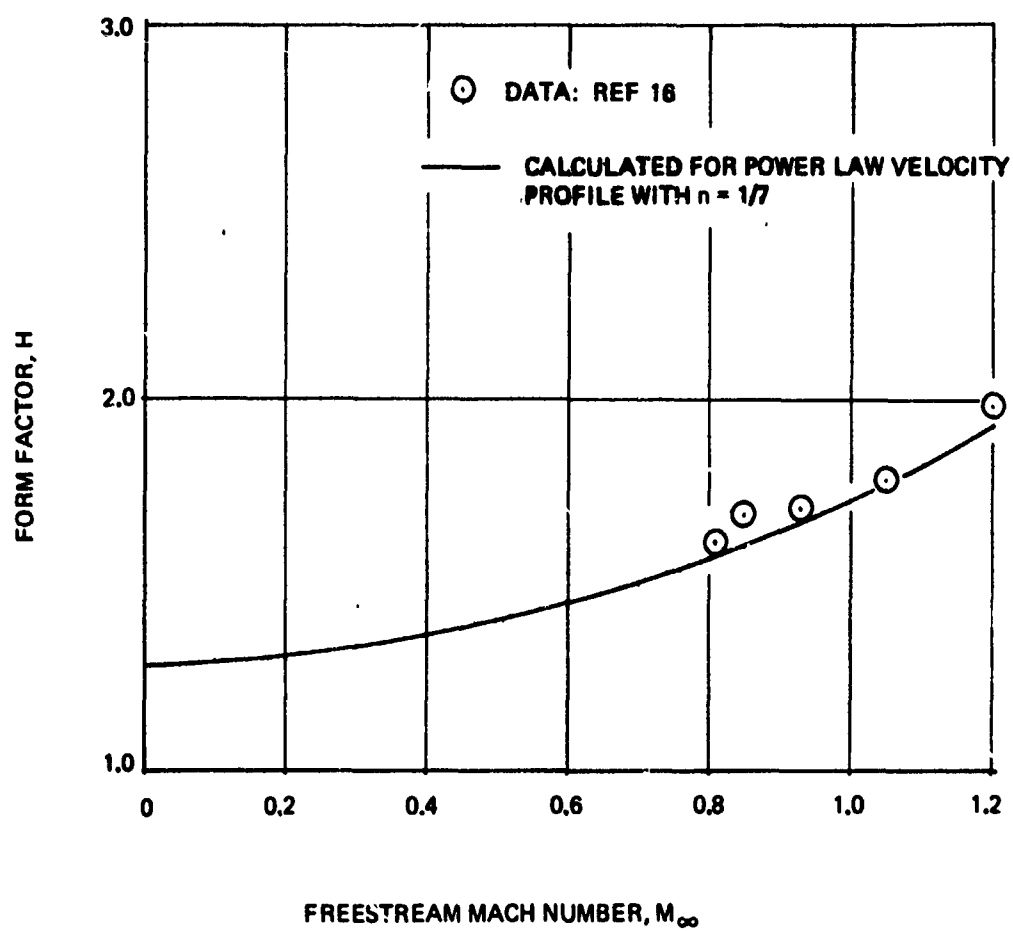


Figure 49: FORM FACTOR DATA FOR CASCADE LATTICES

For a cascade lattice with no stiffeners, it can be shown that

$$\frac{A_{3D}}{A_{2D}} \approx 1 + \frac{\cos \mathcal{S}}{\sigma R} \quad (35)$$

where \mathcal{S} is stagger angle (see Figure 38) and blade aspect ratio R = blade length/chord. If the cascade lattice has stiffeners, their wetted area should be included in the term A_{wall} of

Equation 34. The area ratio A_{3D}/A_{2D} is used to correct $m_{1,2D}$ for losses on end walls and stiffeners.

$$m_{2,3D} = m_{2,2D} \frac{A_{3D}}{A_{2D}} \quad (36)$$

Velocity coefficient is given by

$$C_v = 1 - m_{2,3D} - \Delta C_v) \text{ underexpansion losses (Fig. 6)} \quad (37)$$

Discharge coefficient is given by

$$C_D = 1 - H m_{2,3D} \quad (38)$$

The prediction method computes C_v and C_D for cascade lattices. To obtain reverser efficiency, vector efficiency, and airflow match, the following equations are used:

$$\eta_{Rg} = \frac{C_v \cos \theta_r}{C_{vf}} \quad (39)$$

$$\eta_{Vg} = \frac{C_v}{C_{vf}} \quad (40)$$

$$\bar{z} = \frac{C_D}{C_{Df}} \frac{A_r}{A_f} \quad (41)$$

2.2 Task 1.2--Construct Computerized Analytical Models

The purpose of Task 1.2 was to develop computer programs for predicting TR and TV nozzle performance and evaluating TR and TV influence on the total airplane/engine system. Three computer programs were developed:

- 1) Jet Trajectory and Spreading Program (TEM-356A)
- 2) Reingestion Prediction Program (TEM-356B)
- 3) TR and TV System Performance Program (TEM-357)

The numbers in parenthesis are permanent identification numbers assigned to the programs by Boeing Computer Services, Inc. Further description of the programs is provided in the following sections.

2.2.1 Jet Trajectory and Spreading Program

The purpose of the Jet Trajectory and Spreading Program TEM-356A is to predict the shape of the exhaust plume emanating from a TR or TV nozzle. The exhaust plume definition is used to predict potentially severe aerodynamic interference and control problems that could be caused by plumes impinging on or passing close to flight control surfaces. The program also is used to provide definition of TR exhaust plumes to the Reingestion Prediction Program TEM-356B as described in Section 2.2.2.

As an example of the program's usefulness and purpose, Figures 50 to 52 show a thrust reverser exhaust plume for a two-engine STOL transport. The jet plume was computed by TEM-356A to determine the jet trajectory and plume shape relative to the aerodynamic control surfaces at 110 knot freestream velocity. Most STOL transports are expected to land at about 90 knots, so 110 knots should represent a more critical condition for tail interference effects. The thrust reverser efflux appears to impinge on the horizontal stabilizer in the side view. However, the front view shows that the lower vortex lobe is outboard of the stabilizer. The analysis indicates that the thrust reverser plume would not cause any severe aerodynamic interference problems by impinging on flight control surfaces.

A diagram showing inputs and outputs of the Jet Trajectory and Spreading Program is given in Figure 53. Inputs consist of TR or TV nozzle position, orientation, exhaust flow direction, the type of jet and nozzle and freestream flow conditions. Output consists of the jet centerline in (x, y, z) space and contours of the jet cross sections defining the boundaries between the TR or TV exhaust flow and freestream flow. The analysis uses an empirical equation for the jet centerline, empirical jet spreading coefficients, and theory for the jet cross section. The following sections describe the analysis in more detail.

Jet Trajectory Equation

There are numerous empirical equations that predict the trajectory of a jet in a crossflow (Ref. 17 to 24). Table IV summarizes empirical equations for the jet trajectory, together with their respective ranges of validity. The empirical equations were obtained by curve-fitting data from flow visualization experiments. Comprehensive reviews of the empirical equations were made by Filler (Ref. 25) and Margason (Ref. 24). Filler concluded that empirical equations of Ivanov, Shandorov, and Margason compared favorably within their respective ranges of validity. Margason also concluded that Ivanov's equation provided

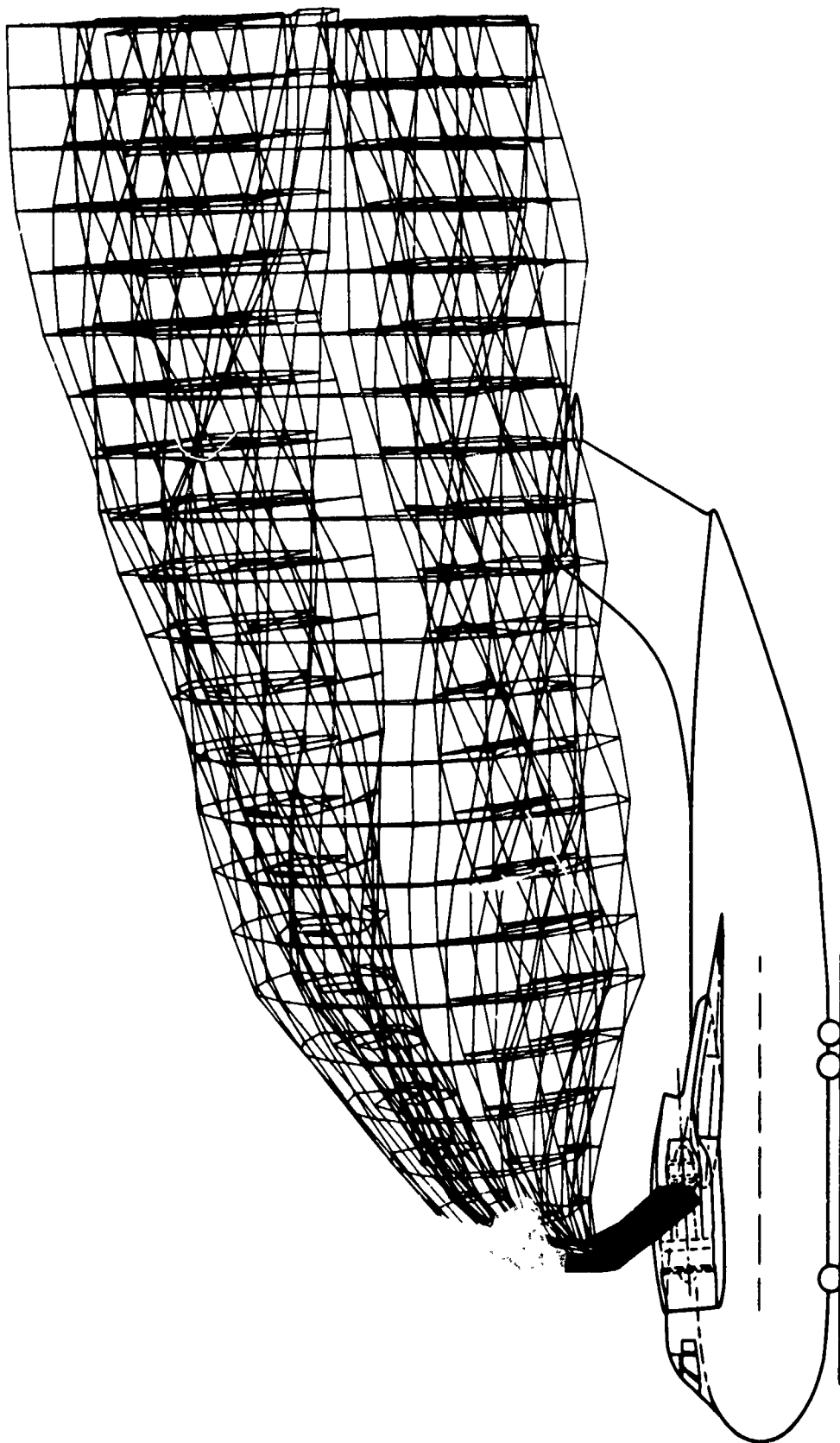


Figure 50: STOL TRANSPORT THRUST REVERSER
PLUME SIDE VIEW

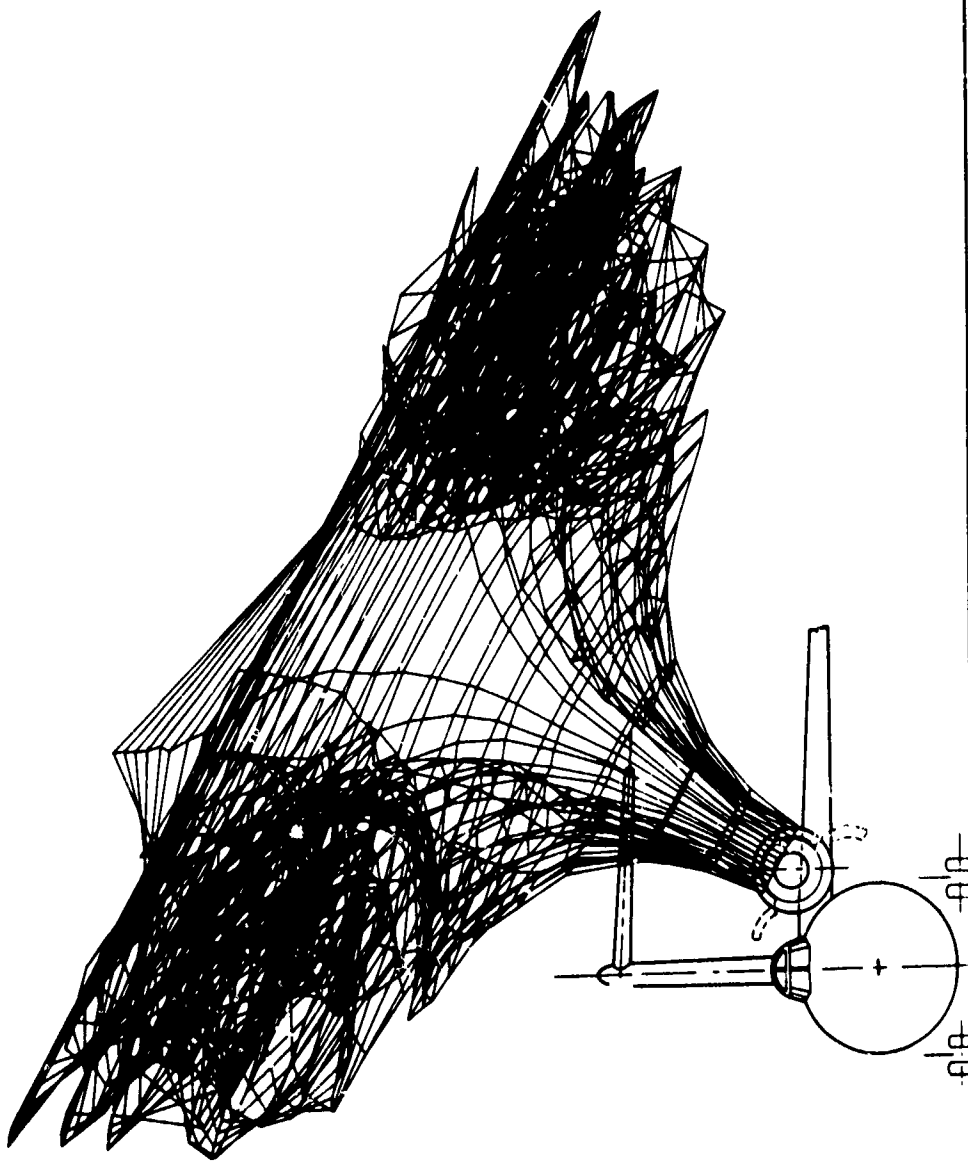


Figure 51: STOL TRANSPORT THRUST REVERSER
PLUME END VIEW

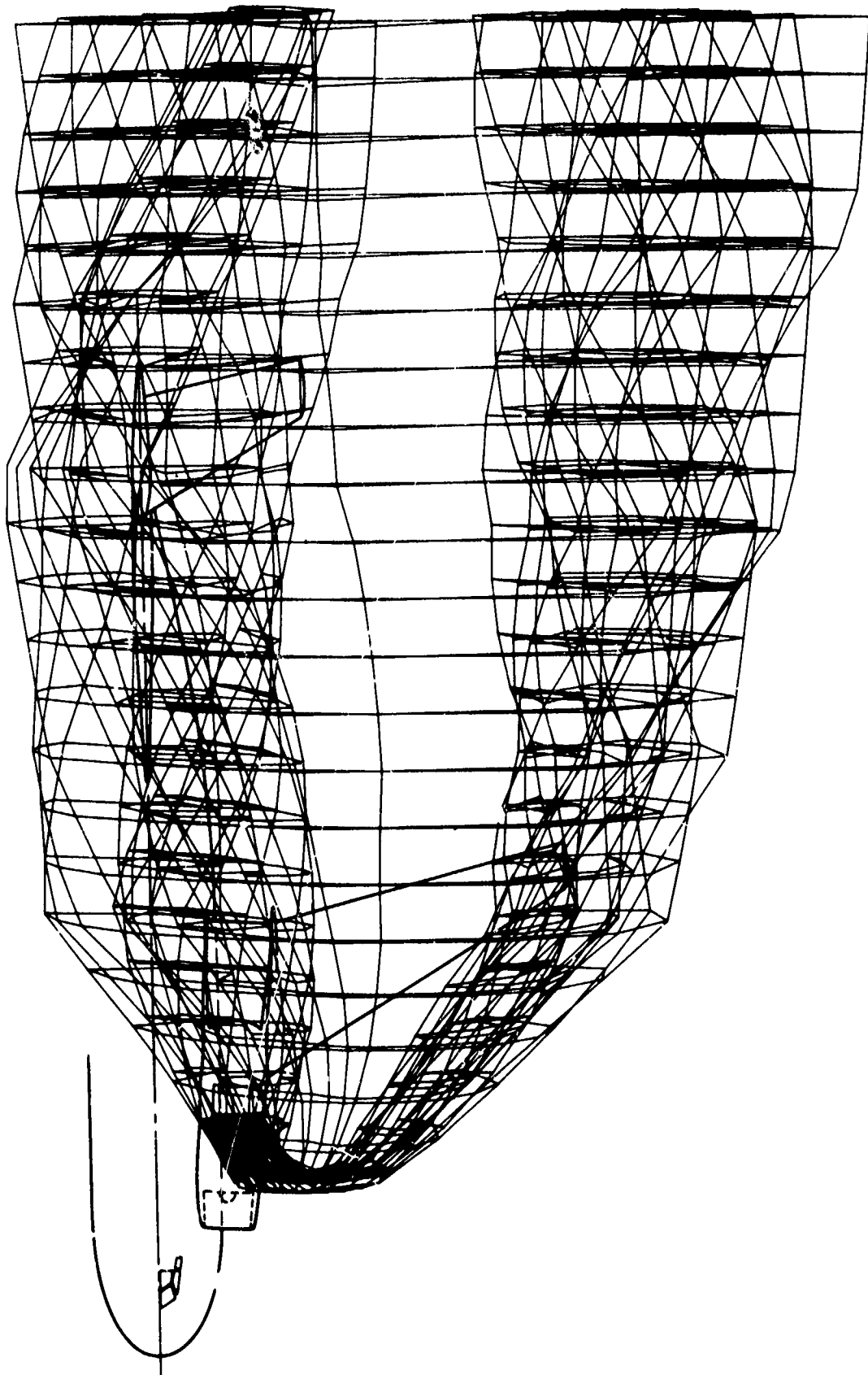


Figure 52: STOL TRANSPORT THRUST REVERSER
PLUME PLAN VIEW

JET TRAJECTORY AND SPREADING PROGRAM

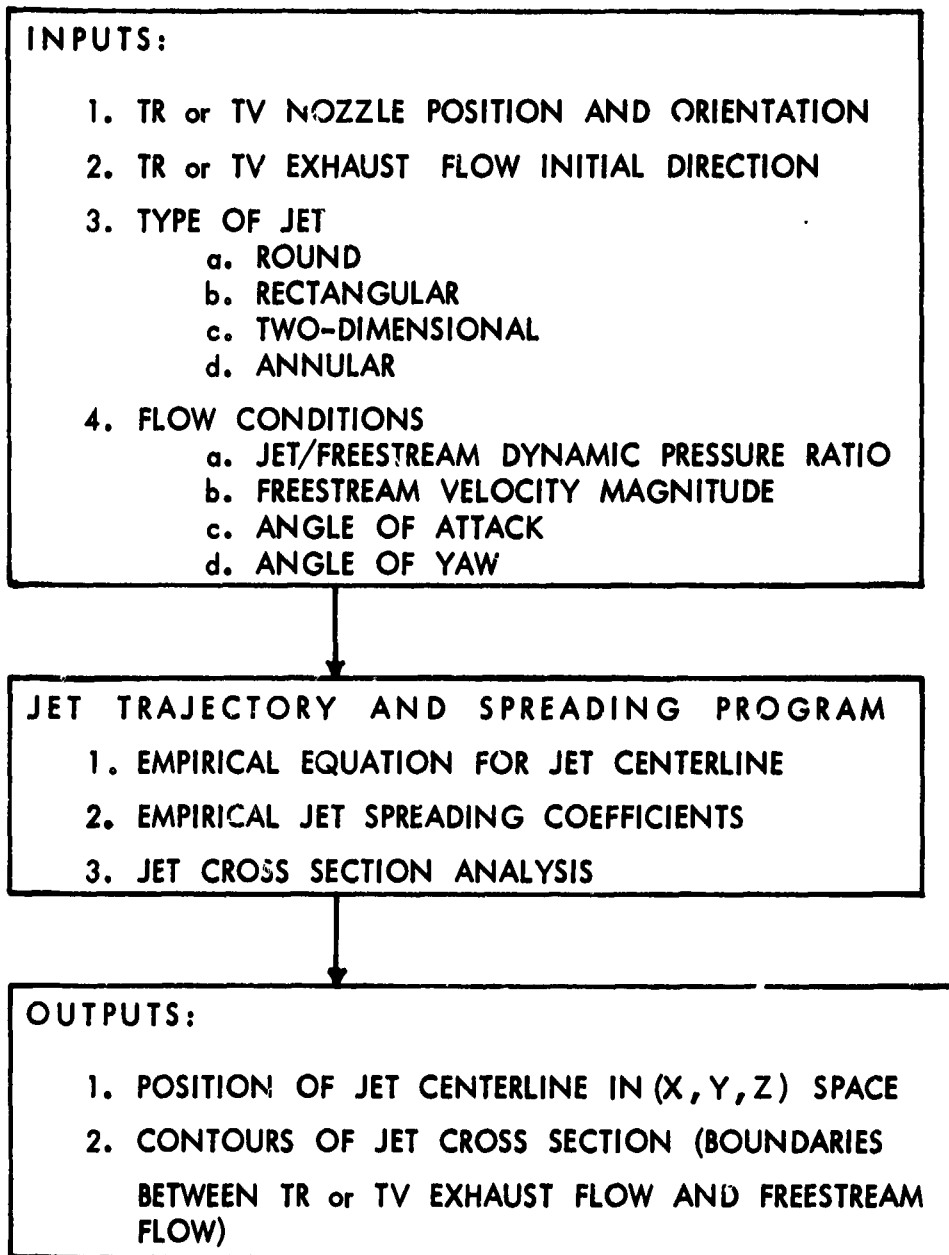


Figure 53: JET TRAJECTORY AND SPREADING PROGRAM DIAGRAM

EQUATION	α_0	q_j / q_∞	T_j / T_∞	REFERENCE
I. $\frac{X}{d_0} = \left(\frac{q_\infty}{q_j}\right)^{1.3} \left(\frac{Z}{d_0}\right)^3 + \frac{Z}{d_0} \cot \alpha_0$	60°—120°	12—1000	1.0	IVANOV REF. 17
II. $\frac{X}{d_0} = \left(\frac{q_\infty}{q_j}\right) \left(\frac{Z}{d_0}\right)^{2.55} + \frac{Z}{d_0} \left(1 + \frac{q_\infty}{q_j}\right) \cot \alpha_0$	45°—90°	2—22	.33—1.0	SHANDOROV REF. 18
III. $\frac{X}{d_0} = 0.25 \left(\frac{V_\infty^2}{V_j Z}\right) \left(\frac{Z}{d}\right)^3 \csc^2 \alpha_0 + \frac{Z}{d_0} \cot \alpha_0$	30°—180°	1.38—100	1.0	MARGASON REF. 24
IV. $\frac{X}{d_0} = 0.118 \left(\frac{\rho_\infty q_\infty}{\rho_j q_j}\right) \left(\frac{Z}{d_0}\right)^{3.3}$	90°	4—50	> 1.0	CALLAGHAN & RUGGERI REF. 19
V. $\frac{X}{d_0} = 2.3 \left(\frac{V_\infty}{V_j}\right)^3 \left(\frac{Z}{d_0}\right)^3$	90°	16—64	1.0	JORDINSON REF. 20
VI. $\frac{X}{d_0} = .195 \left(\frac{V_\infty}{V_j}\right)^2 \left(\frac{Z}{d_0}\right)^3$	90°	16—100	1.0	STORMS REF. 21

DATA TAKEN FROM REFERENCES 24 AND 25

TABLE IV SUMMARY OF EMPIRICAL EQUATIONS FOR JET TRAJECTORY AND RANGE OF VALIDITY

a good fit to his data at most of the deflection angles between 30 and 150 degrees. The range of validity for Ivanov's equation is clearly known and closely meets conditions of thrust reverser/vectoring, namely $0 \leq q_j/q_\infty \leq 200$ and $30 \text{ degrees} \leq \alpha_0 \leq 150 \text{ degrees}$. For these reasons, Ivanov's equation was selected for use in the Jet Trajectory and Spreading Program. Trajectories computed using Ivanov's equation are compared to test data in Figures 54 to 56.

Ivanov also experimented with rectangular jets ($1:5 \leq a/b \leq 5:1$) and concluded that to a first approximation the equation for a circular jet is adequate provided the hydraulic diameter is used instead of the initial jet diameter.

For two-dimensional jets, the equation of Vizel and Mostinskii (Ref. 23) was selected.

$$\frac{x}{t_0} = \frac{0.23 C_x}{\sin \alpha_0} \left(\frac{q_\infty}{q_j} \right) \left(\frac{z}{t_0} \right)^2 + \left(\frac{z}{t_0} \right) \cot \alpha_0 \quad (42)$$

Experimental data for jet penetration coefficient C_x are shown in Figure 57 from Ref. 26. The straight lines drawn through the data are used in program TEM-356A. The line for $\alpha_0 = 90$ degrees is used for discharge angles less than 90 degrees and the line for $\alpha_0 = 135$ degrees is used for angles greater than 135 degrees. Interpolation is used to obtain jet penetration coefficients for $90 \text{ degrees} < \alpha_0 < 135 \text{ degrees}$. Comparisons of Vizel and Mostinskii's results with test data are shown in Figures 58 and 59.

Jet Spreading Coefficients

Experimental jet spreading coefficients obtained for a round jet discharging at 90 degrees to a freestream flow (Ref. 22) are used to predict thickness and width of the exhaust plume. A lack of data exists for other discharge angles and jet shapes. Moreover, there is considerable disagreement for jet thickness to width ratio, δ/w , between the data of several investigators.

Pratte and Baines' jet thickness spreading coefficient data for a round jet in crossflow are presented in Figure 60 from Ref. 22. The following empirical equations provide a good curve fit to the data.

$$\frac{\delta/d_0}{V_j/U_\infty} = 0.36 \left(\frac{S/d_0}{V_j/U_\infty} \right)^{1.35} \quad \text{for } \frac{S/d_0}{V_j/U_\infty} < 3.16 \quad (43)$$

$$\frac{\delta/d_0}{V_j/U_\infty} = 1.16 \left(\frac{S/d_0}{V_j/U_\infty} \right)^{0.33} \quad \text{for } \frac{S/d_0}{V_j/U_\infty} > 3.16 \quad (44)$$

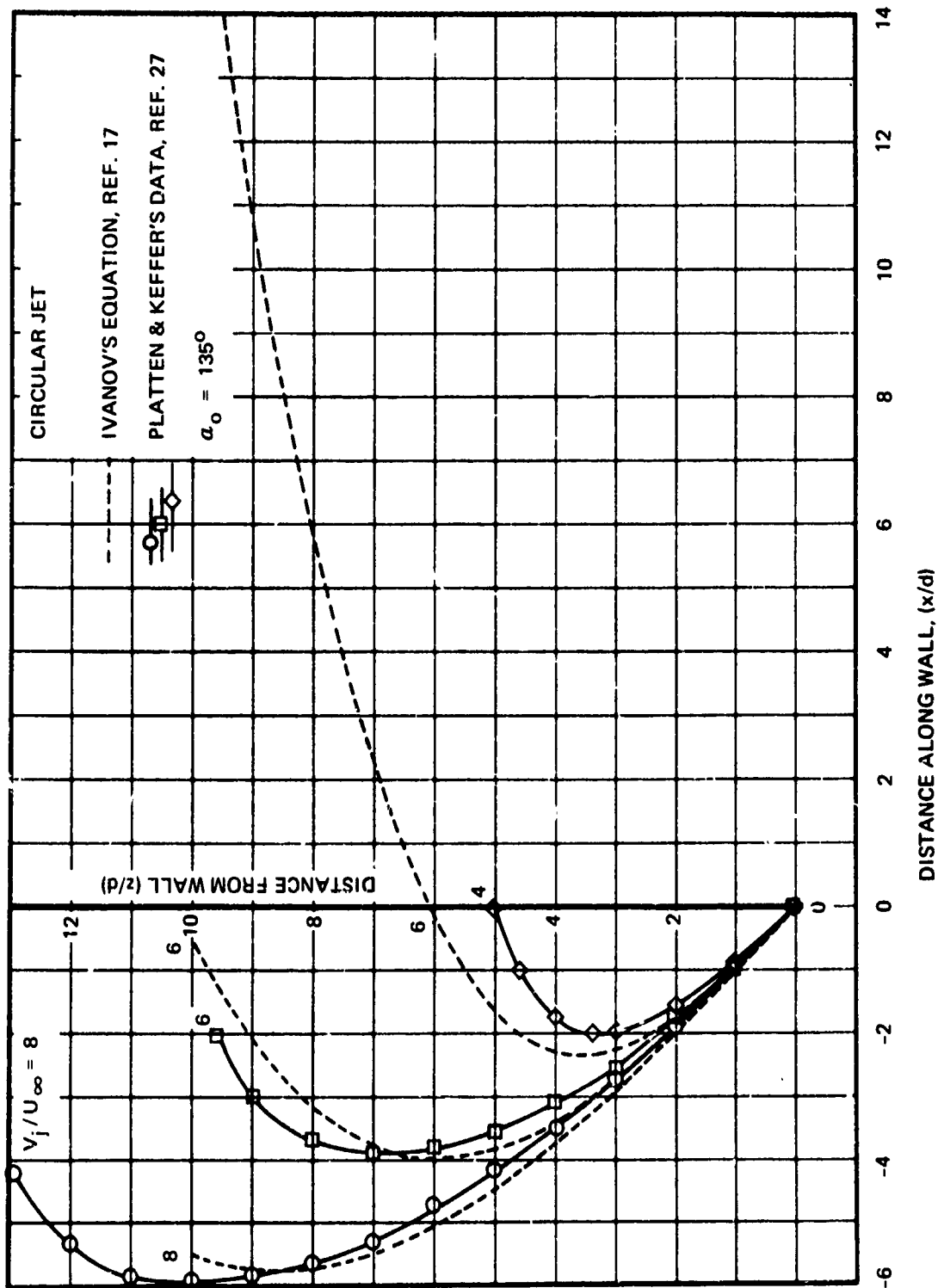


Figure 54: COMPARISON OF JET TRAJECTORY EQUATION WITH DATA FOR $\alpha_0 = 135^\circ$

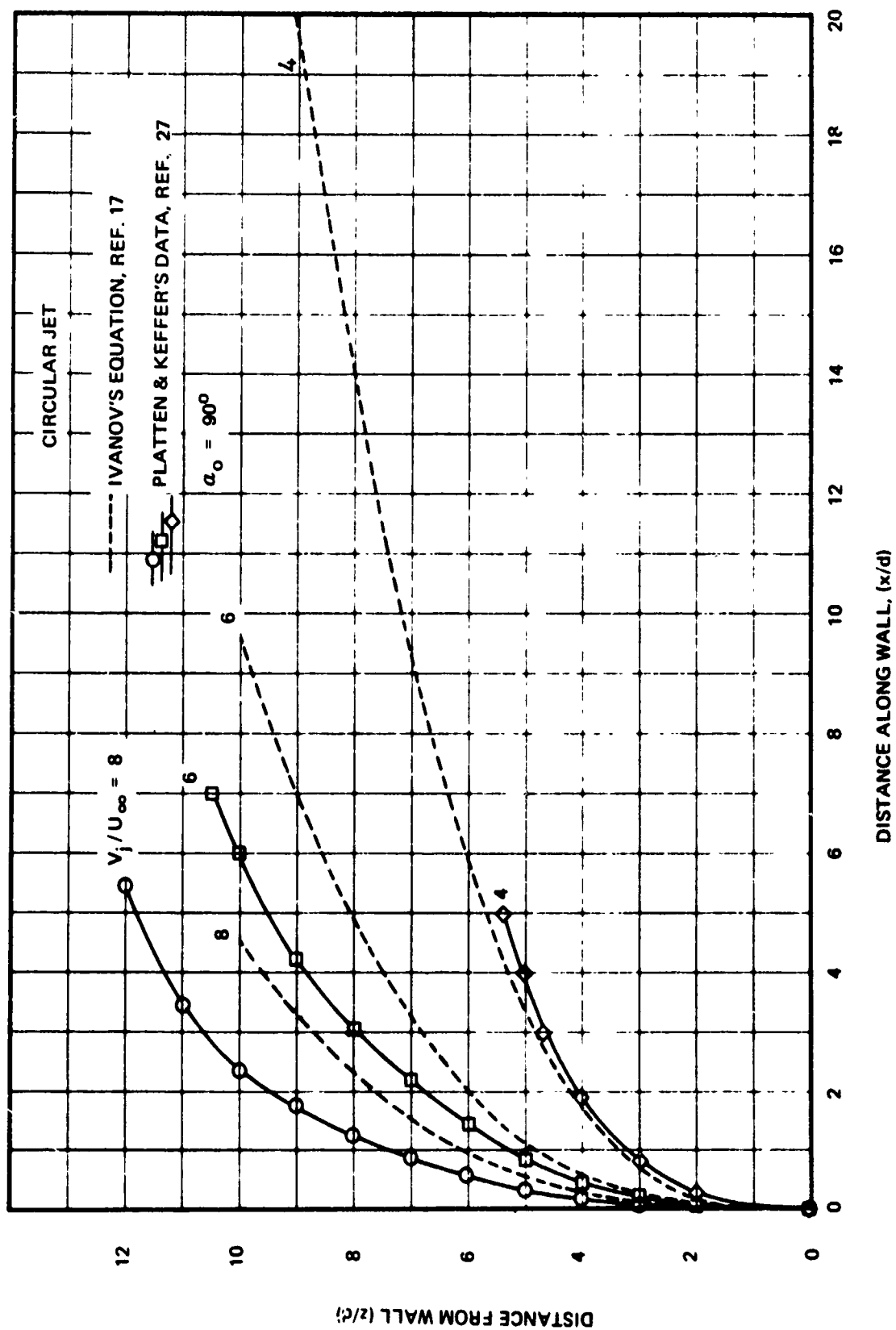


Figure 55: COMPARISON OF JET TRAJECTORY EQUATION WITH DATA FOR $\alpha_0 = 90$ DEGREES

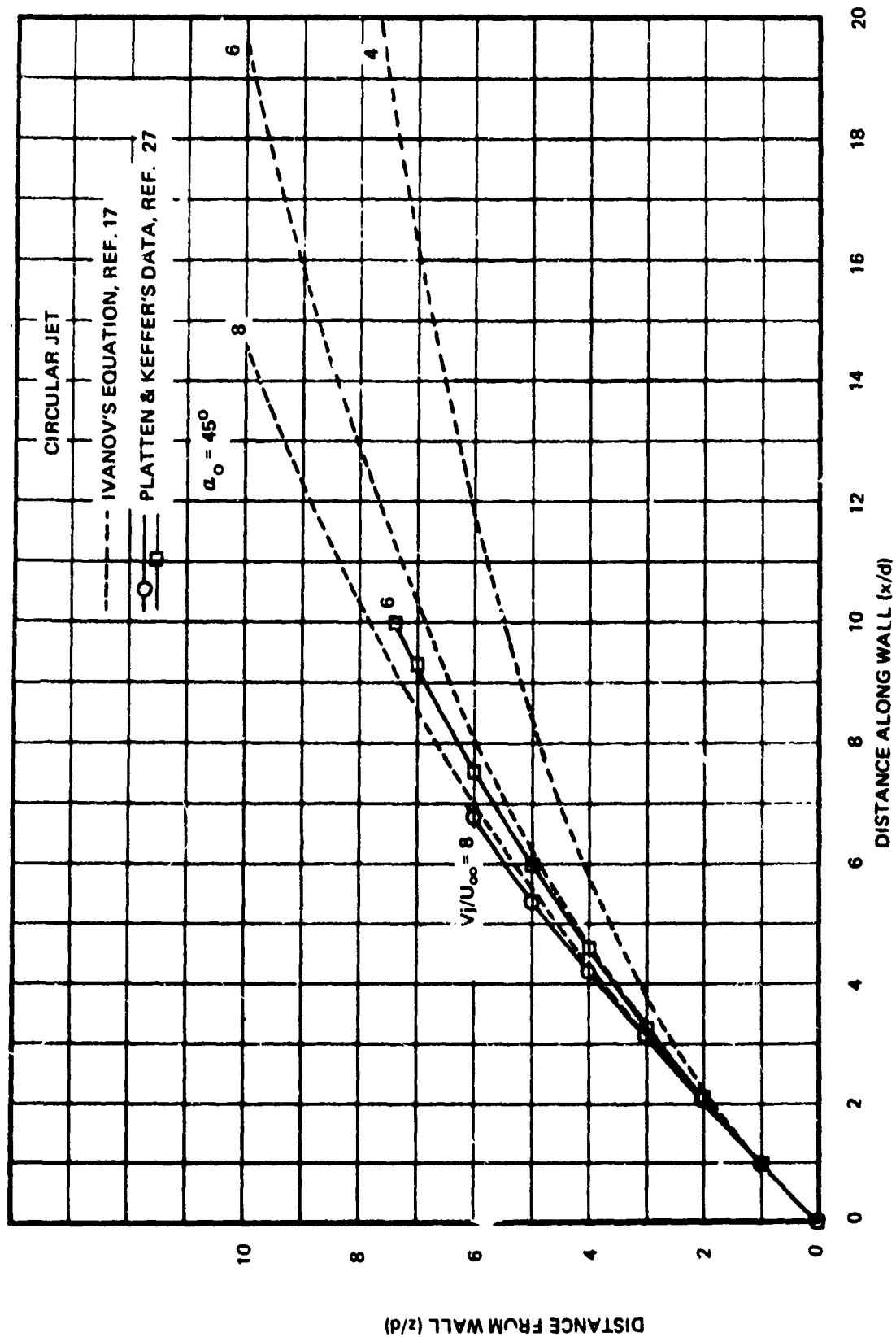


Figure 56: COMPARISON OF JET TRAJECTORY EQUATION WITH DATA FOR $\alpha_0 = 45$ DEGREES

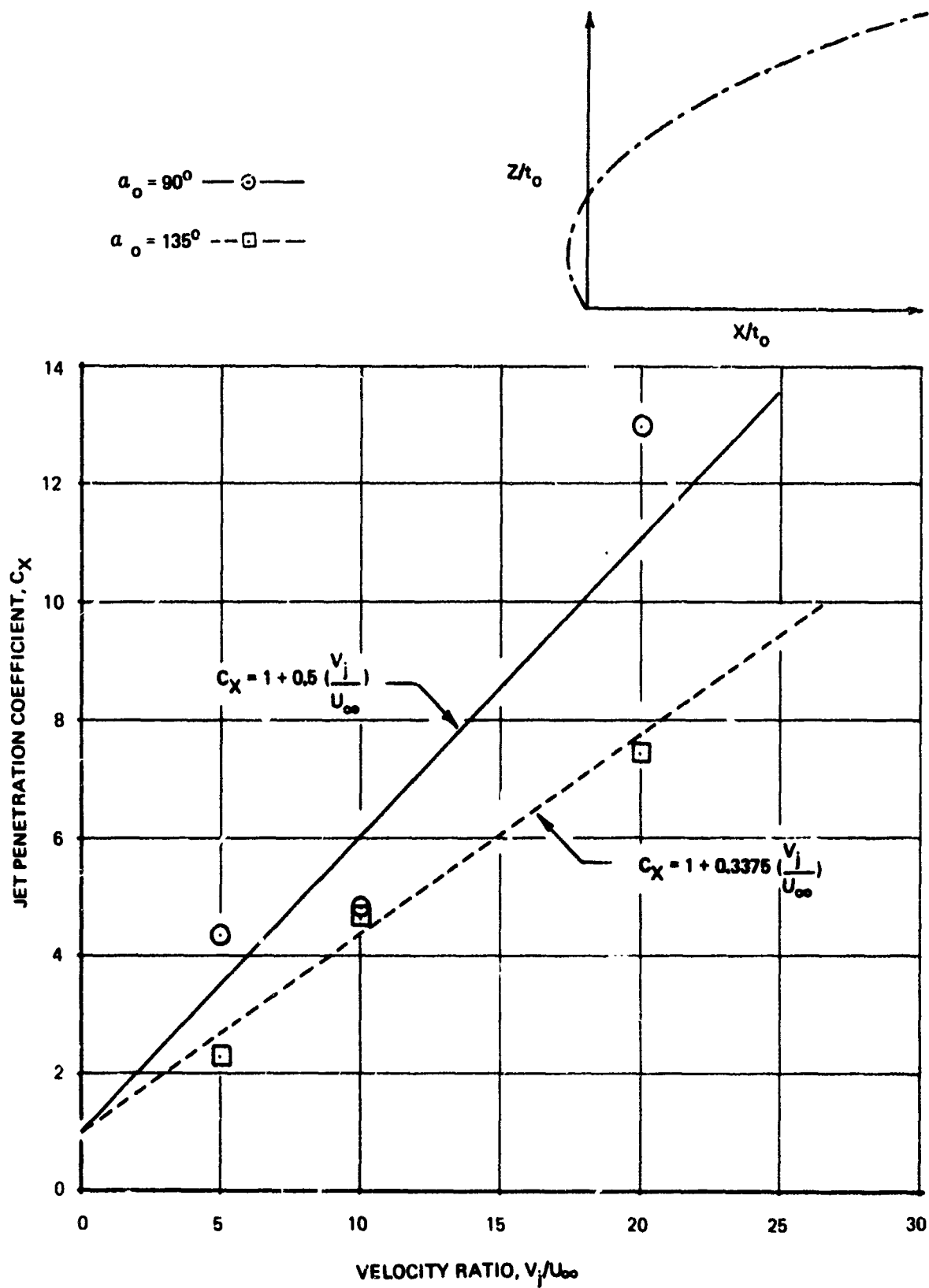


Figure 57: JET PENETRATION COEFFICIENT DATA FOR VIZEL AND MOSTINSKII'S TRAJECTORY EQUATION

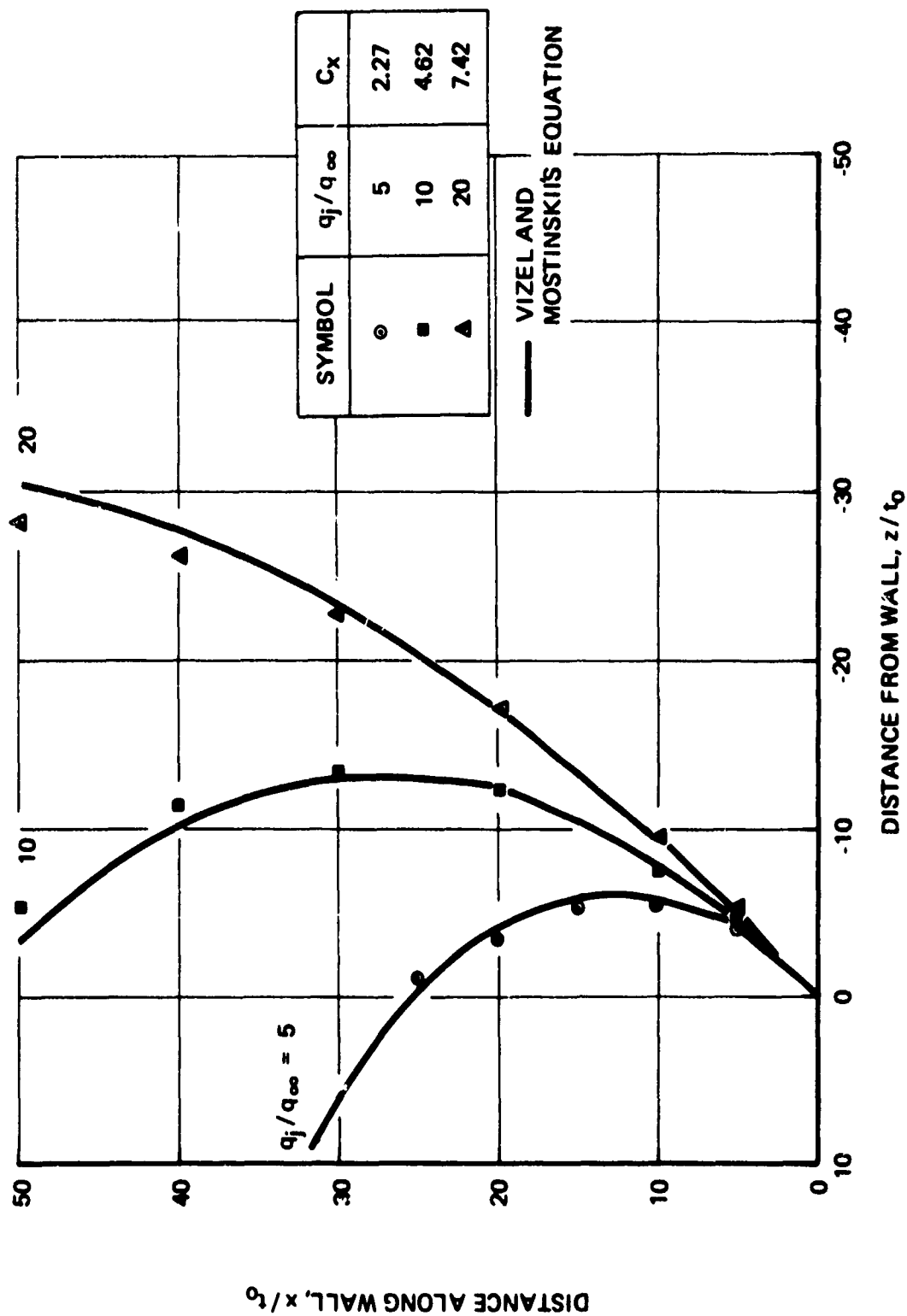


Figure 58: COMPARISON OF TWO DIMENSIONAL JET TRAJECTORY EQUATION TO TEST DATA FOR $\alpha_0 = 135$ DEGREES

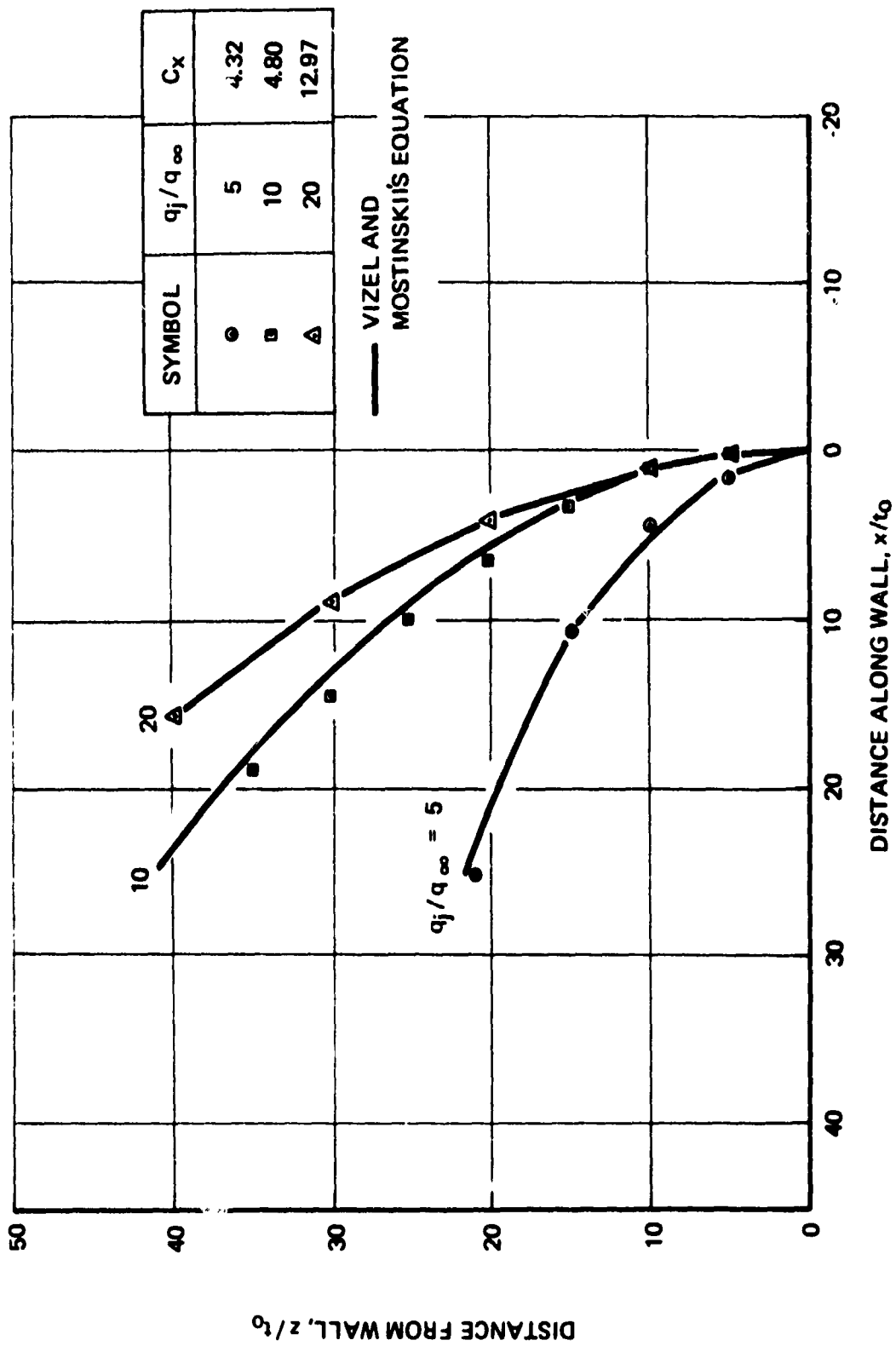


Figure 59: COMPARISON OF TWO DIMENSIONAL JET
 TRAJECTORY EQUATION TO TEST DATA FOR
 $\alpha_0 = 90$ DEGREES

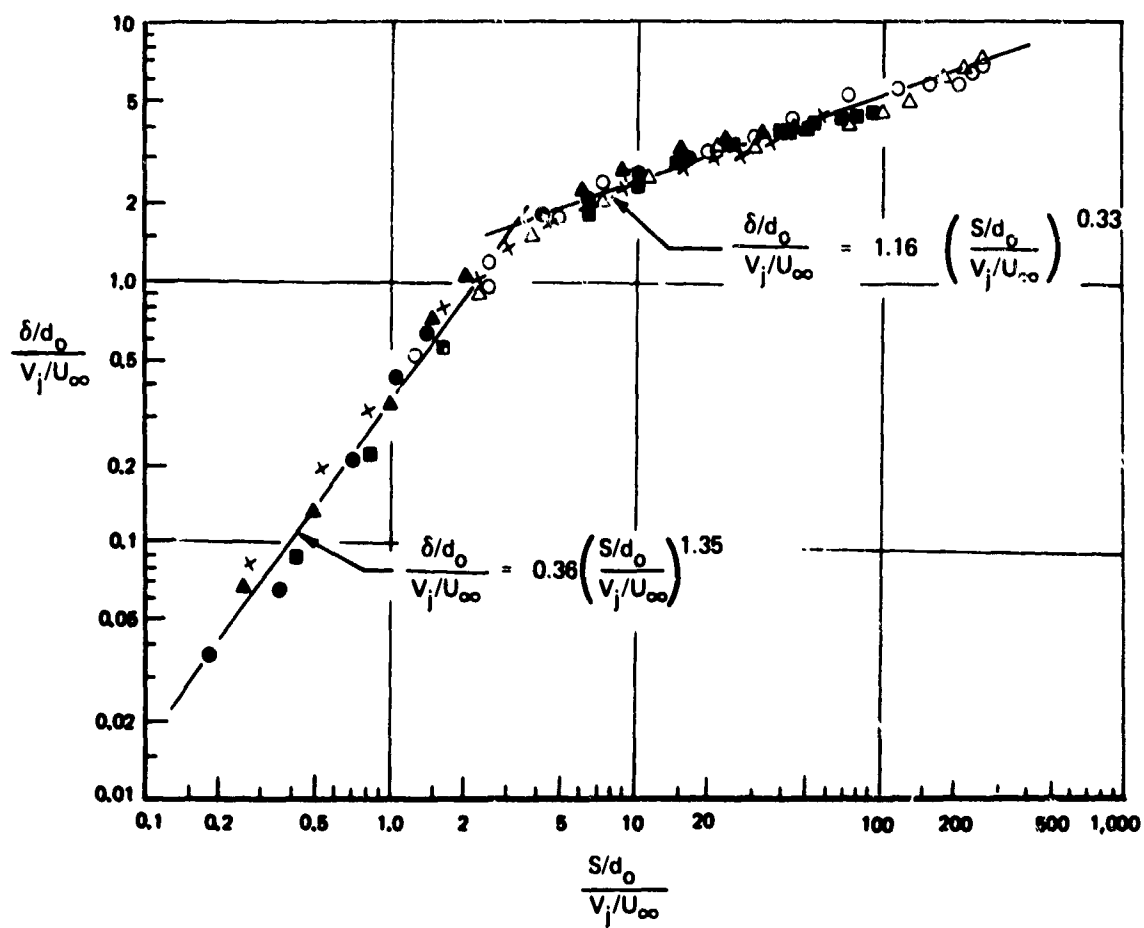


Figure 60: THICKNESS SPREADING CHARACTERISTICS OF A ROUND JET PERPENDICULAR TO A CROSS FLOW

These empirical equations are used downstream of the jet's potential core. In the potential core region, the thickness to diameter ratio is equal to 1.0. Setting $\delta/d_o = 1.0$ in Equation 43 and solving for s/d_o gives

$$\left(\frac{s}{d_o}\right)_{\text{potential core}} = 2.131 \left(\frac{V_j}{U_\infty}\right)^{0.2593} \quad (45)$$

Summarizing, the following equations are used to compute jet thickness.

$$\frac{\delta}{d_o} = 1.0 \quad \text{for} \quad \frac{s}{d_o} < \left(\frac{s}{d_o}\right)_{\text{potential core}} \quad (46)$$

$$\frac{\delta}{d_o} = 0.36 \left(\frac{s}{d_o}\right)^{1.35} \left(\frac{V_j}{U_\infty}\right)^{-0.35} \quad \text{for} \quad \left(\frac{s}{d_o}\right)_{\text{potential core}} < \frac{s}{d_o} < 3.16 \frac{V_j}{U_\infty} \quad (47)$$

$$\frac{\delta}{d_o} = 1.16 \left(\frac{s}{d_o}\right)^{0.39} \left(\frac{V_j}{U_\infty}\right)^{0.67} \quad \text{for} \quad \frac{s}{d_o} > 3.16 \frac{V_j}{U_\infty} \quad (48)$$

Pratte and Baines recommend a jet width-to-thickness ratio of 1.4 based upon their flow visualization experiments. This value compares to width/thickness ratio $w/\delta \approx 1$ measured by Gerend (Ref. 28), $w/\delta = 4$ recommended by Wooler (Ref. 29) and $w/\delta = 5$ suggested by Abramovich (Ref. 17). Pratte and Baines' $w/\delta = 1.4$ was selected because the test section was considered large enough to represent full-scale jet spreading characteristics and because of superior data repeatability.

In the potential core region, jet width is obtained by interpolating between $w/\delta = 1$ at the origin and $w/\delta = 1.4$ at the end of the potential core. Equations for jet width are

$$\frac{w}{d_o} = \left[1 + 0.4 \frac{s/d_o}{\left(s/d_o\right)_{\text{potential core}}}\right] \frac{\delta}{d_o} \quad \text{for} \quad \frac{s}{d_o} < \left(\frac{s}{d_o}\right)_{\text{potential core}} \quad (49)$$

$$\frac{w}{d_o} = 1.4 \frac{\delta}{d_o} \quad \text{for} \quad \frac{s}{d_o} > \left(\frac{s}{d_o}\right)_{\text{potential core}} \quad (50)$$

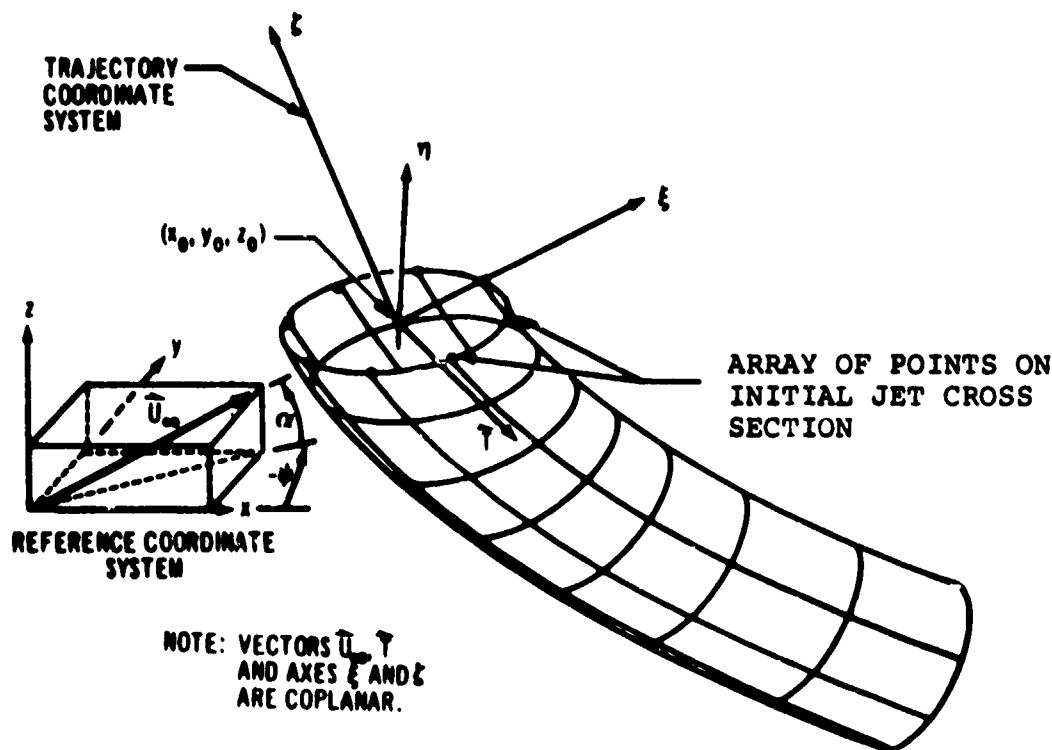
Jet Cross-Section Analysis

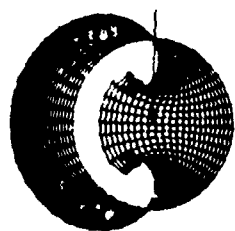
A number of recent theoretical investigations have been made using a theory developed by Chang (Ref. 30 to 33). Chang developed a two-dimensional potential flow theory that predicts the vortex rollup of a cylinder in crossflow. Results of Chang's analysis are shown in Figure 61. The cross section is defined by 48 points and was computed for a velocity ratio $V_j/U_\infty = 8$. Rollup of the cylinder into two counter-rotating vortices is evident. It should be noted that Chang's theory predicts the cross-sectional shape of the jet, but not the trajectory. The cross sections are placed on the trajectory predicted by Ivanov's equation.

Cross sections predicted by Chang's theory are remarkably similar to vortex rollup phenomena observed in flow visualization experiments. Photographs showing vortex rollup are shown in Figure 62. A brief discussion of Chang's theory is given in Appendix I.

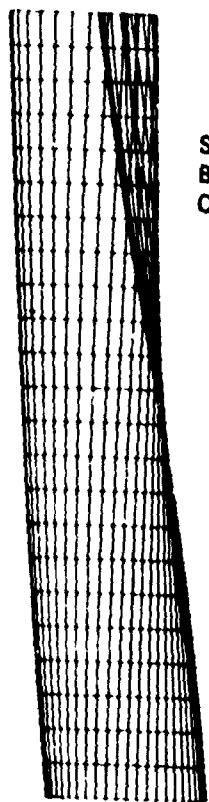
Jet Plume Construction Procedure

The following general procedure is used to construct the jet plume. The freestream velocity vector (defined by angles α and ψ) and the jet initial direction (defined by vector components t_x, t_y, t_z) define a plane, as shown in the following sketch.

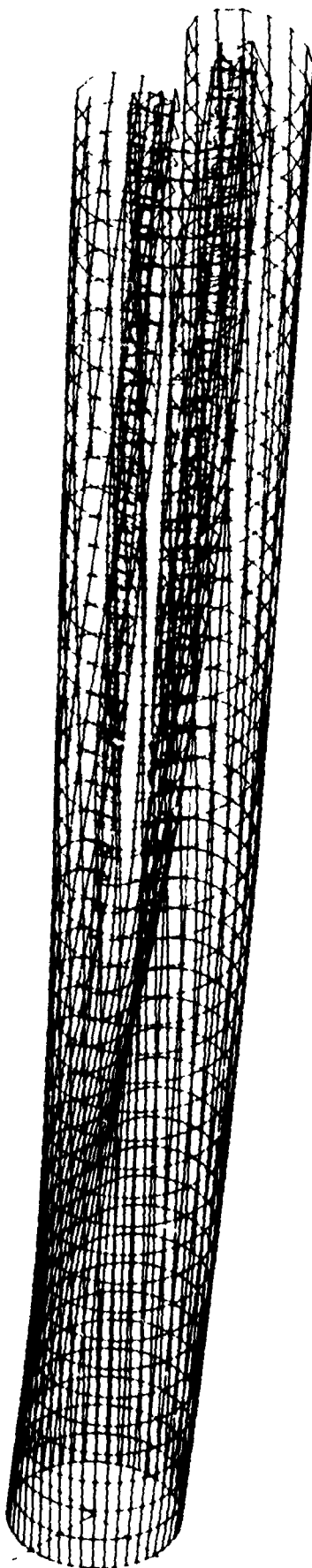




TOP VIEW OF BOTTOM
HALF OF JET



SIDE VIEW OF
BOTTOM HALF
OF JET



ISOMETRIC VIEW

Figure 61: COMPUTER GRAPHIC DISPLAYS OF CHANG
CROSS SECTION FOR $V_{j0}/U_{\infty} = 8$

Approximate value
of q_j/q_{ref}

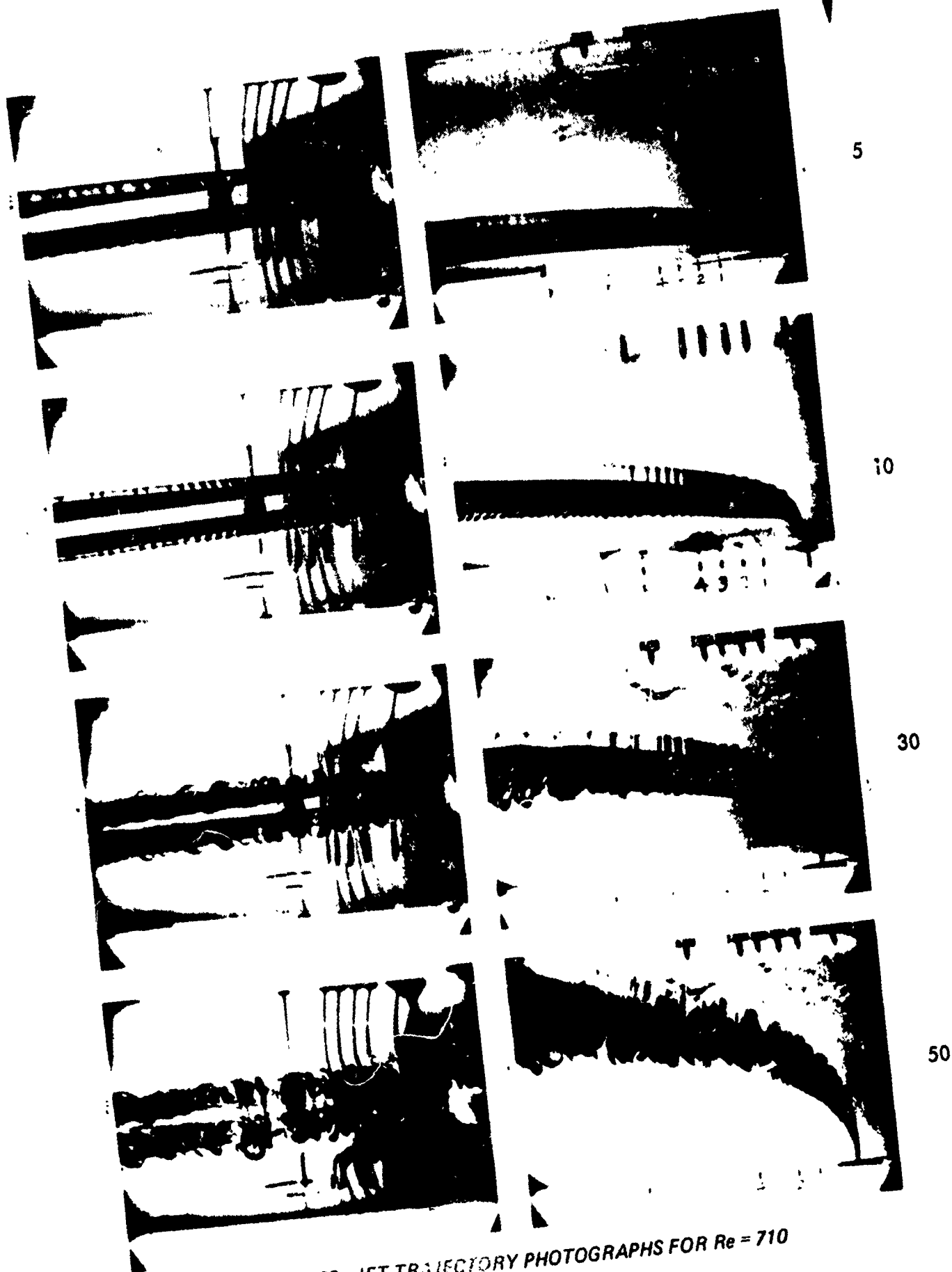
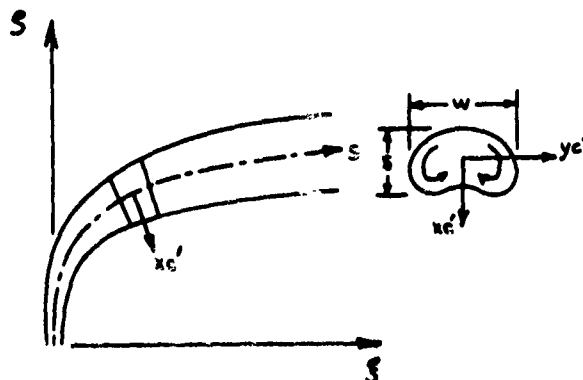


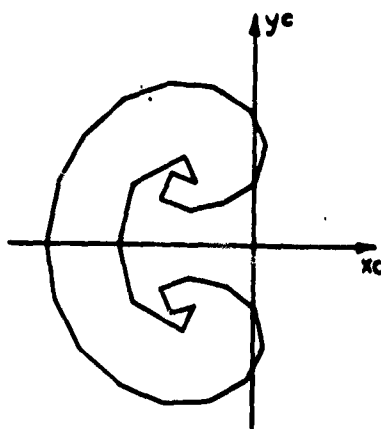
Figure 62: JET TRAJECTORY PHOTOGRAPHS FOR $Re = 710$

The jet centerline is assumed to lie in the plane defined by vectors \vec{U}_∞ and \vec{T} .

Jet cross sections are computed for each station along the jet centerline using Chang's analysis for round or rectangular jets. Thickness and width spreading coefficients are used to define gross deformation of the jet as shown in the following sketch.



The program then centers the cross section on the axis and scales the jet cross-section to the correct size, as shown in the following sketch.



$$\bar{x} = x_{C_{min}} + \frac{\delta}{2} \quad (51)$$

$$\bar{y} = y_{C_{min}} + \frac{\delta}{2} \quad (52)$$

$$x_{c'} = \frac{\delta}{\delta} (x_c - \bar{x}) \quad (53)$$

$$y_{c'} = \frac{w}{\delta} (y_c - \bar{y}) \quad (54)$$

Geometric Capability

The Jet Trajectory and Spreading Program was formulated with considerable flexibility so that it can be applied to a wide variety of TR/TV geometries. The program predicts four types of TR/TV exhaust plumes. Inputs and calculation procedures unique to each jet type are discussed below.

1) TYPE = 1. Circular jet cross-section.

This type of jet models the flow from round nozzles, e.g., three-bearing nozzle, spherical eyeball, or a pure lift engine buried in a fuselage or pod. Inputs for TYPE = 1. are depicted graphically in Figure 63 and summarized in Table V. The calculations use Ivanov's trajectory equation and Pratte and Baines' spreading coefficients. Vortex strengths for Chang's analysis are computed using Equation 11 in Appendix I. A sample case is given in Appendix II.

2) TYPE = 2. Rectangular jet cross-section.

This type of jet is best suited for cascade or target thrust reverser plumes that can be approximated by a rectangular initial cross-section. Inputs for TYPE = 2. are depicted in Figure 64 and summarized in Table VI. The calculations use a hydraulic diameter in Ivanov's trajectory equation

$$d_e = \frac{4(\text{initial area})}{\text{perimeter}} = \frac{2ab}{a+b} \quad (55)$$

where a and b are the length and width of the initial cross-section. Pratte and Baines' empirical jet-spreading coefficients are used for jet thickness and width. Vortex strengths for Chang's analysis are computed from table lookup as described in Appendix I. A sample case is given in Appendix II.

3) TYPE = 3. Two-dimensional jet cross-section.

This type of jet models the flow from a slot nozzle or high aspect ratio rectangular nozzle. Inputs for TYPE = 3. are depicted in Figure 65 and summarized in Table VII. Vizel and Mostinskii's quadratic equation is used for the jet centerline. Pratte and Baines' spreading is used for the jet width. Chang's analysis for the jet cross-section is not used because it was developed for a discrete jet shape, not an infinite jet sheet. A sample case is given in Appendix II.

4) TYPE = 4. Annular jet cross-section.

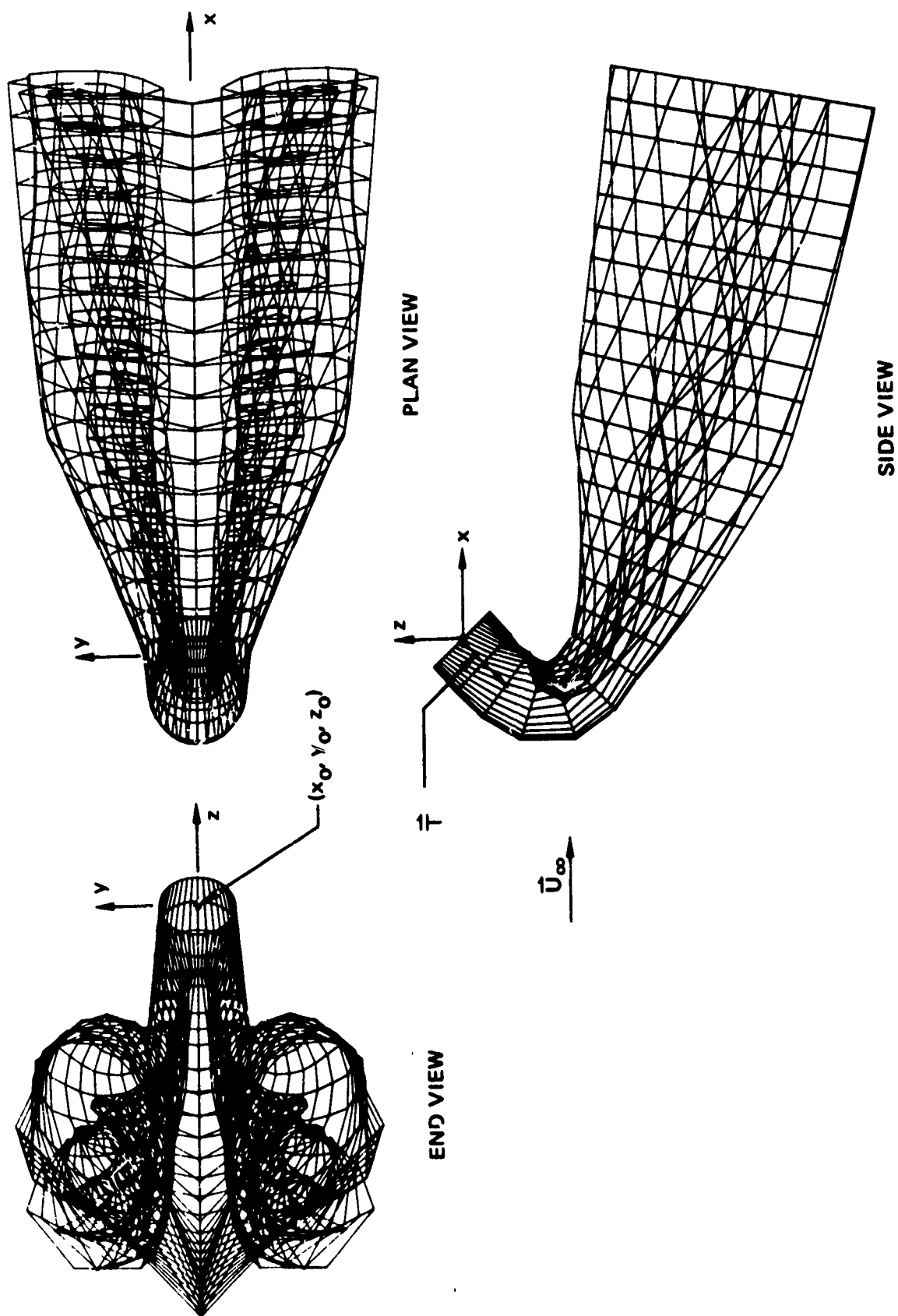


Figure 63: TYPE = 1. CIRCULAR JET CROSS SECTION GEOMETRY

TABLE V INPUTS FOR TYPE = 1., CIRCULAR JET CROSS SECTION

Parameter		Meaning	Units *
Engineering Notation	Program Notation		
TYPE = 1.	TYPE = 1.	indicates circular initial jet cross section	ND
x_o, y_o, z_o	XYZO	jet origin in reference coordinate system	L
t_x, t_y, t_z	TTYZ	vector components defining initial jet direction	ND
D	D	jet initial diameter	L
$\Delta s/D$	DELS D	arc length spacing/initial diameter	ND
q_i/q_∞	QRATI ϕ	jet to freestream dynamic pressure ratio	ND
U_∞	UINF	freestream velocity	L/sec
α	ALPHA	angle of attack	degrees
ψ	PSI	angle of yaw	degrees
PC ϕ DE	PC ϕ DE	punched card code (=0., no cards, = 1., cards)	ND

NOTE: * L indicates length. Any consistent length scale is acceptable, e.g., inches, feet, or meters. ND indicates non-dimensional.

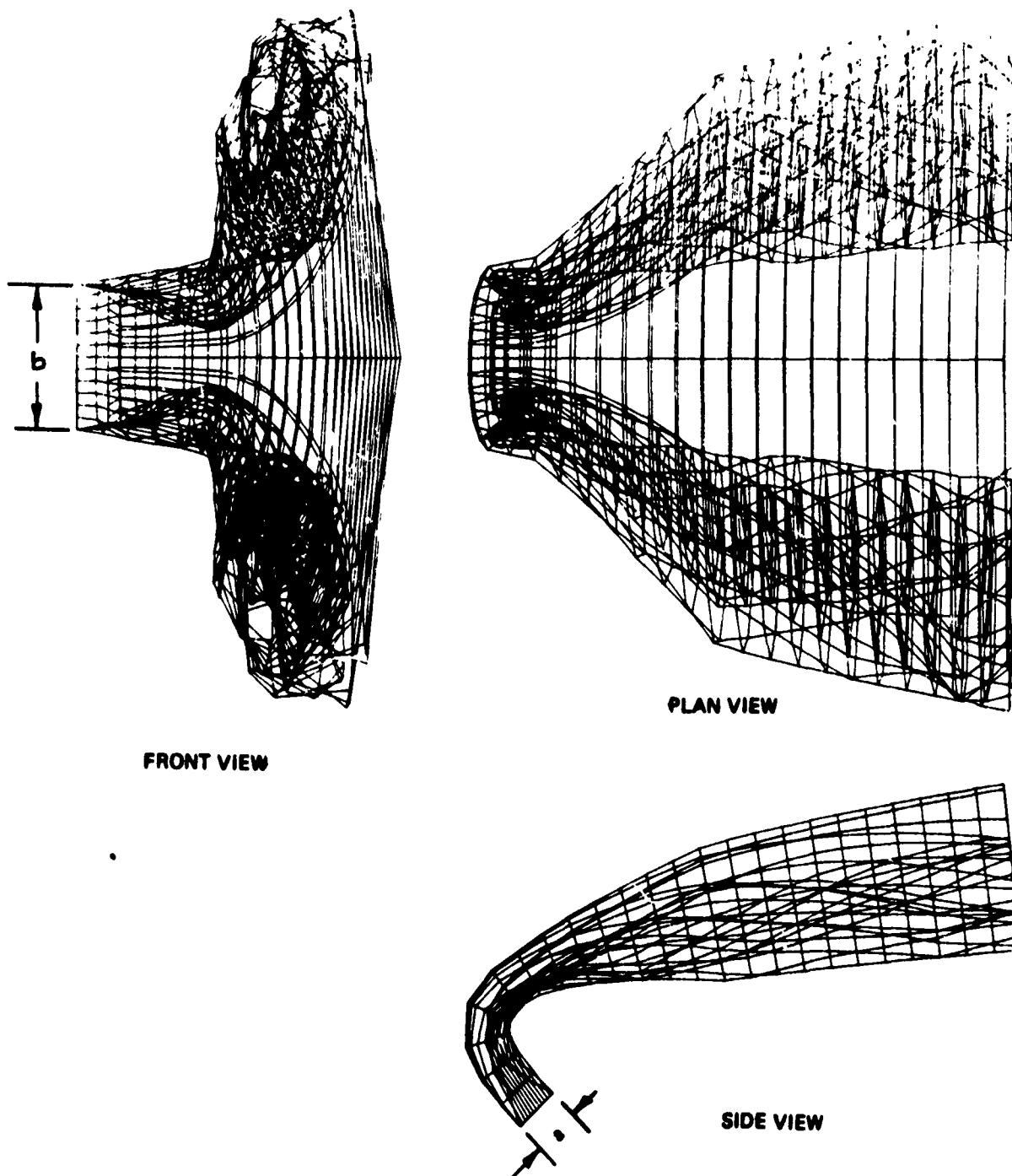
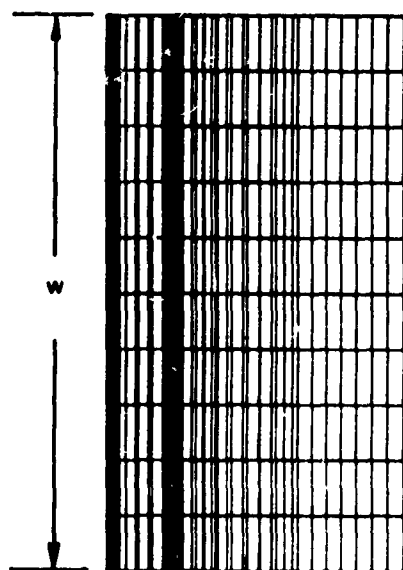


Figure 64: TYPE = 2. RECTANGULAR JET CROSS SECTION GEOMETRY

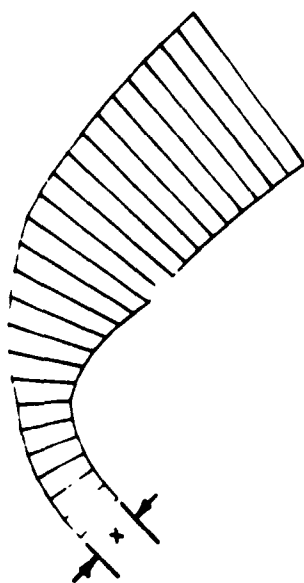
TABLE VI INPUTS FOR TYPE = 2., RECTANGULAR JET CROSS SECTION

Parameter		Meaning	Units *
Engineering Notation	Program Notation		
TYPE = 2.	TYPE = 2.	indicates rectangular initial jet cross section	ND
x_0, y_0, z_0	XYZO	jet origin in reference coordinate system	L
t_x, t_y, t_z	TXYZ	vector components defining initial jet direction	ND
a	A	longitudinal dimension of initial cross section	L
b	B	lateral dimension of initial cross section	L
$\Delta s/De$	DELS	arc length spacing/equivalent diameter	ND
q_j/q_∞	QRATIØ	jet to freestream dynamic pressure ratio	ND
U_∞	UINF	freestream velocity	L/sec
α	ALPHA	angle of attack	degrees
ψ	PSI	angle of yaw	degrees
γ	XNU	skew angle of initial cross section	degrees
PCØDE	PCØDE	punched card code (= 0., no cards, = 1., cards)	ND

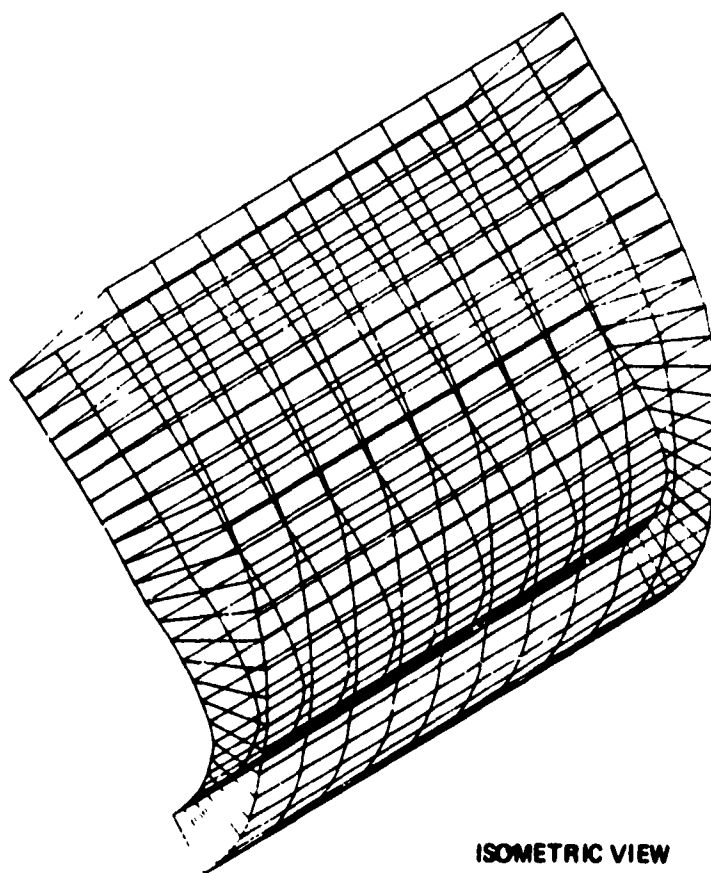
NOTE: * L indicates length. Any consistent length scale is acceptable, e.g., inches, feet, or meters. ND indicates non-dimensional.



PLAN VIEW



SIDE VIEW



ISOMETRIC VIEW

Figure 65: TYPE = 3. TWO DIMENSIONAL JET CROSS SECTION GEOMETRY

TABLE VII INPUTS FOR TYPE = 3., TWO-DIMENSIONAL JET CROSS SECTION

Parameter		Meaning	Units *
Engineering Notation	Program Notation		
TYPE = 3.	TYPE = 3.	indicates two-dimensional initial jet cross section	ND
x_o, y_o, z_o	XYZO	jet origin in reference coordinate system	L
t_x, t_y, t_z	TXYZ	vector components defines initial jet direction	ND
t	T	jet initial thickness	L
w	W	jet initial width	L
$\Delta s/t$	DELS	arc length spacing/jet initial thickness	ND
q_j/q_∞	QRATIØ	jet to freestream dynamic pressure ratio	ND
α	ALPHA	angle of attack	degrees
ψ	PSI	angle of yaw	degrees
PCØDE	PCØDE	punched card code (= 0., no cards; = 1., cards)	ND

NOTE: *L indicates length. Any consistent length scale is acceptable, e.g., inches, feet, or meters. ND indicates non-dimensional.

This type of jet models the flow from annular target or cascade thrust reversers. Inputs for TYPE = 4. are depicted in Figure 66 and summarized in Table VIII. The calculations use Vizel and Mostinskii's trajectory equation and Pratte and Baines' thickness spreading coefficient. Chang's analysis is not applicable for annular shaped jets.

As shown in Figure 66, the output consists of the plume front surface, centerline, and rear surface at a number of radial cutting planes. Origins of the jet arms lie in a plane perpendicular to the \vec{a} vector. Their position in that plane is defined by initial radius R and clock angle θ .

The four types of jets offer sufficient geometric capability for most thrust reverser and vectoring nozzle designs.

Each type of jet requires certain inputs describing the jet's position and orientation in space. All inputs and outputs are made in an airplane (x,y,z,) reference coordinate system defined in Figure 63. The x axis is parallel to the body of the airplane, the y axis is in the spanwise direction of the right half of the wing, and the z axis is upward. The origin is chosen at any convenient point, usually at the airplane nose. The angles of attack and yaw are defined in terms of the direction of the freestream with respect to the reference coordinate system, as shown by the sketch on page 85.

2.2.2 Reingestion Prediction Program

Reingestion occurs when the deflected TR and TV exhaust flow penetrates forward into the freestream flow and is captured by the inlet flow. Pressure and temperature distortions caused by reingestion of the exhaust flow reduce engine thrust and compressor stall margin and can lead to engine surge.

The purpose of the Reingestion Prediction Program is to predict the occurrence of reingestion for arbitrary thrust reverser and airplane configurations as a function of geometry and flow conditions. The program is intended for use as a diagnostic tool to predict severe reingestion problems. The program does not predict inlet temperature rise or the relative severity of reingestion. However, the program printout is designed such that in many cases judgment can be made about the relative severity of reingestion.

In order to develop reingestion prediction methods, reingestion was classified into four categories:

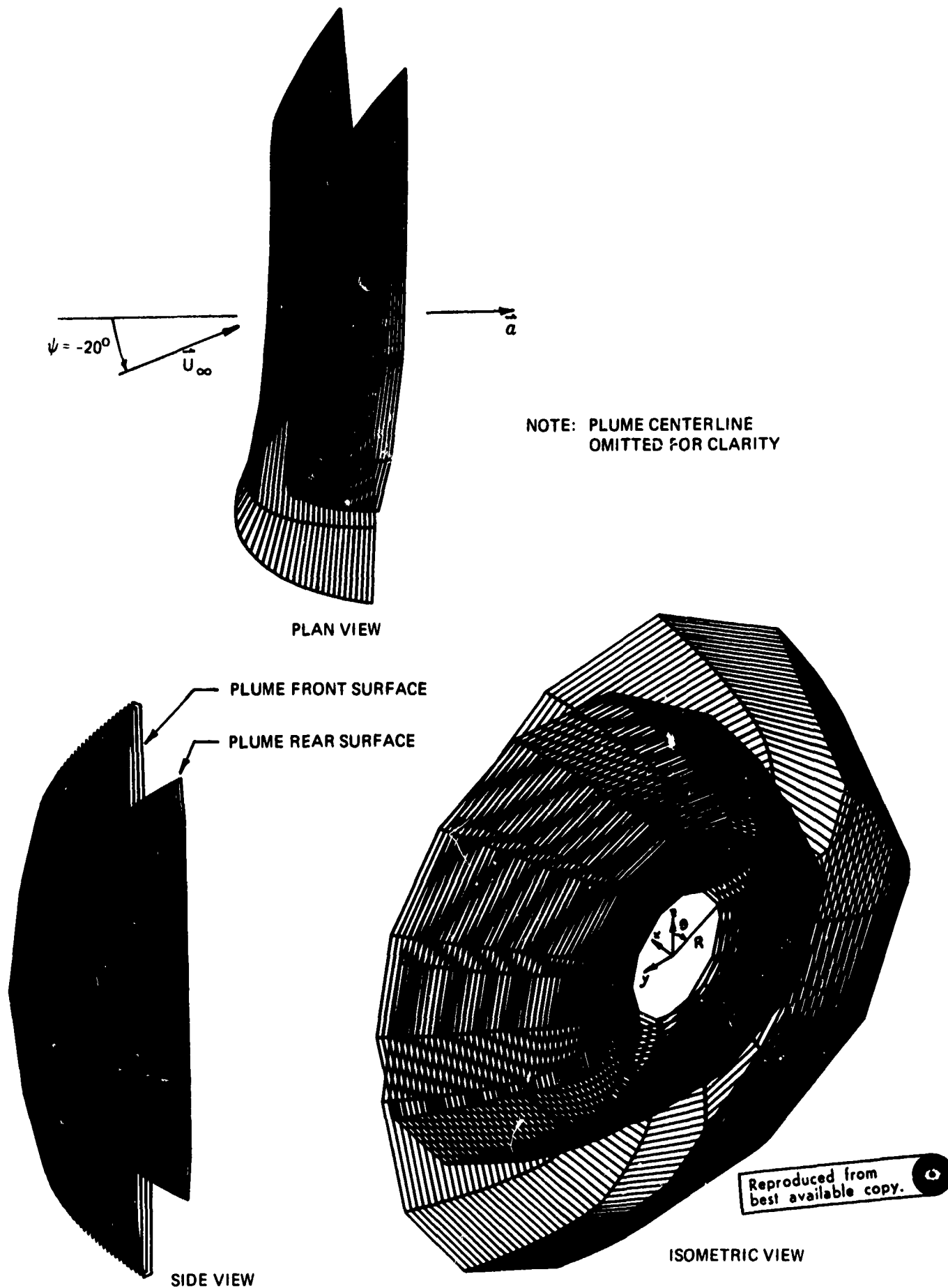


Figure 66: TYPE = 4. ANNULAR JET CROSS SECTION GEOMETRY

TABLE VIII INPUTS FOR TYPE = 4., ANNULAR JET CROSS SECTION

Parameter		Meaning	Units *
Engineering Notation	Program Notation		
TYPE = 4.	TYPE = 4.	indicates annular jet cross section	ND
x_a, y_a, z_a	XYZA	origin of annular jet coordinate system	L
a_x, a_y, a_z	AXYZ	vector components defining cruise nozzle direction	ND
t	T	jet initial thickness	L
r	R	annular jet initial radius	L
$\Delta s/t$	DELS	arc length spacing/jet initial thickness	ND
MR	MR	number of annular jet arms	ND
θ	THETA	arm clock angle	degrees
β	BETA	flow turning angle	degrees
q_j/q_∞	QRATIO	jet to freestream dynamic pressure ratio	ND
α	ALPHA	angle of attack	degrees
ψ	PSI	angle of yaw	degrees
PCODE	PCODE	punched card code (= 0., no cards; = 1., cards)	ND

NOTE: * L indicates length. Any consistent length scale is acceptable, e.g., inches, feet, or meters. ND indicates non-dimensional.

- o Crossflow reingestion
- o Self or closed loop reingestion
- o Near-field fountain reingestion
- o Far-field fountain reingestion

The computer program treats each category of reingestion separately. Computer program inputs are the TR/TV and inlet geometry and flow conditions as diagrammed in Figure 67. Output consists of diagnostic statements predicting whether or not reingestion occurs for the case in question. Methods used to predict each category of reingestion are discussed below.

Crossflow Reingestion

Crossflow reingestion occurs when the exhaust flow from one engine is captured by the inlet flow of an adjacent engine. The most common occurrence of crossflow reingestion is in the outboard engine of a four-engine airplane, as shown in Figure 68.

The method used to predict crossflow reingestion employs thrust reverser exhaust plumes calculated by the Jet Trajectory and Spreading Program. The exhaust plumes are checked for intersections with inlet streamtubes. The program prints out the number of points intersecting an inlet streamtube at each jet station.

To predict crossflow reingestion, definition of the inlet streamtube is required. Streamtubes were calculated for a representative STOL transport inlet using axisymmetric compressible potential flow program TEM-095 (Ref. 34). The inlet hilite to throat contraction ratio is approximately 1.3, diffuser angle equals 5 degrees, and throat Mach is 0.6. Computer-generated plots of streamlines and symbols indicating Mach contours are shown in Figures 69 and 70 for free-stream velocities of 2 and 10 knots, respectively. For low freestream velocities, the stagnation streamline attaches on the cowl outer surface far downstream of the cowl leading edge.

The stagnation streamline defines the pre-entry streamtube used in predicting crossflow reingestion. Streamtubes are summarized in Figure 71 for inlet hilite to freestream velocity ratio from 137.3 to 2.5. Streamtubes for other velocity ratios are obtained by quadratic interpolation or extrapolation to obtain the streamtube radius R at any station.

Arbitrary crosswind angle is accounted for by aligning the axisymmetric streamtube in the direction of the freestream flow, as shown in Figure 72. A local inlet coordinate system is constructed along the streamtube axis. The (x,y,z) coordinates of the exhaust plume computed by the Jet Trajectory and Spreading Program are transferred into this inlet coordinate system and checked for possible intersections.

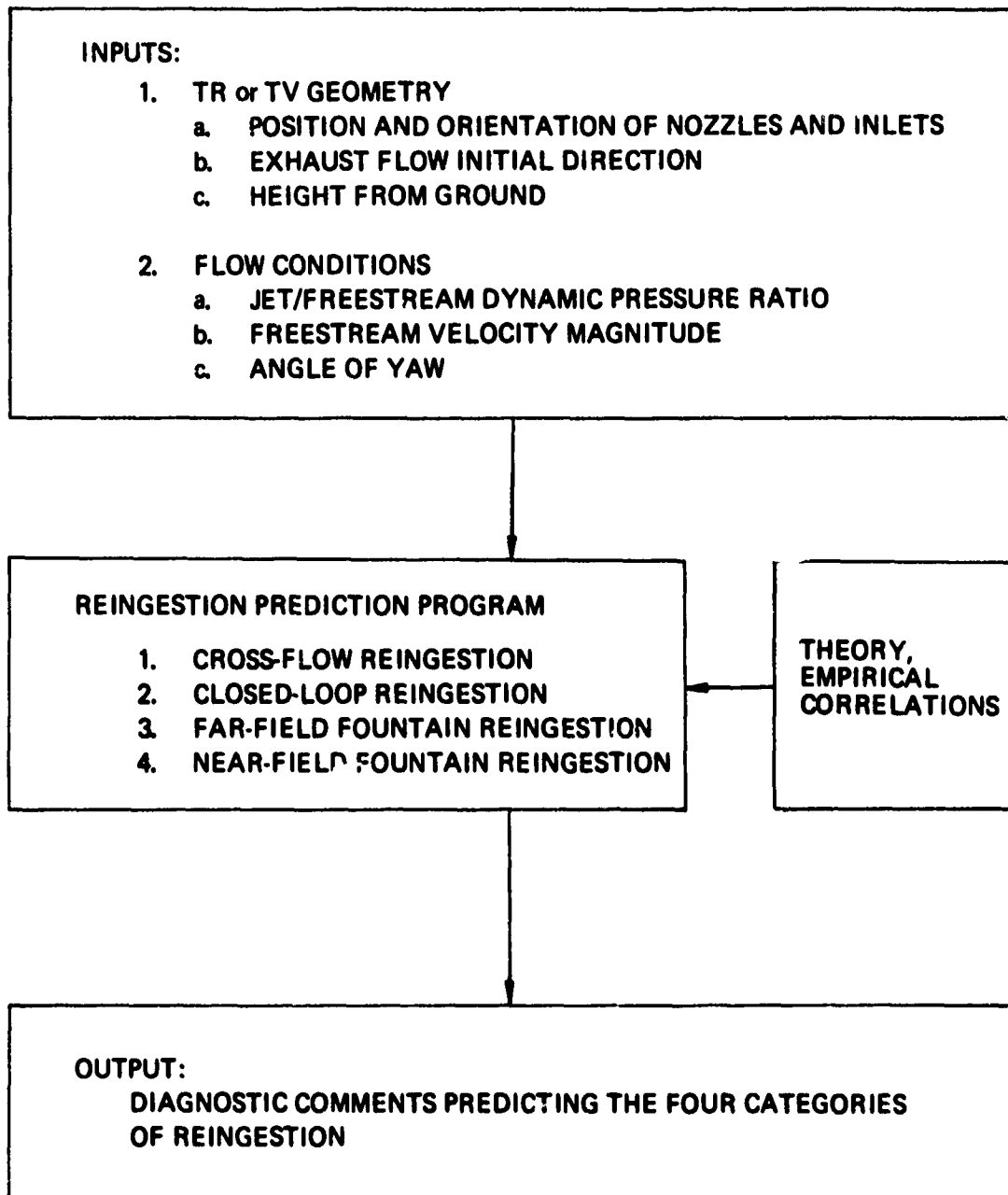


Figure 67: REINGESTION PREDICTION PROGRAM DIAGRAM

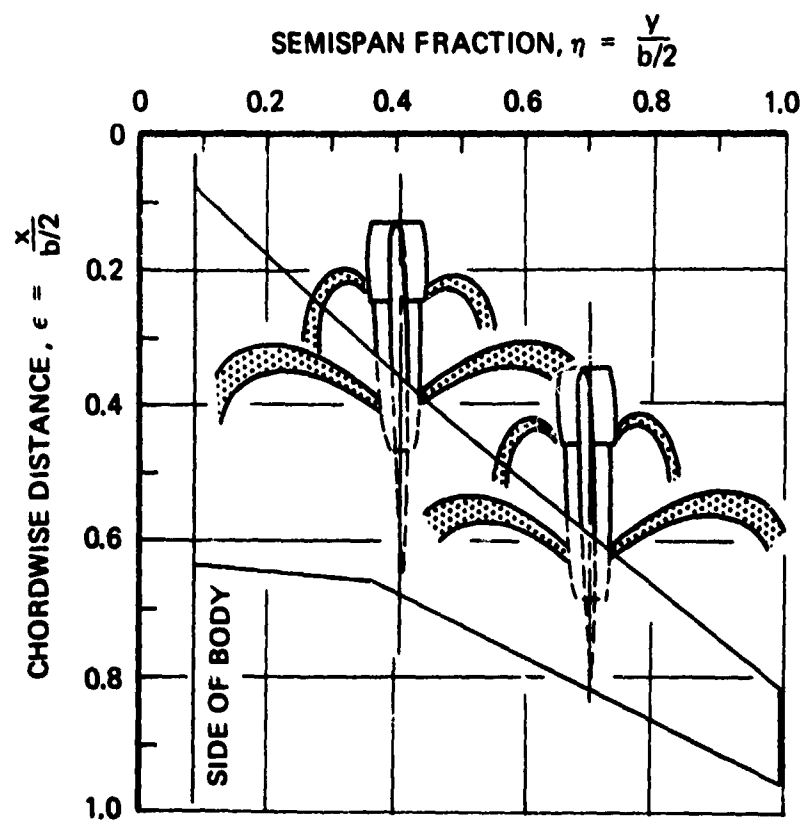


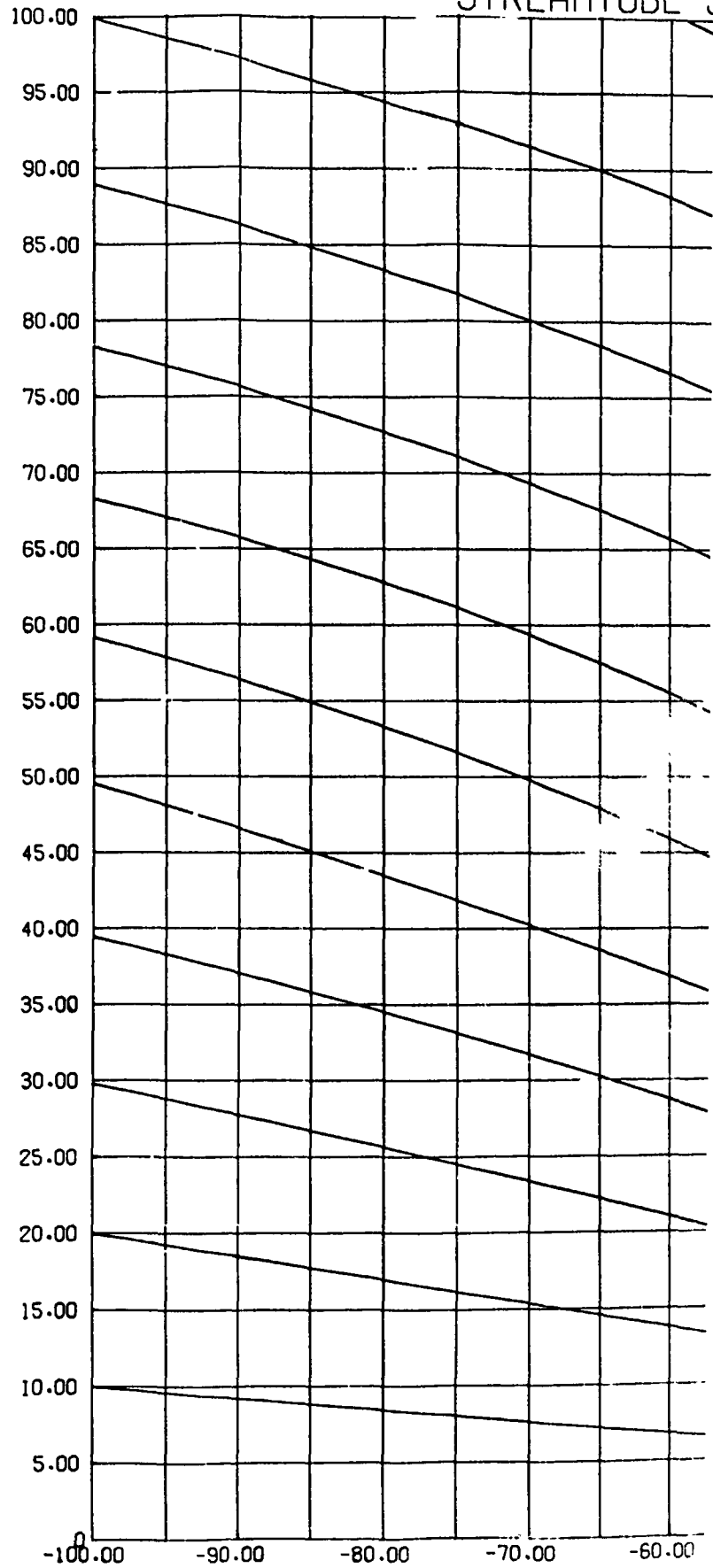
Figure 68: CROSS FLOW REINGESTION

A

SYMBOL MACH NO.

□	.2
○	.3
△	.4
+	.5
x	.6
◇	.7
+	.8

STREAMTUBE S



SHAPES FOR COWL NUMBER C3 CASE 1 $U_{\infty} = 2$ KNOTS $V_{WILITE} / U_{\infty} = 139.33$ M_{THROAT}

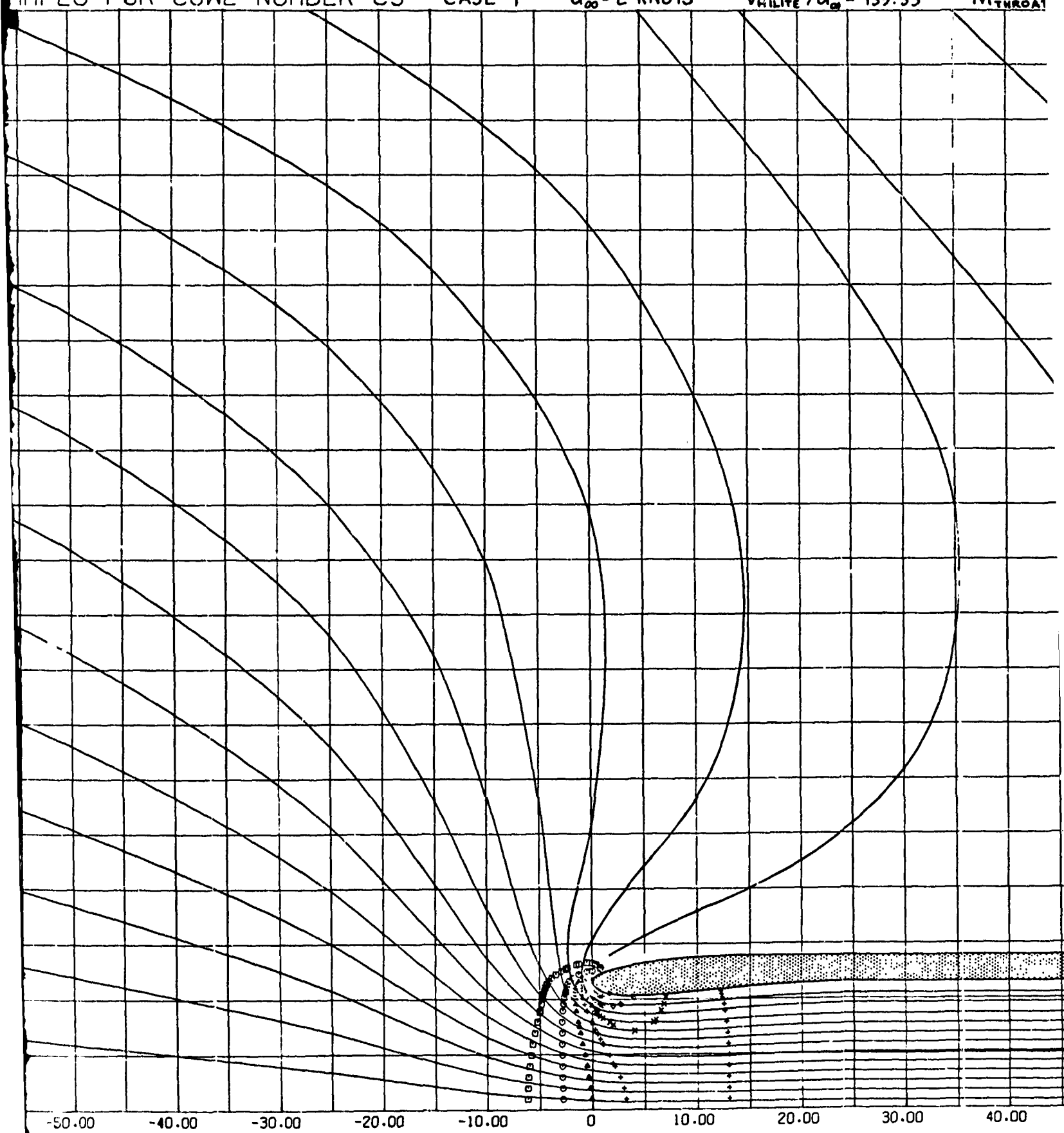


Figure 69

TS

$$V_{HILITE} / u_{\infty} = 139.33$$

$$M_{THROAT} = 0.6$$

$$P_{AA.B} = 14.696 \text{ LBF/IN.}^2$$

$$T_{AMB} = 93^{\circ}\text{F}$$

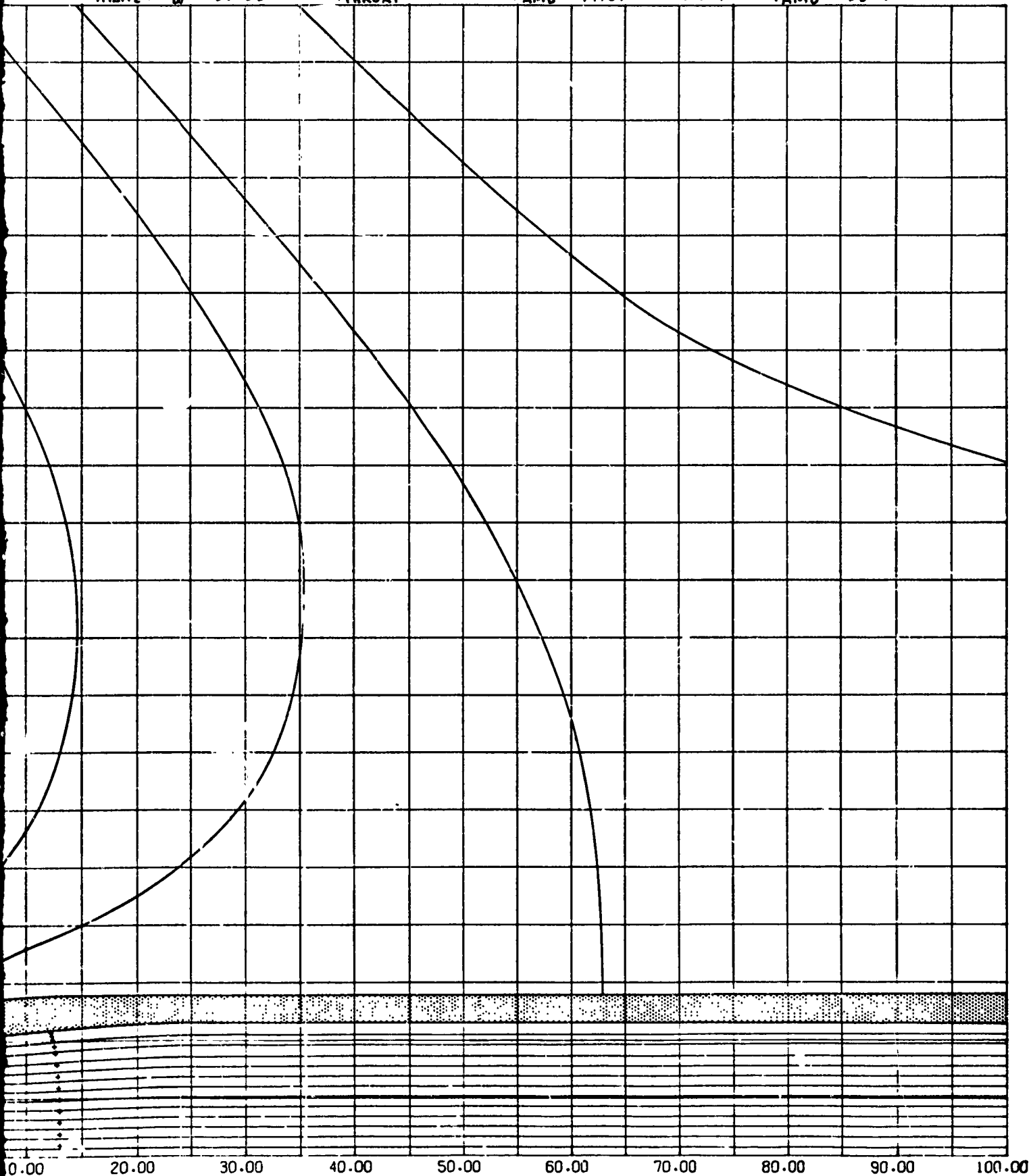
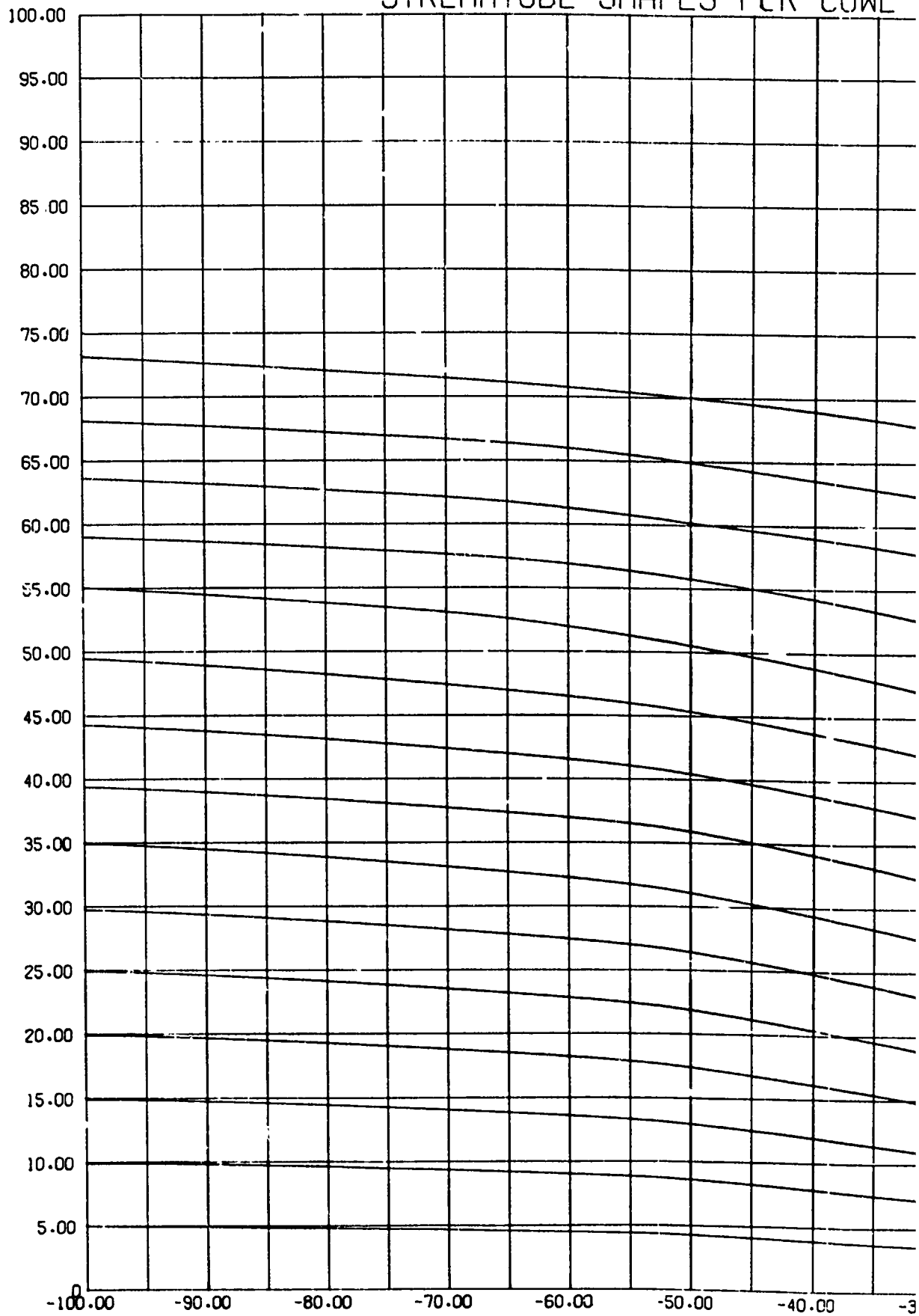


Figure 69: STREAMLINES AND MACH CONTOURS FOR STOL
TRANSPORT INLET

STREAMTUBE SHAPES FOR COWL

71
SYMBOL MACH NO.

□	.2
○	.3
△	.4
+	.5
×	.6
◇	.7
↑	.8



NUMBER C3

CASE 2

$U_{\infty} = 10$ KNOTS

$V_{NILITE} / U_{\infty} = 27.87$

$M_{THROAT} = 0.6$

$P_{AMB} = 14$

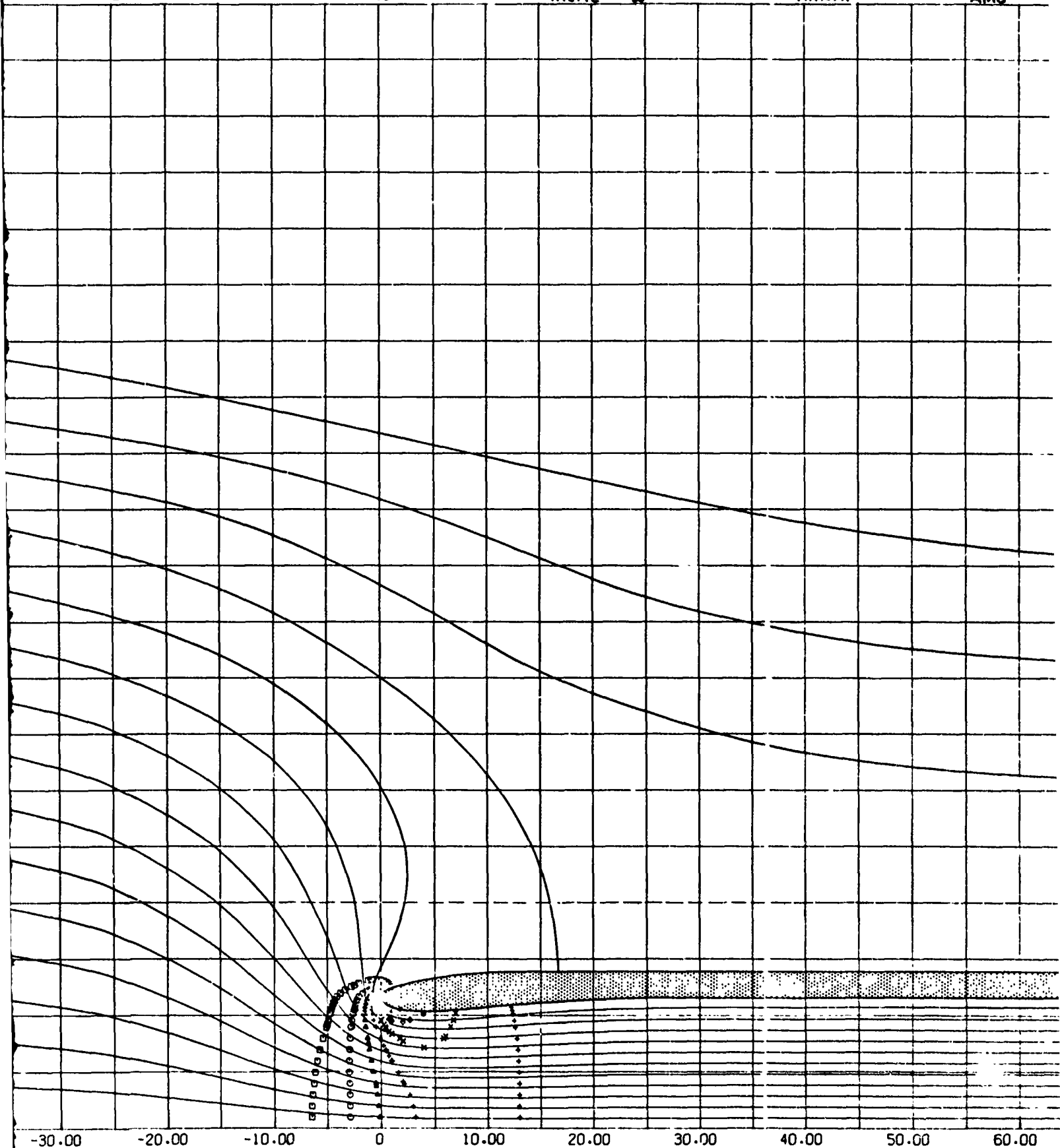


Figure 70: STREAM
TRANSP

$V_{HILITE} / u_{\infty} = 27.87$

$M_{THROAT} = 0.6$

$P_{AMB} = 14.696 \text{ LBF/IN}^2$

$T_{AMB} = 93^{\circ}\text{F}$

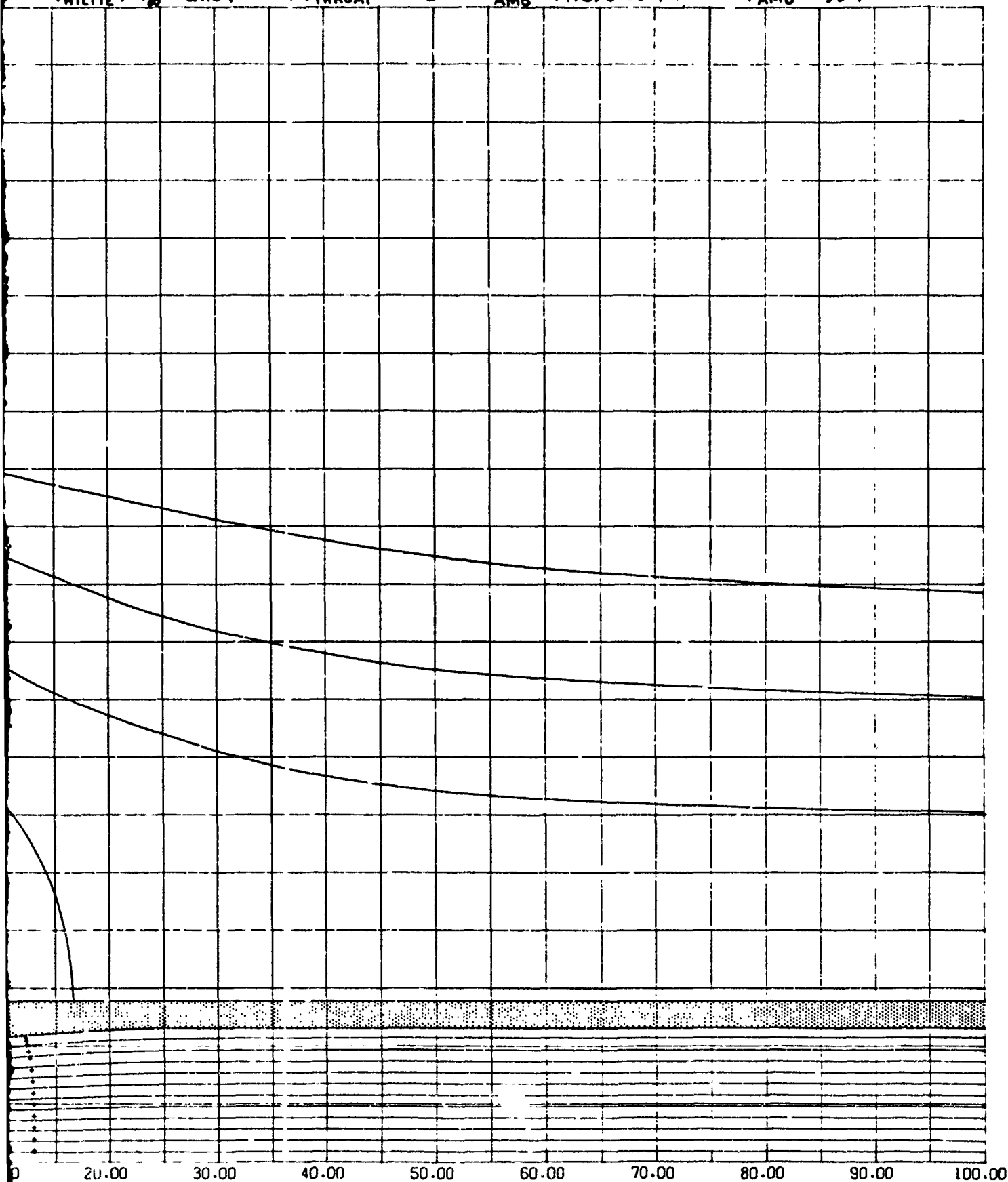


Figure 70: STREAMLINES AND MACH CONTOURS FOR STOL TRANSPORT INLET

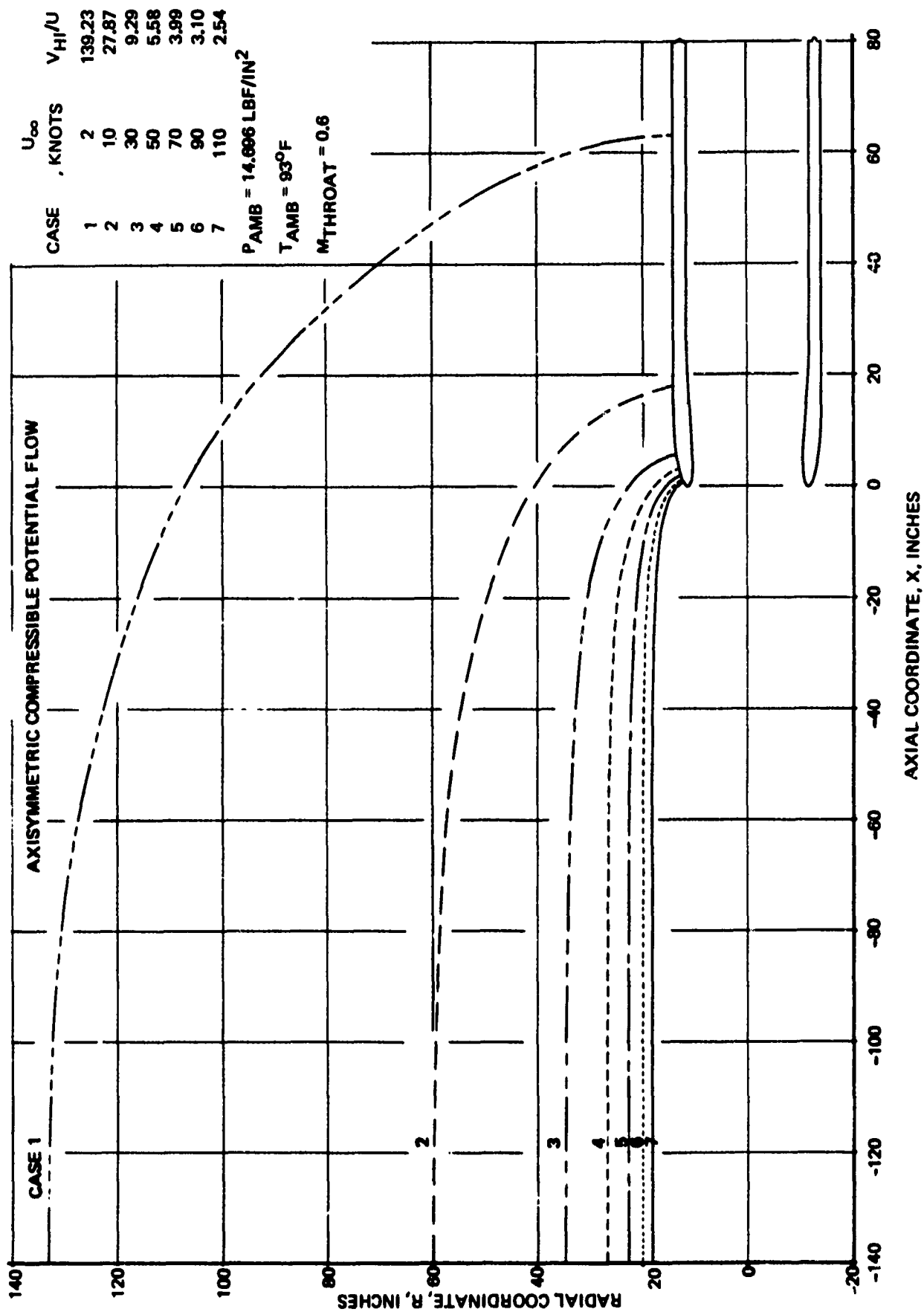
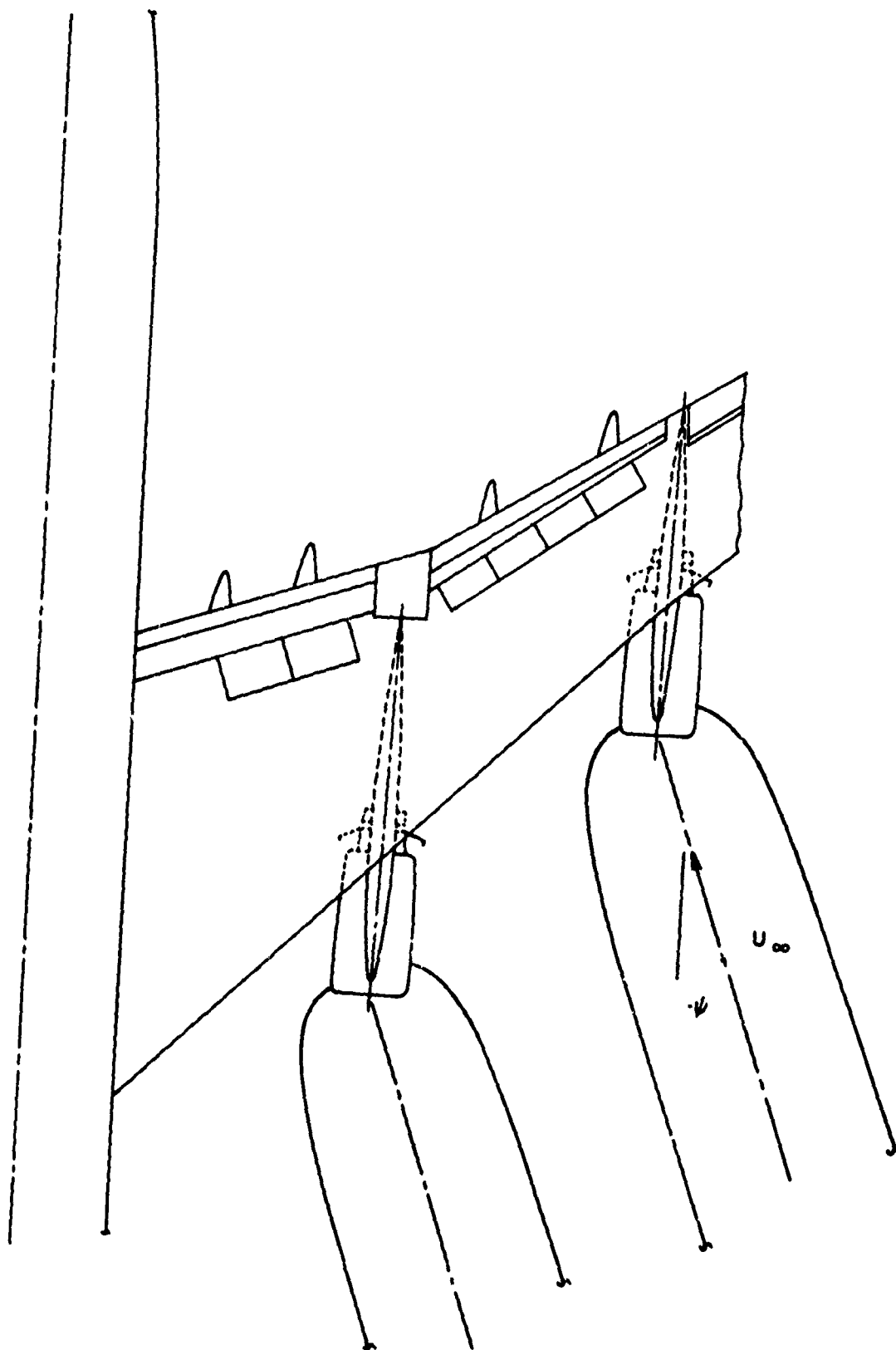


Figure 71: EFFECT OF INLET VELOCITY RATION ON PRE-ENTRY STAGNATION STREAMTUBES FOR A REPRESENTATIVE STOL TRANSPORT INLET



**Figure 72: ALIGNMENT OF THE INLET STREAMTUBE
COORDINATE SYSTEM WITH THE FREESTREAM
VELOCITY VECTOR**

Existing jet penetration data (Ref. 35) show that the thrust reverser plume is extremely unsteady and that large turbulent fluctuations occur in the mixing region with the freestream flow. To account for flowfield unsteadiness in predicting crossflow reingestion, the correlation shown in Figure 73 is used. Data are shown for the jet maximum penetration point (MPP) as a function of velocity ratio and discharge angle. The scatter radius is given by

$$\left(\frac{r_s}{d}\right)_{MPP} = 2 + 0.45 \left(\frac{V_j}{U_\infty}\right)^{0.94} \left[1 - 0.734 (\sin \theta)^{0.685}\right] \quad (57)$$

From the nozzle exit to the MPP, a linear interpolation is used to obtain scatter radius.

$$\frac{r_s}{d} = \frac{s/d}{(s/d)_{MPP}} \left(\frac{r_s}{d}\right)_{MPP} \quad \text{for } \frac{s}{d} < \left(\frac{s}{d}\right)_{MPP} \quad (58)$$

Downstream of the maximum penetration point, the scatter radius at the MPP is used

$$\frac{r_s}{d} = \left(\frac{r_s}{d}\right)_{MPP} \quad \text{for } \frac{s}{d} \geq \left(\frac{s}{d}\right)_{MPP} \quad (59)$$

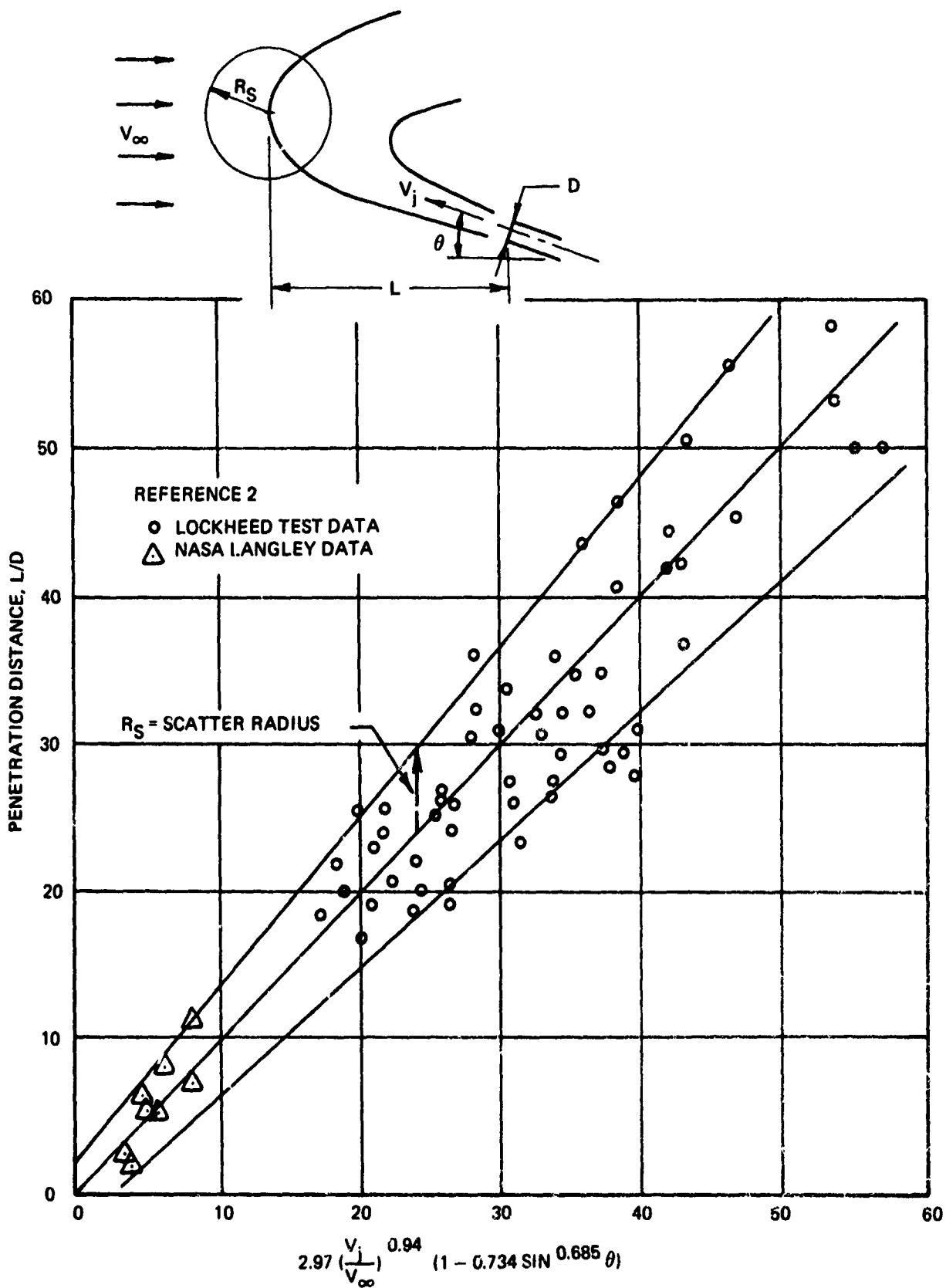
The scatter radius is a measure of uncertainty in predicting the plume's position due to large-scale turbulent fluctuations of exhaust flow. Because of this uncertainty, the plume's forward boundary is increased by the scatter radius. The adjusted plume surface is checked for crossflow reingestion.

Crossflow reingestion results are shown in Figure 74. The configuration is an early version of the 747 airplane with long duct nacelles and annular target thrust reversers. The configuration was tested for reingestion characteristics in a low-speed wind tunnel test. The computer program predicts crossflow reingestion at about 90 knots. The wind tunnel test indicated crossflow reingestion at 90 knots (Ref. 36).

The main limitation to the crossflow prediction method is that inlet and exhaust flows are assumed to act independently. Effects of inlet suction on the exhaust flow are not included. Mutual interactions between impinging jet flows are also not included.

Self or Closed Loop Reingestion

Self or closed loop reingestion occurs when the TR or TV exhaust flow forms a continuous closed path back into the engine inlet. Two types of self-reingestion are shown in



**Figure 73: JET PENETRATION CORRELATION
ILLUSTRATING DATA SCATTER DUE TO
TURBULENT FLUCTUATIONS OF FLOW**

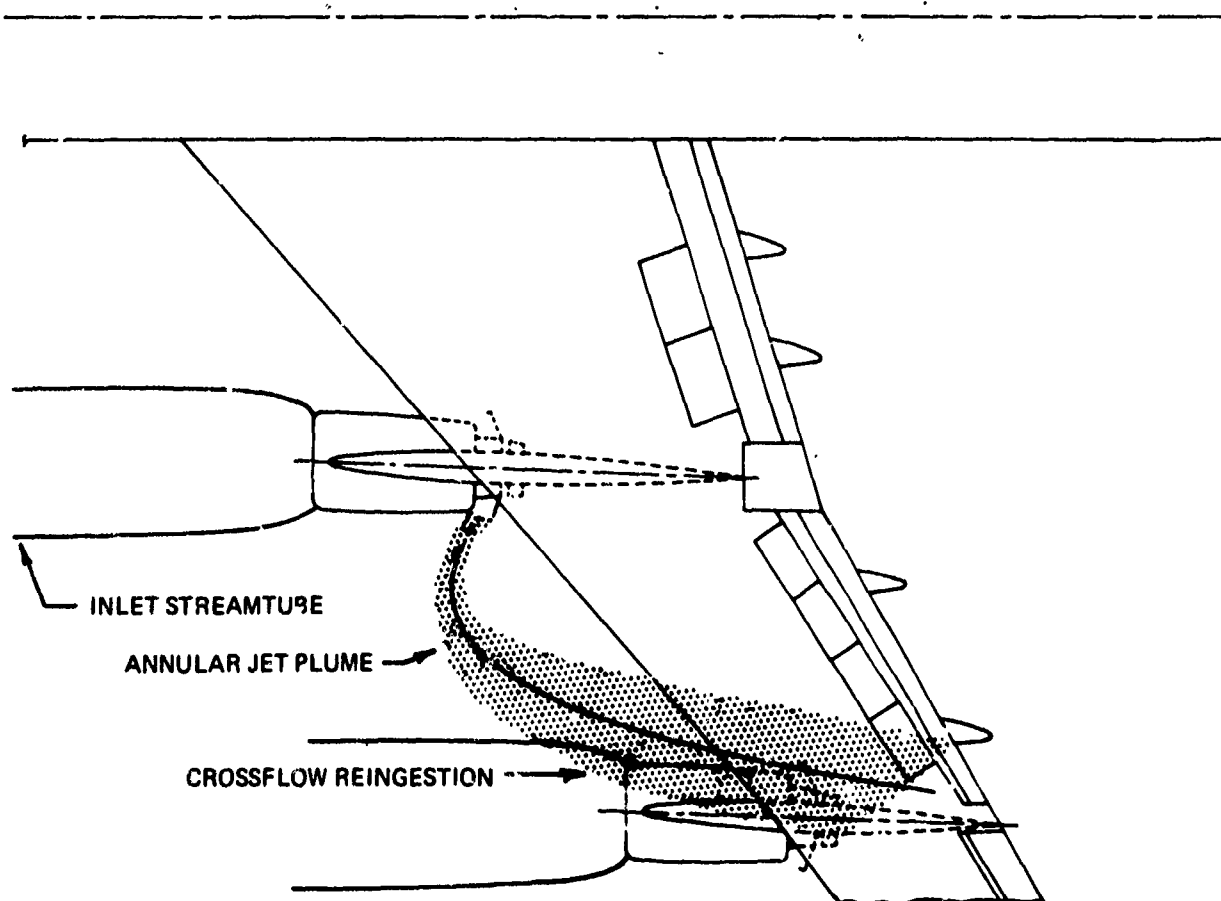


Figure 74: CROSSFLOW REINGESTION RESULTS FOR 90 KNOTS FREESTREAM VELOCITY

Figure 75. The first type is caused by the thrust reverser exhaust flow attaching to the cowl surface and penetrating forward into the oncoming flow, where it is captured by the inlet flow. For the second type, the exhaust flow does not attach to the cowl, but the proximity of inlet and nozzle causes exhaust flow to be captured. This type of self-reingestion is treated by the procedure discussed previously for crossflow reingestion.

In order to predict self-reingestion due to exhaust flow reattachment, it was first necessary to develop reattachment criteria. For a two-dimensional jet discharging obliquely from a plate, it is well known that under certain conditions the jet bends towards the plate and reattaches due to reduced pressures caused by entrainment in the separation bubble. As shown by the data in Figure 76, the jet will always be separated for discharge angles greater than about 60 degrees. As the discharge angle decreases, the value of plate length over slot width required for attached flow also decreases. Figure 76 is used to predict reattachment for two-dimensional and annular jets (TYPE = 3. and 4.).

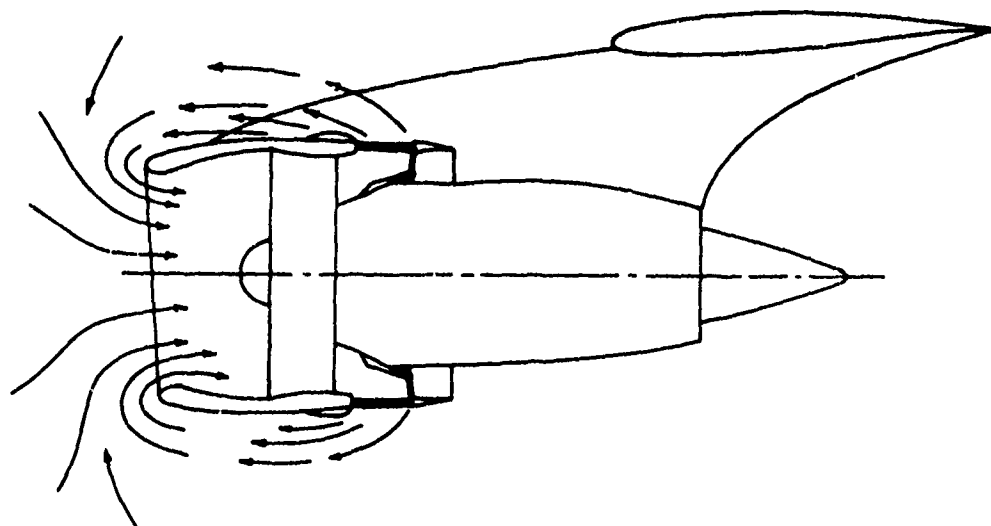
The reattachment of a three-dimensional and annular jet behaves differently from a two-dimensional jet. Freestream flow enters the separation bubble from the side as illustrated in Figure 77, thus relieving reduced pressures in the bubble. Presence of a counterflow further complicates the flow field. Considerable effort was made in searching for data or theory to predict the reattachment of a three-dimensional jet. No theory and very little data were discovered. Test data from an SST thrust reverser concept with a 30-degree discharge angle revealed a strong reattachment under static conditions. A schematic of the thrust reverser and flow field is shown in Figure 78a. Oil flow visualization proved that reattachment occurred along the centerline of the second door as shown in Figure 78b.

Reingestion testing conducted during the development of the 707 cascade thrust reverser resulted in the following general criteria for jet discharge angles

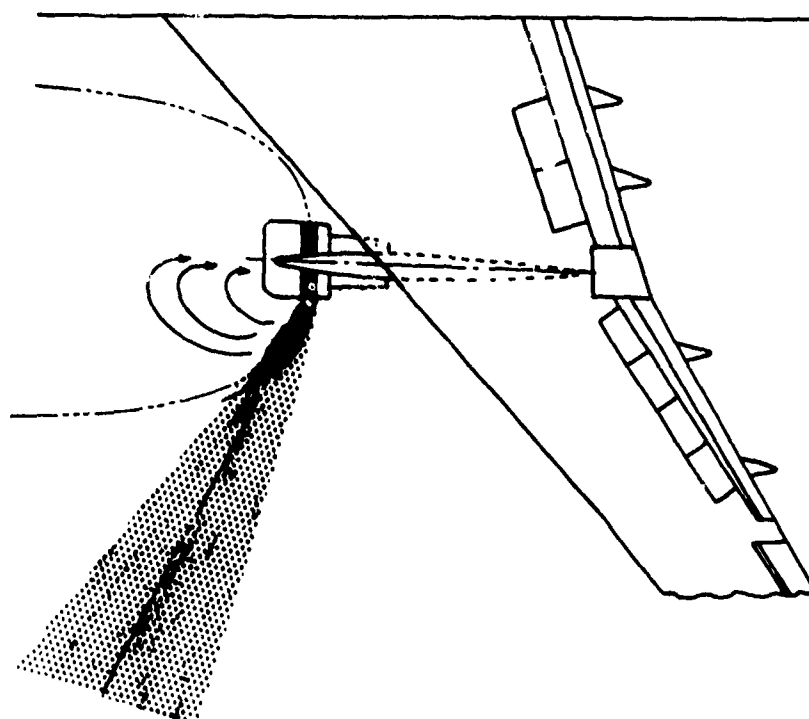
$$\theta = \begin{cases} 55 \text{ degrees, jet will no reattach} \\ 45 \text{ degrees, jet may or may not reattach} \\ 30 \text{ degrees, jet will reattach} \end{cases} \quad (60)$$

Based on the 707 and SST test data, the criteria given by Equation (60) are used to predict reattachment for discrete jets (TYPE = 1. and 2.).

No method has been developed to predict whether or not reingestion occurs once a jet has reattached to the cowl. Conceivably, it could separate again in presence of a strong counterflow. Experience has shown, however, that reingestion



a) SELF REINGESTION DUE TO THRUST REVERSER EXHAUST FLOW ATTACHMENT ON COWL SURFACE



b) SELF REINGESTION DUE TO PROXIMITY OF INLET AND THRUST REVERSER NOZZLE

Figure 75: SELF REINGESTION

SYMBOL REFERENCE

- ⊙ BOURQUE AND NEWMAN, REF 37
- NACA TN 4272, NACA TN 4377, REF 38

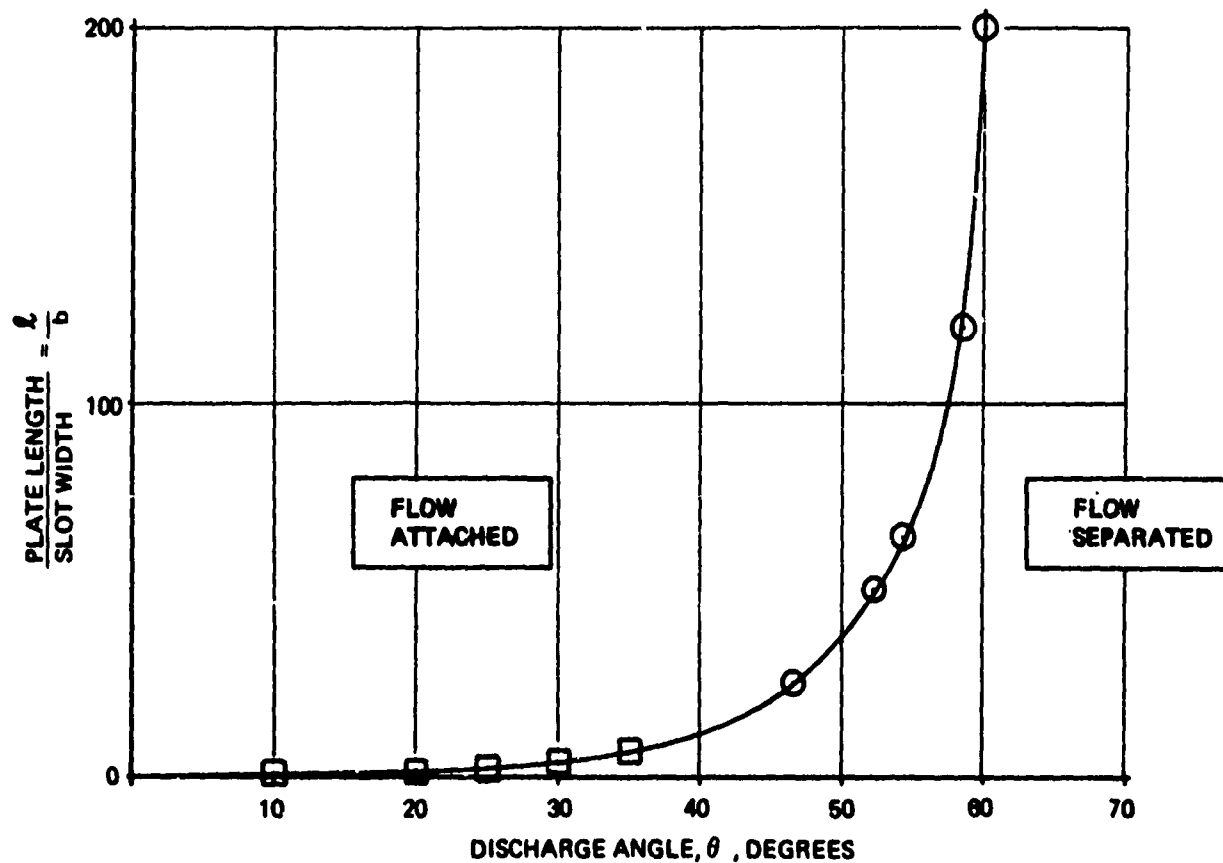
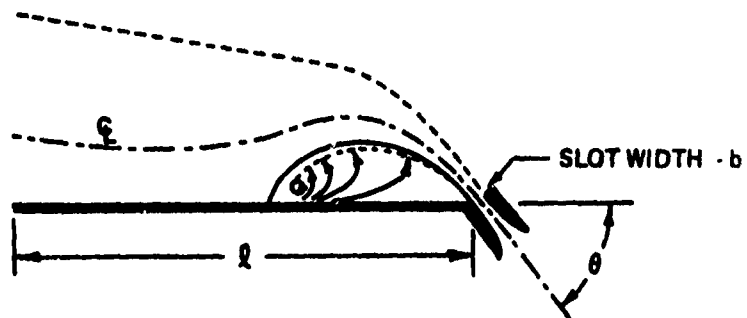


Figure 76: EFFECT OF DISCHARGE ANGLE AND PLATE LENGTH ON THE REATTACHMENT OF A TWO DIMENSIONAL INCOMPRESSIBLE JET

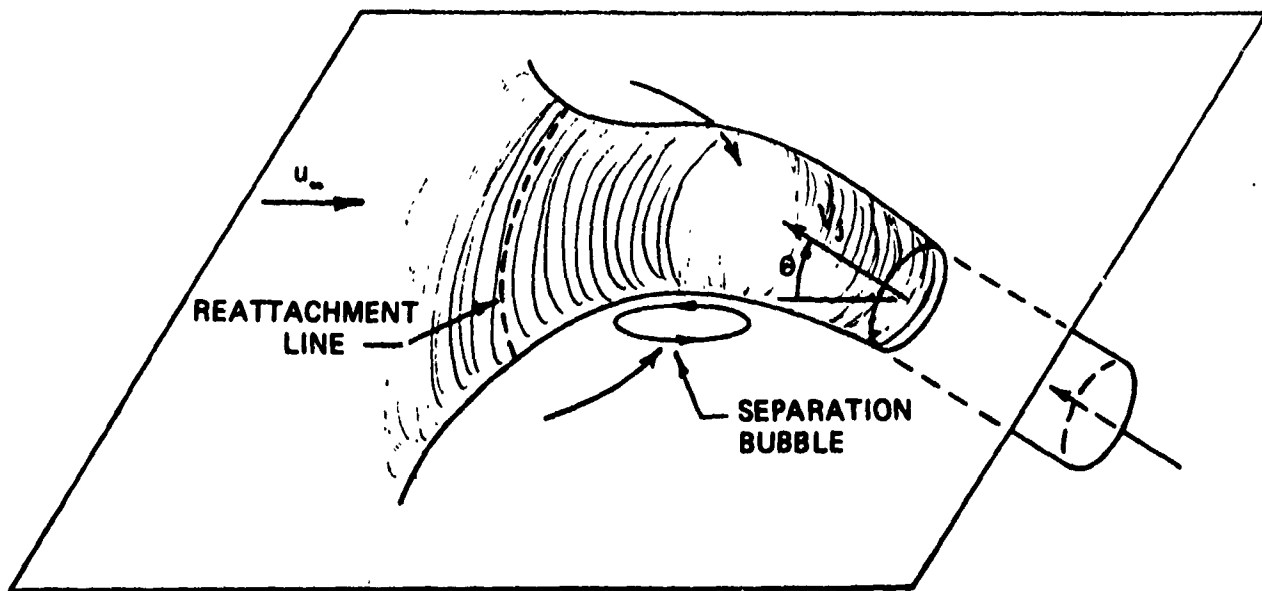
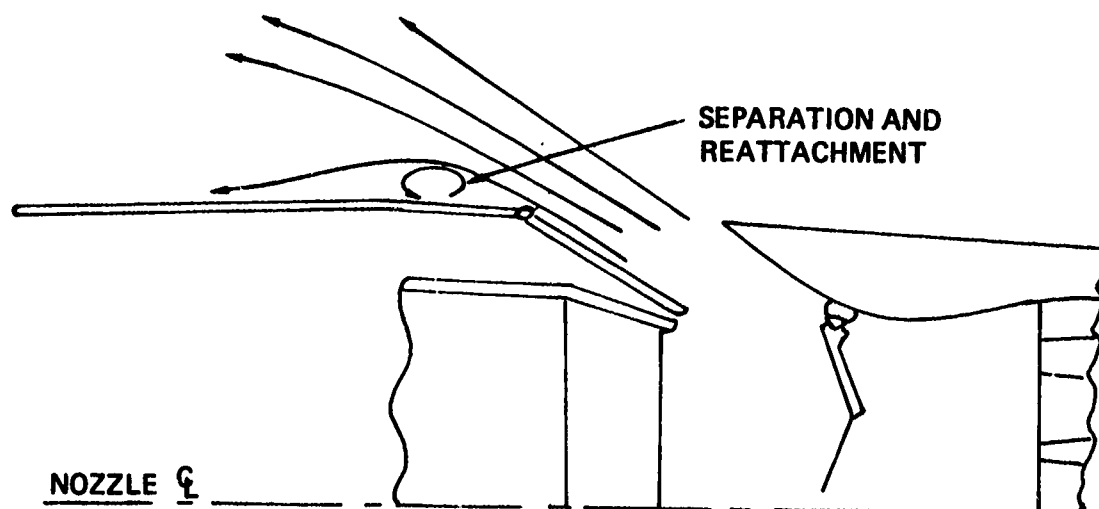
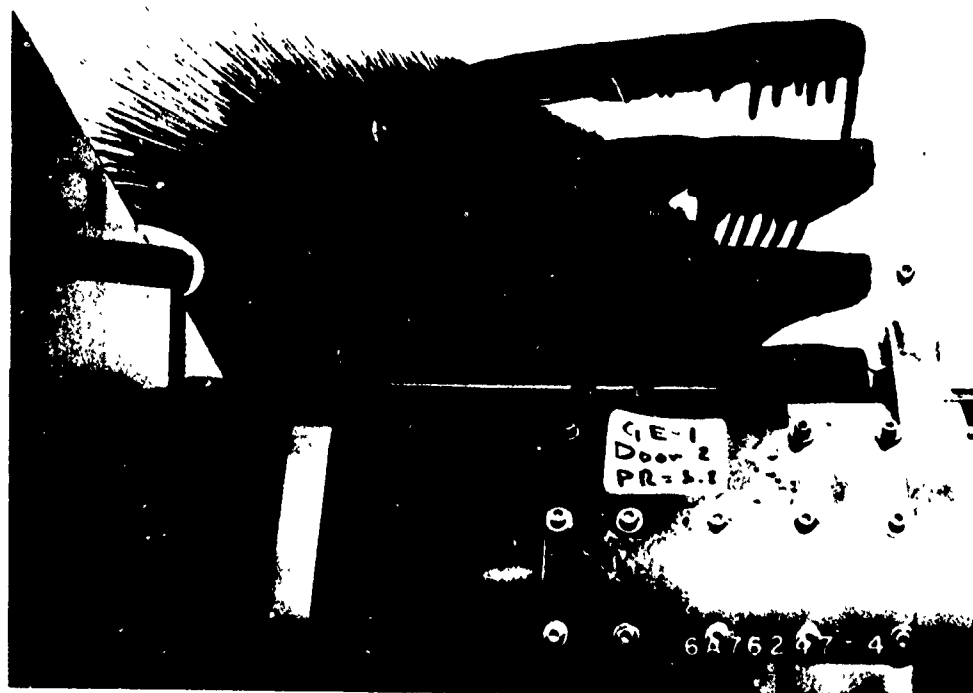


Figure 77: REATTACHMENT OF A THREE DIMENSIONAL JET



a) SCHEMATIC OF THRUST REVERSER AND FLOW FIELD



b) OIL FLOW VISUALIZATION

Figure 78: EXHAUST FLOW REATTACHMENT ON SST THRUST REVERSER

usually occurs if the flow reattaches. Consequently, the approach taken for self-reingestion is that the reattachment criteria also predict reingestion. Thus, if reattachment is predicted from Figure 76 or Equation 60, then reingestion also is predicted.

There are several limitations to the self-reingestion prediction method. Inlet and exhaust flows are assumed to act independently. Effects of inlet suction on exhaust flow are not included. Secondly, there is no definitive reattachment criterion for discrete jets. Also, there is no method to predict whether a reattached jet will continue to propagate forward or separate and be blown rearward. Nevertheless, the method fulfills the major objective of providing a diagnostic tool for reingestion problems.

Near-Field Fountain Reingestion

Near-field fountain reingestion occurs when two or more adjacent jets impinge nearly vertically on the ground plane. Spreading ground flows collide and cause "fountains" of high velocity air to rise vertically as shown in Figure 79. These fountains can be ingested into nearby inlets. The prediction method for near-field fountain reingestion employs existing NASA test data from Ref. 39. The test evaluated recirculation effects resulting from a pair of heated jets impinging on a ground plane. Significant conclusions reached about conditions causing near-field fountain reingestion are summarized below:

- 1) Upwash and inlet temperature rises were extremely sensitive to small nozzle cant angles that result in configuration asymmetries as viewed looking normal to the common plane of the nozzles. A sketch of the flow-field with canted nozzles is shown in Figure 80a. Conversely, the upwash and inlet temperature rises were relatively insensitive to small nozzle cant angles that maintained symmetry as viewed looking normal to the common plane of the nozzles as shown in Figure 80b.
- 2) The inlet flow rate had almost no effect on inlet temperature rise. The upwash flow was established predominantly by the jets with the inlets merely swallowing air in their proximity. The upwash between nozzles generally was concentrated in a region about three diameters in width, with velocities frequently in excess of 100 feet per second. No data for upwash temperature or velocity were presented for the plane of symmetry between the two nozzles. However, flow visualization photographs and pressure surveys on the ground plane indicate the fountain was at least six diameters wide along the stagnation streamline dividing flows. It can therefore be

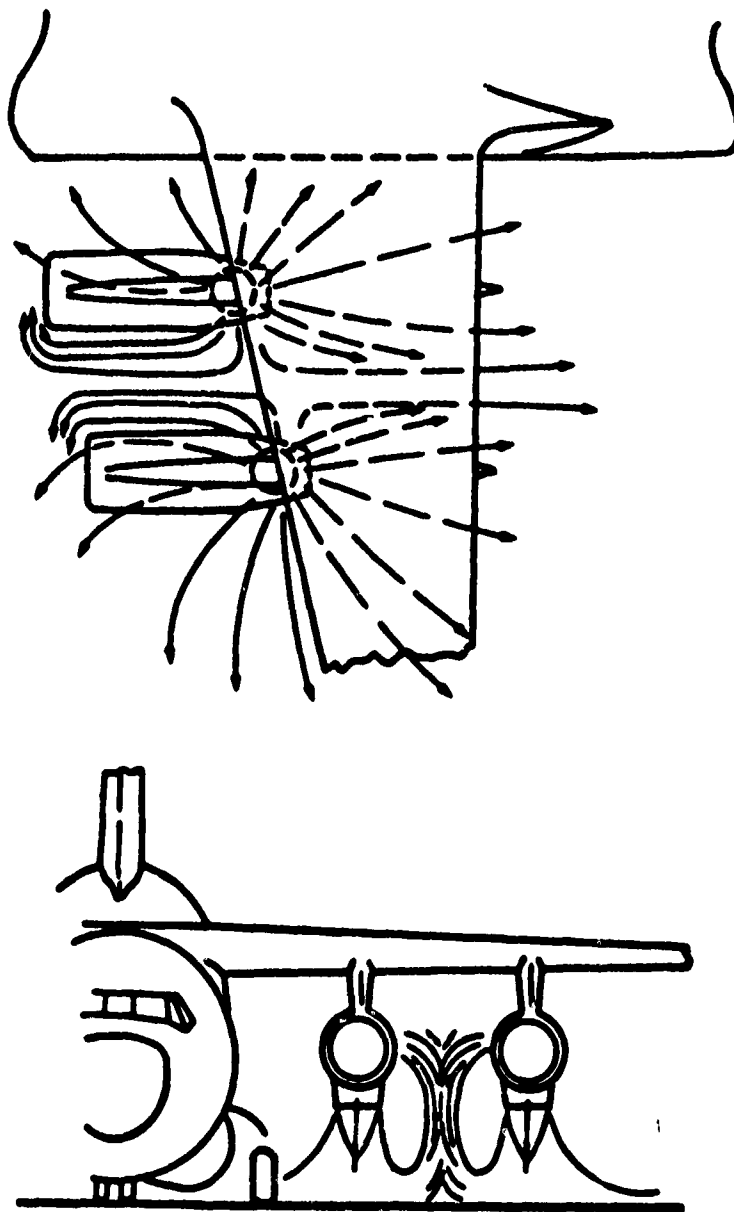
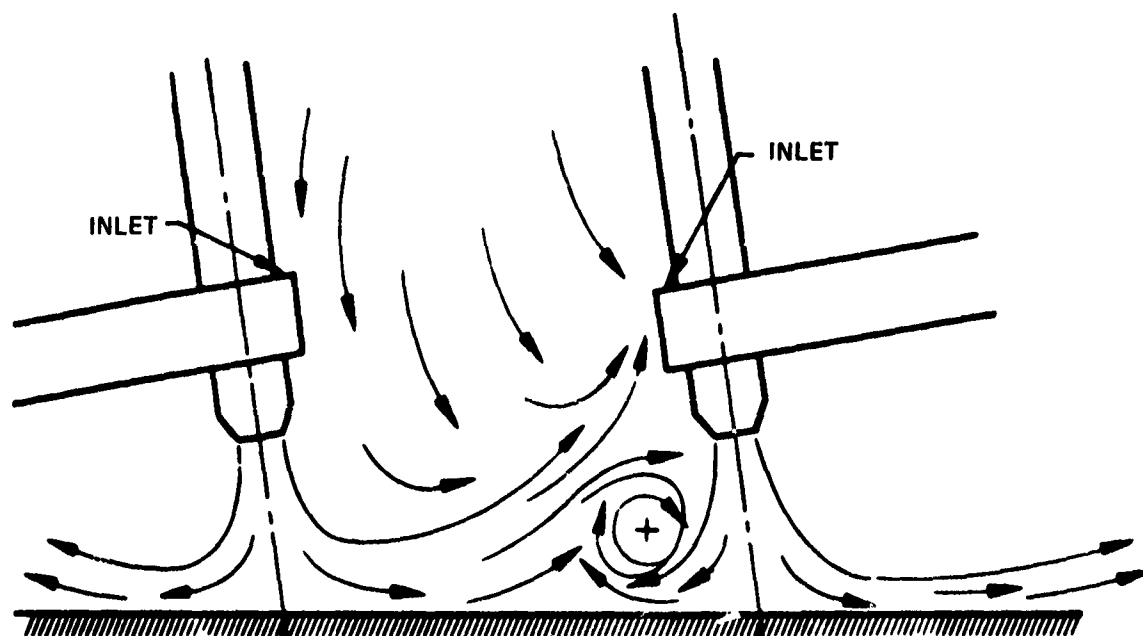
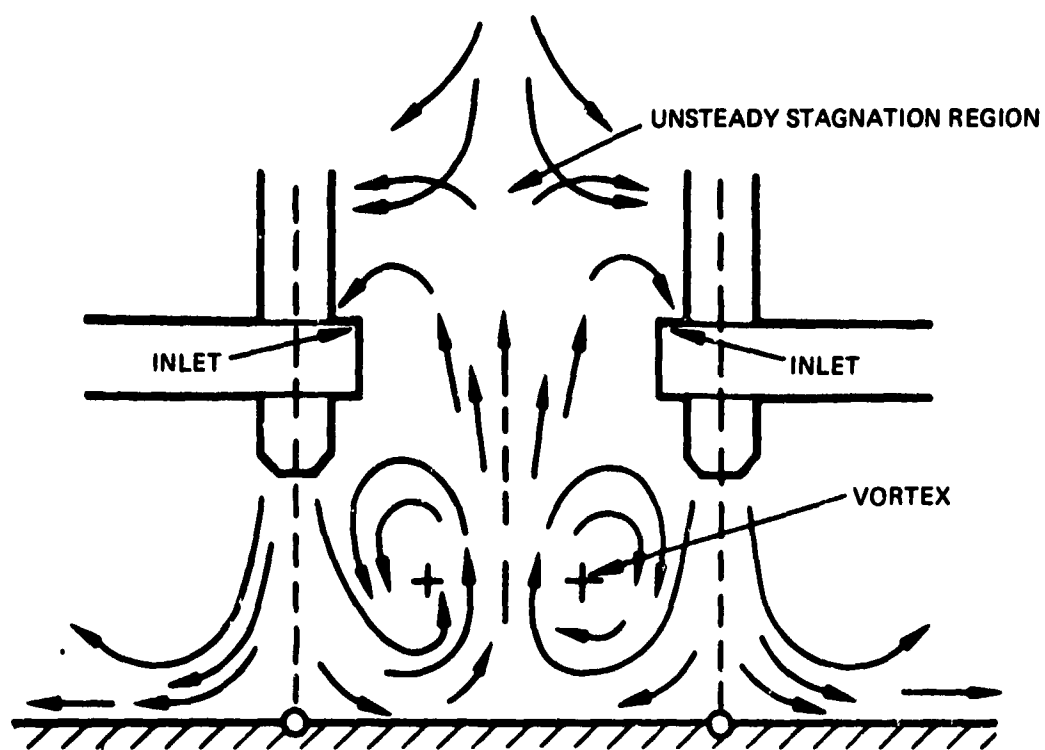


Figure 79: NEAR-FIELD FOUNTAIN REINGESTION



a) FLOW FIELD WITH CANTED NOZZLES



b) NOMINAL FLOW FIELD WITH SYMMETRIC NOZZLES AND
EQUAL NOZZLE PRESSURE

Figure 80: NEAR-FIELD FOUNTAIN FLOW FIELDS

assumed that inlets located parallel to the symmetry plane also reingest flow from the fountain.

- 3) The jets merged if they were located close together and high off the ground. The criterion for a pair of parallel jets to merge is given by

$$\left(\frac{S}{D}\right)_{\text{jets merge}} \leq 1 + 2 \frac{H}{D} \tan \alpha \quad (61)$$

where α is the half angle of the spreading jet plume, S is the spacing between jets, and H is the height. Using a spreading angle of 7 degrees gives

$$\left(\frac{S}{D}\right)_{\text{jets merge}} \leq 1 + 0.246 \frac{H}{D} \quad (62)$$

When the jets merged, no fountain or reingestion occurred.

- 4) The effect of wind in altering the near flowfield was negligible for wind speeds less than 6 feet per second. With the wind parallel to the common plane of the nozzles, further increases in wind speed shifted the fountain downstream, until at about 16 feet per second, the upwash was shifted beyond the downstream jet, thus eliminating the fountain between the jets.

With the wind at 90 degrees to the common plane of the nozzles, no significant change in either the upwash flow or inlet temperature rise was detected within the range of wind speeds investigated, i.e., wind speed < 16 feet per second. However, analysis of the jet trajectory of the fountain shows that for wind speeds greater than about 25 feet per second, the fountain will be swept downstream.

Based upon these conclusions, certain criteria have been established for near-field fountain reingestion to occur, namely:

- 1) Near-field fountain reingestion will not occur for free-stream velocities greater than about 25 feet per second because the fountain is swept downstream by the freestream flow.
- 2) There must be a minimum of two jets directed downward for a fountain to form.
- 3) The jet pairs are checked to see whether they merge. If the jets merge before impinging on the ground, no fountain or reingestion occurs.

- 4) If the cant angles are symmetric when viewed in their common plane, near-field fountain reingestion will occur for cant angles up to ± 20 degrees. If the cant angles are not symmetric, near-field reingestion will occur for cant angles up to about 6 degrees.

The Reingestion Prediction Program checks all jets against the above criteria. If a pair of jets satisfying the criteria are found, then reingestion diagnostic comments are printed out.

The principal limitation of the near-field fountain reingestion prediction method is the fact that the test hardware represented a lift engine having an inlet located very close to the exhaust nozzle (Figure 80). STOL transports employing thrust vectoring of the cruise engines will have inlets located several nozzle diameters in front of the nozzle. This type of configuration will be less susceptible to near-field reingestion than the NASA hardware. Therefore, reingestion predictions using NASA data will be conservative.

Far-Field Fountain Reingestion

Far-field fountain reingestion occurs when the spreading ground flow from one of more impinging jets separates from the ground, rises in a cloud, and is blown back into the inlet. Separation is caused by buoyancy forces in the absence of a free-stream flow or by interaction with a headwind.

Figure 81 depicts the major elements used to predict far-field reingestion. The dividing streamline between jet and freestream flow is determined first. Secondly, the upper surface of the exhaust cloud is located. Finally, the exhaust cloud is checked for intersections with the inlet streamtubes. Details of this procedure are discussed in the following paragraphs.

To predict far-field reingestion, the separation point of the spreading ground jet is required. Separation data from Ref. 40 to 43 are compared in Figure 82. Abbott's data agree fairly well with Binion's data and with NASA's single and dual pod data over a limited range of dynamic pressure ratios. Discrepancies are probably due to configuration differences and measurement inaccuracies. Abbott correlated data for a wide range of dynamic pressure ratios and impingement angles and developed a criterion to predict the separation distance (Ref. 40). Abbott's separation criterion, depicted in Figure 83, states that separation occurs at a distance where the dynamic pressure for a stationary nozzle is equal to four times the dynamic pressure of the still air relative to a moving nozzle, i.e.,

$$(q_s)_{\text{stationary nozzle}} = 4(q_\infty)_{\text{moving nozzle}} \quad (63)$$

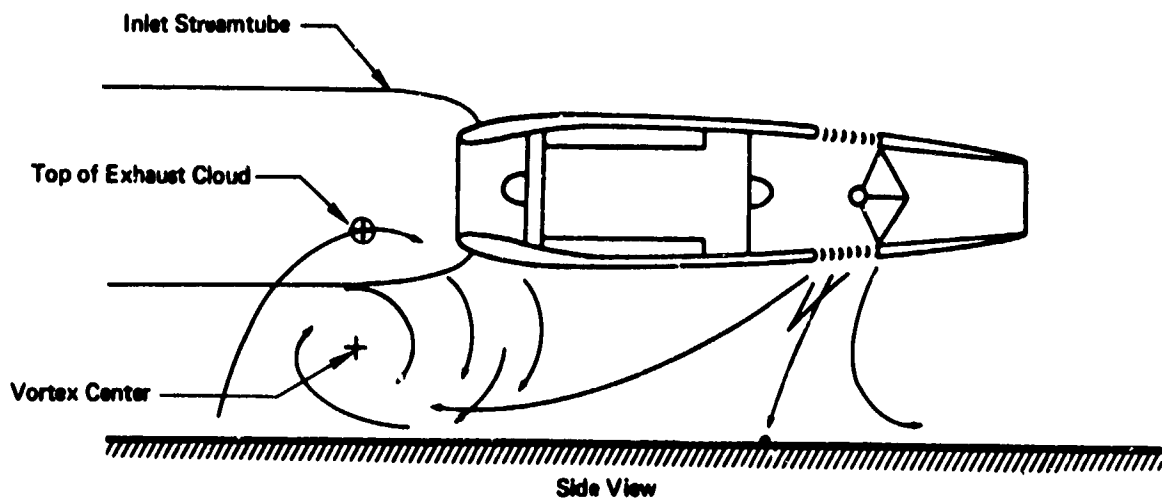
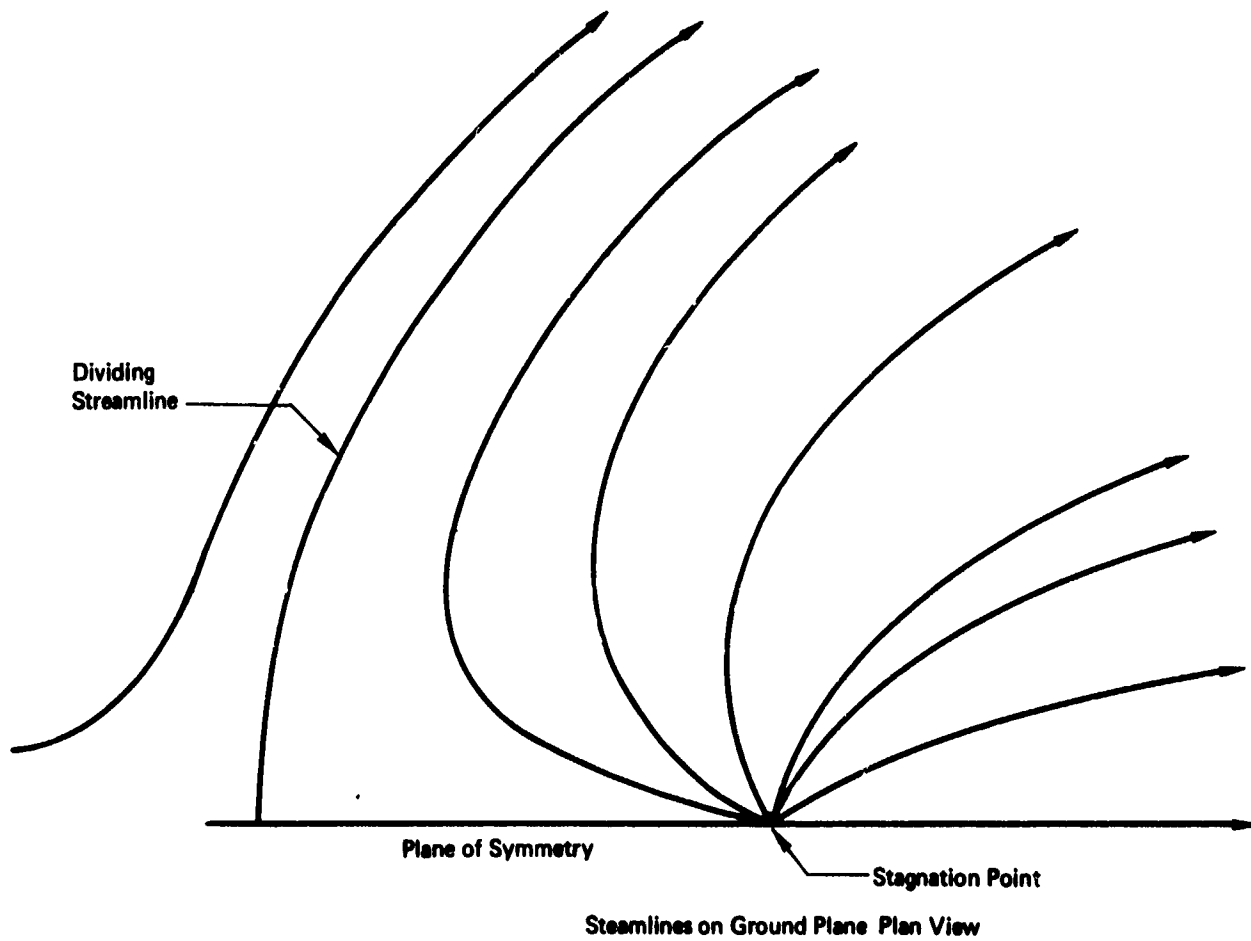


Figure 81: FAR-FIELD FOUNTAIN REINGESTION

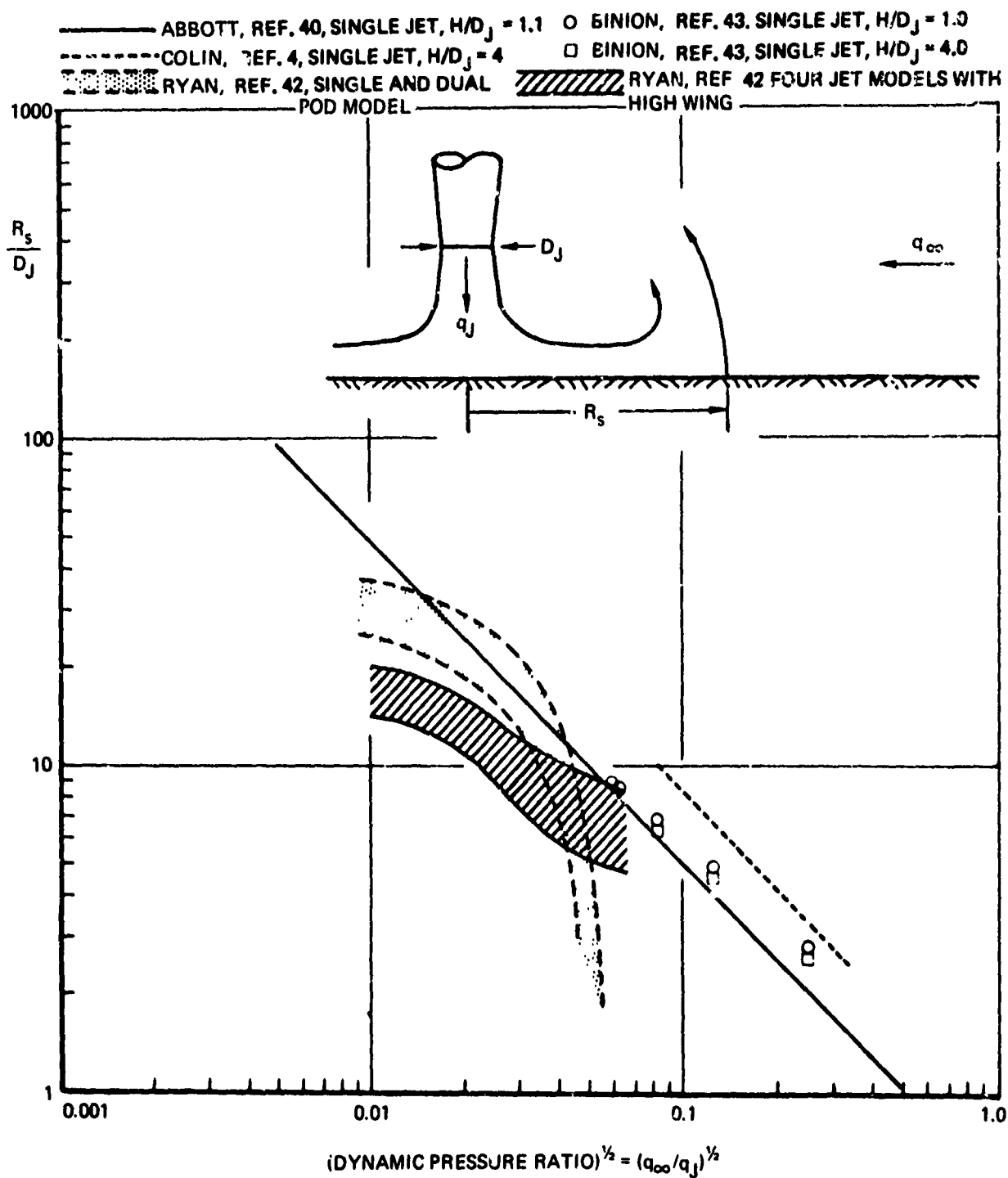
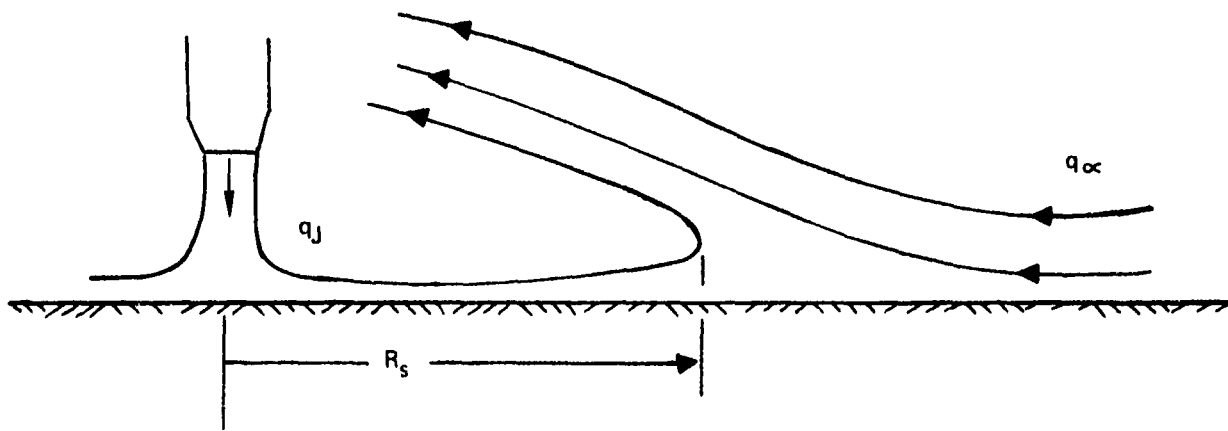


Figure 82: COMPARISON OF FLOW SEPARATION DATA
 FOR 90° JET IMPINGEMENT

(A) MOVING NOZZLE



(B) STATIONARY NOZZLE

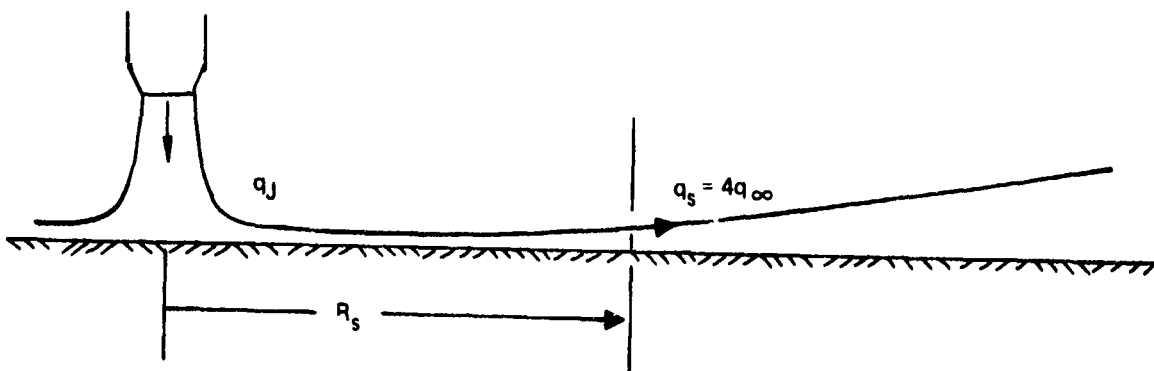


Figure 83: ABBOTT'S CRITERION FOR PREDICTING FAR FIELD FOUNTAIN FLOW SEPARATION

Abbott conducted extensive dynamic pressure surveys for stationary nozzles and used flow visualization for moving nozzles in order to develop this criterion. Results are shown in Figure 84 for impingement angles from 40 to 150 degrees and dynamic pressure ratios from 4 to 40,000.

Abbott's correlation for separation distance of the spreading ground jet applies only in the vertical plane of symmetry. The general case of far-field reingestion involves inlets located to the right or left of this plane. Therefore, it is necessary to predict the position of the dividing streamline out of the plane of symmetry. Potential flow theory was used by Colin with good results to predict the peeling line for a jet impinging at 90 degrees (Ref. 41). Comparison of Colin's theory to test data is shown in Figure 85. His potential flow model consisted of a line source combined with a freestream flow. The source strength was sized to make the dividing streamline match data in the plane of symmetry.

Colin's theory was extended to jets impinging at arbitrary angles by specifying a nonuniform outflow velocity distribution around the periphery of the jet's cross section projected on the ground plane. The outflow velocity was determined by balancing the momentum of radial streamlines leaving the stagnation point. Computer-plotted results are shown in Figures 86 to 88 for 0, 45, and 90-degree wind direction. Streamlines are shown emanating from the jet stagnation point and in the freestream surrounding the zone of jet flow. Streamlines without symbols were traced from separate computer submissions. Jet impingement angles of 30, 60, 90, 120, and 150 degrees were run with 0, 45, and 90-degree wind direction at velocity ratios $V_j/U_\infty = 1$ to 100. Wind direction has a pronounced influence on the dividing streamline as shown by Figure 89. However, when the dividing streamlines are aligned along the direction of approach flow as in Figure 90 the effect of wind direction is seen to be small. As expected, velocity ratio had a large influence on the dividing streamline as shown in Figure 91. However, the influence of jet impingement angle on dividing streamline shape was unexpectedly small, indicating that total jet strength is more important in determining dividing streamline shape than the relative distribution of outflow velocity.

As discussed previously, Abbott's criterion is used to predict the separation point in the plane of symmetry. The peeling line radius out of the plane of symmetry is determined from the dividing streamline for 90 degree impingement. Because the jet impingement angle has only a small influence on dividing streamline shape, the dividing streamline for 90 degree impingement is used for all impingement angles.

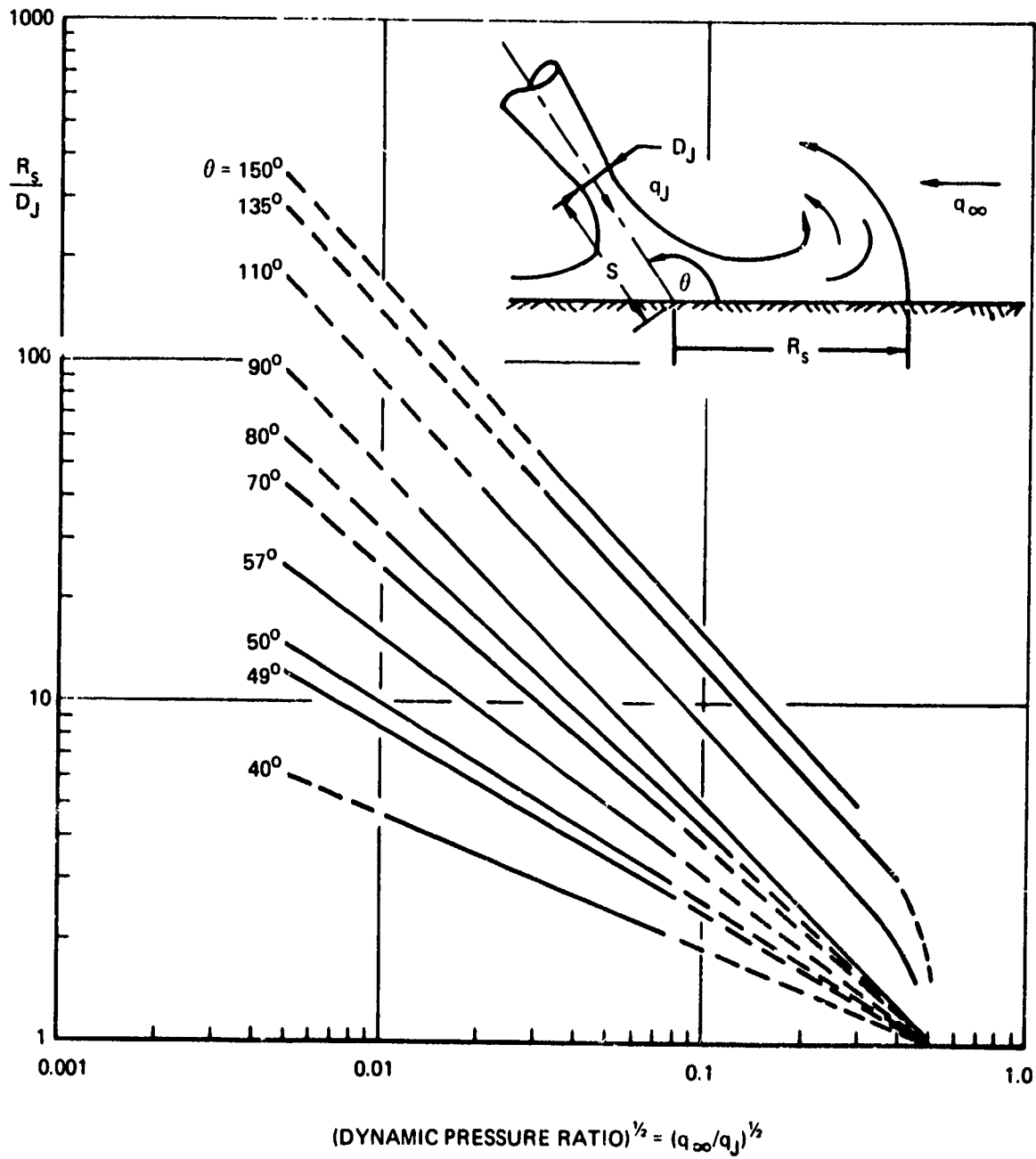
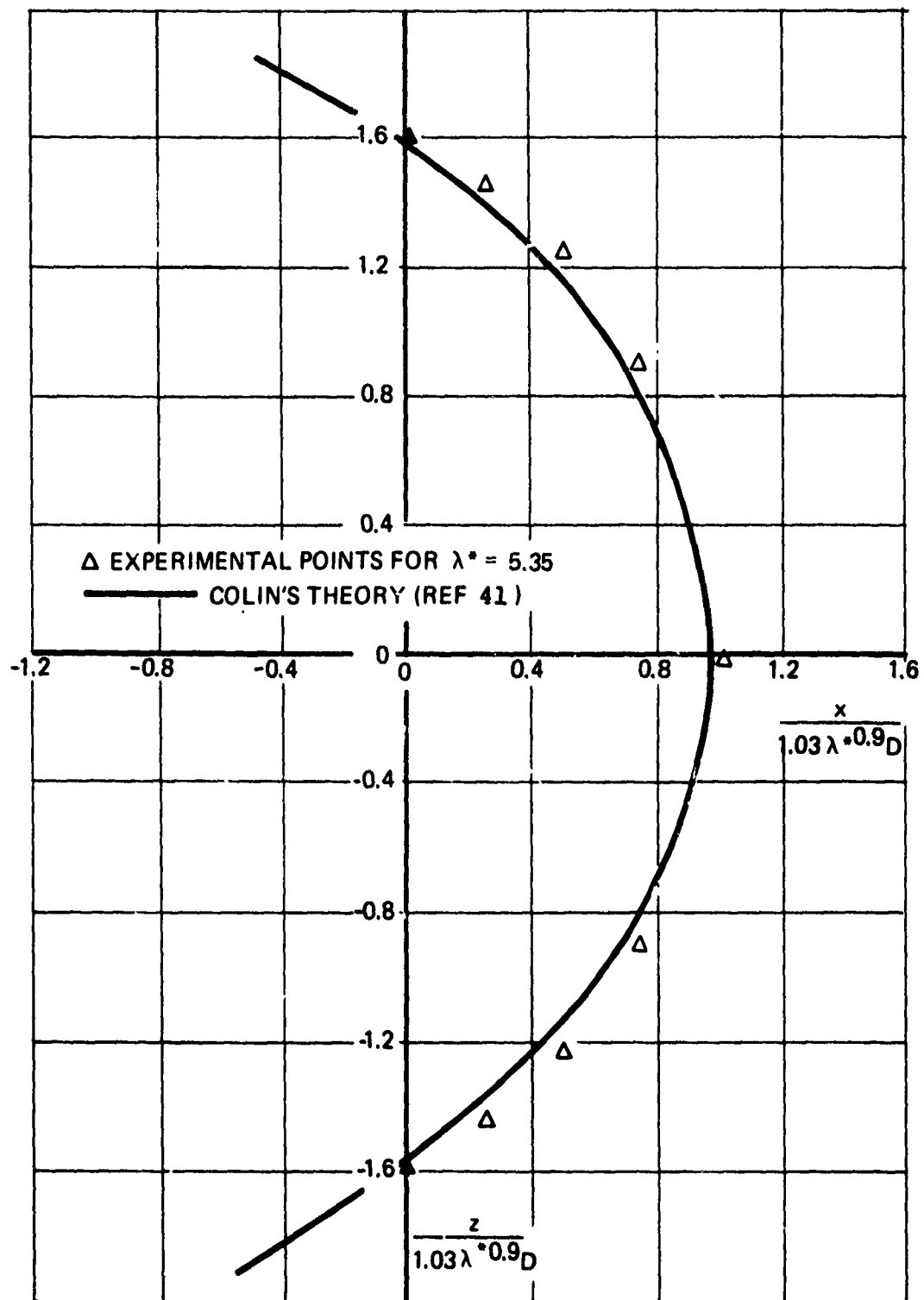


Figure 84 : EFFECT OF IMPINGEMENT ANGLE AND DYNAMIC PRESSURE RATIO ON FAR FIELD FOUNTAIN FLOW SEPARATION



$$\lambda^* = \frac{V_{REF}}{U_{\infty}}$$

$$V_{REF} = \sqrt{\frac{2(P_{STAGNATION POINT} - P_{\infty})}{\rho}}$$

Figure 85: DIVIDING STREAMLINE COMPARISON
 BETWEEN THEORY AND EXPERIMENT

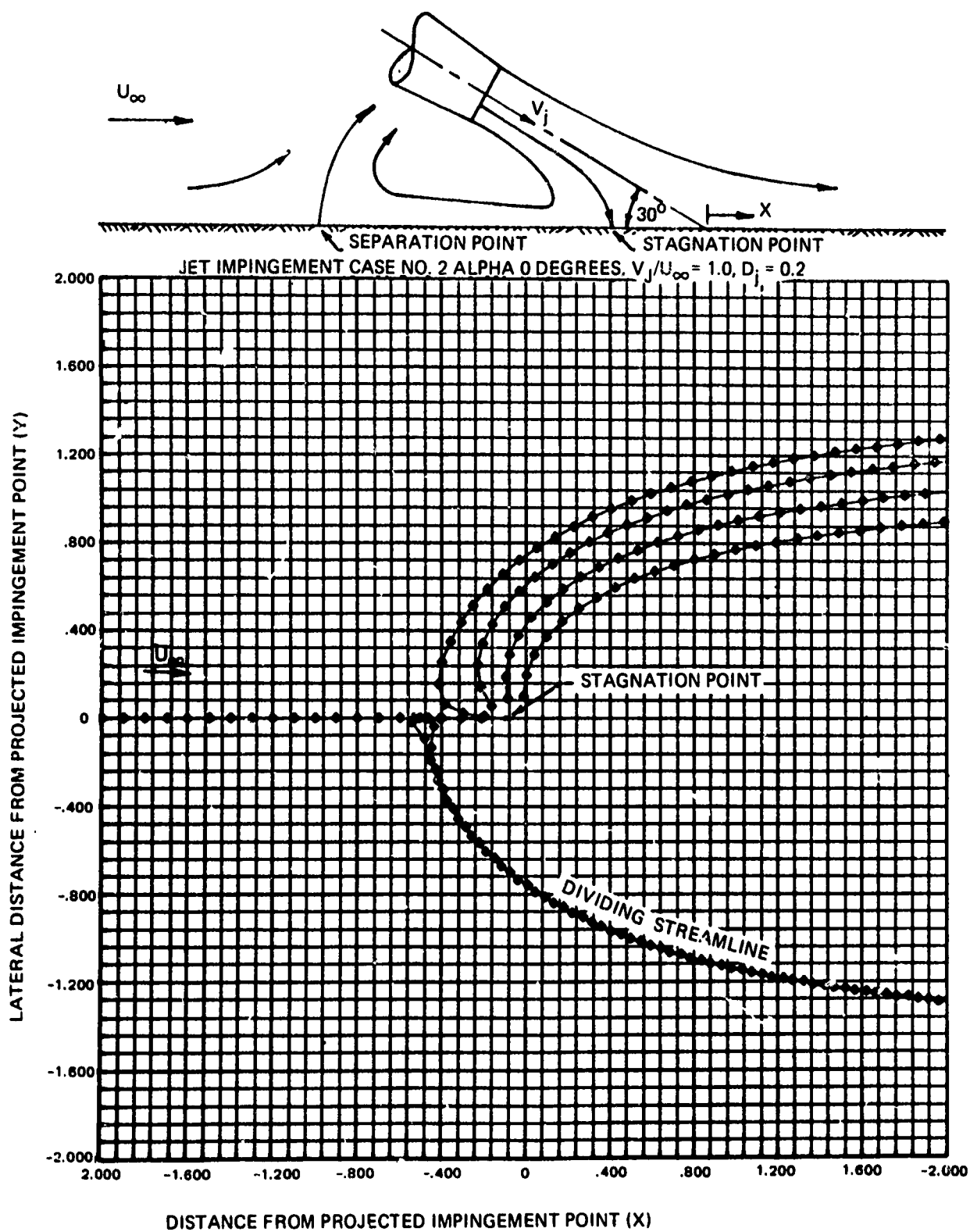


Figure 86: GROUND PLANE STREAMLINES FOR 30° JET IMPINGEMENT ANGLE AND VELOCITY RATIO $V_j/U_\infty = 1.0$

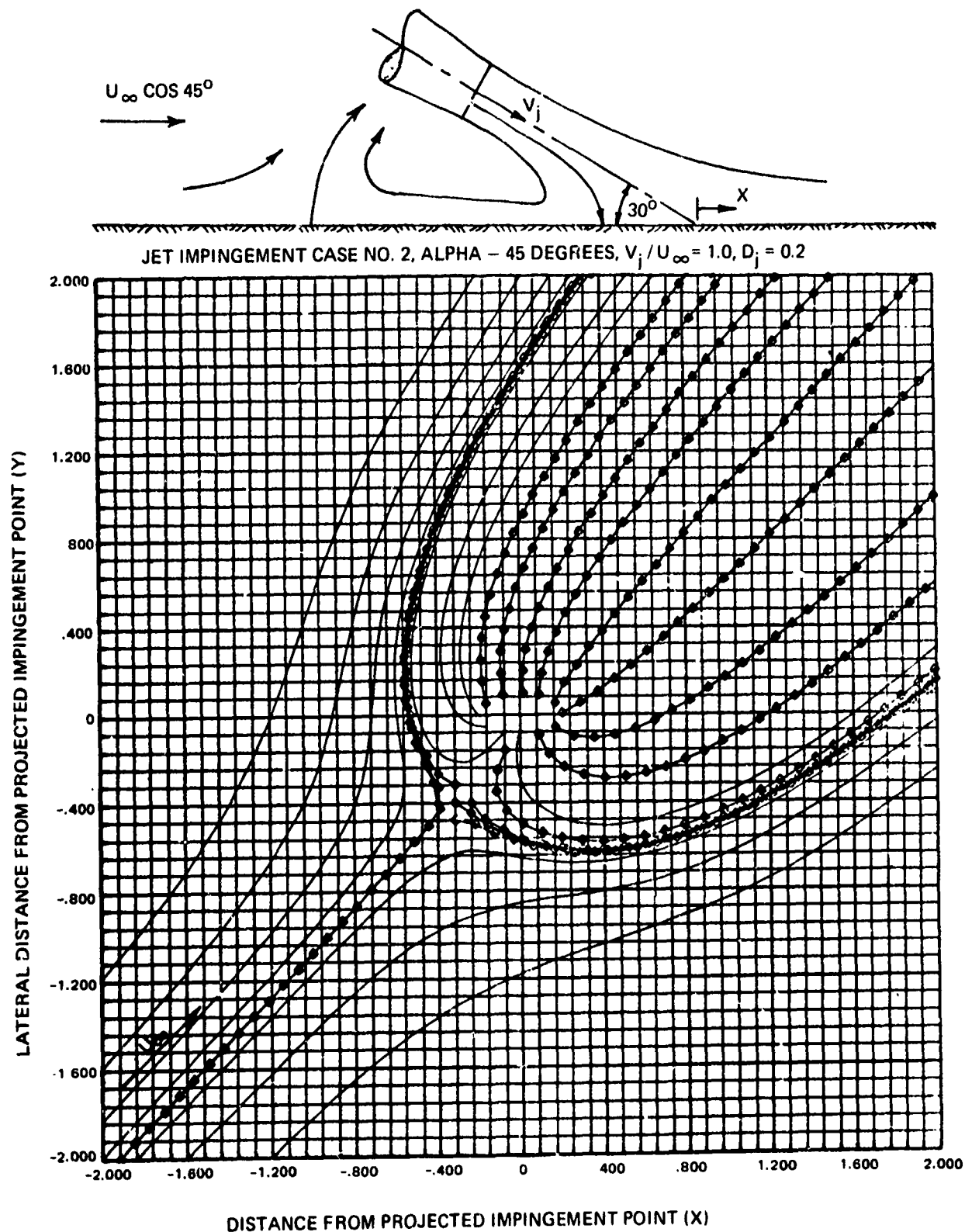


Figure 87: GROUND PLANE STREAMLINES FOR 30° JET IMPINGEMENT ANGLE AND 45° WIND DIRECTION

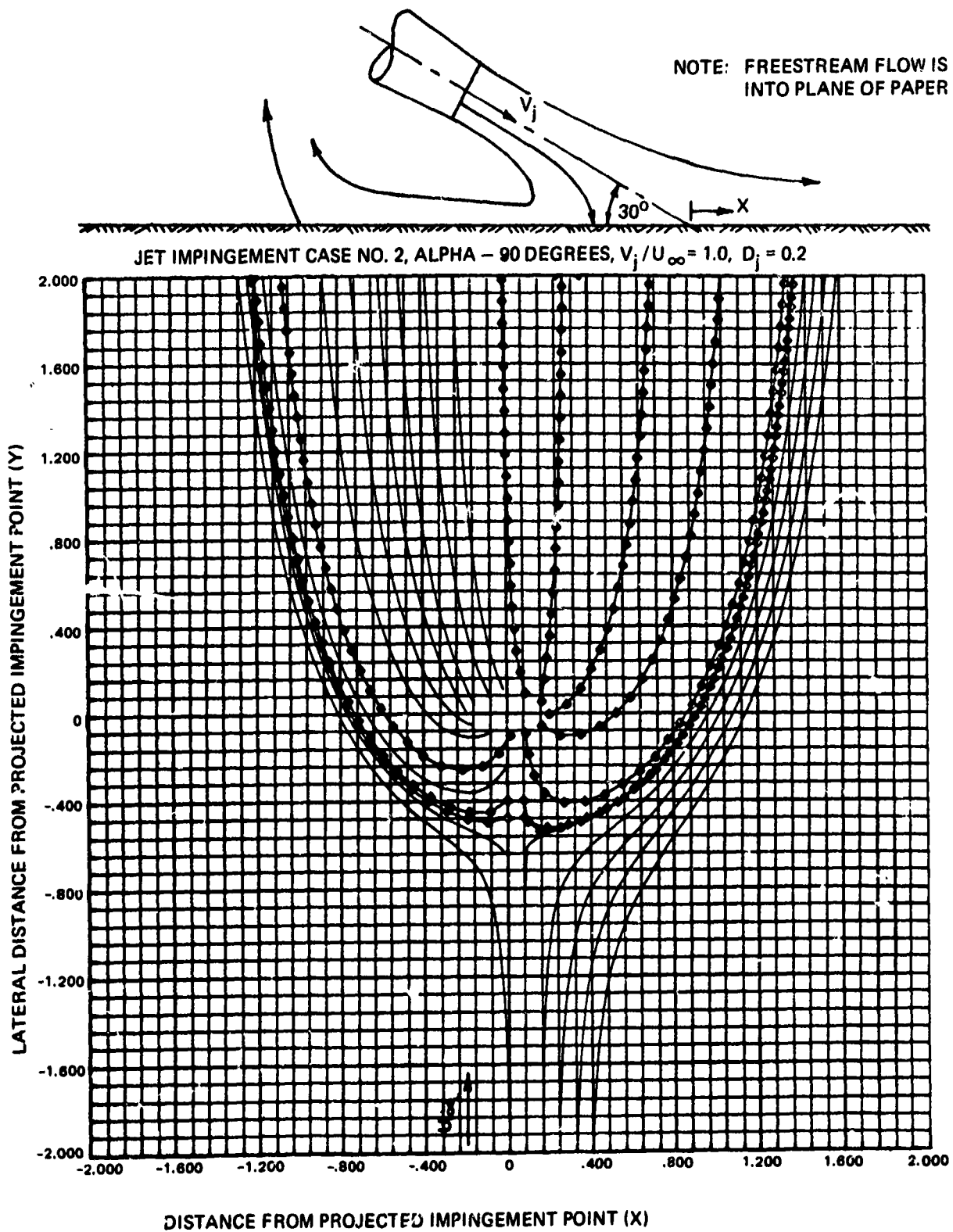


Figure 88: GROUND PLANE STREAMLINES FOR 30° JET IMPINGEMENT ANGLE AND 90° WIND DIRECTION

$$D_j = 0.2$$

$$V_j / U_\infty = 1.0$$

$$\text{IMPINGEMENT ANGLE} = 30^\circ$$

$$\text{WIND DIRECTION} = \psi$$

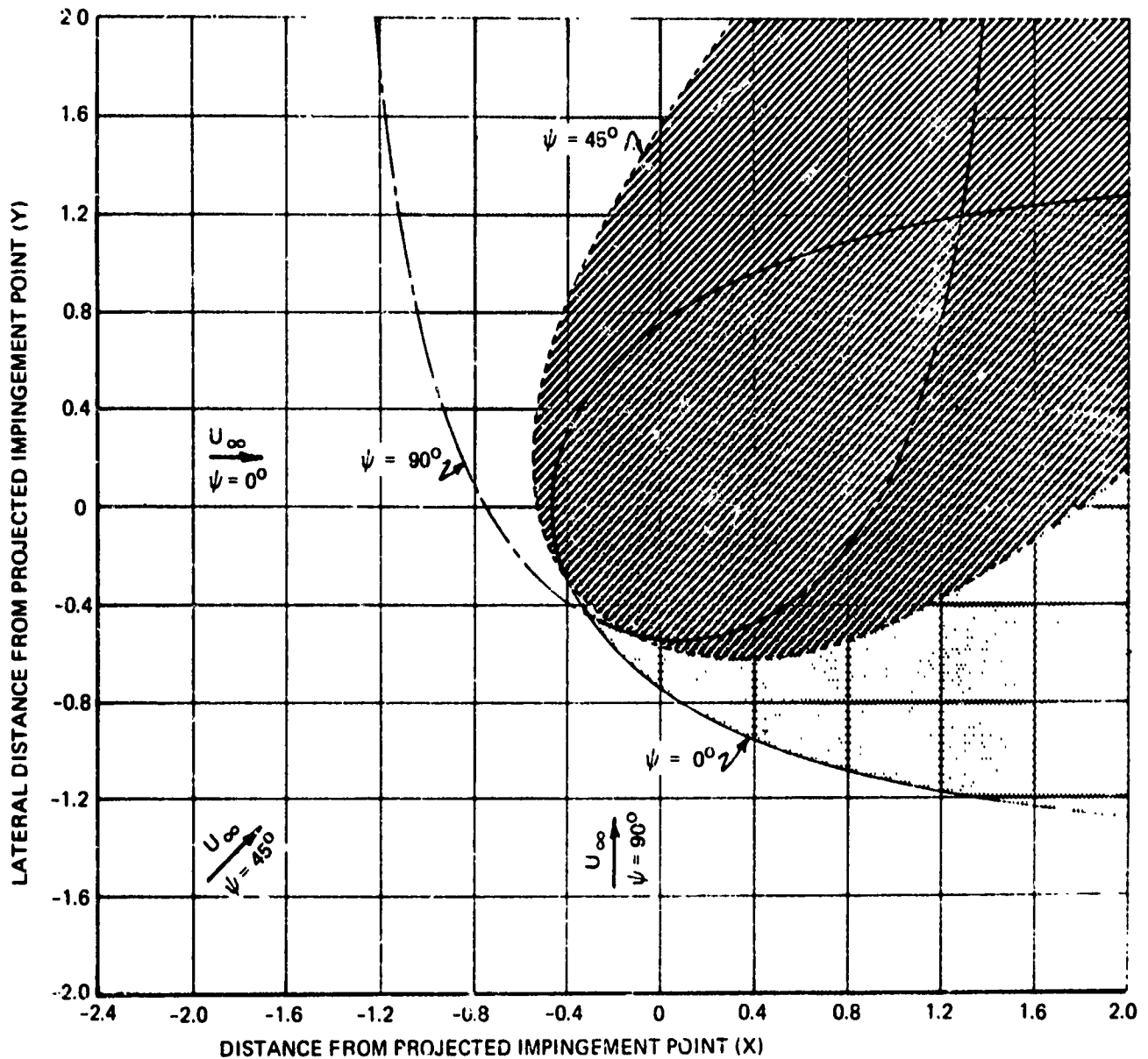


Figure 89: EFFECT OF WIND DIRECTION ON DIVIDING STREAMLINE SHAPE

$$D_j = 0.2$$

$$V_j / U_\infty = 1.0$$

IMPINGEMENT ANGLE = 30°

———— WIND DIRECTION = 0°

- - - - - WIND DIRECTION = 45°

- · - · - WIND DIRECTION = 90°

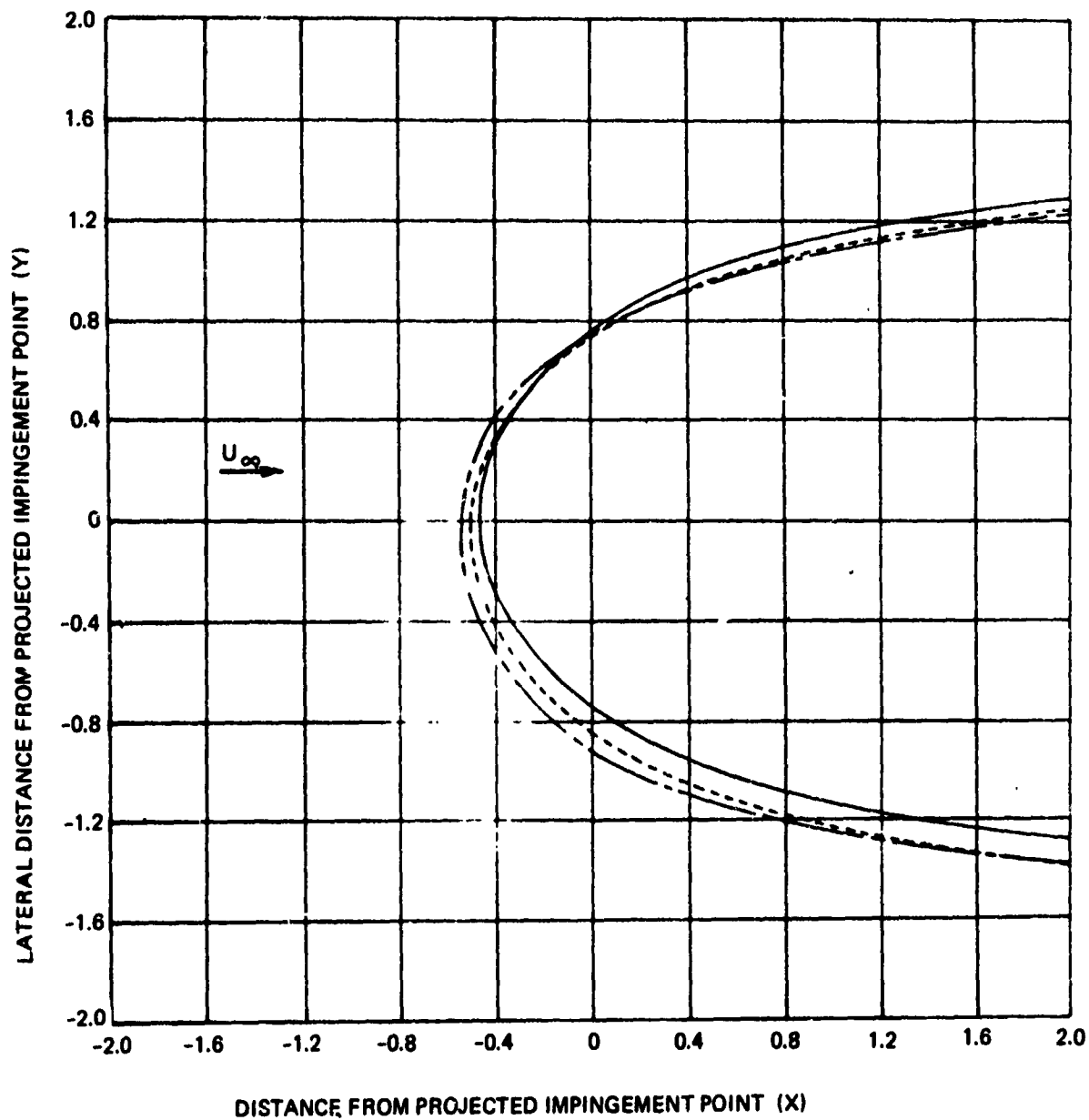


Figure 90: EFFECT OF WIND DIRECTION ON DIVIDING STREAMLINE SHAPE

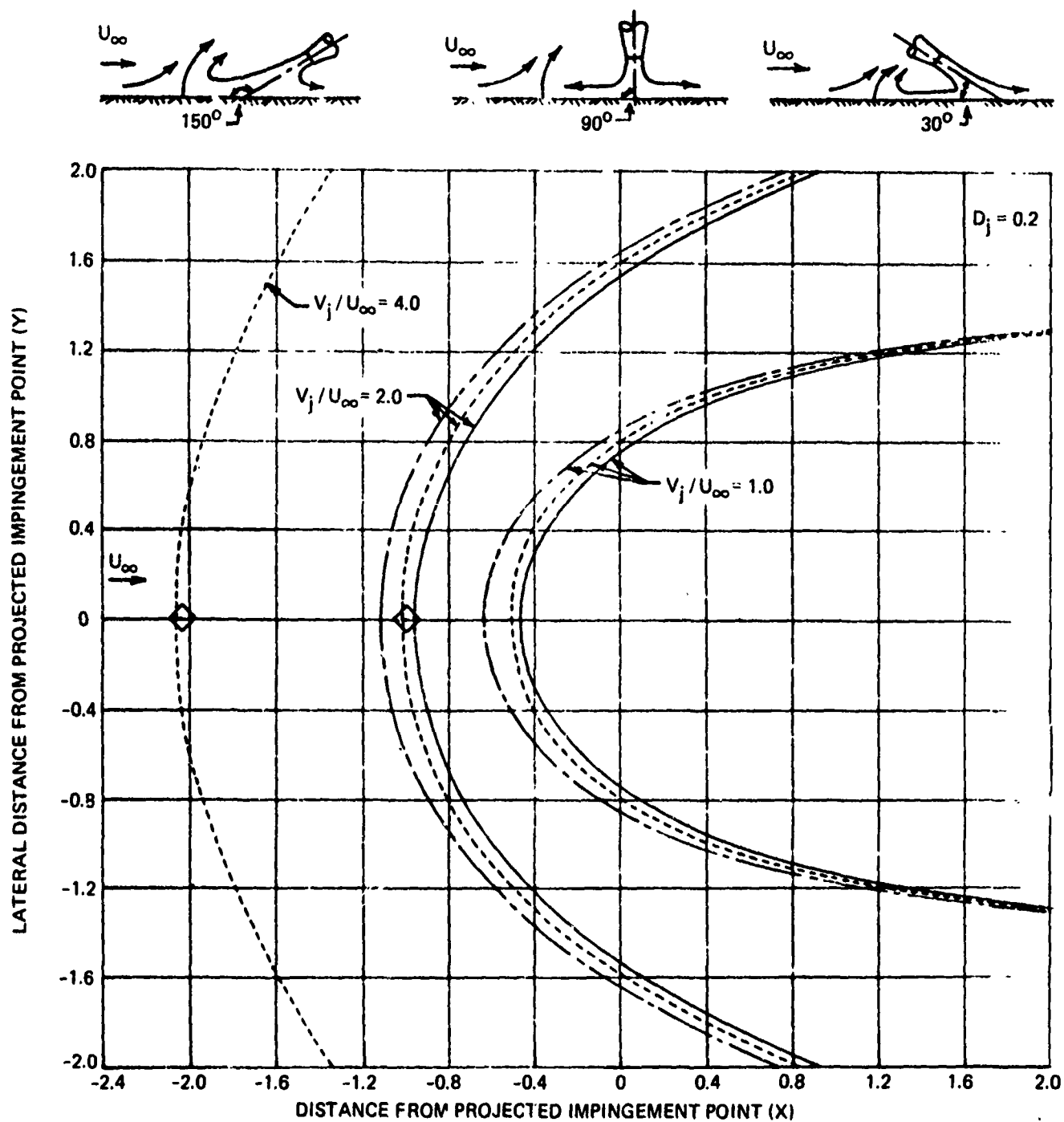


Figure 91: EFFECT OF VELOCITY RATIO AND IMPINGEMENT ANGLE ON DIVIDING STREAMLINE SHAPES

Once the position of the dividing streamline is determined, it is necessary to predict the height of the exhaust cloud. Abbott's data shown in Figure 92 are used for this purpose. Data scatter is due in part to turbulent fluctuations present in the exhaust cloud. The top line is used to provide a factor of conservatism in the prediction method. The radial position of the top of the exhaust cloud is assumed to lie above the vortex center given by Colin's data, as shown in Figure 93.

The final step necessary to predict far-field reingestion is to check the exhaust cloud upper surface for possible intersections with inlet streamtube surfaces. The Re-ingestion Prediction Program checks a limited number of points in the cloud for intersections with inlet streamtube surfaces. As shown in Figure 94, points are checked at azimuth angles from 30 to 330 degrees. This simplified intersection procedure was chosen because the exhaust cloud surface is not known with sufficient accuracy to warrant a more sophisticated surface intersection technique.

Steps used to predict near-field fountain reingestion are summarized below.

- 1) Separation of the spreading ground jet is predicted using Abbott's data correlation.
- 2) The dividing streamline in the ground plane is predicted by potential flow.
- 3) The exhaust cloud upper surface is predicted by Abbott's and Colin's data.
- 4) The exhaust cloud is checked for intersection with inlet streamtubes.

2.2.3 TR and TV System Performance Program

The TR and TV System Performance Program consists of four modules containing empirical data correlations and some analyses developed during Tasks 1.1 and 1.3. Inputs and outputs of the program are shown in Figure 95. Detailed description of the four performance modules follows.

Internal Performance Module

Data correlations developed during Tasks 1.1 and 1.3 were incorporated into the Internal Performance Module, which contains data correlations for the following types of cruise nozzles, thrust reversers, and vectoring nozzles.

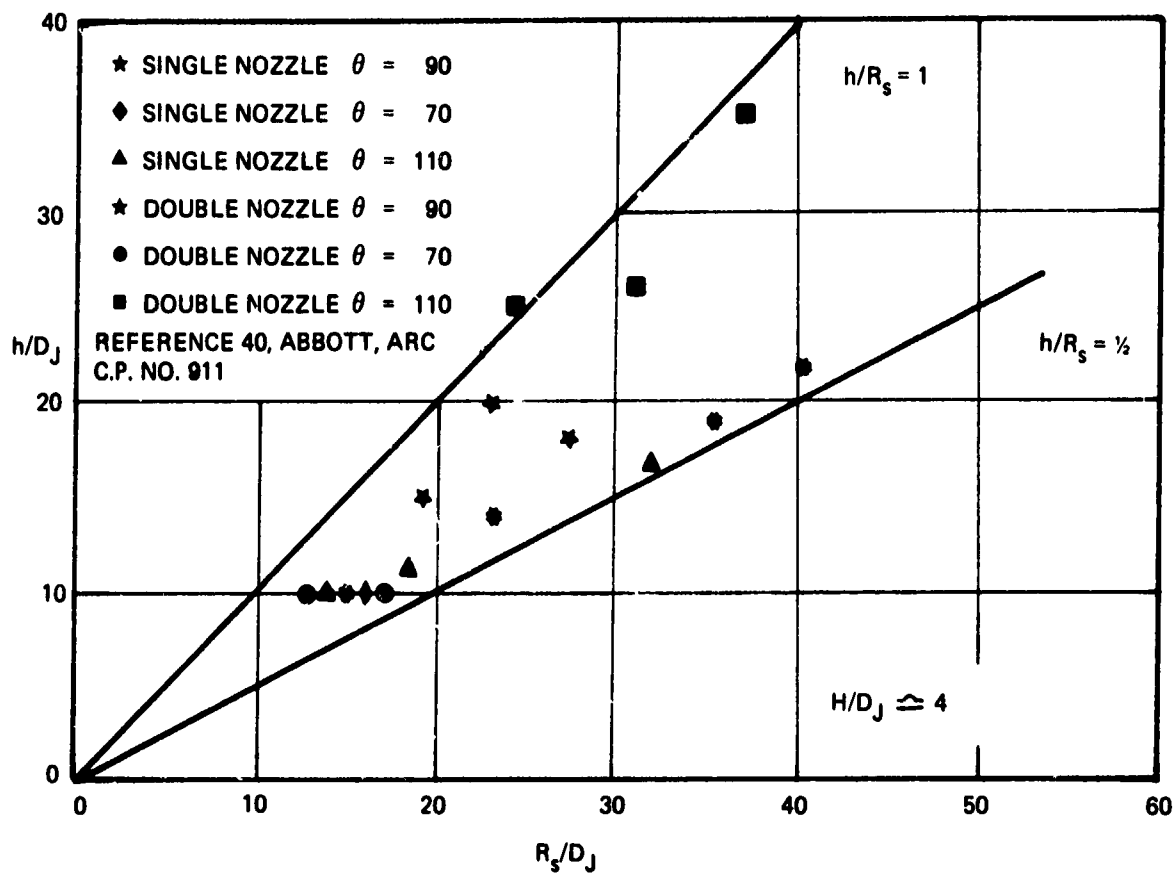
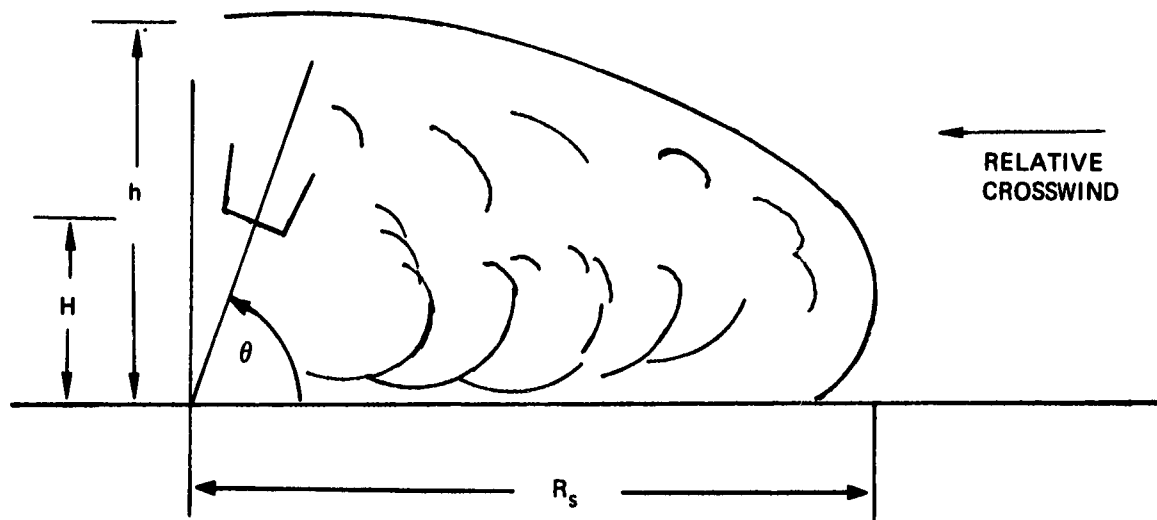


Figure 92: HEIGHT OF FAR FIELD FOUNTAIN EXHAUST CLOUD

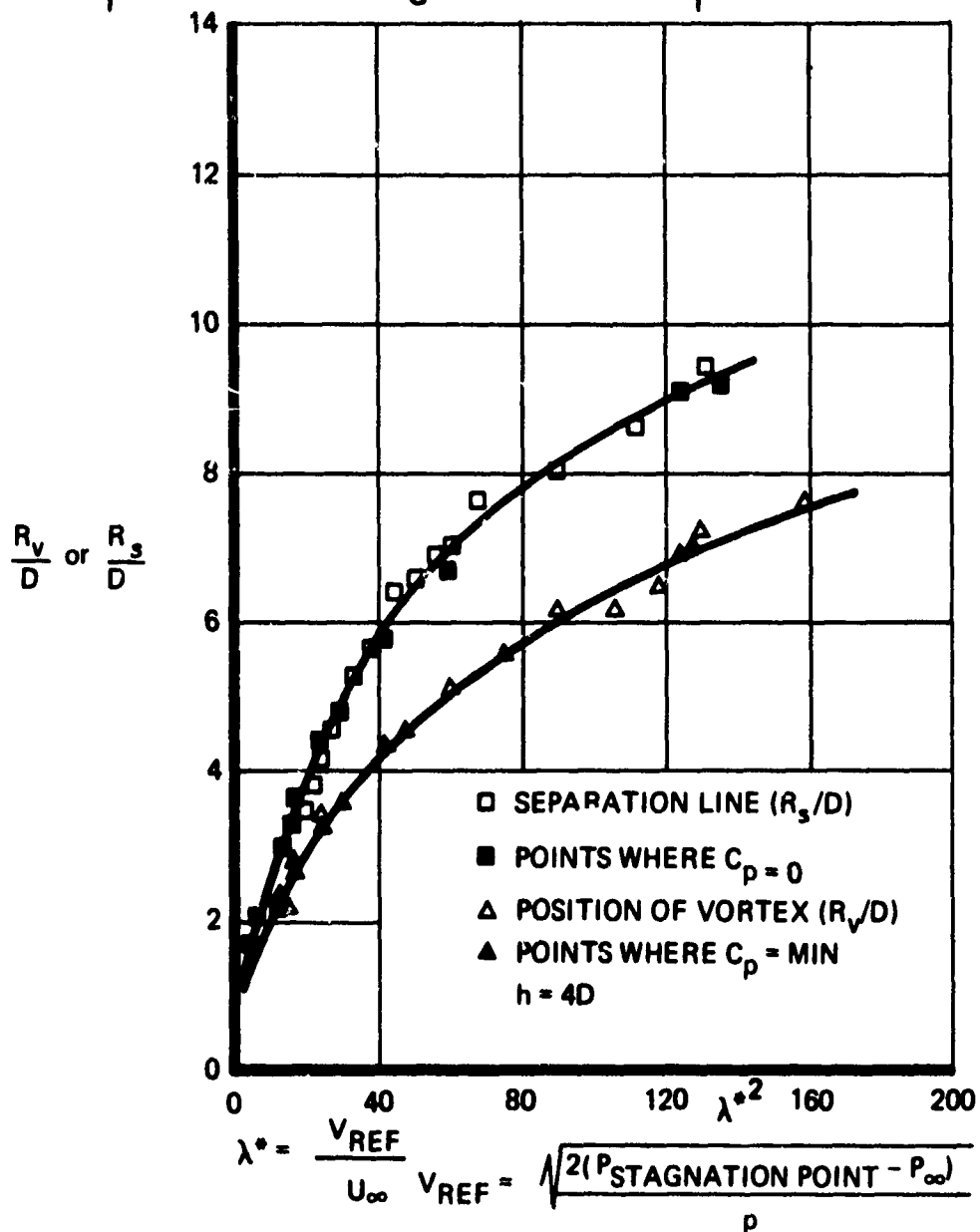
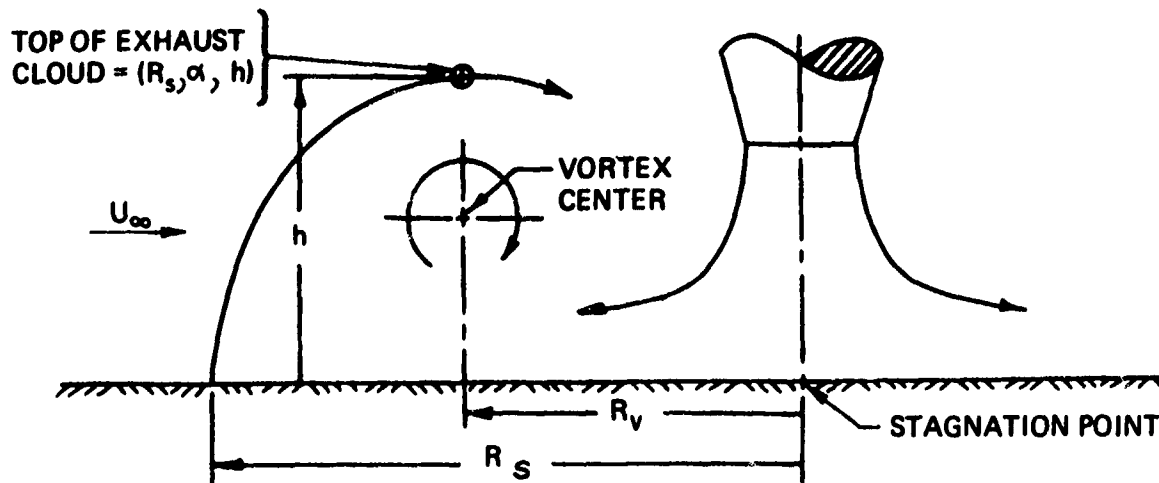


Figure 93: POSITION OF VORTEX AND SEPARATION LINE VS CORRECTED DYNAMIC PRESSURE RATIO

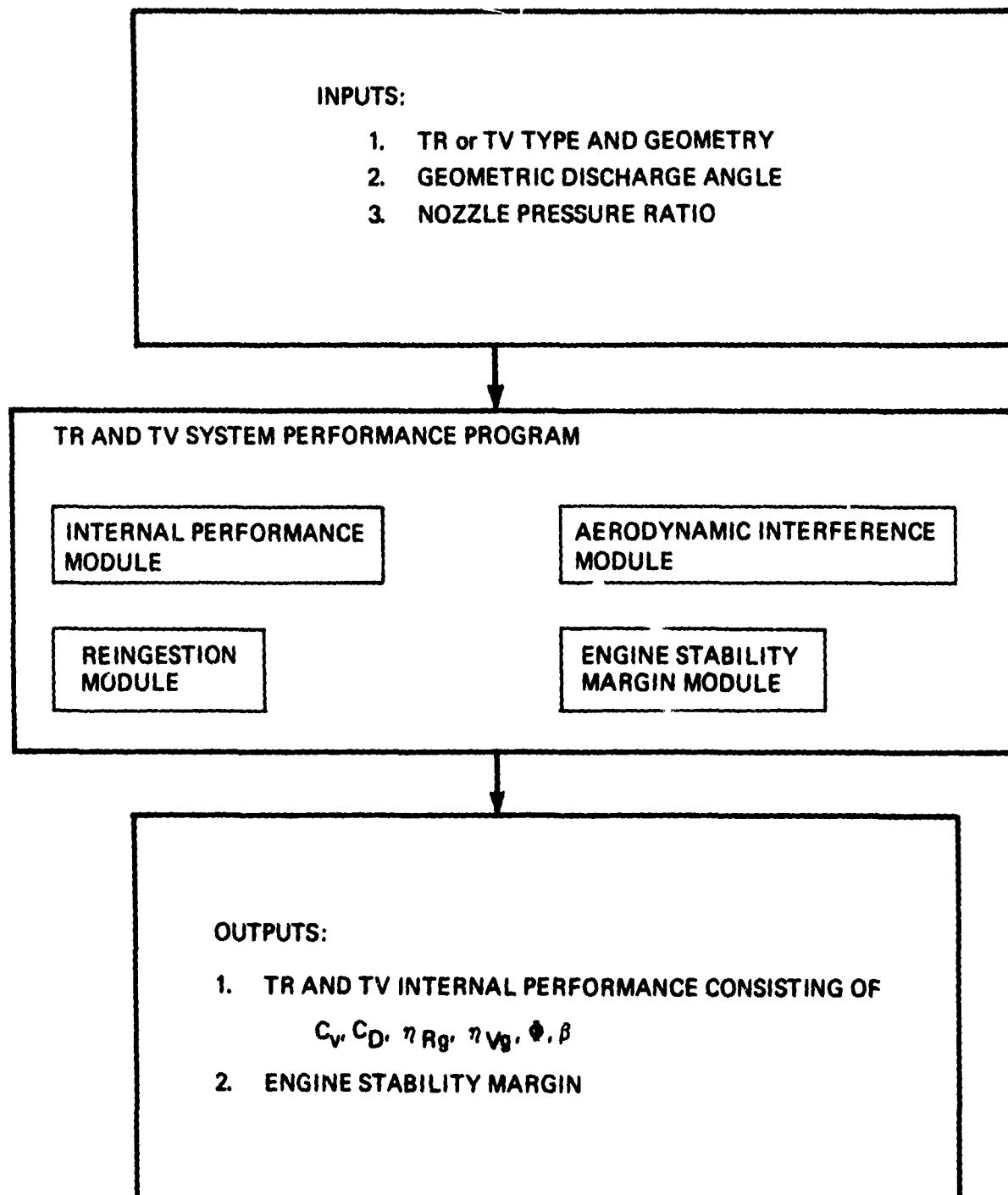


Figure 95: TR AND TV SYSTEM PERFORMANCE PROGRAM

- 1) Cruise nozzles
 - a) Conical
 - b) Annular
 - c) Noncircular
- 2) Thrust reversers
 - a) Target (clamshell and annular)
 - b) Blocker deflector and blocker cascade
- 3) Thrust vectoring nozzles
 - a) Single bearing
 - b) Three bearing
 - c) Spherical eyeball
 - d) Lobstertail
 - e) External deflector
- 4) Cascade lattices applicable to cascade TR and TV nozzles

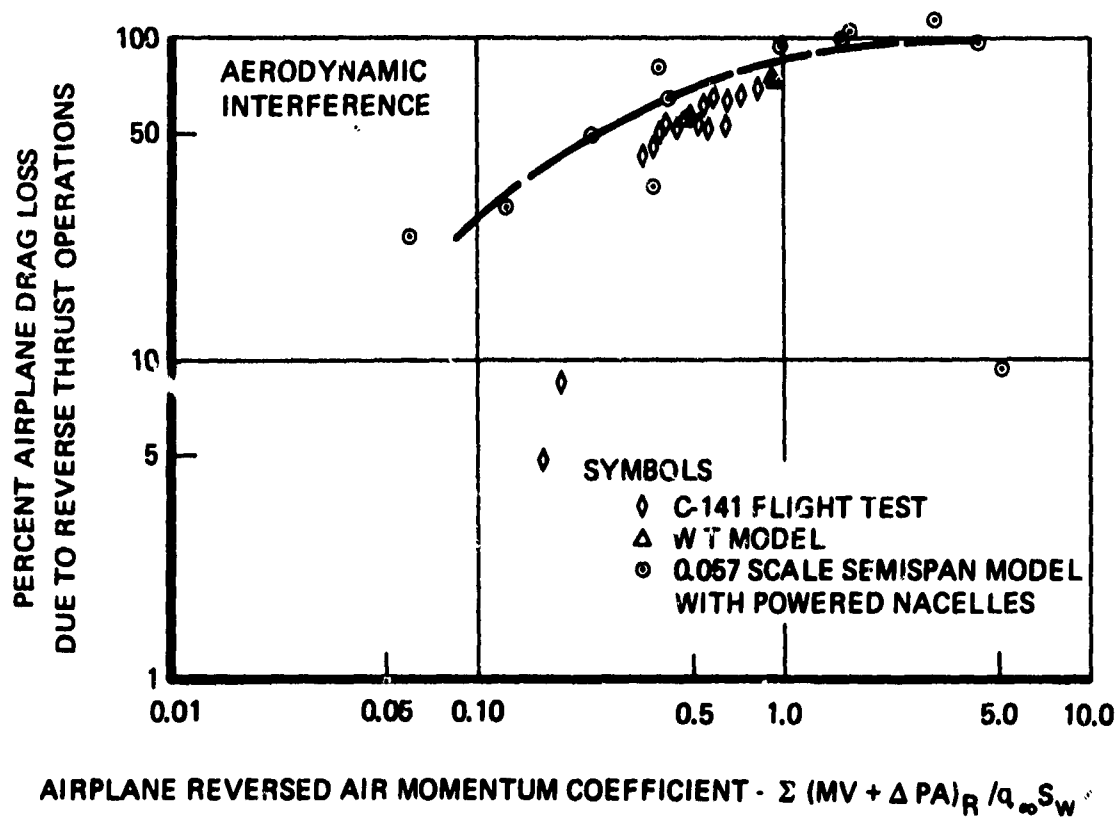
Data correlations for the above nozzles are discussed in Sections 2.1 and 2.3. Computer program usage is described in Section 3.3.

Aerodynamic Interference Module

Existing aerodynamic data for thrust reverser systems are for low-wing, four-engine jet transport aircraft. Thrust reverser operation frequently caused unfavorable aerodynamic interference problems, such as bouyancy lift forces on the wing and a loss in the flap drag. Both effects were experienced by the original 737 clamshell reverser deployed in front of the flaps. When the new target reverser was installed behind the wing flaps, favorable interference, i.e., decreased lift, increased drag, resulted.

High-wing transport aircraft with pylon-mounted engines experience an increase in flap and spoiler drag due to reverser operation, as shown in Figure 96. The data correlation from Ref. 44 gives the percent reduction in drag as a function of reverser momentum coefficient.

Thrust reversers for STOL transports will be designed to deflect the flow forward and up to avoid aerodynamic interference and reingestion problems. Existing data are inadequate to predict aerodynamic interference for configurations of this type. Data are required showing the effects of TR type, location, forward speed, pressure ratio, and discharge pattern.



**Figure 96: EFFECT OF REVERSE THRUST ON AIRPLANE
DRAG DURING GROUND ROLL**

Logic has been formulated in TEM-357 that allows easy incorporation of aerodynamic data into the Aerodynamic Interference Module as data become available.

Reingestion Module

The purpose of the Reingestion Module is to predict inlet temperature rise and total pressure distortion as a function of thrust reverser type, location, forward speed, and discharge pattern. A vast amount of reingestion data have been accumulated for commercial transport thrust reversers. However, the data are of little value to candidate STOL transport thrust reverser installations because of significant differences from commercial transport TR designs.

Logic has been formulated in TEM-357 that allows easy incorporation of reingestion data into the Reingestion Module as data become available.

Engine Stability Margin Module

The purpose of the Engine Stability Margin Module is to predict effects of thrust reverser area mismatch, engine transient response, and inlet pressure and temperature distortion on engine stability margin. The engine stability margin analysis was performed by Pratt & Whitney Aircraft. The results have been tabulated and incorporated into the Engine Stability Margin Module. The analysis is summarized in the following paragraphs and described in detail in Ref. 45. A sample case is provided in Appendix II.

Stability margin studies were performed on three Pratt & Whitney Aircraft turbofan engines using a transient computer program. These engines were extracted from the Pratt & Whitney Aircraft file of study engine cycles and consist of a 2.0 BPR mixed flow, and a 6.0 and 12.0 nonmixed flow design, each with a fanhigh compression system. These cycles are typical of those considered at different BPR levels for STOL application. The objective of these stability margin studies was to obtain a set of data which would permit evaluation of engine stability margin during normal STOL operation as a function of distortion, reverser operation and thrust level to ultimately define the distortion tolerance for each engine. The reverser effect on the engine was defined to be a change in exhaust nozzle effective area.

The assumed exhaust nozzle area variation is shown in Figure 97. The definition of the deployment characteristic was selected because a review of several thrust reversers showed an over area of at least 20 percent sometime during deployment. The review also showed that an under area usually occurs near the end of the deployment stroke. The

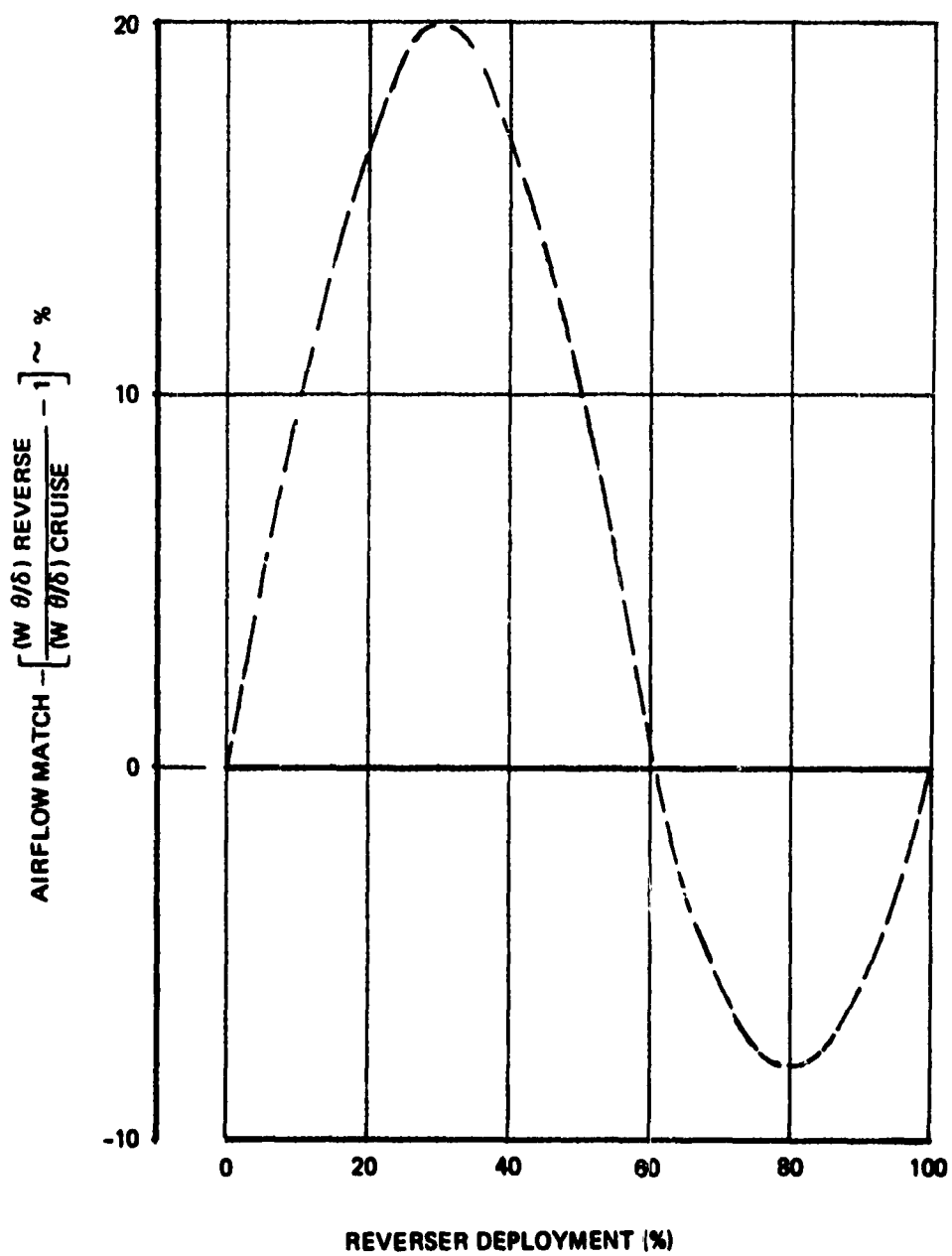


Figure 97: AIRFLOW MATCH CURVE REPRESENTING REVERSER DEPLOYMENT

deployment rate in all cases was one second from stowed to fully deployed. This rate was identified as a goal for thrust reverser design studies conducted in Part 1B of the program.

Data were calculated for both steady and transient operation at a sea level flight condition. Steady state data show the effect of thrust reverser area variation on the stability margin of the fan and compressor, as well as the thrust split between the flowstream. The thrust split can be used to estimate the reverse thrust of different types of reversers. The steady state data were obtained from each engine model by simulating the effect of a thrust reverser as a change in either primary or duct stream effective area. The effective area values investigated were the extremes of minimum and maximum area positions as identified by Boeing.

Transient operation consisted of engine accels and decels at various area values, as well as thrust reverser transitions. Accels and decels were obtained to determine the influence of off design area value on stability margin as well as the time it takes to achieve a desired thrust change. Thrust reverser transitions were obtained for the one second deployment rate with engines set at 80 percent of takeoff power, and were made from stowed to deployed as well as from deployed to stowed.

It is concluded from analysis of these data that the influence of a thrust reverser on component stability margin during transient operation is approximately equivalent to changes obtained during steady operation at the same nozzle positions. This can be observed by examination of accel and decel data, as well as thrust reverser deployment data. This conclusion simplifies thrust reverser analysis because it eliminates the need for incorporating transient stability margin data into the analysis.

A further simplification was derived for accel and decel influence on high compressor stability margin. These data have been reduced to a set of curves that define the loss or gain in stability margin as a function of engine power.

Other factors that influence stability margin are pressure and temperature distortion. Data were obtained for each engine on a "change in stability margin" basis. The effect of distortion was obtained using parallel compressor theory resulting from 180 degree square wave patterns.

2.3 Task 1.3--Plan and Conduct Supplemental Tests

Task 1.3 consisted of planning and conducting supplemental tests in conjunction with development of computer programs for thrust reverser and thrust vectoring systems. The purpose of the tests was to fill data voids discovered in the literature that would have impeded development of computer programs.

2.3.1 Identification of Technology Voids

Boeing considered identification of data voids to be an important task of this program. Computer programs developed during Task 1.2 are based on results of the literature review. Also, voids discovered formed the basis for supplemental tests. Consequently, considerable effort was made in reviewing data to accurately identify data voids and justify selection of models for supplemental tests.

A guideline established early in the planning of supplemental tests was that the tests would supply data required to complete development of the Internal Performance Module of the TR and TV System Performance Program (see Section 2.2.3). Obviously, data voids exist for new thrust reverser and thrust vectoring concepts. However, it is believed that model testing of new concepts should be deferred to Part 1C after adequate design and evaluations have been completed.

The data review resulted in identification of the following data voids in the open literature:

Blocker Door Geometry

There was a lack of a consistent set of data that isolate effects of blocker door geometry on the performance of blocker/deflector and blocker/cascade thrust reversers.

Multibearing Vectoring Nozzles

There was a lack of data for multibearing vectoring nozzles that show the effect of:

- o Duct contraction ratio
- o Turning radius
- o Low nozzle pressure ratios (<1.5)

Also, there was no data that evaluate the multibearing vectoring nozzle as a combined thrust reverser and vectoring system (120 degree deflection). Available data for other types of thrust reverser and vectoring systems are adequate to formulate the Internal Performance Module of the TR and TV System Performance Program.

2.3.2 Supplemental Static Tests

On the basis of the data review, a test plan (Ref. 46) was formulated for supplemental static tests to determine:

- 1) Multibearing vectoring nozzle performance as a function of parametric geometry variations.
- 2) Blocker door geometry effects on performance of blocker/cascade and blocker/deflector thrust reversers.

The test plan was submitted to the Air Force program manager in September 1971 and was approved in October. Static testing was conducted from 20 December 1971 to 14 February 1972 on the thrust vector rig at the Boeing Propulsion/Noise Laboratories.

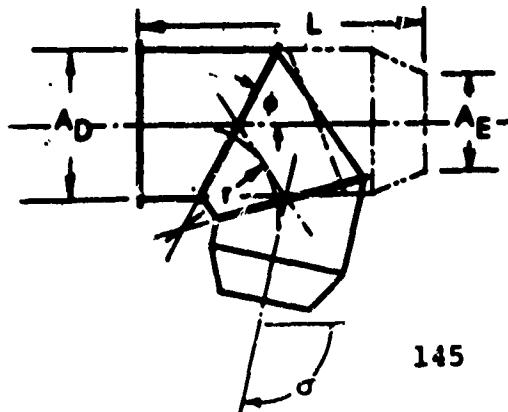
A test report (Ref. 47) was prepared and submitted to the Air Force program manager in March 1972. Descriptions of test models and results are summarized in the following sections. The test results have been incorporated into the Internal Performance Module of ER and TV System Performance Program TEM-357.

Multibearing Vectoring Nozzle Static Test

The objectives of the multibearing vectoring nozzle static tests were to:

- 1) Evaluate the vectoring nozzle internal performance (thrust and mass flow) for variations of:
 - a) Bearing angle
 - b) Duct turning Mach number (inlet and exit)
 - c) Duct turning radius
 - d) Overall duct and nozzle length
 - e) Thrust vector angle
 - f) Nozzle pressure ratio
- 2) Evaluate the multibearing vectoring nozzle as a thrust reverser system.
- 3) Establish design criteria for full-scale nozzle design.

A total of 10 multibearing nozzle test configurations were tested including the following geometric variations:



- 1) Bearing angle, $\phi = 65^\circ, 60^\circ$
- 2) Duct contraction ratio:
 $\phi = 65^\circ, A_D/A_E = 1.345, 1.760, 2.94$
 $\phi = 60^\circ, A_D/A_E = 1.345, 2.94$
- 3) Duct turning radius ratio:
 $\phi = 65^\circ, (r/D)_{\min} = 0.641, 0.926$
 $\phi = 60^\circ, (r/D)_{\min} = 0.645, 0.840$
- 4) Overall duct and nozzle length:
 $\phi = 65^\circ, L/D = 2.415, 1.996$
 $\phi = 60^\circ, L/D = 2.944, 2.301$
- 5) Thrust vector angle
 $\phi = 65^\circ, \sigma = 0^\circ, 30^\circ, 60^\circ, 100^\circ$
 $\phi = 65^\circ, \sigma = 0^\circ, 30^\circ, 60^\circ, 90^\circ, 120^\circ$

In addition, one of the models tested has a converging duct section that accelerated flow through the duct turn. The model had a contraction ratio of $A_D/A_E = 2.94$ and bearing plane angles of 60 degrees. All models were tested over the pressure ratio range from 1.1 to 3.0. A test model is shown installed on the vectoring rig in Figure 98.

Many of the configurations had nearly equivalent performance. Therefore to improve readability, data points are not shown on the following comparison plots. Plotted data for each nozzle configuration are presented in Appendix I of Ref. 47. Results of the multibearing static test are summarized below.

- 1) Vector efficiency and airflow match are decreased as duct contraction ratio decreases (and duct Mach number increases) especially below contraction ratio of 1.760. Airflow match was significantly lower for contraction ratio of 1.345 at maximum deflection angle (Figure 99 through 101).
- 2) The duct turning radius was not a significant influence on vectoring nozzle performance. Generally, vectoring efficiency was improved 0.5 to 1.5 percent and airflow match was improved by two percent when the turning radius ratio was increased at maximum deflection (Figure 102 and 103).

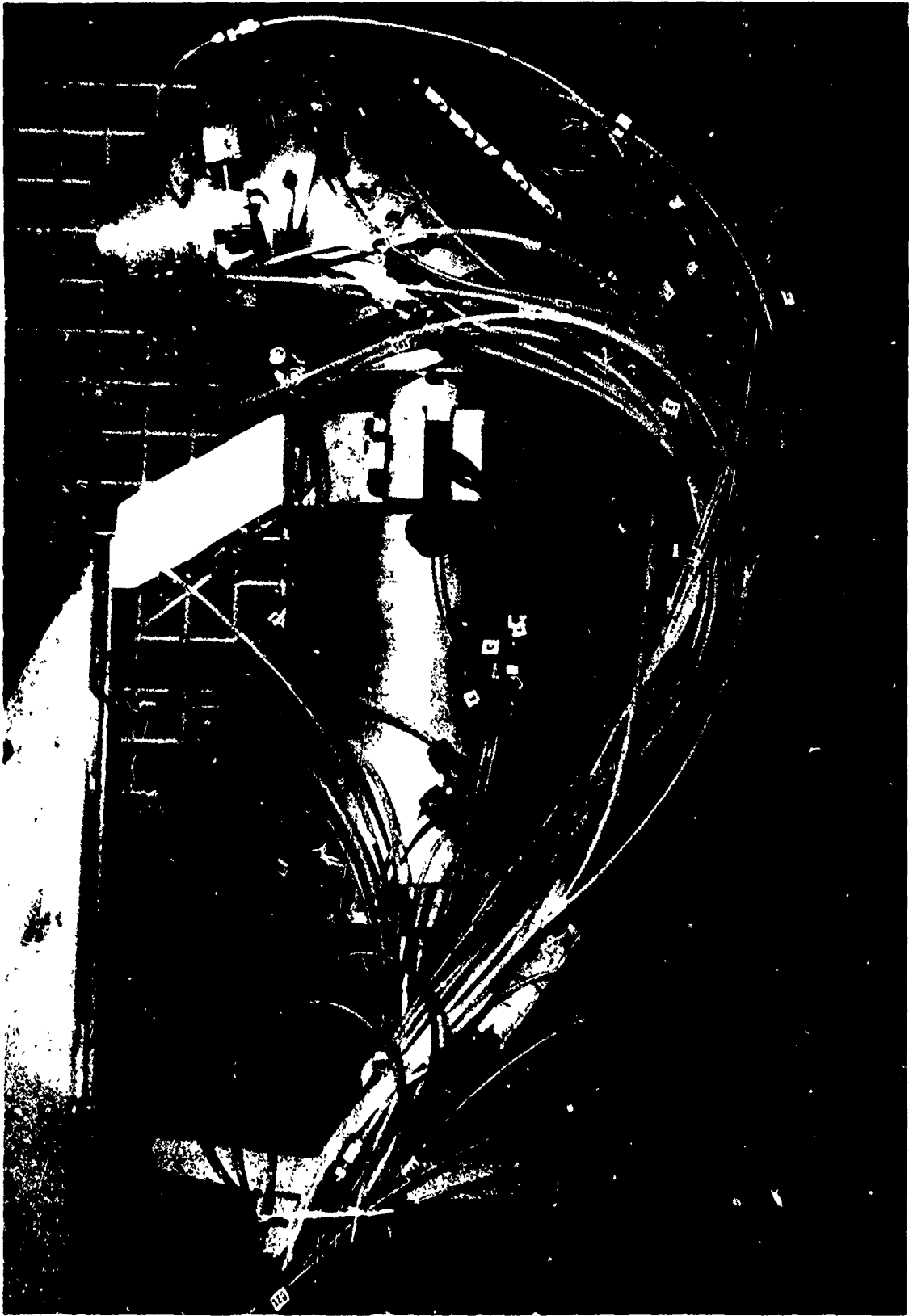


Figure 98: **MULTIBEARING VECTORING NOZZLE MODEL INSTALLATION**

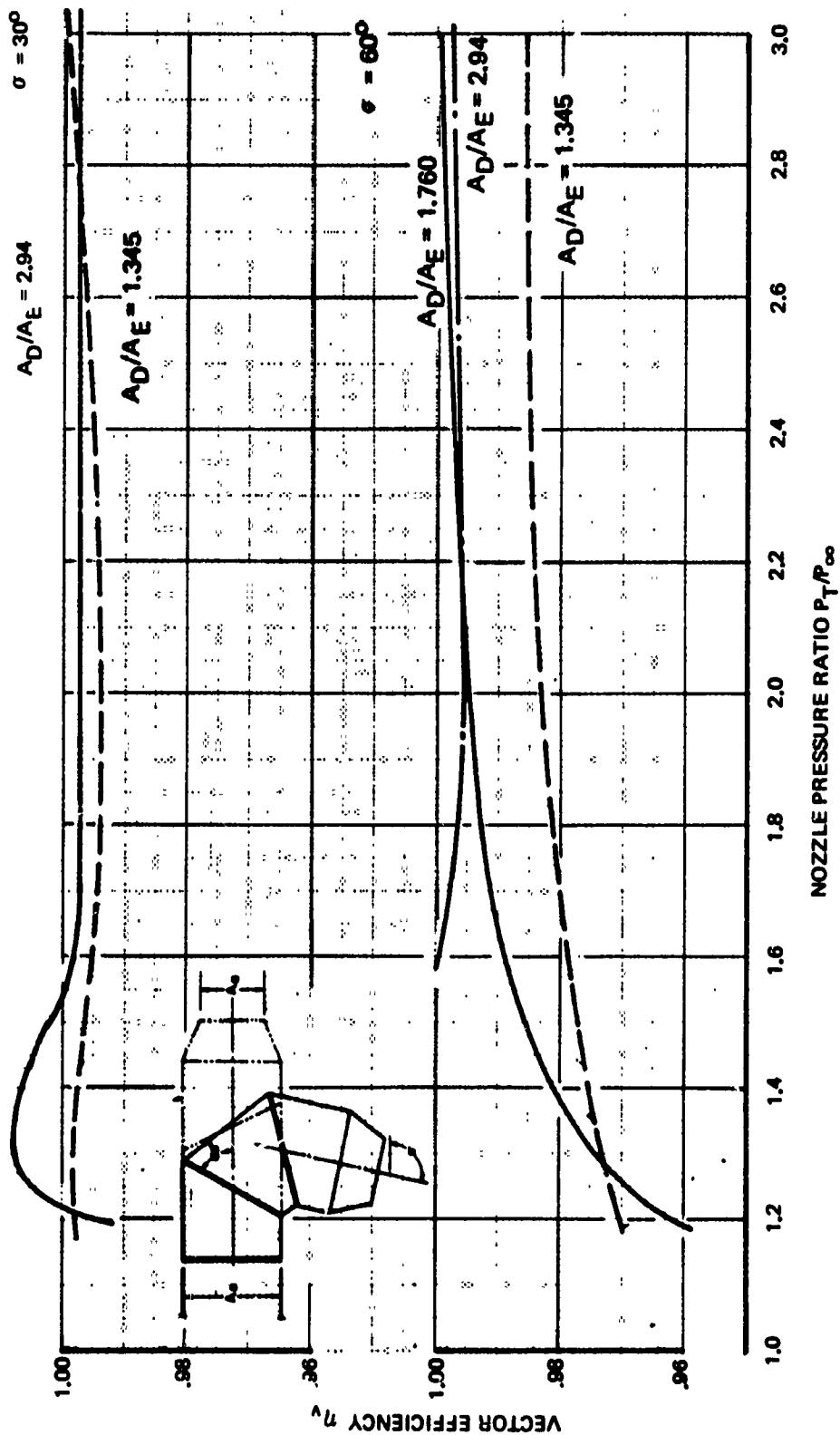


Figure 99: EFFECT OF DUCT CONTRACTION RATIO ON VECTOR EFFICIENCY $\phi = 65^\circ$

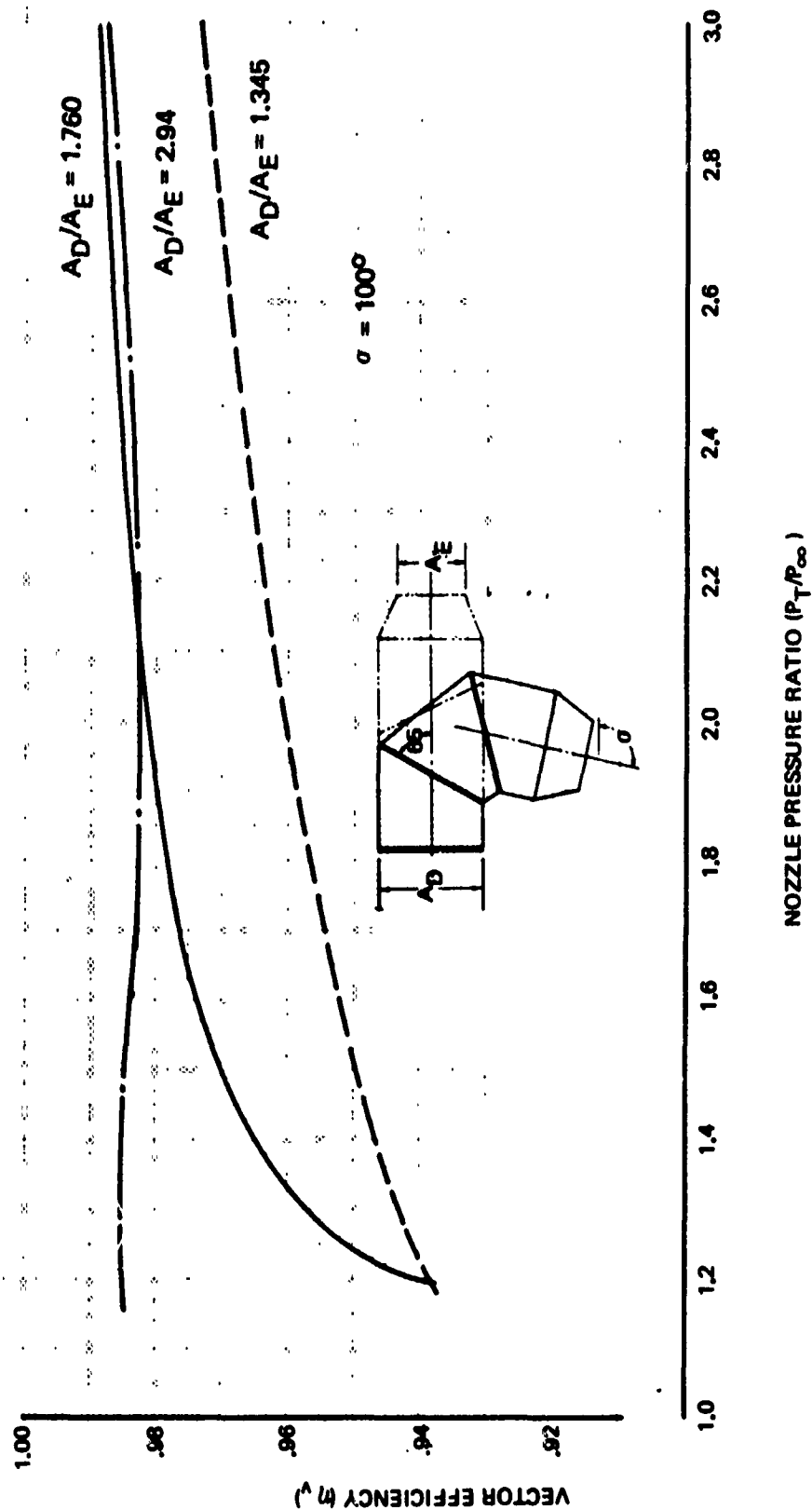


Figure 99: (Concluded) EFFECT OF DUCT CONTRACTION RATIO ON VECTOR EFFICIENCY $\phi = 65^\circ$

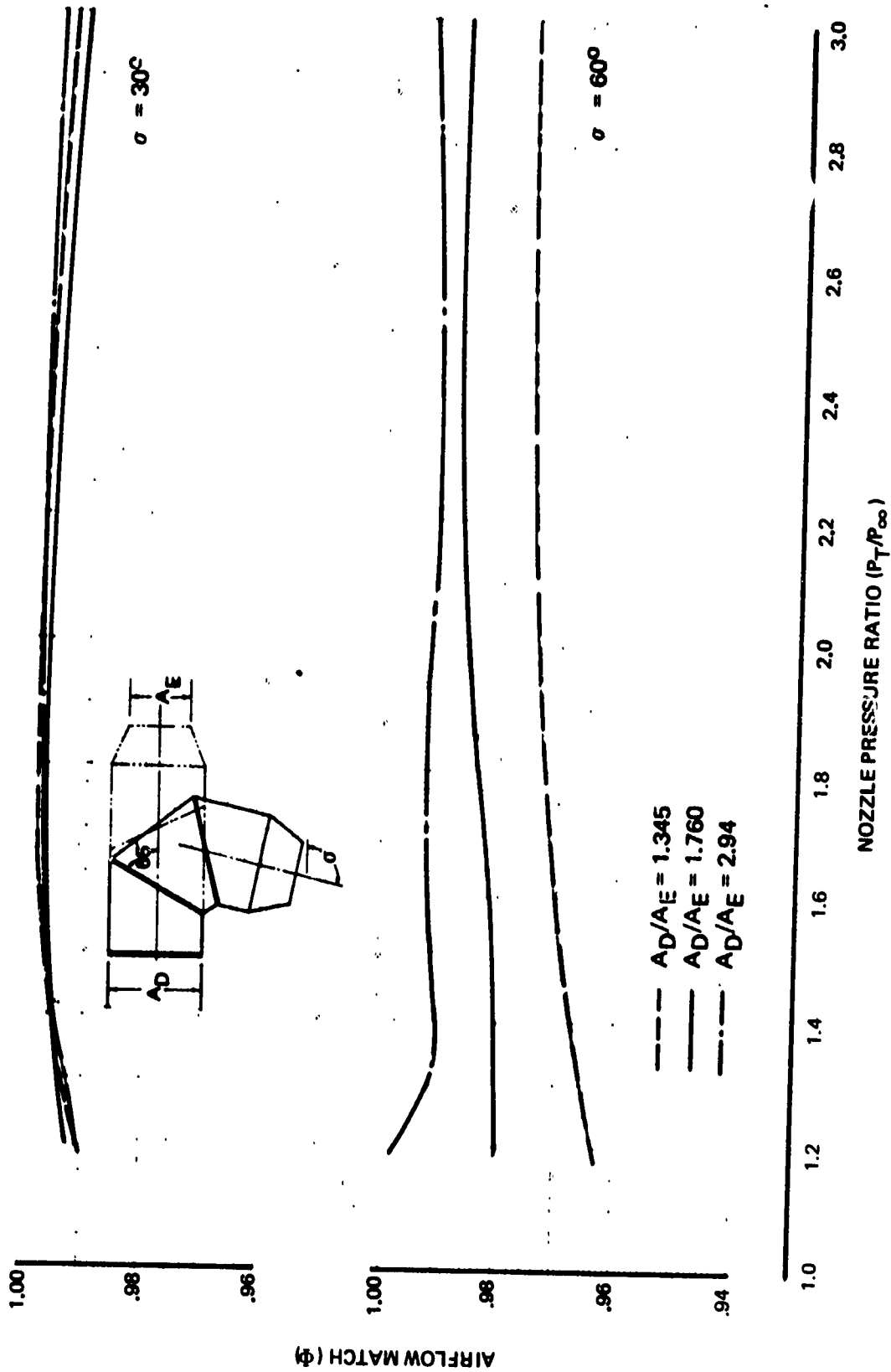


Figure 100: EFFECT OF DUCT CONTRACTION RATIO ON AIRFLOW MATCH $\phi = 65^\circ$

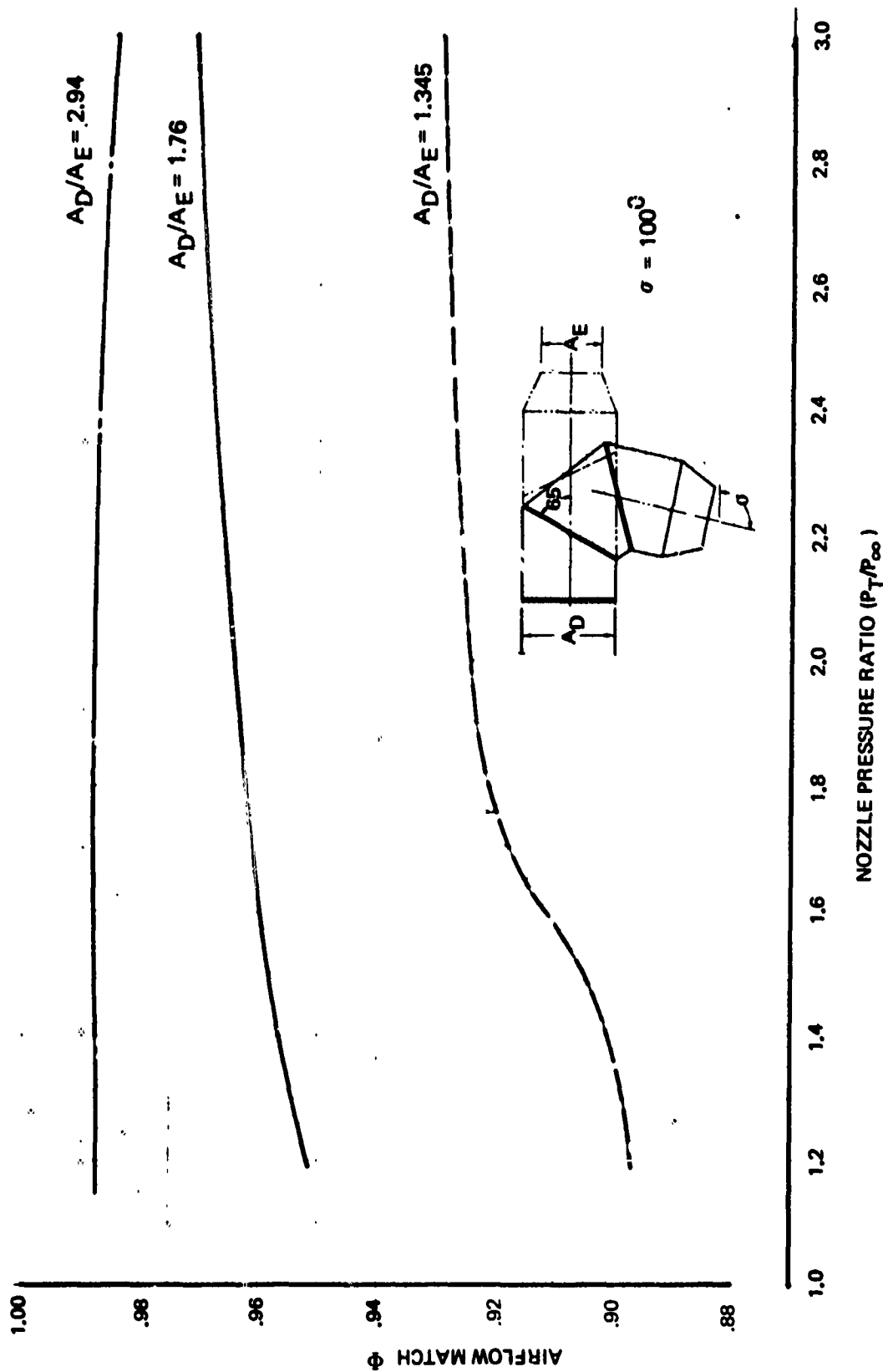


Figure 100: (Concluded) EFFECT OF DUCT CONTRACTION RATIO ON
AIRFLOW MATCH $\phi = 65^\circ$

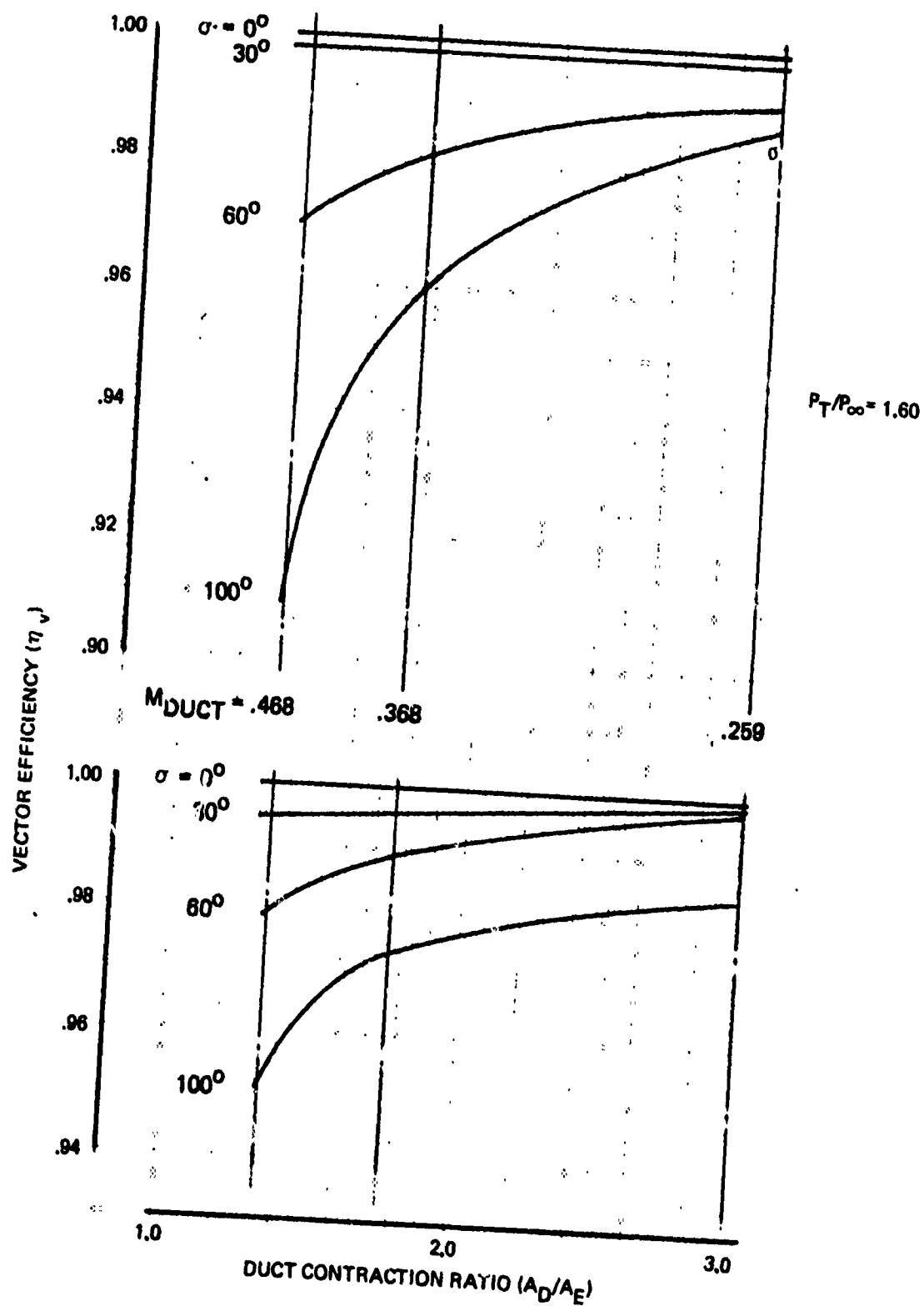


Figure 101: EFFECT OF DUCT CONTRACTION RATIO AT $P_T/P_\infty = 1.60$

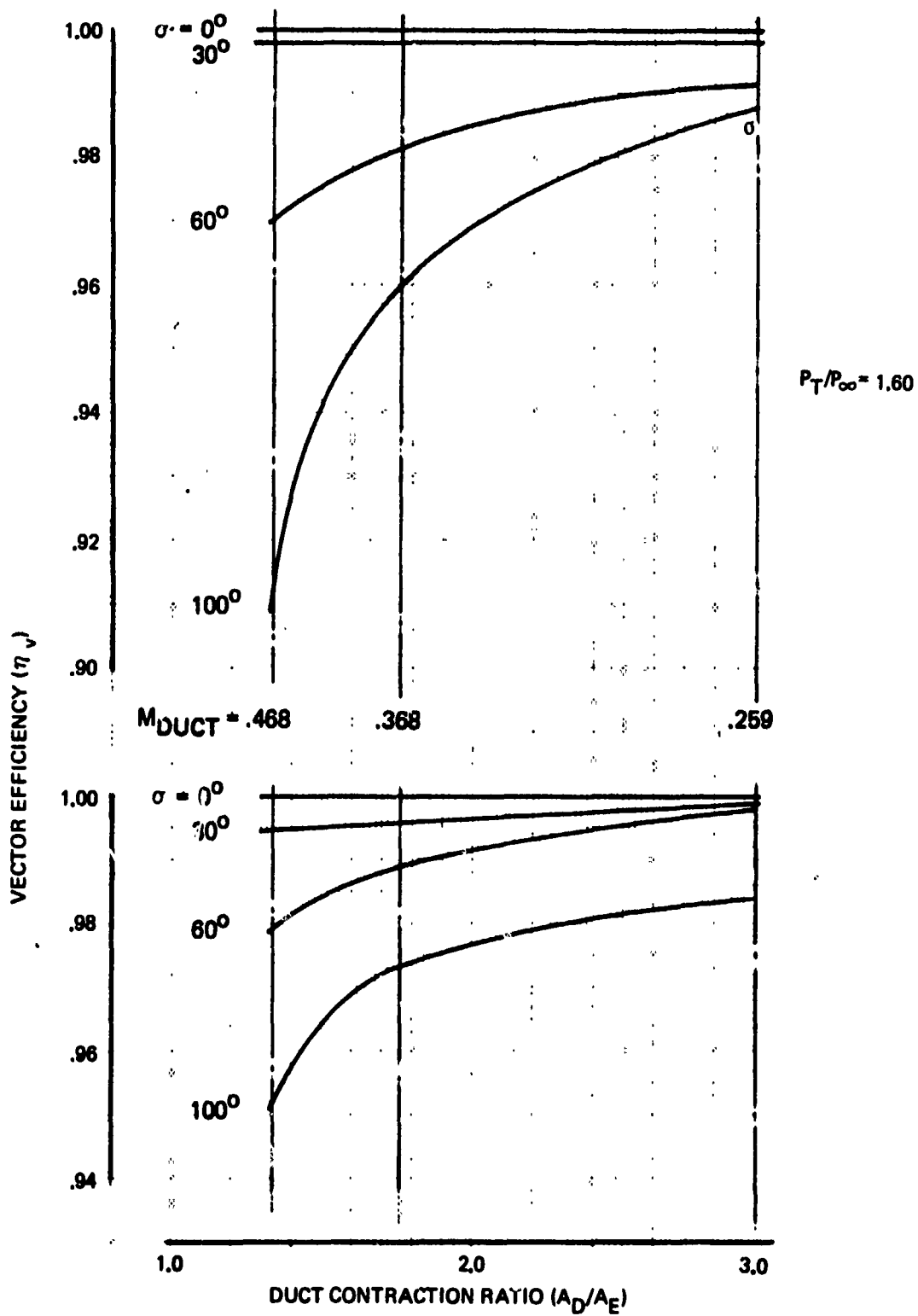


Figure 101: EFFECT OF DUCT CONTRACTION RATIO AT $P_T/P_\infty = 1.60$

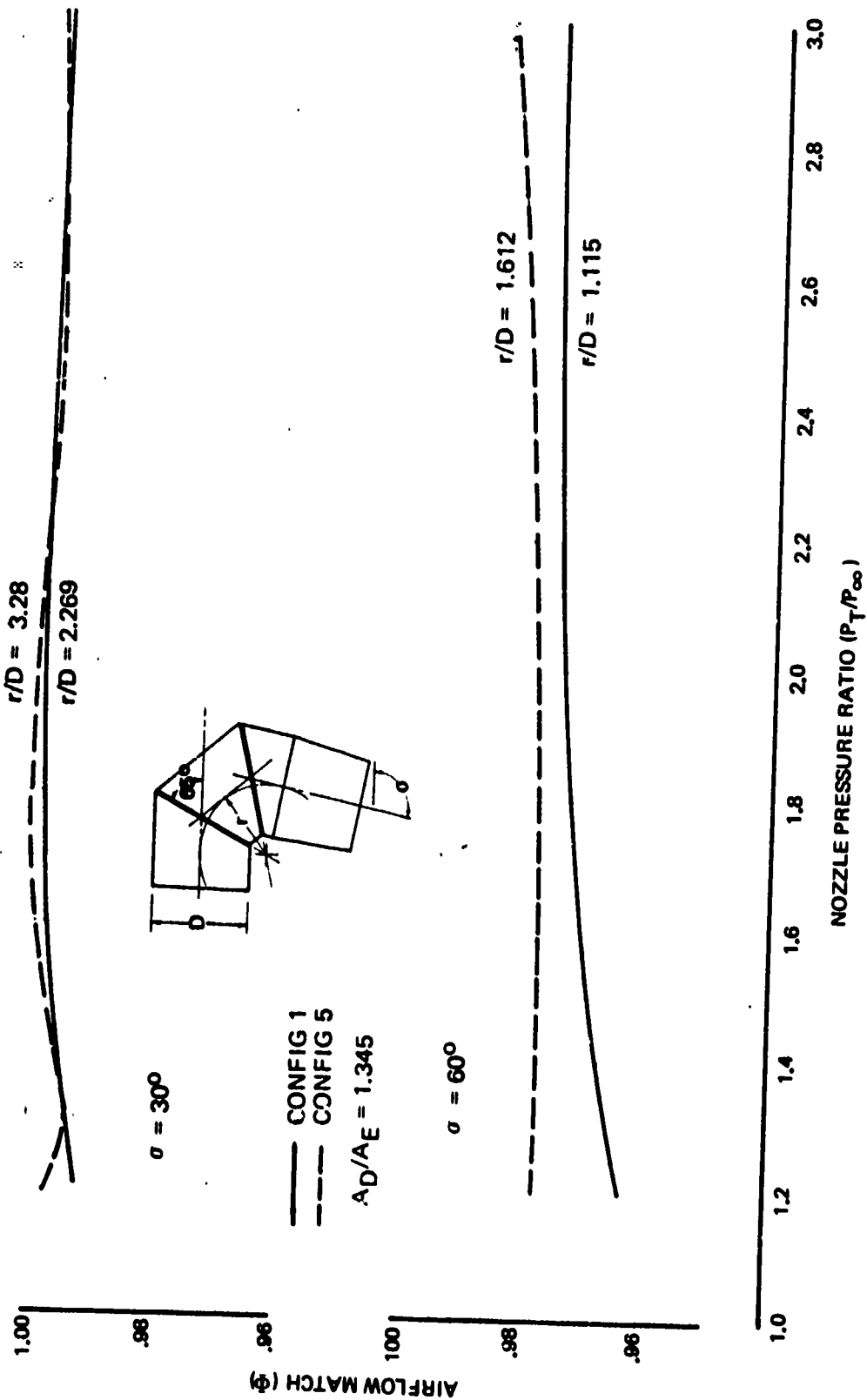


Figure 103: EFFECT OF DUCT TURNING RADIUS ON AIRFLOW MATCH, $\phi = 65^\circ$

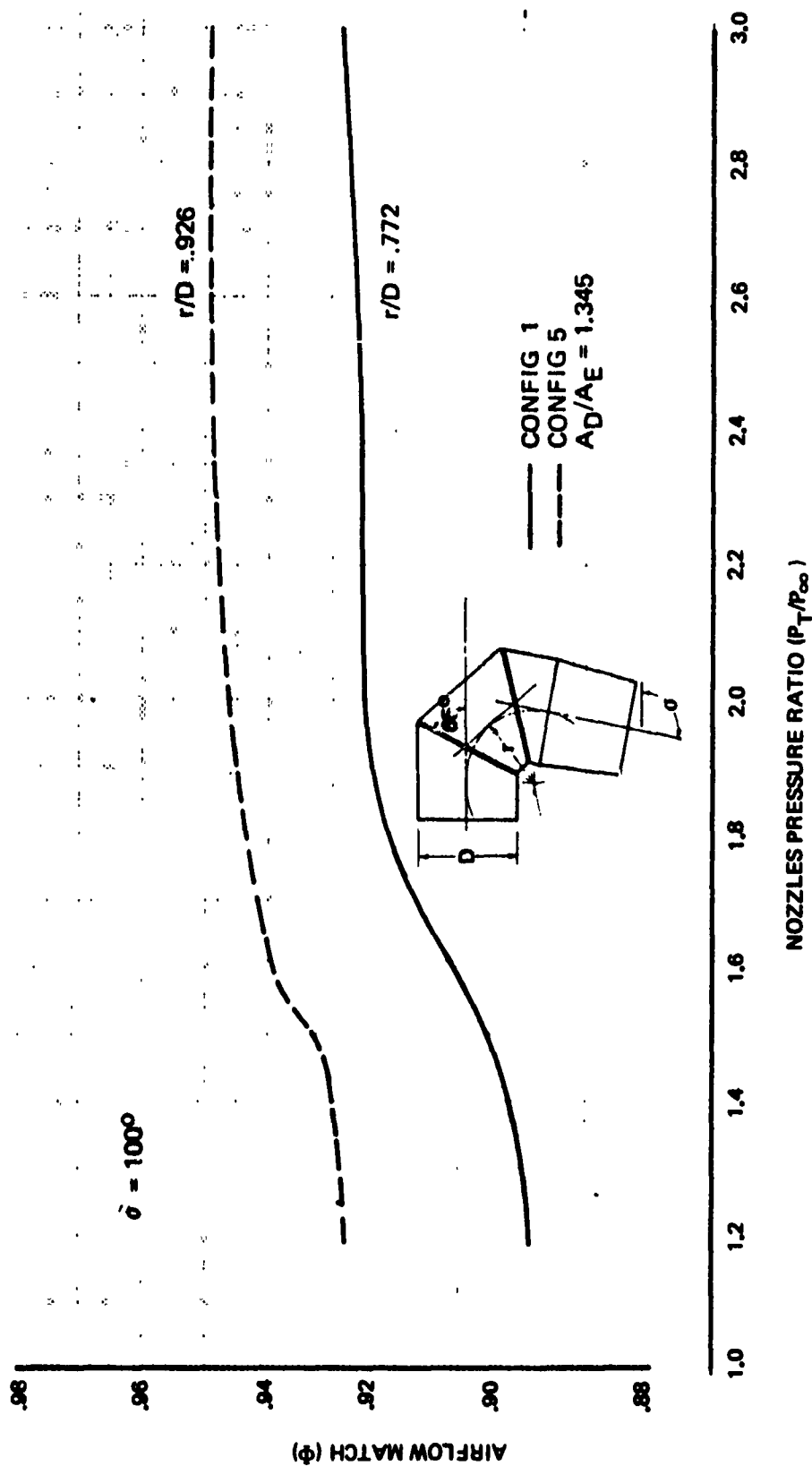


Figure 133: (Concluded) EFFECT OF DUCT TURNING RADIUS ON AIRFLOW MATCH, $\phi = 65^\circ$

- 3) The effect of overall duct length indicated duct and nozzle length can be made as short as possible without severe penalty to vectoring nozzle performance (Figures 104 and 105).
- 4) Reverser efficiency of 47 to 49 percent was obtained when the 60 degree bearing plane angle configurations were tested at 120 degree deflection angle. The data indicate that satisfactory levels of reverser performance are possible when the multibearing nozzle is used as a thrust reverser (Figure 106).
- 5) The converging duct model configuration had equivalent vectoring performance when compared to a constant area duct configuration with the same contraction ratio. This design is attractive because it is shorter than constant area duct designs and therefore will have less weight (Figures 107 and 108).

Thrust Reverser Blocker Door Geometry Static Test

The purpose of this static test was to investigate blocker door geometry effects on thrust reverser performance. Test objectives were:

- 1) Determine the effect of blocker door deflection angle and setback distance on performance of blocker/deflector and blocker/cascade thrust reversers installed in the following ducts:
 - a) Annular duct of a fan nozzle
 - b) Circular duct of a primary (or mixed flow nozzle)
- 2) Establish design criteria for the above thrust reverser installations.

Initial planning for this test included four types of thrust reversers:

- o Annular duct blocker/cascade
- o Annular duct blocker/deflector
- o Circular duct blocker/cascade
- o Circular duct blocker/deflector

However, static testing of the blocker door geometry model was terminated after completion of the annular duct blocker/cascade model testing. It was decided that the results obtained would satisfy the overall objectives of the program without expenditure of funds beyond the budgeted amount. Since effects of blocker door geometry were found to be relatively small, lack of data for untested configurations will not significantly affect the accuracy of internal performance predictions of the TR and TV System Performance Program.

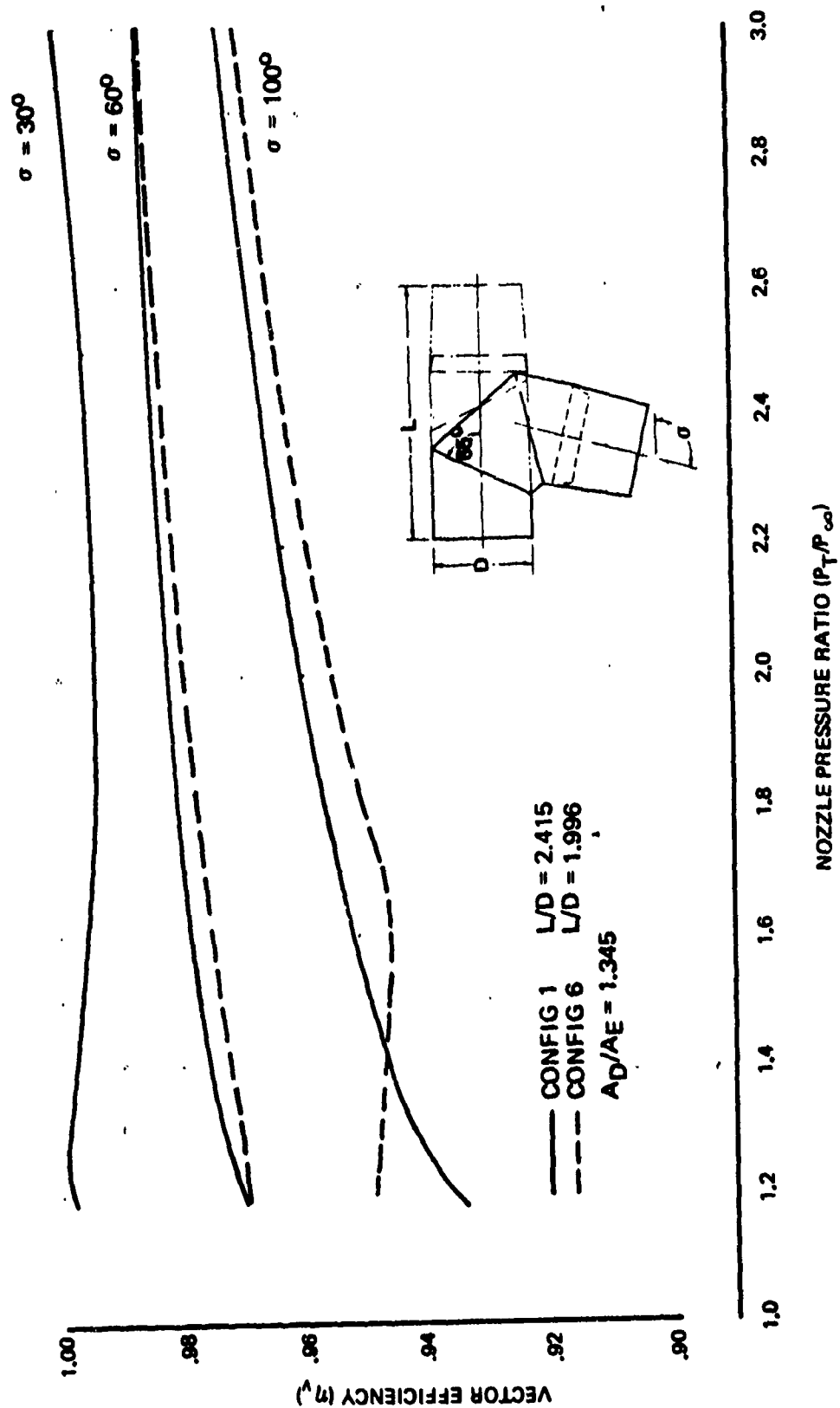


Figure 104: EFFECT OF DUCT AND NOZZLE LENGTH ON VECTOR EFFICIENCY, $\phi = 65^\circ$

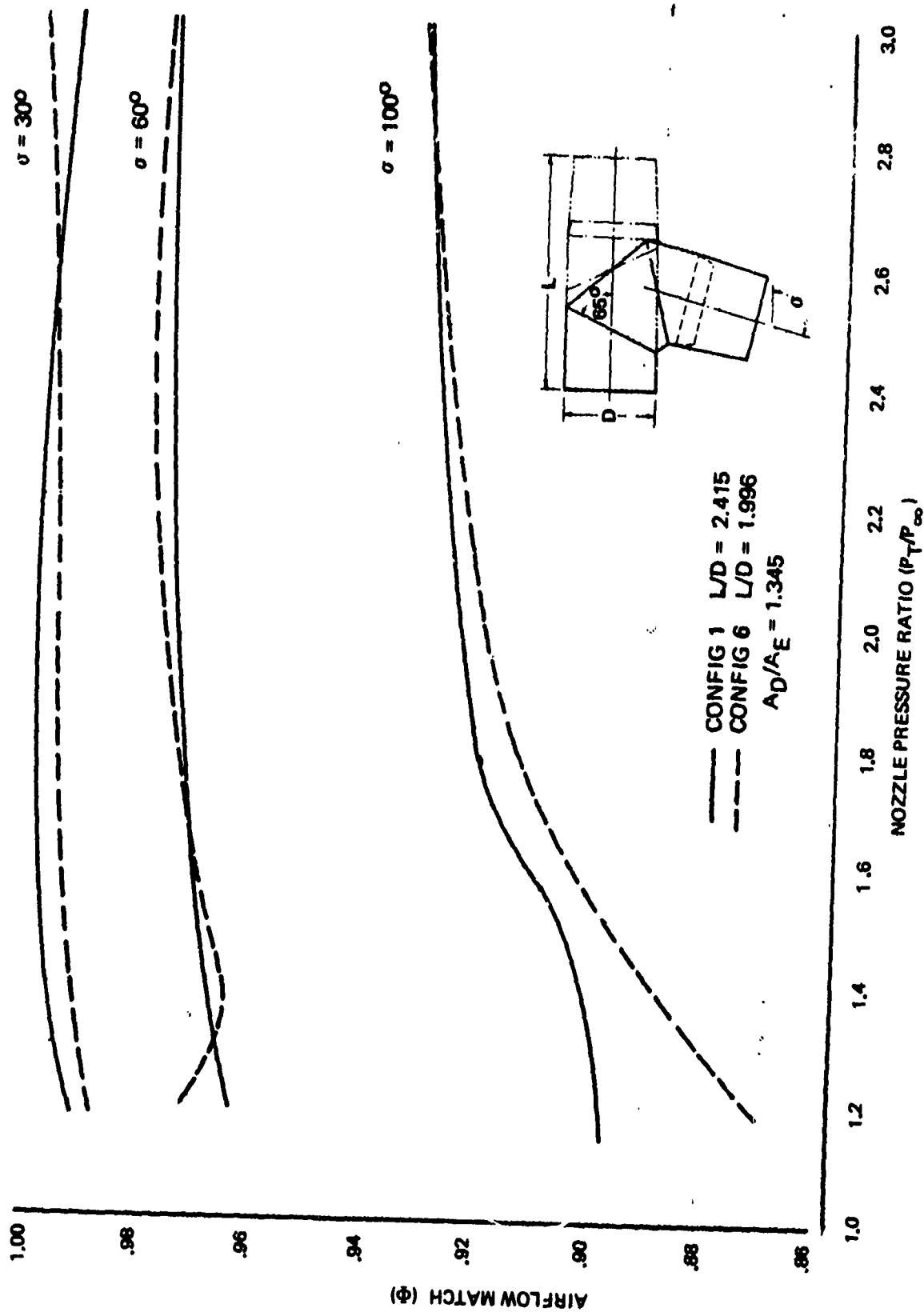


Figure 105: EFFECT OF DUCT AND NOZZLE LENGTH ON AIRFLOW MATCH, $\phi = 65^\circ$

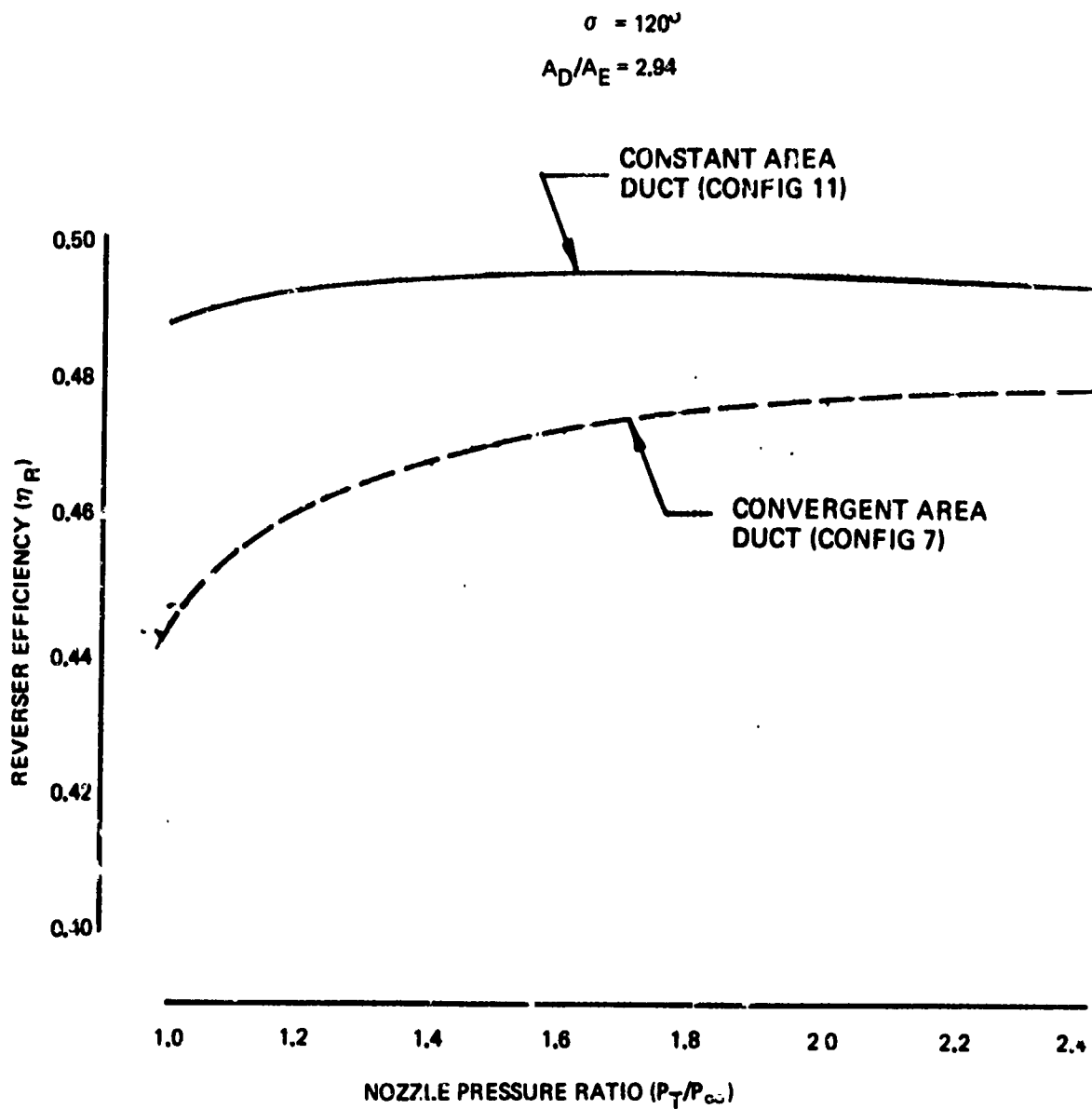


Figure 106: EVALUATION OF THRUST REVERSER PERFORMANCE

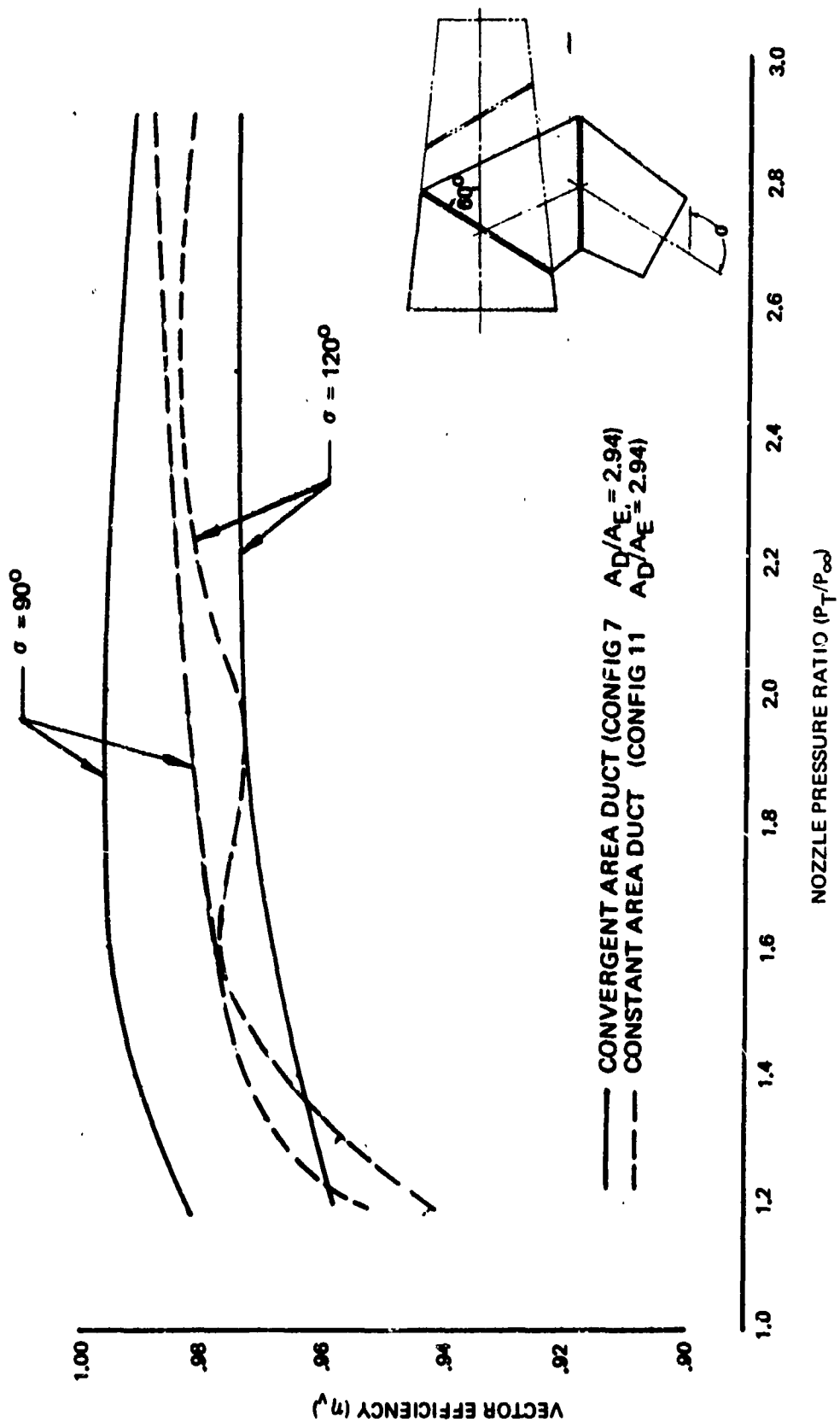


Figure 107: EFFECT OF ACCELERATING DUCT FLOW ON VECTOR EFFICIENCY

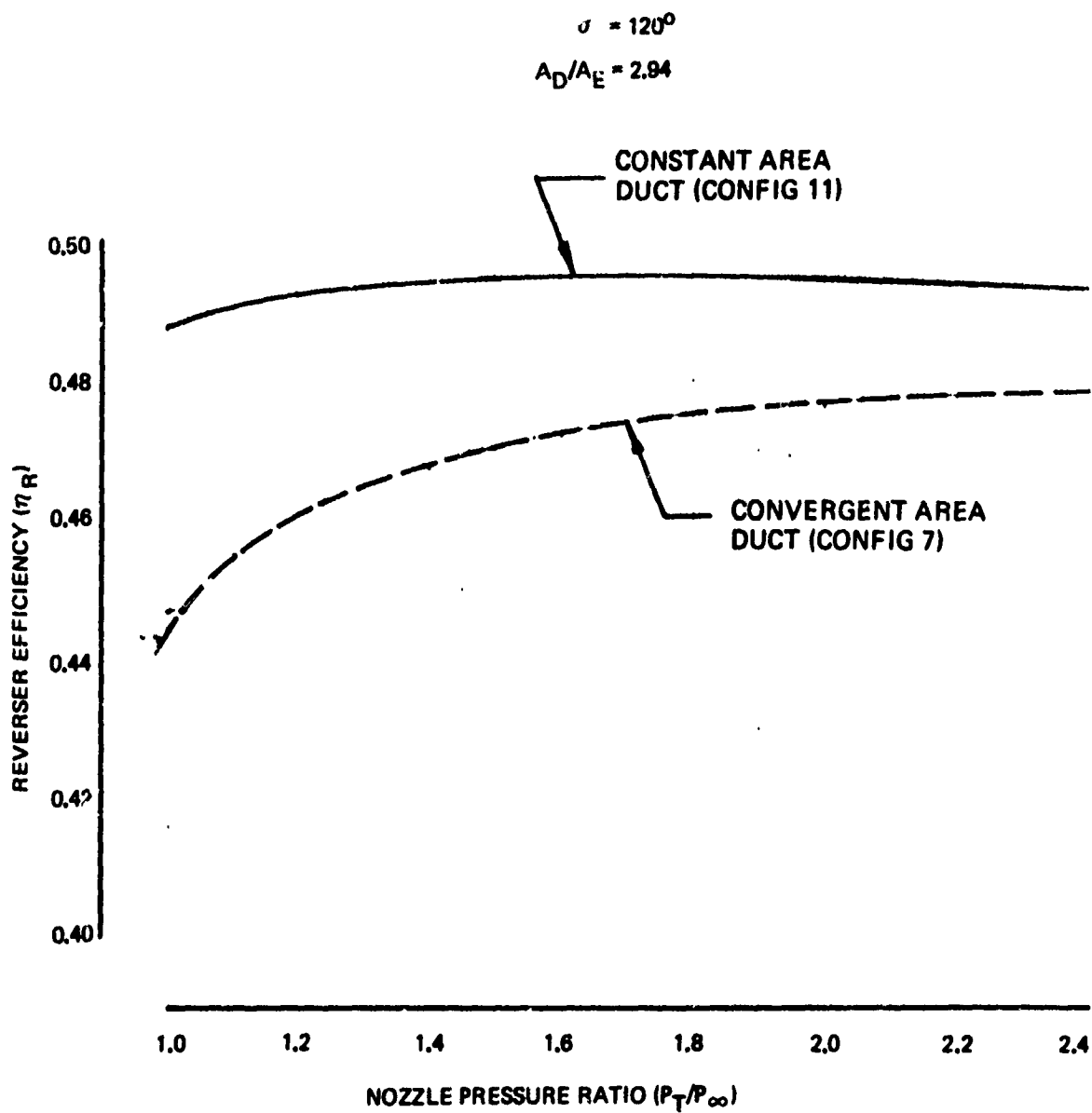


Figure 106: EVALUATION OF THRUST REVERSER PERFORMANCE

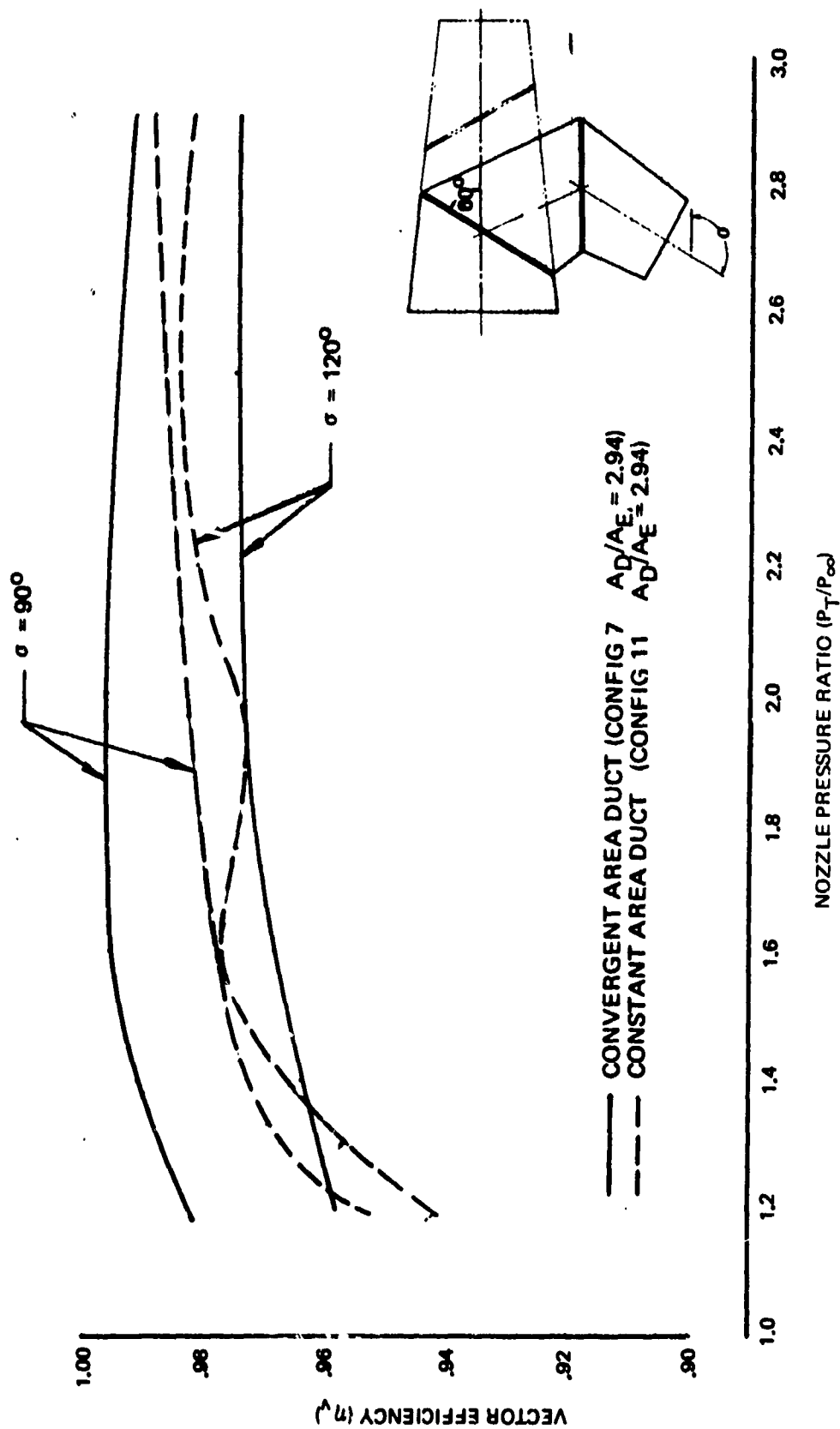


Figure 107: EFFECT OF ACCELERATING DUCT FLOW ON VECTOR EFFICIENCY

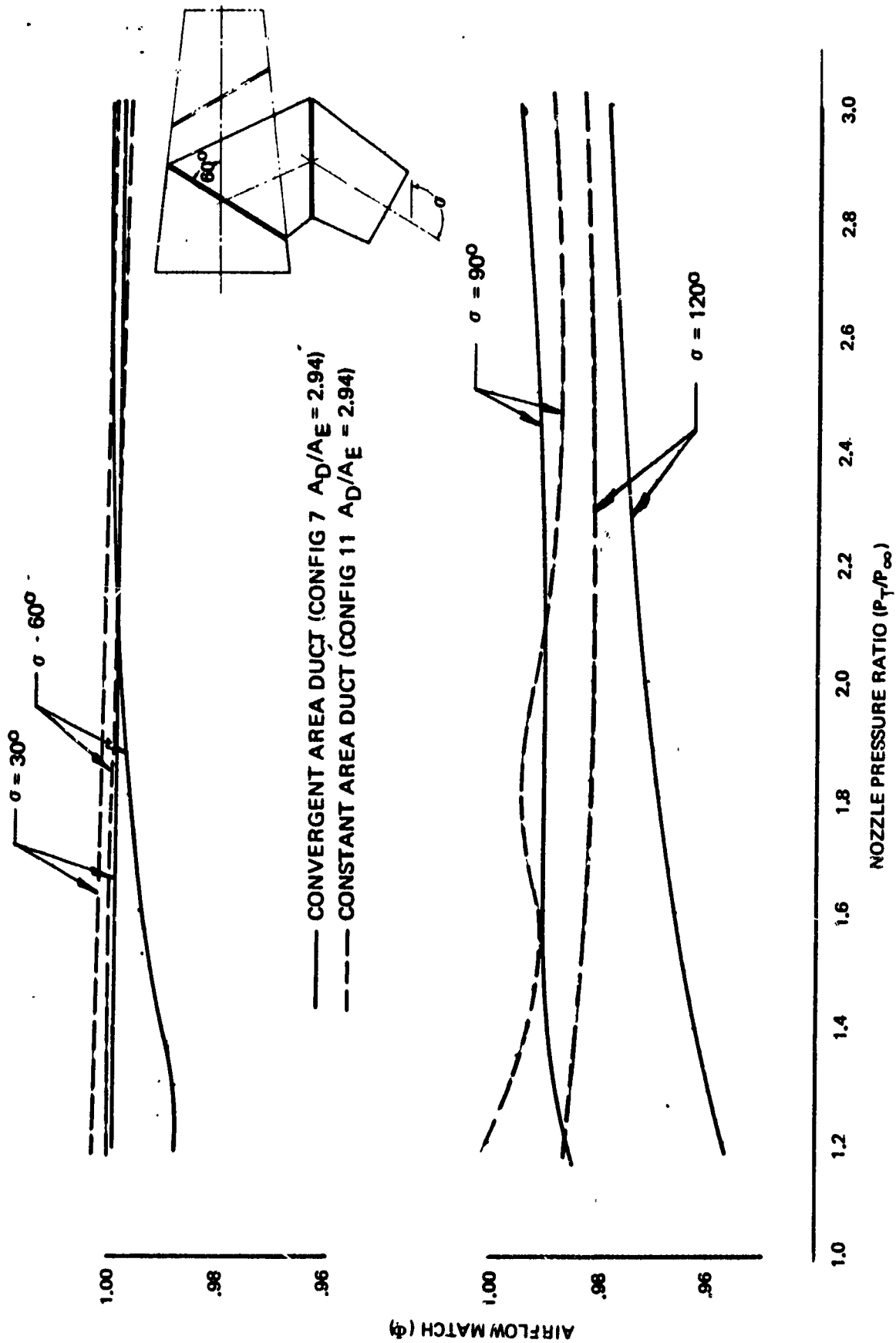
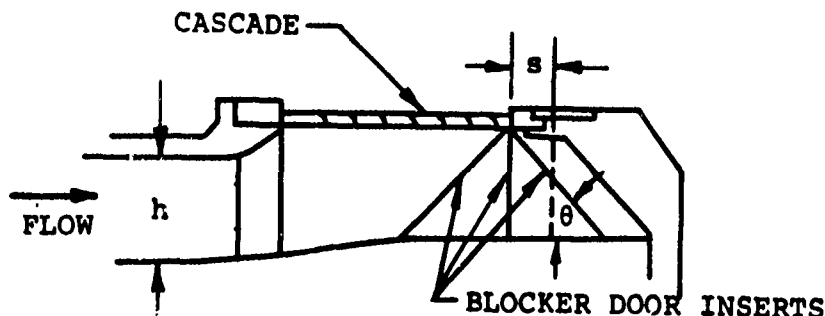


Figure 108: EFFECT OF ACCELERATING DUCT FLOW ON AIRFLOW MATCH

The blocker door geometry static test model consisted of an annular flow duct simulating a fan exhaust duct, a simulated engine strut (internal), and a cascade reverser model similar to the type used on the fan reverser on the Model 747 JT9D-3A engine. A photograph of the model installation is shown in Figure 109.



Inserts for 45, 90, and 135 degrees were used to simulate the blocker door geometry. The model was tested with setback distances of $s/h = 0$ and 0.50.

The effects of blocker door geometry were evaluated as increments relative to the $\theta = 90$ degrees, $s/h = 0$, blocker door configuration. Data points are not shown in the comparison curves. Test data for each model configuration showing absolute levels are shown in Appendix I of Ref. 47. The results of the test are summarized as follows:

- 1) Data indicate optimum blocker door design for an annular cascade reverser is the 90 degree door geometry. Reverser performance was lower for the 45 and 135 degree blocker door geometry configurations. (Figure 110)
- 2) Blocker door setback distance has minimal effect on reverser performance, as shown in Figure 111. The data show that small positive or negative changes in reverser efficiency occurred when the blocker door was set back from the cascade depending on the nozzle pressure ratio.

Details of test models and installation, instrumentation, procedure, and results of the multibearing vectoring nozzle and blocker door geometry static tests are presented in Ref. 47.

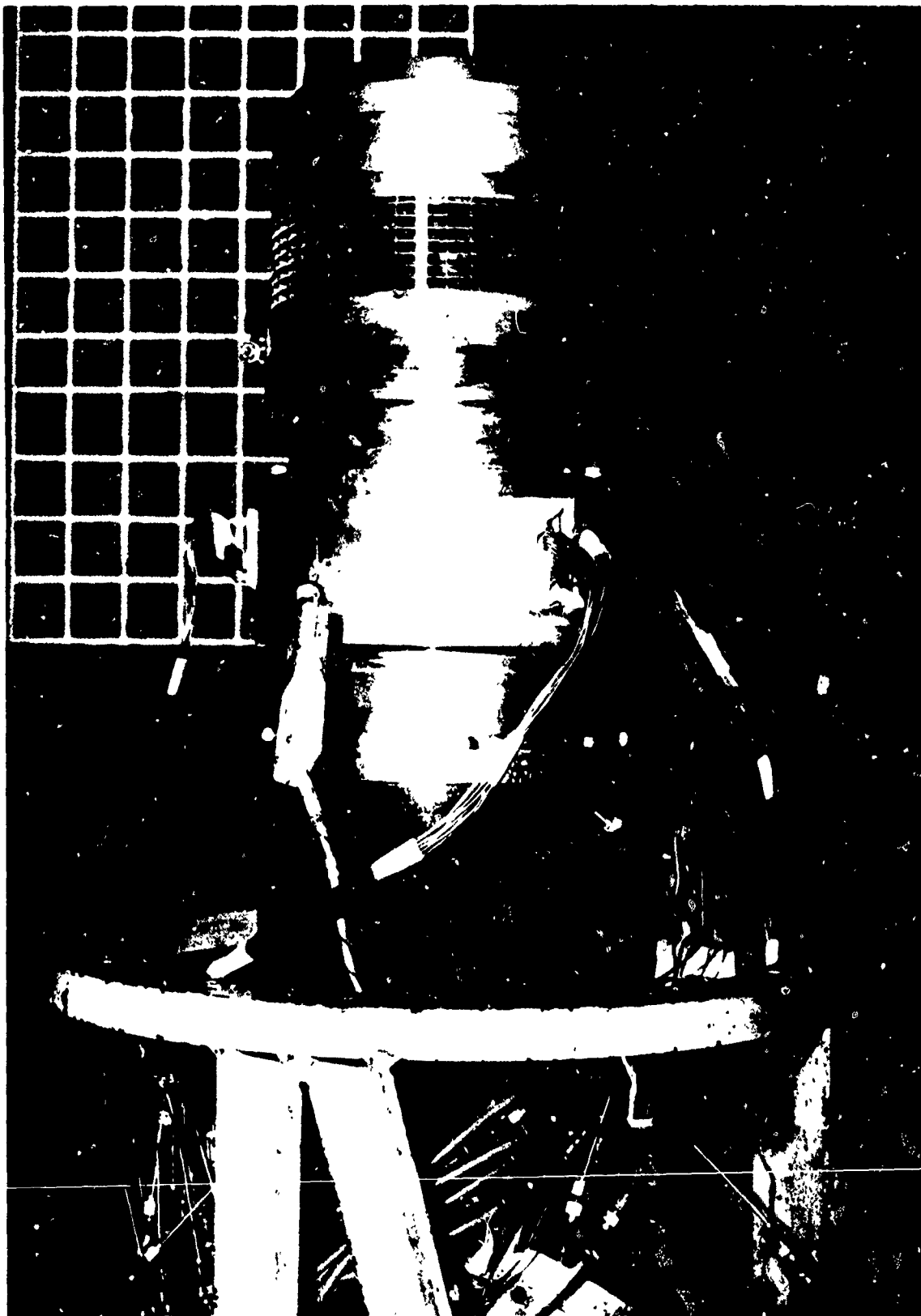


Figure 109: BLOCKER DOOR GEOMETRY MODEL INSTALLATION

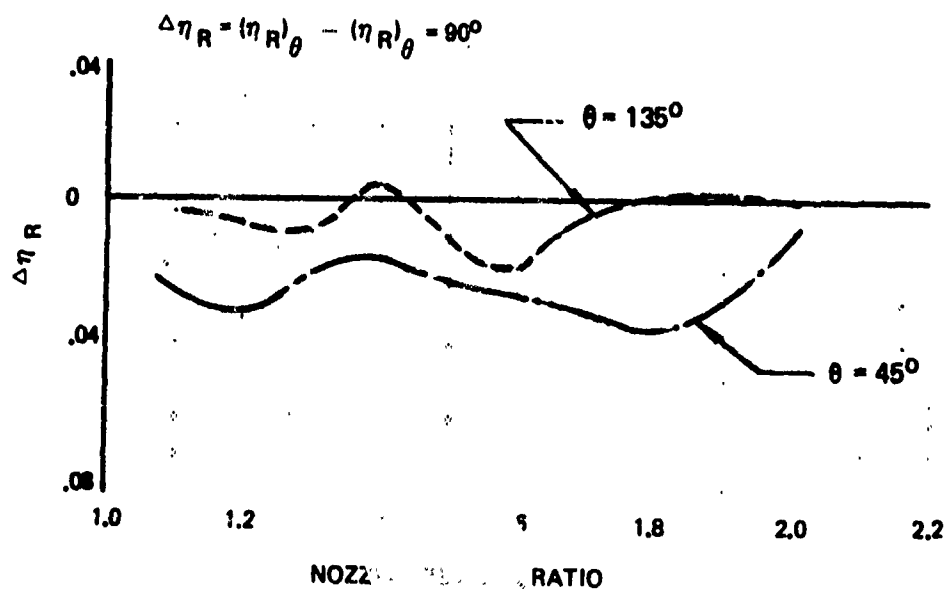
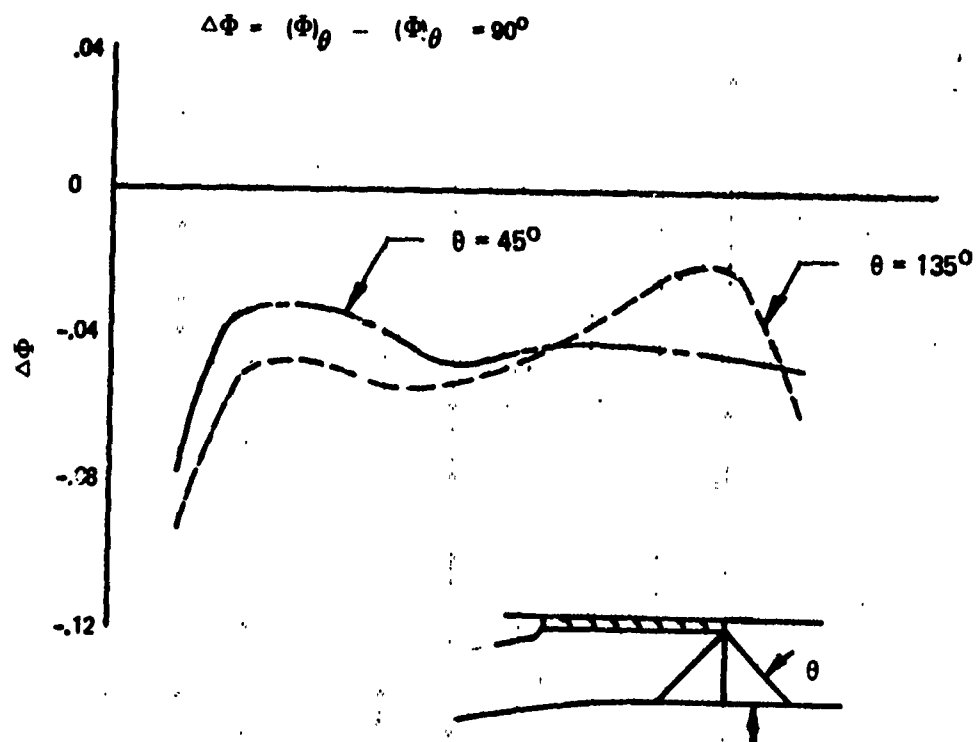


Figure 110. EFFECT OF BLOCKER DOOR ANGLE ON CASCADE REVERSER PERFORMANCE

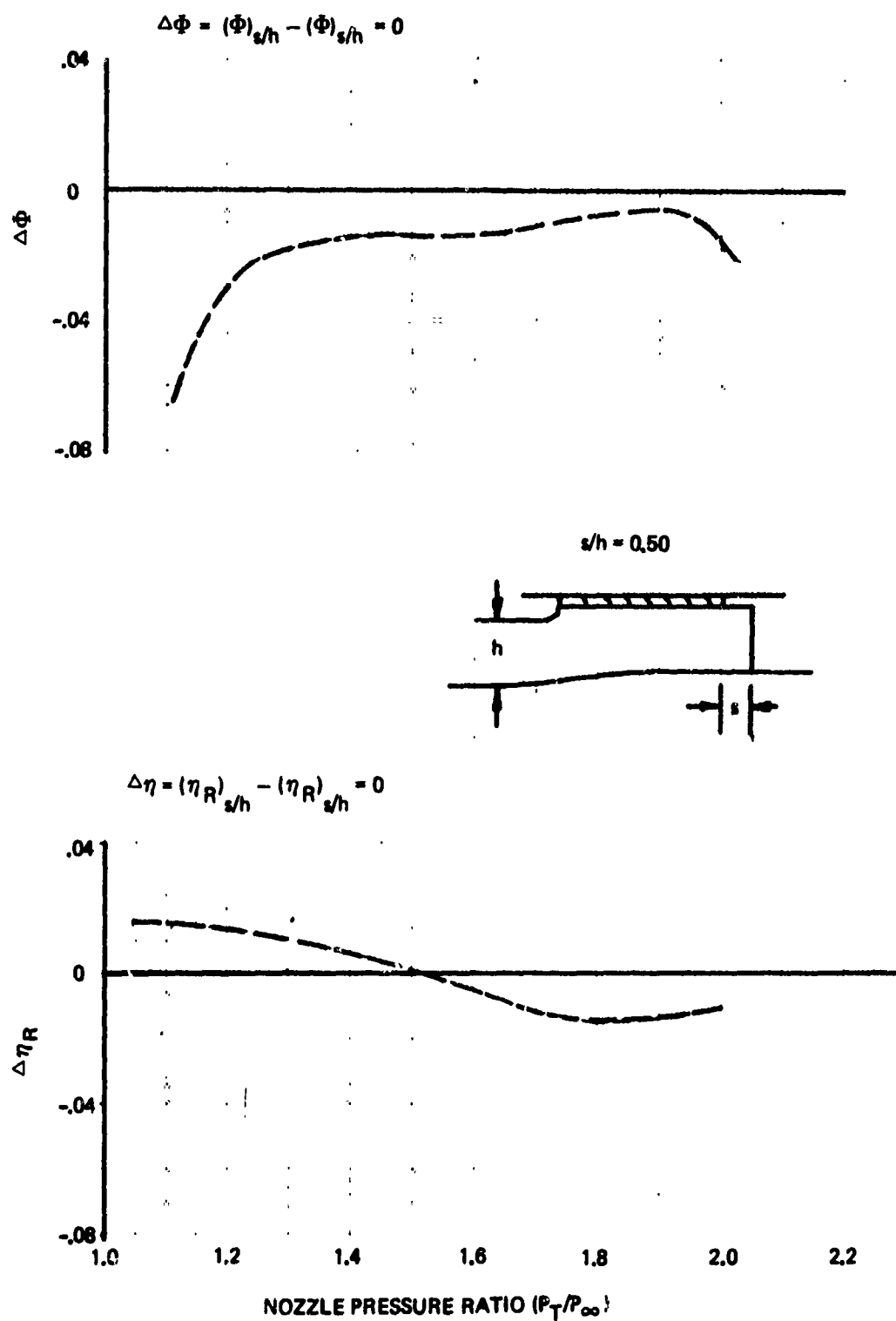


Figure 111: EFFECT OF BLOCKER DOOR SETBACK DISTANCE ON CASCADE REVERSER PERFORMANCE

SECTION III

CONCLUSIONS AND RECOMMENDATIONS

The tasks conducted during Part 1A of this program have produced several useful tools for thrust reverser and vectoring nozzle design studies:

- 1) Thrust Reverser and Thrust Vectoring Literature Review Document (Ref. 1) --to allow a reader to easily determine sources of data related to his particular interest.
- 2) Jet Trajectory and Spreading Program--to predict the trajectory and shape of the thrust reverser or vectoring nozzle exhaust plume.
- 3) Reingestion Prediction Program--to predict the on-set of reingestion for arbitrary thrust reverser and airplane configurations as a function of geometry and flow condition.
- 4) TR and TV System Performance Program--to predict TR and TV nozzle performance and engine stability margin characteristics.

In addition, static tests were conducted to determine:

- 1) Multibearing vectoring nozzle performance as a function of parametric geometry variations.
- 2) Blocker door geometry effects on the performance of annular blocker/cascade thrust reversers.

The test results filled data voids discovered during the literature review and were incorporated into the TR and TV System Performance Program. The primary conclusions to be drawn from the Part 1A analytical work are:

- 1) The analytical and semi-empirical methods developed provide relatively simple design tools to evaluate the performance of many types of thrust reverser and thrust vectoring systems and to determine potential exhaust flow interference and reingestion problems. They are limited only by the current-state-of-the-art of analysis and existing empirical data.

- 2) There are many sources of thrust reverser reingestion and aerodynamic interference data for current CTOL transports. However, application of the data to STOL transports is limited because the specific requirements of STOL transports cause the thrust reverser installation to be highly configuration dependent. The requirements of exhaust flow directional control to minimize reingestion result in thrust reverser types that are significantly different than conventional designs. The aircraft high lift system has a direct influence on the nacelle location, reverser type, and hence reingestion and aerodynamic interference characteristics.
- 3) The methods used to predict the onset of reingestion would benefit from comparisons with experimental results that isolate the specific type of reingestion i.e., crossflow, self (closed loop), near field fountain, or far field fountain.
- 4) The influence of thrust reverser operation on engine stability margin during transients is approximately equivalent to changes obtained during steady state operation at the corresponding partially deployed reverser position.
- 5) Existing data for flat plate and curved external deflectors is inadequate to predict effects of setback distance and door length for other types of deflector nozzles. Static tests were conducted during Part 1C on a hinged deflector nozzle and data correlation showing effects of setback distance were incorporated into the TR and TV System Performance Program.

Recommendations for future thrust reverser and thrust vectoring work pertinent to the tools developed for Part 1A include the following:

- 1) Interactions between thrust reverser and inlet flow fields and the effects on airplane aerodynamic characteristics should be studied using three-dimensional potential flow techniques.
- 2) The closed loop reingestion criteria should be improved by using a free streamline analysis or by experiment. A parametric test of variables influencing self reingestion is recommended.
- 3) Improvements should be made to the Jet Trajectory and Spreading Program to handle multiple, merging jets, including effects of inlet suction and nonuniform flow field.

- 4) A low speed wind tunnel test should be conducted to obtain thrust reverser and thrust vectoring performance data allowing correlations of aerodynamic interference and reingestion as a function of TR and TV system type, location, forward speed, pressure ratio, vector angle, and angle of attack and yaw.

SECTION IV
COMPUTER PROGRAM USAGE

Three computer programs have been developed:

- 1) Jet Trajectory and Spreading Program TEM-356A
- 2) Reingestion Prediction Program TEM-356B
- 3) TR and TV System Performance Program TEM-357

The programs are coded in FORTRAN IV language for the Control Data Corporation 6600 (131K) digital computer. They may be compiled with either FORTRAN IV (Extended) or FORTRAN IV (Run) compilers by changing the end-of-file test in input routines. The standard FORTRAN system library (FTN) is used. There is no overlaying or use of scratch tapes. Control of the computer during checkout was by the KRONOS operating system.

Card deck arrangements for the programs are shown in Figures 112 and 113. Each program consists of control cards, either a symbolic or binary deck, and a group of data cards. The control cards shown are common for the three programs but are characteristic of the particular computer installation. Data cards for the particular problem and the first two control cards, which contain run priority, time estimate, and user identification are inserted into the deck. The other cards normally remain unchanged.

The remainder of this section describes mechanics of input data preparation. Complete descriptions of card inputs to each program are presented. Appendix II contains sample cases to acquaint users with input card format and printout format for each program. These sample cases are also intended for use in checking out the programs on computer facilities.

3.1 Jet Trajectory and Spreading Computer Program Usage

Program TEM-356A provides a simple method of obtaining jet plume shapes for four types of initial jet cross sections.

TYPE =	Initial Jet Cross Section	Page
1.	Circular	174
2.	Rectangular	176
3.	Two-dimensional	178
4.	Annular	180

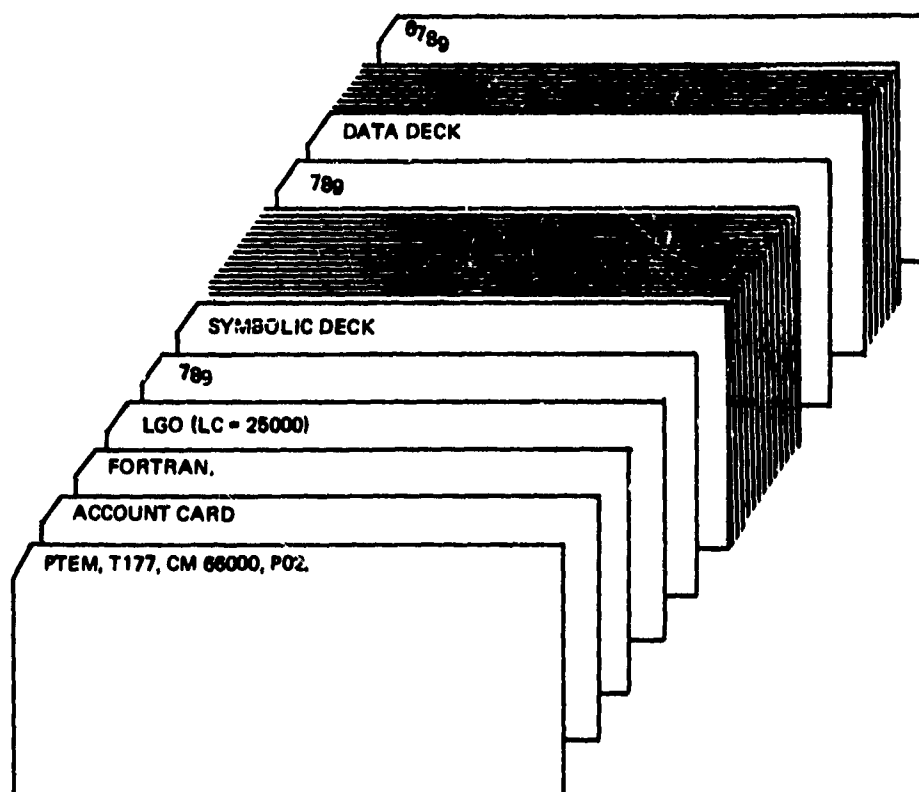


Figure 112: DECK ARRANGEMENT FOR PROGRAMS TEM-356A, TEM-356B, AND TEM-357 WHEN USING A SYMBOLIC DECK

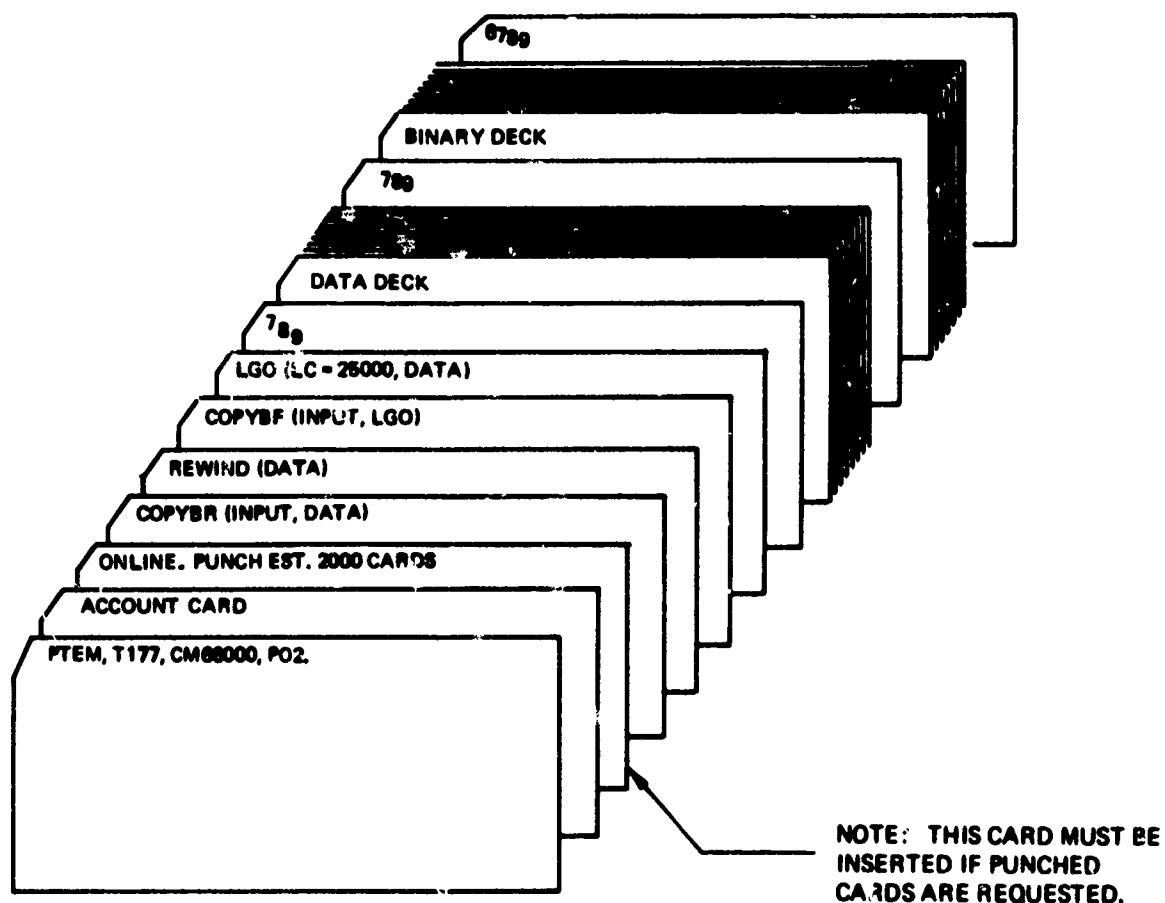


Figure 113: DECK ARRANGEMENT FOR PROGRAMS TEM-356A, TEM-356B, AND TEM-357 WHEN USING A BINARY DECK

Data Input Format

All input to program TEM-356A is in the "NAMELIST" format, except one table of values used for TYPE = 4. (page 181). The following rules must be followed to use NAMELIST format.

- 1) Card Column 1 must be blank, always.
- 2) A data set begins with a \$NEW card and ends with a \$END card.
- 3) Commas are used to separate numbers and variable names.
- 4) Variable names must be properly spelled.
- 5) Card Columns 1 to 80 are read using NAMELIST. This means that CC 73-80 cannot be used for identification purposes.
- 6) Variable names and values are read "free field." This means imbedded blanks may be used at the user's discretion, and that more than one variable may be input per card. However, the input system described on the following pages is recommended because it separates the numbers and makes data checking easier.

The general card stacking arrangement is shown in Figure 114. The user may run as many jet plumes as he desires in a single computer submission. There are no restrictions as to sequence of the four types. Detailed card inputs for the four types are contained in the next section. Users are cautioned to check their inputs carefully before submitting a computer run.

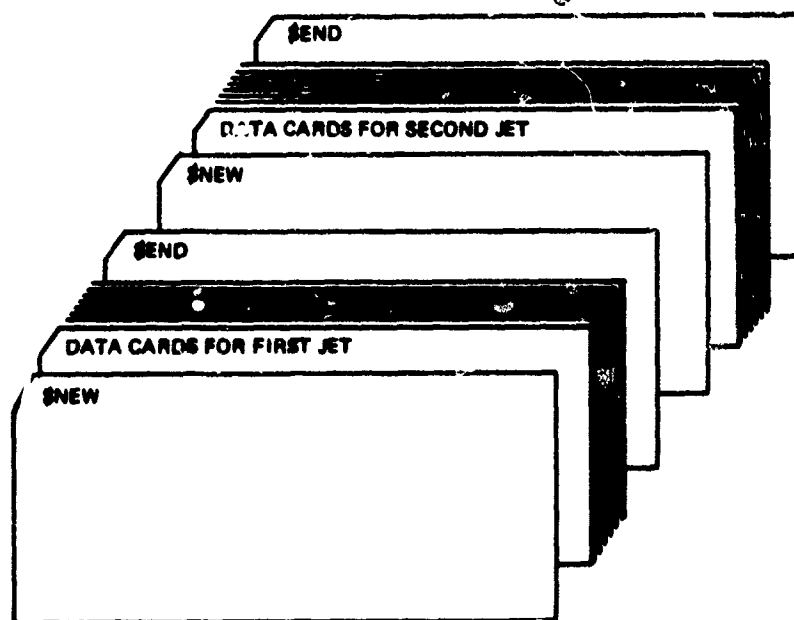


Figure 114: DATA CARD ARRANGEMENT FOR SEVERAL CASES, PROGRAM TEM-356A

Jet Trajectory and Spreading Program Card Input

TYPE = 1. Figure 115 displays the data card arrangement for circular jet plumes. A description of the card input follows:

Card	Column	Code	Explanation
<u>\$NEW</u>	2-10	\$NEW	\$NEW must be punched in CC 2-10.
<u>Card 1</u>	2-10	TYPE =	TYPE = must be punched in CC 2-10.
	11-20	1.,	indicates circular jet
<u>Card 2</u>	2-10	XYZ0 =	XYZ0 = must be punched in CC 2-10.
	11-20	x_o'	jet origin in reference co-ordinate system
	21-30	y_o'	
	31-40	z_o'	Note: The fourth character in XYZ0 is a "zero", not the letter "O".
<u>Card 3</u>	2-10	TXYZ =	TXYZ = must be punched in CC 2-10.
	11-20	t_x'	vector components defining initial jet direction
	21-30	t_y'	
	31-40	t_z'	
<u>Card 4</u>	2-10	D =	D = must be punched in CC 2-10.
	11-20	d,	jet initial diameter
<u>Card 5</u>	2-10	DELSD =	DELSD = must be punched in CC 2-10.
	11-20	$\Delta s/d,$	arc length spacing/initial diameter
<u>Card 6</u>	2-10	QRATIØ =	QRATIØ = must be punched in CC 2-10.
	11-20	$q_j/q_{\infty},$	jet to freestream dynamic pressure ratio
<u>Card 7</u>	2-10	UINF =	UINF = must be punched in CC 2-10.
	11-20	$U_{\infty},$	freestream velocity

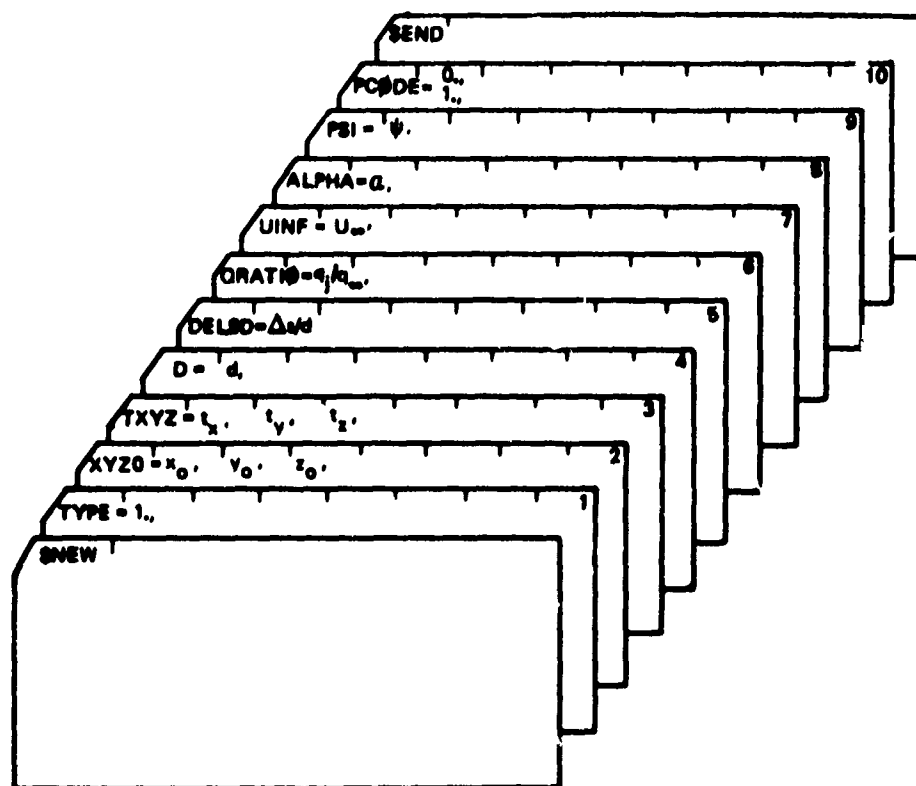


Figure 115: DATA CARD ARRANGEMENT FOR TYPE = 1, CIRCULAR JET

TYPE = 2. Figure 116 displays the data card arrangement for rectangular jet plumes. A description of the card input follows:

Card	Column	Code	Explanation
<u>\$NEW</u>	2-10	\$NEW	\$NEW must be punched in CC 2-10.
<u>Card 1</u>	2-10 11-20	TYPE = 2.,	TYPE = must be punched in CC 2-10. indicates rectangular jet
<u>Card 2</u>	2-10 11-20 21-30 31-40	XYZ0 = $x_o,$ $y_o,$ $z_o,$	XYZ0 must be punched in CC 2-10. jet origin in reference co- ordinate system Note: The fourth character in XYZ0 is a "zero", not the letter "O".
<u>Card 3</u>	2-10 11-20 21-30 31-40	TXYZ = $t_x,$ $t_y,$ $t_z,$	TXYZ = must be punched in CC 2-10. vector components defining initial jet direction
<u>Card 4</u>	2-10 11-20	A = a,	A = must be punched in CC 2-10. longitudinal dimension of initial cross section
<u>Card 5</u>	2-10 11-20	B = b,	B = must be punched in CC 2-10. lateral dimension of initial cross section
<u>Card 6</u>	2-10 11-20	DELSD = $\Delta s/de,$	DELSD = must be punched in CC 2-10. arc length spacing/equivalent diameter
<u>Card 7</u>	2-10 11-20	QRATIO = $q_j/q_\infty,$	QRATIO = must be punched in CC 2-10. jet to freestream dynamic pressure ratio
<u>Card 8</u>	2-10 11-20	UINF = $U_\infty,$	UINF = must be punched in CC 2-10. freestream velocity
<u>Card 9</u>	2-10 11-20	ALPHA = $\alpha,$	ALPHA = must be punched in CC 2-10. angle of attack

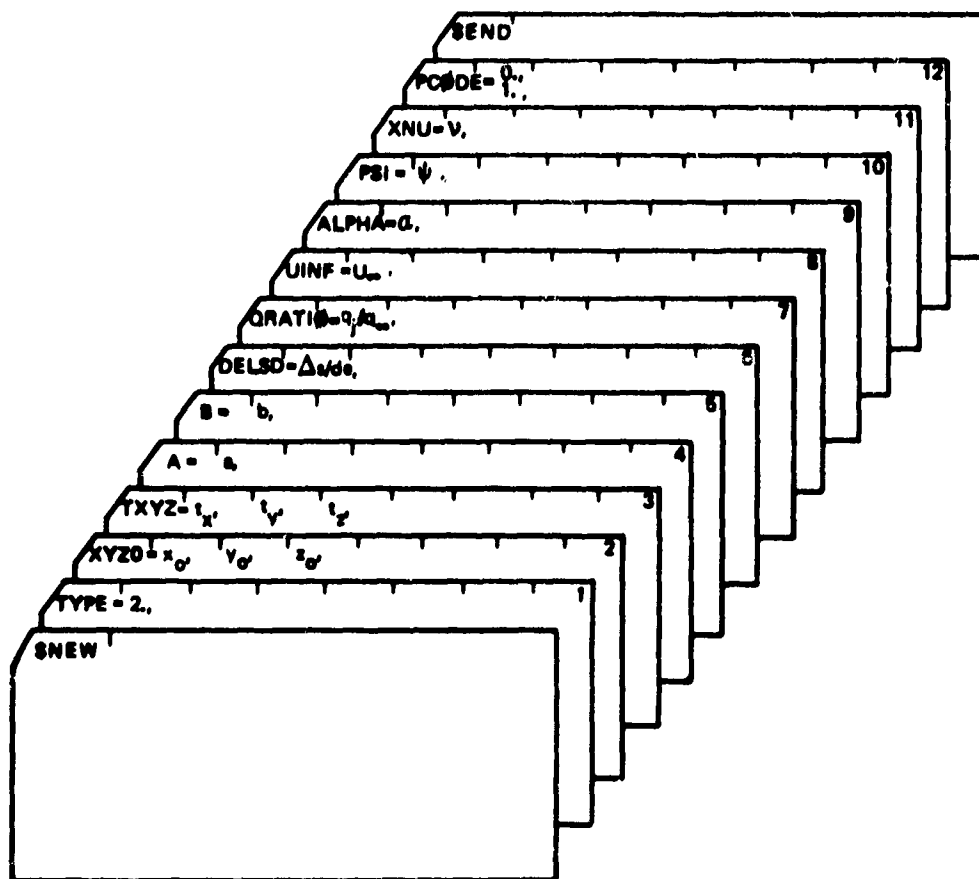


Figure 116: DATA CARD ARRANGEMENT FOR TYPE - 2. RECTANGULAR JET

TYPE = 3. Figure 117 displays the data card arrangement for two-dimensional jet plumes. A description of the card input follows:

Card	Column	Code	Explanation
<u>\$NEW</u>	2-10	\$NEW	\$NEW must be punched in CC 2-10.
<u>Card 1</u>	2-10	TYPE =	TYPE = must be punched in CC 2-10.
	11-20	3.,	indicates two-dimensional cross section
<u>Card 2</u>	2-10	XYZ0 =	XYZ0 = must be punched in CC 2-10.
	11-20	x_0 ,	jet origin in reference co-
	21-30	y_0 ,	ordinate
	31-40	z_0 ,	system Note: The fourth character in XYZ0 is a "zero", not the letter "O".
<u>Card 3</u>	2-10	TXYZ =	TXYZ = must be punched in CC 2-10.
	11-20	t_x ,	vector components defining
	21-30	t_y ,	initial
	31-40	t_z ,	jet direction
<u>Card 4</u>	2-10	T =	T = must be punched in CC 2-10.
	11-20	t,	jet initial thickness
<u>Card 5</u>	2-10	W =	W = must be punched in CC 2-10.
	11-20	w,	jet initial width
<u>Card 6</u>	2-10	DELSD =	DELSD = must be punched in CC 2-10.
	11-20	$\Delta s/t$,	arc length spacing/jet initial thickness
<u>Card 7</u>	2-10	QRATIO =	QRATIO = must be punched in CC 2-10.
	11 20	q_j/q_∞ ,	jet to freestream dynamic pressure ratio
<u>Card 8</u>	2-10	ALPHA =	ALPHA = must be punched in CC 2-10.
	11-20	α ,	angle of attack
<u>Card 9</u>	2-10	PSI =	PSI = must be punched in CC 2-10.
	11-20	γ ,	angle of yaw

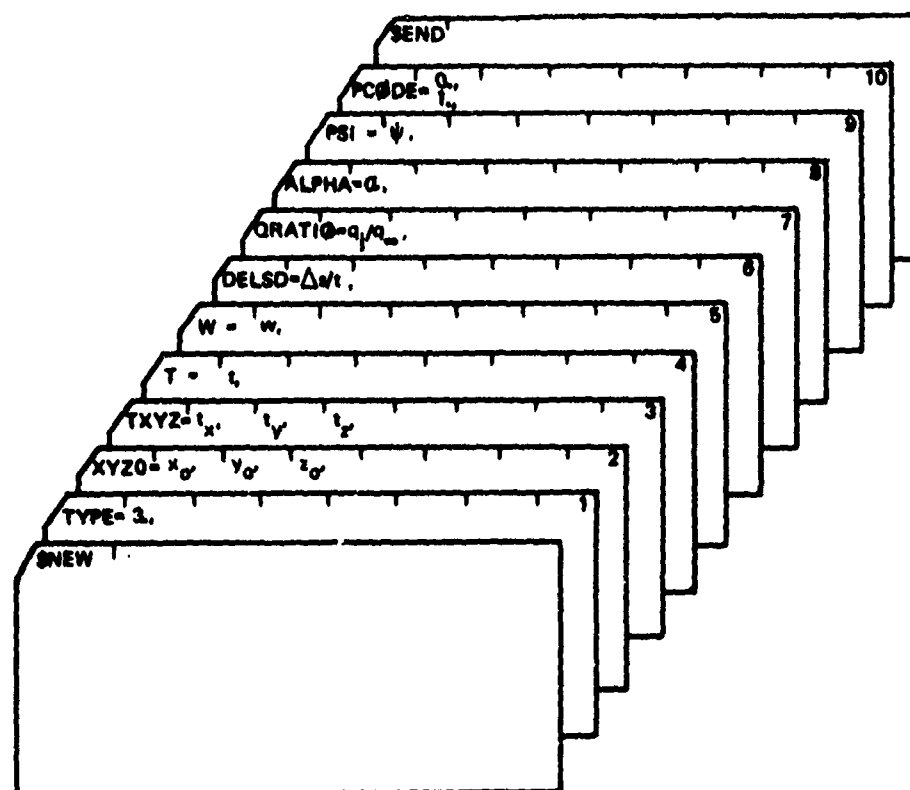


Figure 117: DATA CARD ARRANGEMENT FOR TYPE = 3, TWO DIMENSIONAL JET

TYPE = 4. Figure 118 displays the data card arrangement for annular jet plumes. A description of the card input follows:

Card	Column	Code	Explanation
<u>\$NEW</u>	2-10	\$NEW	\$NEW must be punched in CC 2-10.
<u>Card 1</u>	2-10	TYPE =	TYPE = must be punched in CC 2-10.
	11-20	4.,	indicates annular jet cross section
<u>Card 2</u>	2-10	XYZA =	XYZA - must be punched in CC 2-10.
	11-20	x_a'	origin of annular jet coordinate system
	21-30	y_a'	
	31-40	z_a'	
<u>Card 3</u>	2-10	AXYZ =	AXYZ = must be punched in CC 2-10.
	11-20	a_x'	vector components defining cruise
	21-30	a_y'	nozzle direction
	31-40	a_z'	
<u>Card 4</u>	2-10	T =	T = must be punched in CC 2-10.
	11-20	t,	jet initial thickness
<u>Card 5</u>	2-10	R =	R = must be punched in CC 2-10.
	11-20	r,	annular jet initial radius
<u>Card 6</u>	2-10	DELSD =	DELSD = must be punched in CC 2-10.
	11-20	$\Delta s/t$	arc length spacing/jet initial thickness
<u>Card 7</u>	2-10	MR =	MR = must be punched in CC 2-10.
	11-20	MR,	number of annular jet arms
<u>Card 8</u>	2-10	QRATI ϕ =	QRATI ϕ = must be punched in CC 2-10.
	11-20	q_j/q_∞ ,	jet to freestream dynamic pressure ratio
<u>Card 9</u>	2-10	ALPHA =	ALPHA = must be punched in CC 2-10.
	11-20	α ,	angle of attack

Card	Column	Code	Explanation
<u>Card 10</u>	2-10 11-20	PSI = ?,	PSI = must be punched in CC 2-10. angle of yaw
<u>Card 11</u>	2-10 11-20	PCODE = PCODE,	PCODE = must be punched in CC 2-10. = 0., no punched cards produced = 1., punched cards produced
<u>\$END</u>	2-10	\$END	\$END must be in CC 2-10.

The following additional data must be input for TYPE = 4.,
Note that NAMELIST format is not used for these inputs. Input
format is 2F10.0 (two fields, each ten digits wide).

Card	Column	Code	Explanation
<u>Card</u> <u>Set A</u>	1-10 11-20	Θ β	arm clock angle flow turning angle

Note: There must be MR of the cards, two numbers per card,
where MR is the number of annular jet arms.

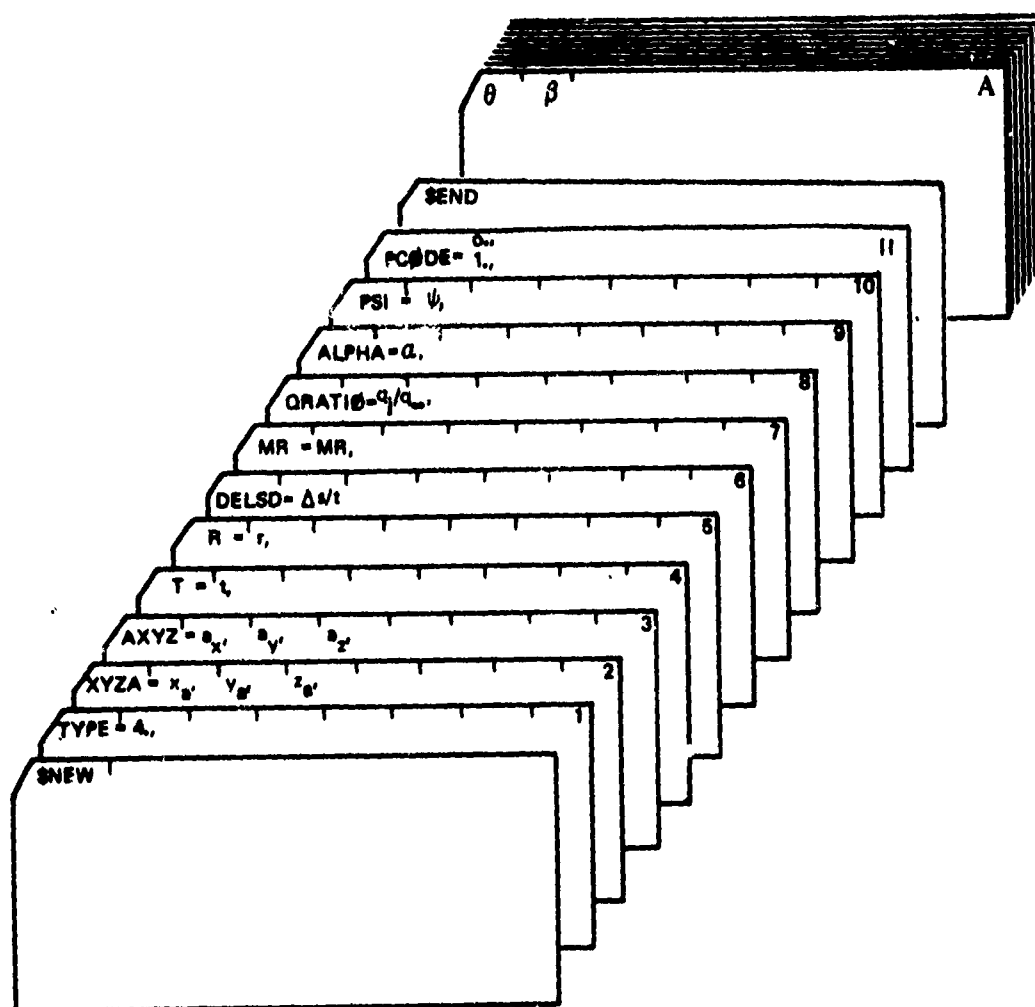


Figure 118: DATA CARD ARRANGEMENT FOR TYPE = 4. ANNULAR JET

3.2 Reingestion Prediction Computer Program Usage

Data Input Format

Inputs describing jet plume geometry use the NAMELIST format and are nearly identical to that described for the Jet Trajectory and Spreading Program. The only exceptions are noted below:

- 1) ALPHA is not input. The theory assumes the freestream flow is parallel to the ground plane and automatically sets $\alpha = 0$. Yaw angle ψ is input as usual.
- 2) PCODE is not input. The program assumes PCODE = 0.
- 3) A new parameter, XCWL, is input for all jet types. XCWL is the length of the cowl from the inlet leading edge to the front of the thrust reverser exit. XCWL is used in place of plate length in the criterion for reattachment of exhaust flow to the cowl surface (see Figure 76).
- 4) A new parameter, NOI, is input for all jet types. NOI is the inlet number associated with a particular jet.
- 5) UINF must be input for all type jets. In TEM-356A, UINF is required for TYPE = 1. and 2. only.
- 6) The inlet data are input in 10F7.0 format.

The general card stacking arrangement is shown in Figure 119. The user may submit up to four inlets and four jets (other than TYPE = 4.) in a single case. Only one TYPE = 4. jet may be run per case. However, as many cases as are desired can be stacked for a single computer submission.

REINGESTION PREDICTION PROGRAM CARD INPUT

Figure 119 displays the data card arrangement for the Reingestion Prediction Computer Program. All numbers must be punched with a decimal point. The inlet card input data are input in 7F10.0 format rather than NAMELIST.

Card	Column	Code	Explanation
<u>Card 1</u>	1-10	NI	= number of inlets $1. \leq NI \leq 4.$
	11-20	ZGRND	height of (x,y,z) reference coordinate system from ground plane
<u>Card Set 2</u>	1-10	x_i	position of inlet center in reference coordinate system
	11-20	y_i	
	21-30	z_i	
	31-40	d_i	inlet diameter
	41-50	V_{hi}	inlet hilite velocity Note: There must be NI cards in Card Set 2, five numbers per card.
<u>Card 3</u>	1-10	NJ	= number of jets $1. \leq NJ \leq 4.$

Figure 120 displays additional NAMELIST data cards for use in program TEM-356B. The cards are inserted in any order between the \$NEW and \$END cards with the other NAMELIST cards describing the jet geometry. A description of the additional input follows:

Card	Column	Code	Description
<u>Card N1</u>	2-10	XCØWL =	XCØWL - must be punched in CC 2-10. length of cowl surface
	11-20	$x_{cowl},$	
<u>Card N2</u>	2-10	NØI =	NØI = must be punched in CC 2-10. inlet number associated with this jet
	11-20	NØI,	
<u>Card N3</u>	2-10	UINF =	UINF = must be punched in CC 2-10. freestream velocity, ft/sec
	11-20	$U_{\infty},$	

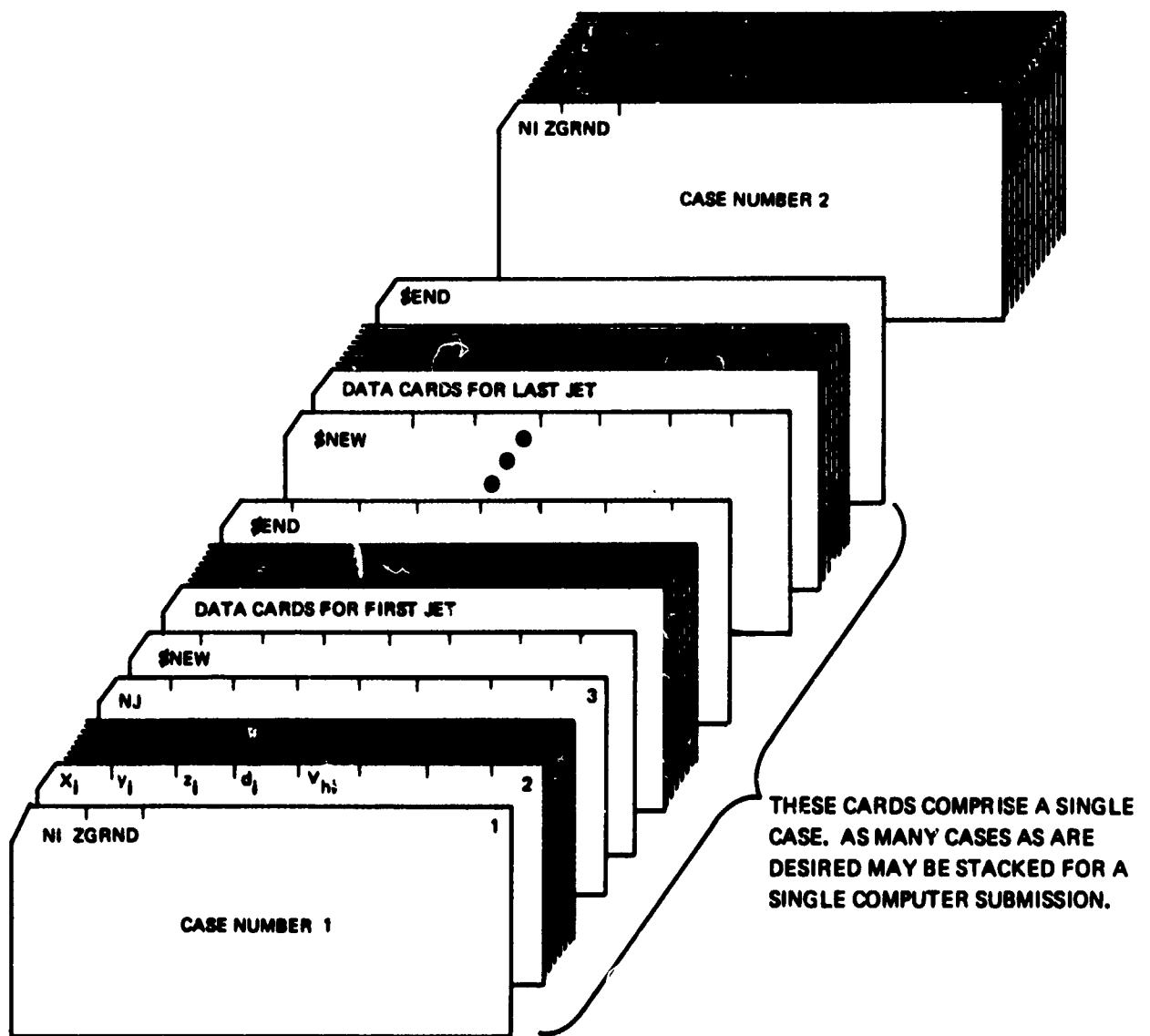
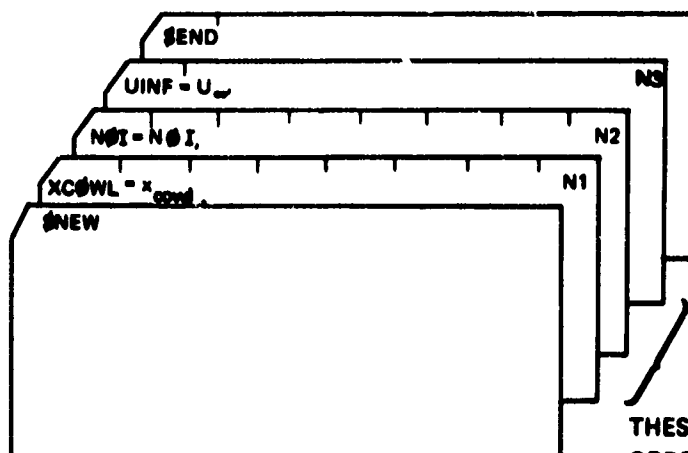


Figure 119: DATA CARD ARRANGEMENT FOR REINGESTION PREDICTION PROGRAM TEM-356B



THESE CARDS ARE INSERTED IN ANY ORDER BETWEEN THE \$NEW AND \$END CARDS WITH THE OTHER NAMELIST CARDS DESCRIBING THE JET GEOMETRY.

Figure 120: ADDITIONAL NAME LIST DATA CARDS FOR REINGESTION PREDICTION PROGRAM TEM-356B

3.3 TR and TV System Performance Computer Program Usage

Program TEM-357 consists of four modules as noted below. Four-letter capitalized control words are used to direct program execution to the appropriate subroutine.

Internal Performance Module (INTE)

Engine Stability Margin Module (ENGI)

Aerodynamic Interference Module (AERO)

Reingestion Module (REIN)

Data Input Format

Input to TEM-357 falls into three categories: control cards, title cards, and numeric input. As their name implies, the control cards control execution of the program. The control cards must be punched in card columns 1 to 4. All input data, except title cards and control cards, are punched in number fields seven columns wide, with ten fields per card. Decimal points should always be punched for every input number.

The general card stacking arrangement is shown in Figure 121. There are no restrictions as to sequence of the four major modules. The control word END punched in card columns 1 to 3 terminates program execution. Detailed card inputs for the four modules are contained in the following sections.

Internal Performance Module (INTE)

The Internal Performance Module contains data correlations for the following types of cruise nozzles, thrust reversers, and vectoring nozzles.

	Nozzle	Control Word	Page
cruise nozzles {	conical	CONI	190
	annular	ANNU	192
	noncircular	EQUI	194
thrust reversers {	target (clamshell and annular)	TARG	196
	blocker deflector	BLOC	200
thrust vectoring nozzles {	single bearing	SING	202
	three-bearing	THRE	204
	spherical eyeball	SPHE	206
	lobstertail external deflector	LOBS	208
cascade losses {	cascade lattices	CASC	210

(Blank)

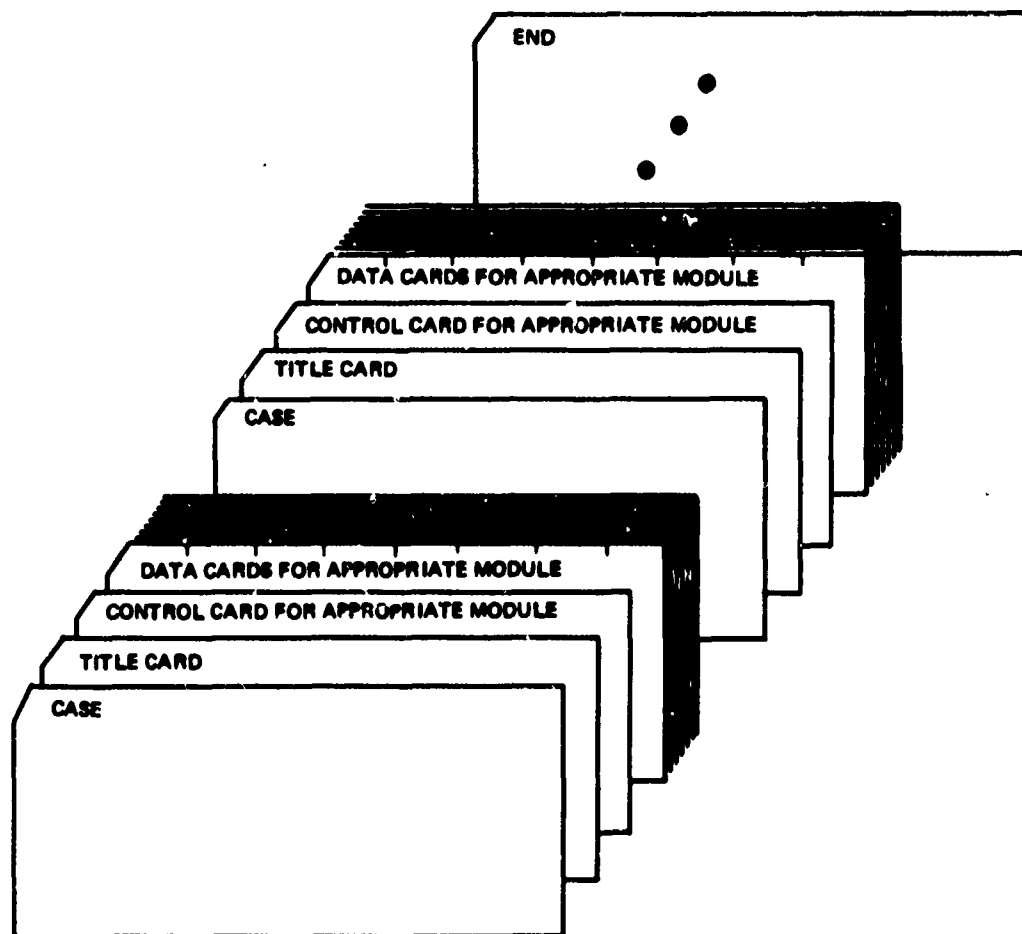


Figure 121: DATA CARD ARRANGEMENT FOR SEVERAL CASES, PROGRAM TEM-357

Detailed card inputs for each type of nozzle are described on the pages noted in the foregoing table. Several of the subroutines (CONI, ANNU, EQUI, SING, THRE, SPHE, LOBS) were modified during Task 3.2 in order to make Reynolds number scale corrections. The full scale Reynolds number (calculated at a reference nozzle pressure ratio of 1.5) is punched in the eighth field (card column 50-56) in the E format and must be right adjusted. For example, a full scale Re of 10.4×10^6 would be punched as follows:

Card Column						
50	51	52	53	54	55	56
✓	1	0	.	4	E	6

The check mark (✓) indicates a blank. Sample Case Number Two in Appendix II (page 259) illustrates the scale correction inputs and outputs.

CONI Input

Figure 122 displays the data card arrangement for conical cruise nozzles. A description of the card input follows.

Card	Column	Code	Explanation
<u>Card 1</u>	1-4	CØNI	Control card - contains the word CØNI
<u>Card 2</u>	1-7	LEVEL	= 1. indicates "Level 1" performance predictions = 2. indicates "Level 2" performance predictions
	8-14 15-21	$\Delta R/L$ α	nozzle offset/duct length internal wall angle at nozzle trailing edge in degrees Omit α if LEVEL = 1.
	22-28	D_1/D_2	nozzle entrance/exit diameter Omit D_1/D_2 if LEVEL = 1.
	50-56	Re _{fs}	full scale Reynolds number at a reference nozzle pressure ratio of 1.5. Punched in E Format and right adjusted. See above example. Omit if scale corrections are not desired.

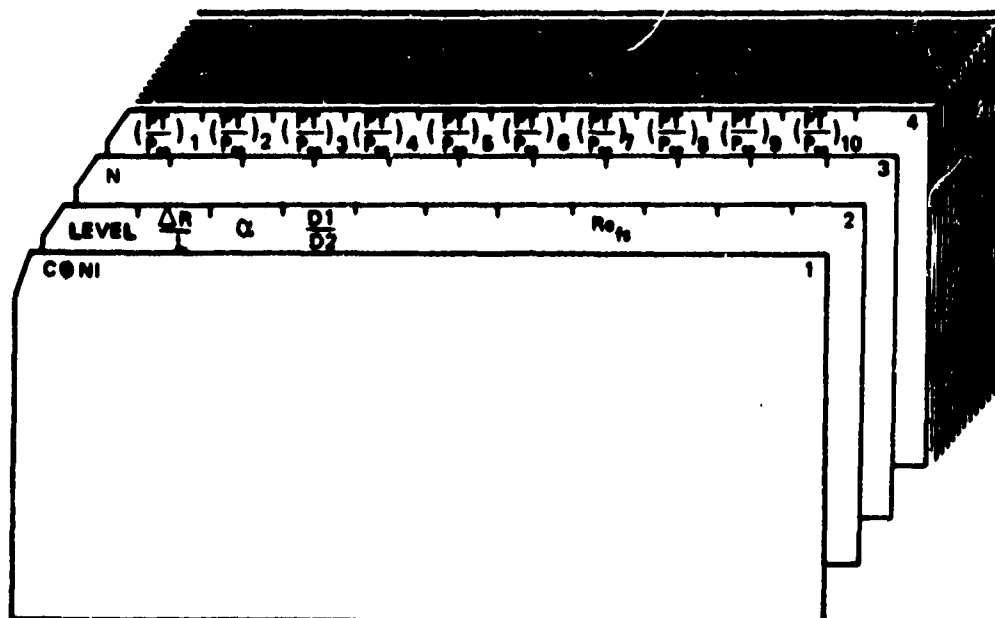


Figure 122: DATA CARD ARRANGEMENT FOR CONICAL CRUISE NOZZLES

ANNU Input

Figure 123 displays the data card arrangement for annular cruise nozzles. A description of the card input follows.

Card	Column	Code	Explanation
<u>Card 1</u>	1-4	ANNU	control card - contains the word ANNU
<u>Card 2</u>	1-7	LEVEL	= 1. indicates "Level 1" performance predictions = 2. indicates "Level 2" performance predictions
	8-14	$\Delta R/L$	nozzle offset/duct length
	15-21	α	internal wall angle at nozzle trailing edge in degrees. Omit α if LEVEL = 1.
	22-28	A_D/A_E	duct entrance/nozzle exit area Omit A_D/A_E if LEVEL = 1.
	29-35	R_O	nozzle exit outer radius
	36-42	R_i	nozzle exit inner radius
	50-56	Re_{fs}	full scale Reynolds number at a reference nozzle pressure ratio of 1.5. Punched in E format and right adjusted. See example on page 190. Omit if scale corrections are not desired.
<u>Card 3</u>	1-7	N	= number of pressure ratios in Card Set 4. $1. \leq N \leq 20$.
<u>Card Set 4</u>	1-7	(P_T/P_∞) 1	nozzle pressure ratios at which performance predictions are desired. There must be N of these values, ten numbers per card.
	8-14	(P_T/P_∞) 2	
	15-21	(P_T/P_∞) 3	
	22-28	(P_T/P_∞) 4	
	29-35	(P_T/P_∞) 5	
	36-42	(P_T/P_∞) 6	
	43-49	(P_T/P_∞) 7	
	50-56	(P_T/P_∞) 8	
	57-63	(P_T/P_∞) 9	
	64-70	(P_T/P_∞) 10	

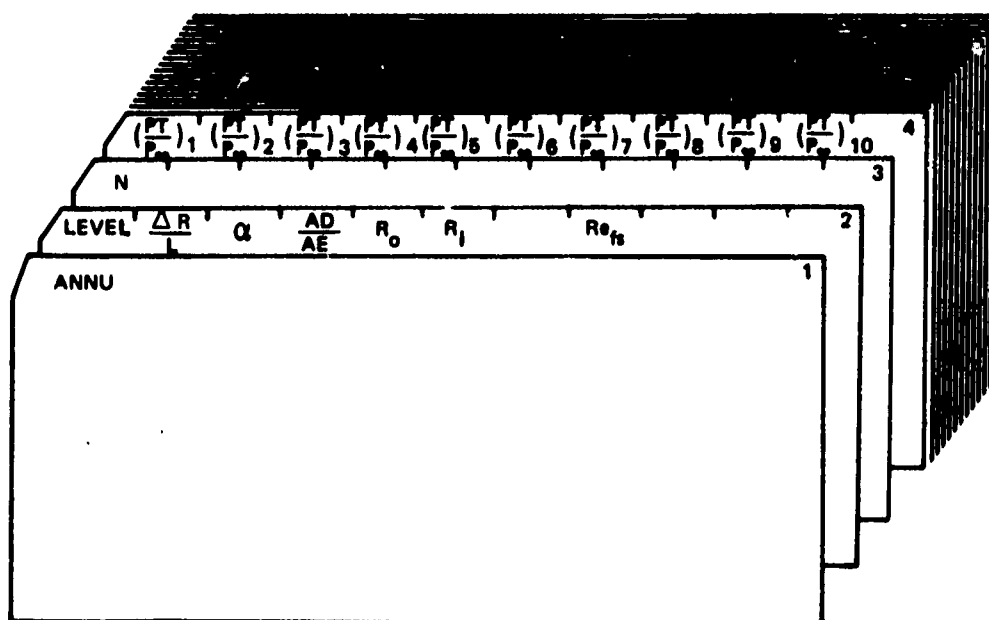


Figure 123: DATA CARD ARRANGEMENT FOR ANNULAR CRUISE NOZZLES

EQUI Input

Figure 124 displays the data card arrangement for noncircular shaped cruise nozzles. A description of the card input follows:

Card	Column	Code	Explanation
<u>Card 1</u>	1-4	EQUI	control card - contains the word EQUI
<u>Card 2</u>	1-7	LEVEL	= 1. indicates "Level 1" performance predictions = 2. indicates "Level 2" performance predictions
	8-14	$\Delta R/L$	nozzle offset/duct length
	15-21	α	internal wall angle at nozzle trailing edge in degrees Omit α if LEVEL = 1.
	22-28	D_1/D_2	nozzle entrance/exit diameter Omit D_1/D_2 if LEVEL = 1.
	53-60	Re_{fs}	full scale Reynolds number at a reference nozzle pressure ratio of 1.5. Punched in E format and right adjusted. See example on page 190. Omit if scale corrections are not desired.
<u>Card Set 4</u>	1-7	$(P_T/P_{O_2})_1$	nozzle pressure ratios at which performance predictions are desired. There must be N of these values, ten numbers per card.
	8-14	$(P_T/P_{\infty})_2$	
	15-21	$(P_T/P_{\infty})_3$	
	22-28	$(P_T/P_{\infty})_4$	
	29-35	$(P_T/P_{\infty})_5$	
	36-42	$(P_T/P_{\infty})_6$	
	43-49	$(P_T/P_{\infty})_7$	
	50-56	$(P_T/P_{\infty})_8$	
	57-63	$(P_T/P_{\infty})_9$	
	64-70	$(P_T/P_{\infty})_{10}$	

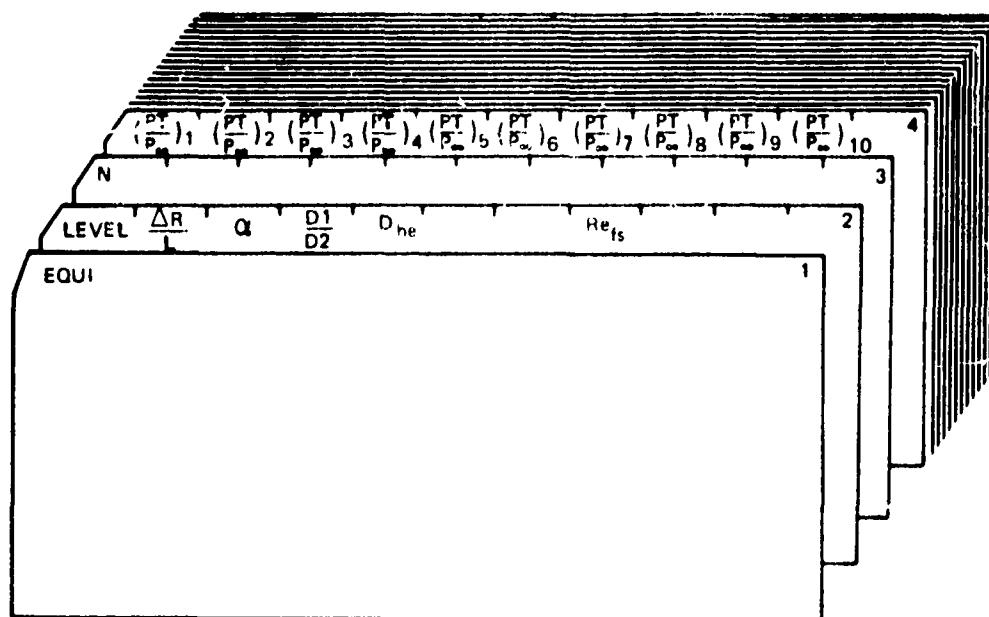


Figure 124: DATA CARD ARRANGEMENT FOR IRREGULAR SHAPED CRUISE NOZZLES

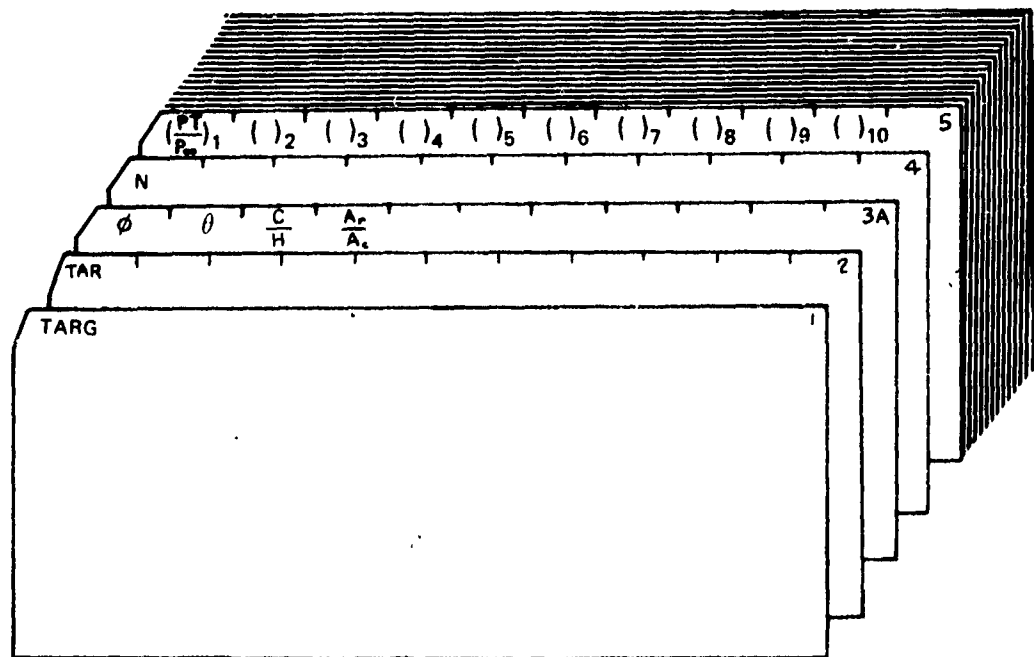
TARG Input

Figures 125a and 125b display the data card arrangement for annular and clamshell target thrust reversers. A description of the card input follows:

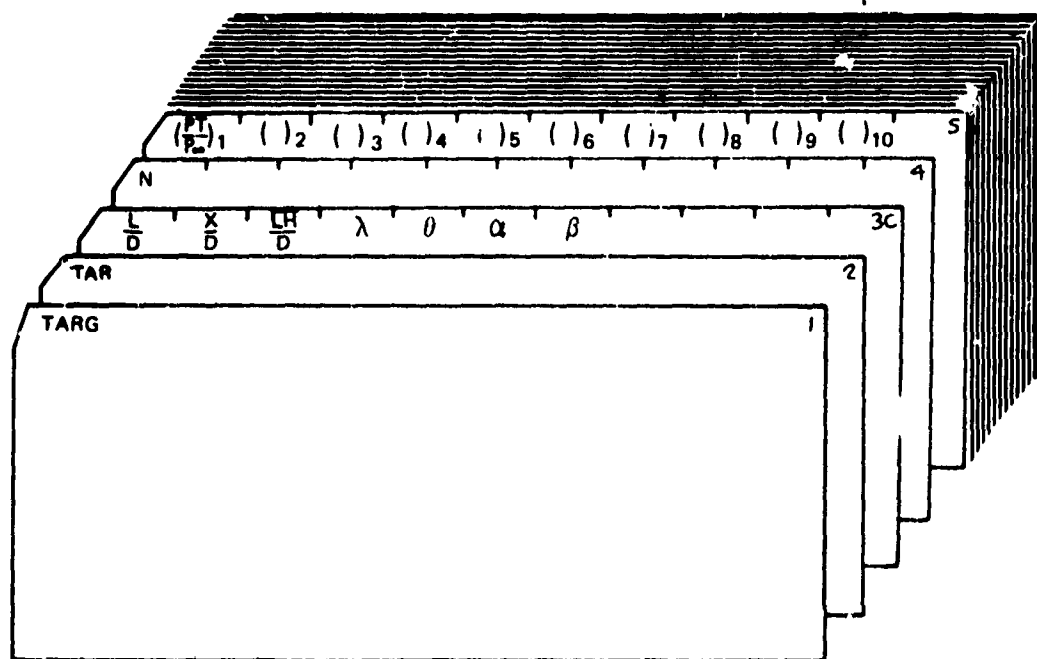
Card	Column	Code	Explanation
<u>Card 1</u>	1-4	TARG	control card - contains the word TARG
<u>Card 2</u>	1-7	TAR	= 1. indicates clamshell target thrust reverser = 2. indicates annular target reverser
<u>Card 3A*</u>	1-7	ϕ	blockage angle in degrees, see Figure 23
	8-14	θ	door angle in degrees, see Figure 23
	15-21	C/H	throat gap/annulus height, see Figure 23
	22-28	A_r/A_c	reverser exit area/cruise nozzle exit area
<u>Card 3C**</u>	1-7	L/D	door length/nozzle exit diameter
	8-14	X/D	setback distance/nozzle exit diameter
	15-21	\overline{LH}/D	average lip height/nozzle exit diameter
	22-28	λ	sweep angle in degrees, see Figure 13
	29-35	Θ	arc angle in degrees, see Figure 13
	36-42	α	cone angle in degrees, see Figure 13
	43-49	β	bevel angle in degrees, see Figure 13

Note: * Omit card 3A for clamshell target thrust reversers.
 ** Omit Card 3C for annular target thrust reversers.

Card	Column	Code	Explanation
<u>Card 4</u>	1-7	N	= number of pressure ratios in Card Set 4. $1. \leq N \leq 20$.
<u>Card Set 5</u>	1-7	(P_T/P_∞) 1	nozzle pressure ratios at which performance predictions are desired. There must be N of these values, ten numbers per card.
	8-14	(P_T/P_∞) 2	
	15-21	(P_T/P_∞) 3	
	22-28	(P_T/P_∞) 4	
	29-35	(P_T/P_∞) 5	
	36-42	(P_T/P_∞) 6	
	43-49	(P_T/P_∞) 7	
	50-56	(P_T/P_∞) 8	
	57-63	(P_T/P_∞) 9	
	64-70	(P_T/P_∞) 10	



a) ANNULAR TARGET THRUST REVERSER INPUTS



b) CLAMSHELL TARGET THRUST REVERSER INPUTS

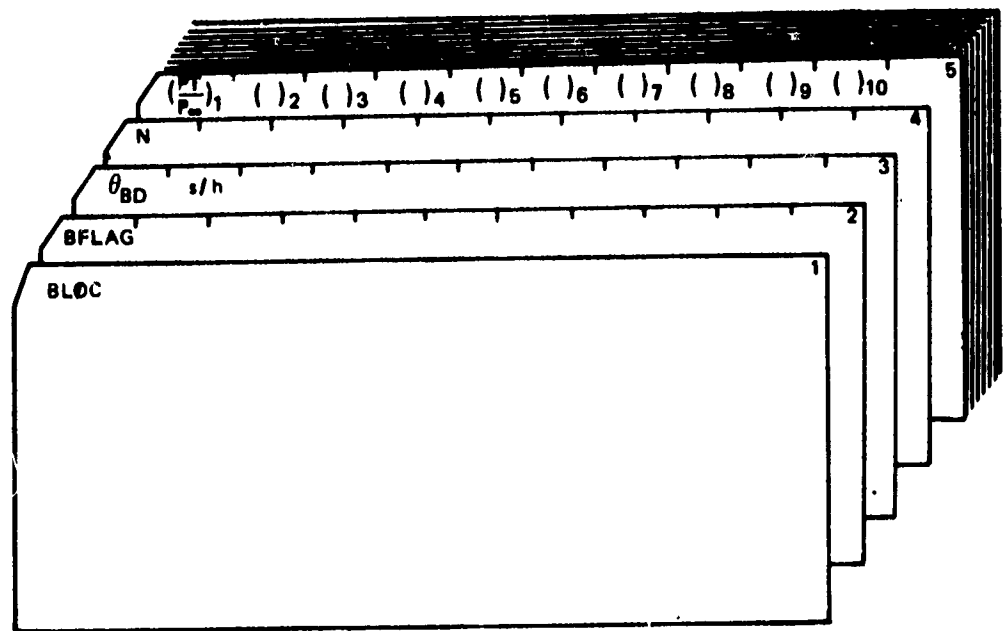
Figure 125: DATA CARD ARRANGEMENT FOR TARGET THRUST REVERSERS

Preceding page blank

BLØC Input

Figure 126 displays the data card arrangement for blocker deflector and blocker cascade thrust reversers. A description of the card input follows:

Card	Column	Code	Explanation
<u>Card 1</u>	1-4	BLØC	control card - contains the word BLØC
<u>Card 2</u>	1-7	BFLAG	= 0. indicates blocker deflector thrust reverser = 1. indicates blocker cascade thrust reverser
<u>Card 3</u>	1-7	Θ_{80}	blocker door angle in degrees, see page 162
	8-14	s/h	blocker door setback/annulus height, see page 162. Omit if BFLAG = 0.
<u>Card 4</u>	1-7	N	= number of pressure ratios in Card Set 4. $1. \leq N \leq 20$.
<u>Card Set 5</u>	1-7	$(P_T/P_\infty)_1$	nozzle pressure ratios at which performance predictions are desired. There must be N of these values, ten numbers per card.
	8-14	$(P_T/P_\infty)_2$	
	15-21	$(P_T/P_\infty)_3$	
	22-28	$(P_T/P_\infty)_4$	
	29-35	$(P_T/P_\infty)_5$	
	36-42	$(P_T/P_\infty)_6$	
	43-49	$(P_T/P_\infty)_7$	
	50-56	$(P_T/P_\infty)_8$	
	57-63	$(P_T/P_\infty)_9$	
	64-70	$(P_T/P_\infty)_{10}$	



**Figure 126: DATA CARD ARRANGEMENT FOR BLOCKER DEFLECTOR AND
BLOCKER CASCADE THRUST REVERSERS**

SING Input

Figure 127 displays the data card arrangement for single bearing vectoring nozzles. A description of the card input follows:

Card	Column	Code	Explanation
<u>Card 1</u>	1-4	SING	control card - contains the word SING
<u>Card 2</u>	1-7	α	bearing plane angle in degrees, see Figure 28
	8-14	β	bearing duct angle in degrees, see Figure 28
	15-21	ϕ	bearing rotation angle in degrees, see Figure 28
	22-28	Ω	flow turning angle measured from cruise nozzle centerline in degrees. See page 42. Program automatically calculates Ω if it is not input.
	29-35	$\Delta R/L$	nozzle offset/duct length
	50-56	Re_{fs}	full scale Reynolds number at a reference nozzle pressure ratio at 1.5. Punched in E format and right adjusted as shown on page 190. Omit if scale corrections are not desired.
<u>Card 3</u>	1-7	N	= number of pressure ratios in Card Set 4. $1 \leq N \leq 20$.
<u>Card Set 4</u>	1-7	$(P_T/P_\infty)_1$	nozzle pressure ratios at which performance predictions are desired. There must be N of these values, ten numbers per card.
	8-14	$(P_T/P_\infty)_2$	
	15-21	$(P_T/P_\infty)_3$	
	22-28	$(P_T/P_\infty)_4$	
	29-35	$(P_T/P_\infty)_5$	
	36-42	$(P_T/P_\infty)_6$	
	43-49	$(P_T/P_\infty)_7$	
	50-56	$(P_T/P_\infty)_8$	
	57-63	$(P_T/P_\infty)_9$	
	64-70	$(P_T/P_\infty)_{10}$	

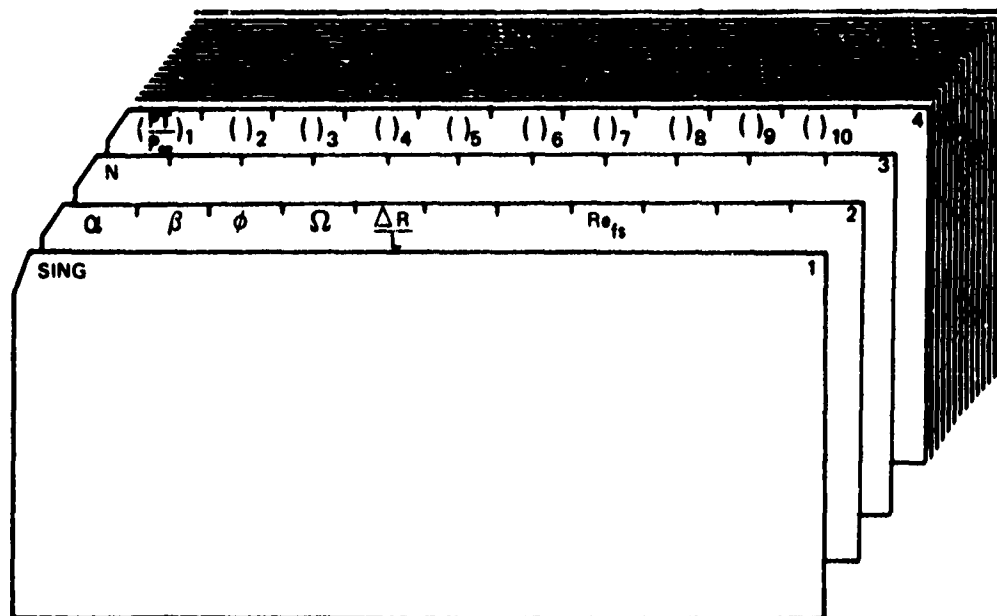


Figure 127. DATA CARD ARRANGEMENT FOR SINGLE BEARING NOZZLES

THRE Input

Figure 128 displays the data card arrangement for three bearing vectoring nozzles. A description of the card input follows:

Card	Column	Code	Explanation
<u>Card 1</u>	1-4	THRE	control card - contains the word THRE
<u>Card 2</u>	1-7	ϕ	bearing plane angle in degrees, see page 145
	8-14	A_D/A_E	duct entrance/nozzle exit area
	15-21	σ	vector angle in degrees, see page 145
	22-28	A	length of center section
	29-35	L	total nozzle length
	36-42	D	duct entrance diameter
<u>Card Set 4</u>	50-56	Re_{fs}	full scale Reynolds number at a reference nozzle pressure ratio of 1.5. Punched in E format and right adjusted as shown on page 190. Omit if scale corrections are not desired.
	1-7	$(P_T/P_\infty)_1$	nozzle pressure ratios at which performance predictions are desired. There must be N of these values, ten numbers per card.
	8-14	$(P_T/P_\infty)_2$	
	15-21	$(P_T/P_\infty)_3$	
	22-28	$(P_T/P_\infty)_4$	
	29-35	$(P_T/P_\infty)_5$	
	36-42	$(P_T/P_\infty)_6$	
	43-49	$(P_T/P_\infty)_7$	
	50-56	$(P_T/P_\infty)_8$	
	57-63	$(P_T/P_\infty)_9$	
	64-70	$(P_T/P_\infty)_{10}$	

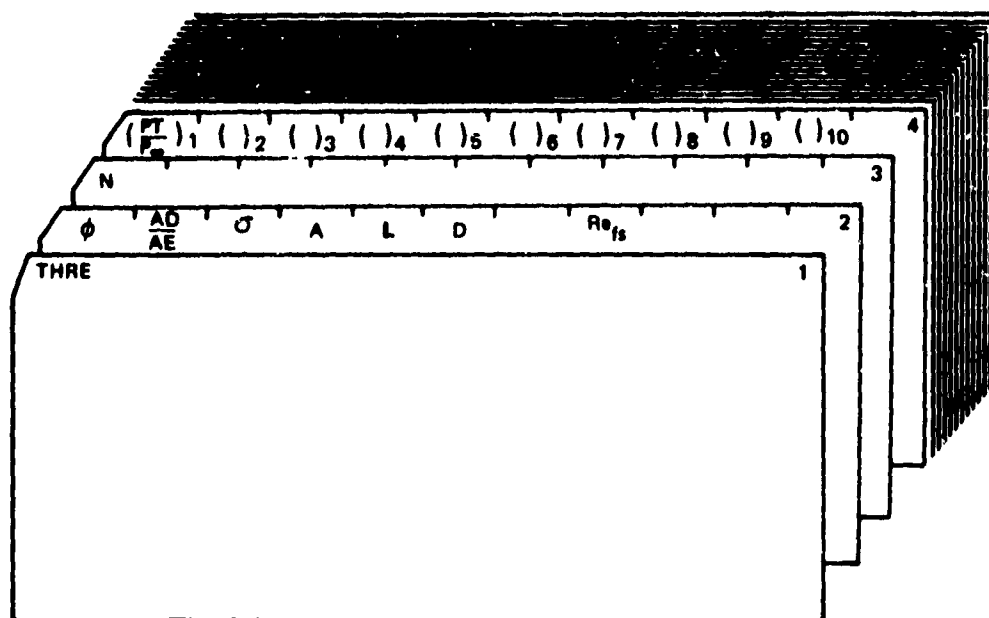


Figure 128: DATA CARD ARRANGEMENT FOR THREE BEARING NOZZLES

SPHE Input

Figure 129 displays the data card arrangement for spherical eyeball vectoring nozzles. A description of the card input follows:

Card	Column	Code	Explanation
<u>Card 1</u>	1-4	SPHE	control card - contains the word SPHE
<u>Card 2</u>	1-7	θ	mechanical vector angle in degrees
	50-56	Re_{fs}	full scale Reynolds number at a reference nozzle pressure ratio of 1.5. Punched in E format and right adjusted as shown on page 190. Omit if scale corrections are not desired.
<u>Card 3</u>	1-7	N	= number of pressure ratios in Card Set 4. $1 \leq N \leq 20$.
<u>Card Set 4</u>	1-7	(P_T/P_∞) 1	nozzle pressure ratios at which performance predictions are desired. There must be N of these values, ten numbers per card.
	8-14	(P_T/P_∞) 2	
	15-21	(P_T/P_∞) 3	
	22-28	(P_T/P_∞) 4	
	29-35	(P_T/P_∞) 5	
	36-42	(P_T/P_∞) 6	
	43-49	(P_T/P_∞) 7	
	50-56	(P_T/P_∞) 8	
	57-63	(P_T/P_∞) 9	
	64-70	(P_T/P_∞) 10	

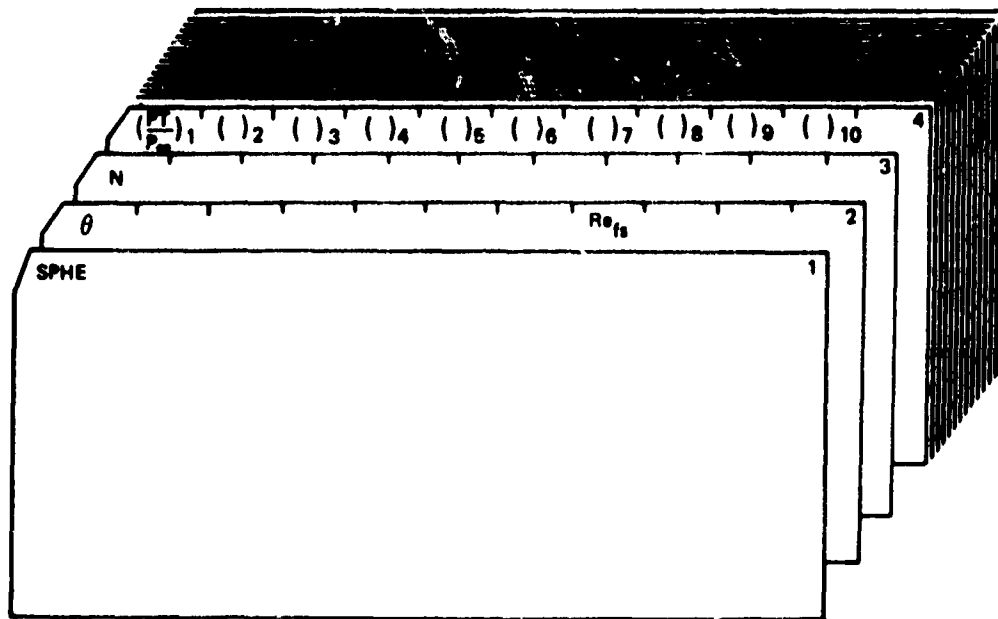


Figure 129: DATA CARD ARRANGEMENT FOR SPHERICAL EYEBALL NOZZLES

LØBS Input

Figure 130 displays the data card arrangement for lobstertail or aft-hood deflector nozzles. A description of the card input follows:

Card	Column	Code	Explanation
<u>Card 1</u>	1-4	LØBS	control card - contains the word LØBS
<u>Card 2</u>	1-7	θ	mechanical vector angle in degrees
	50-56	Re_{fs}	full scale Reynolds number at a reference nozzle pressure ratio of 1.5. Punched in E format and right adjusted as shown on page 190. Omit if scale corrections are not desired.
<u>Card 3</u>	1-7	N	= number of pressure ratios in Card Set 4. $1. \leq N \leq 20$.
<u>Card Set 4</u>	1-7	$(P_T/P_\infty)_1$	nozzle pressure ratios at which performance predictions are desired. There must be N of these values, ten numbers per card.
	8-14	$(P_T/P_\infty)_2$	
	15-21	$(P_T/P_\infty)_3$	
	22-28	$(P_T/P_\infty)_4$	
	29-35	$(P_T/P_\infty)_5$	
	36-42	$(P_T/P_\infty)_6$	
	43-49	$(P_T/P_\infty)_7$	
	50-56	$(P_T/P_\infty)_8$	
	57-63	$(P_T/P_\infty)_9$	
	64-70	$(P_T/P_\infty)_{10}$	

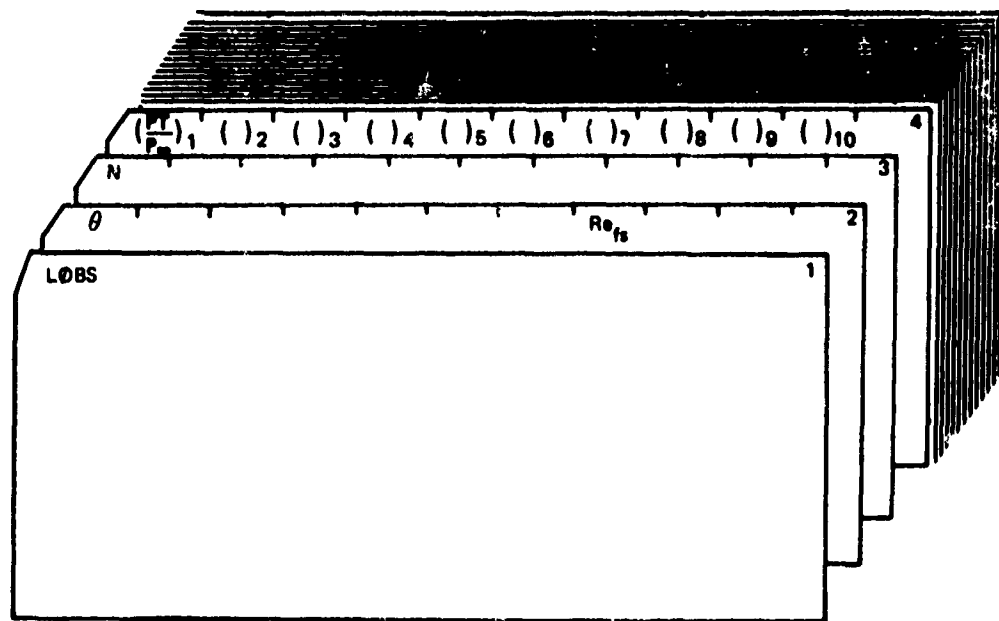


Figure 130: DATA CARD ARRANGEMENT FOR LOBSTERTAIL OR AFT-HOOD DEFLECTOR NOZZLES

EXTE Input

Figure 131 displays the data card arrangement for external deflector nozzles. A description of the card input follows:

Card	Column	Code	Explanation
<u>Card 1</u>	1-4	EXTE	control card - contains the word EXTE
<u>Card 2</u>	1-7	CFLAG	= 0. indicates flat plate deflector = 1. indicates curved deflector = 2. indicates hinged external deflector
	8-14	Θ	mechanical vector angle in degrees. Omit if CFLAG = 2.
	15-21	X/D_n	hinged deflector setback distance/nozzle diameter in TV mode, see page 266. Omit if CFLAG = 0. or 1.
	22-28	D_n/D	nozzle diameter in TV mode/cruise nozzle diameter, see page 266. Omit if CFLAG = 0. or 1.
	29-35	γ	deflection angle defined in sketch on page 266. Omit if CFLAG = 0. or 1.
<u>Card 3</u>	1-7	N	= number of pressure ratios in Card Set 4. $1. \leq N \leq 20$.
<u>Card Set 4</u>	1-7	$(P_T/P_\infty)_1$	nozzle pressure ratios at which performance predictions are desired. There must be N of these values, ten numbers per card.
	8-14	$(P_T/P_\infty)_2$	
	15-21	$(P_T/P_\infty)_3$	
	22-28	$(P_T/P_\infty)_4$	
	29-35	$(P_T/P_\infty)_5$	
	36-42	$(P_T/P_\infty)_6$	
	43-49	$(P_T/P_\infty)_7$	
	50-56	$(P_T/P_\infty)_8$	
	57-63	$(P_T/P_\infty)_9$	
	63-70	$(P_T/P_\infty)_{10}$	

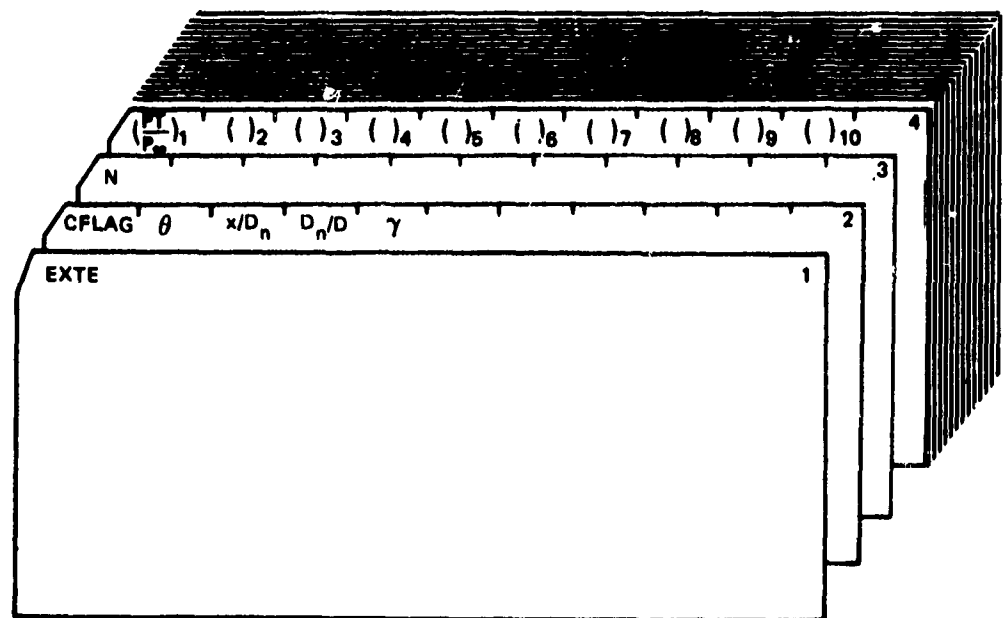


Figure 131: DATA CARD ARRANGEMENT FOR EXTERNAL DEFLECTOR NOZZLES

CASC Input

Figure 132 displays the data card arrangement for cascade loss predictions. A description of the card input follows:

Card	Column	Code	Explanation
<u>Card 1</u>	1-4	CASC	control card - contains the word CASC
<u>Card 2</u>	1-7	β_1	inlet blade angle in degrees, see Figure 38
	8-14	α_1	gas inlet angle in degrees, see Figure 38
	15-21	c/s	blade chord/pitch ratio, see Figure 38
	22-28	o/s	opening/pitch ratio, see Figure 38
	29-35	s/e	pitch/curvature ratio, see Figure 38
	36-42	t/c	thickness/chord ratio, see Figure 38
	43-49	t_e/s	trailing edge thickness/pitch ratio, see Figure 38
	50-56	T_{TN}	nozzle total temperature, °R
	57-63	γ	ratio of specific heats
	64-70	l	blade length, see Figure 38
<u>Card 3</u>	1-7	c	blade chord, see Figure 38
	8-14	$\frac{A_{wall}}{A_{blade}}$	end wall and stiffener wetted area/blade wetted area
<u>Card 4</u>	1-7	N	= number of pressure ratios in Card Set 4. $1. \leq N \leq 20$.

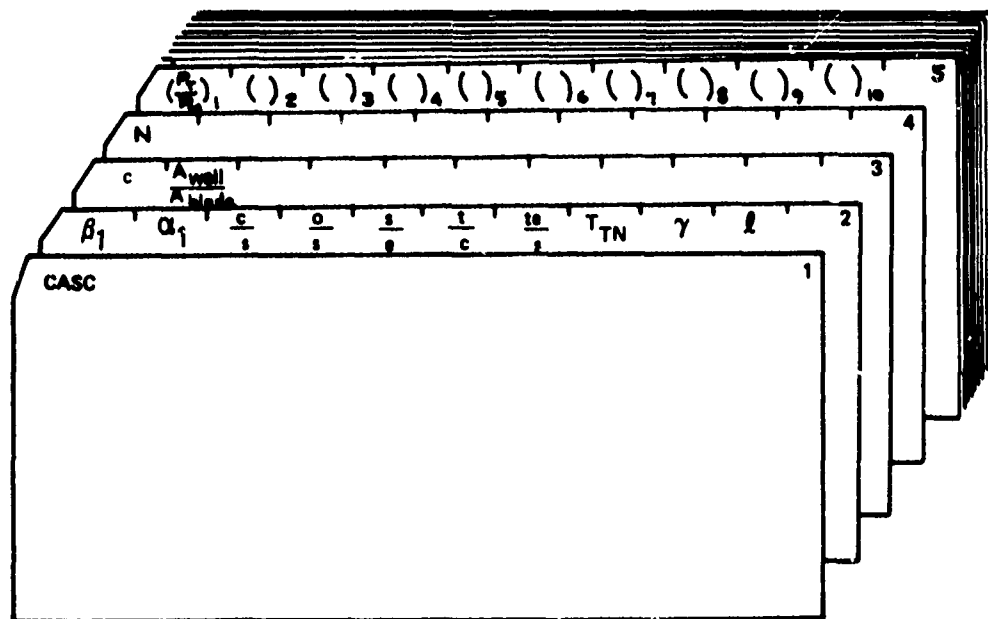


Figure 132: DATA CARD ARRANGEMENT FOR CASCADE LOSS PREDICTIONS

Engine Stability Margin Module (ENGI) Input

Figure 133 displays the data card arrangement for the Engine Stability Margin Module. A description of the card input follows:

Card	Column	Code	Explanation
<u>Card 1</u>	1-4	ENGI	control card - contains the word ENGI
<u>Card 2</u>	1-7	BPR	bypass ratio, $2. \leq BPR \leq 12$.
	8-14	TRMIX	= 1. indicates mixed flow engine = 2. indicates non-mixed flow engine
	15-21	TRAN	= -1. indicates engine decel = 0 indicates steady state operation = +1. indicates engine accel
	22-28	TTRAN	time at which engine accel or decel is initiated, seconds
	29-35	POWER	if TRAN = -1., percent engine power level at <u>end</u> of engine decel from 100 percent power if TRAN = 0., percent steady state power level if TRAN = +1., percent engine power level at <u>start</u> of engine accel to 100 percent power
<u>Card 3</u>	1-7	N	number of times and area matches to follow in Card Set 4. $1. \leq N \leq 20$.

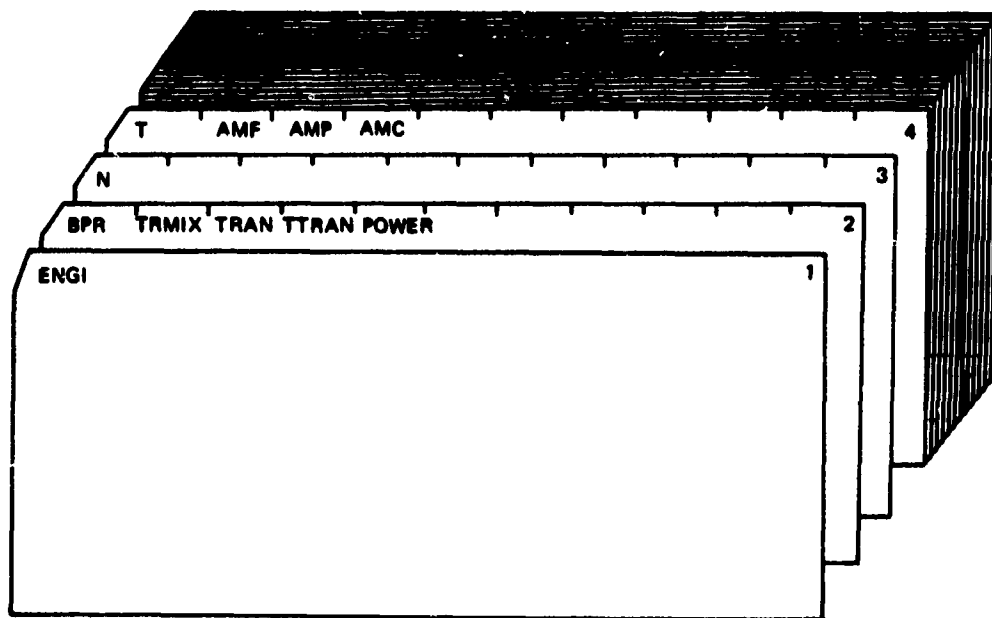


Figure 133: DATA CARD ARRANGEMENT FOR ENGINE STABILITY MARGIN MODULE

APPENDIX I

CHANG'S THEORY FOR THE ROLLUP OF A JET IN CROSSFLOW

The complex potential for flow around a circular cylinder is given by

$$w = U_{\infty} \left(z + \frac{a^2}{z} \right) \quad (1)$$

where $w = U_{\infty} z$ is the complex potential for uniform flow, and the second term is a doublet of strength $\mu = 2\pi U_{\infty} a$ located at the origin with its axis in the $-x$ direction, and "a" is the radius of the cylinder. The complex variables w and z are given by

$$w = \phi + i\psi \quad (2)$$

$$z = x + iy = r e^{i\theta} \quad (3)$$

where ϕ and ψ are the potential and stream functions. The complex velocity field is given by

$$\frac{dw}{dz} = u - i v \quad (4)$$

From Equations 1 and 2 the complex potential w is separated into its real and imaginary parts ϕ and ψ .

$$\phi = U_{\infty} \left(r + \frac{a^2}{r} \right) \cos \theta \quad (5)$$

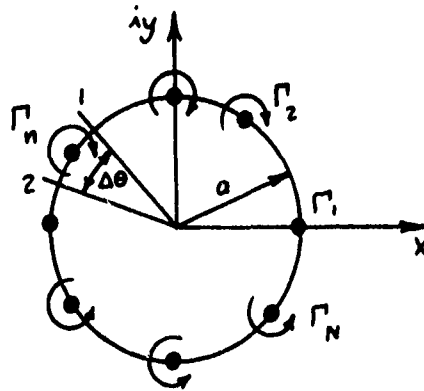
$$\psi = U_{\infty} \left(r - \frac{a^2}{r} \right) \sin \theta \quad (6)$$

The velocity components are given by

$$v_r = \frac{\partial \phi}{\partial r} = U_{\infty} \left(1 - \frac{a^2}{r^2} \right) \cos \theta \quad (7)$$

$$v_{\theta} = \frac{1}{r} \frac{\partial \phi}{\partial \theta} = -U_{\infty} \left(1 + \frac{a^2}{r^2} \right) \sin \theta \quad (8)$$

The circulation strength for a segment of the circle can be replaced by a discrete vortex filament, as shown on the following sketch:



$$\theta_1 = (n-1) \frac{2\pi}{N} - \frac{\pi}{N}$$

$$\theta_2 = (n-1) \frac{2\pi}{N} + \frac{\pi}{N}$$

$$\Delta\theta = \frac{2\pi}{N}$$

The circulation is found by integrating the velocity vector along a path from point 1 to point 2.

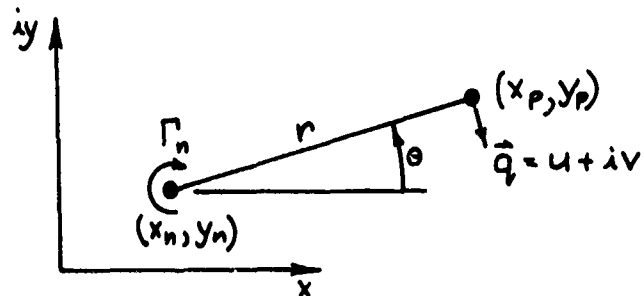
$$\Gamma_n = - \int_{\theta_1}^{\theta_2} \vec{q} \cdot d\vec{s} = - \int_{\theta_1}^{\theta_2} v_\theta r d\theta \quad (9)$$

$$\Gamma_n = \int_{\theta_1}^{\theta_2} u_\infty \left(1 + \frac{a^2}{r^2}\right) \sin\theta r d\theta \quad (10)$$

Integration of Equation 10 gives the vortex strength:

$$\Gamma_n = 4\pi u_\infty a \sin \frac{\pi}{N} \sin \left[\frac{\pi}{N} (n-1) \right] \quad (11)$$

Referring to the following sketch:



the velocity components induced at a point (x_p, y_p) by a vortex of strength Γ_n at the point (x_n, y_n) are given by

$$u_n = \frac{\Gamma_n}{2\pi r} \sin\theta = \frac{\Gamma_n}{2\pi} \frac{y_p - y_n}{(x_p - x_n)^2 + (y_p - y_n)^2} \quad (12)$$

$$v_n = -\frac{\Gamma_n}{2\pi r} \cos\theta = -\frac{\Gamma_n}{2\pi} \frac{x_p - x_n}{(x_p - x_n)^2 + (y_p - y_n)^2} \quad (13)$$

The deformation of the jet cross section, comprised of the vortex filaments, is found by assuming that the filaments are free to move in space for a finite time period. Their direction of travel is in the direction of the velocity vector induced by all the other elements. Thus, the lateral displacement of each vortex filament is found by:

$$\Delta x = \Delta t \sum_n u_n \quad (14)$$

$$\Delta y = \Delta t \sum_n v_n \quad (15)$$

where Δt is the time interval that is fixed by the jet velocity and the distance chosen for steps between cross sections, Δs .

The procedure is similar for finding the deformation of a cross section other than circular, the difference being the strength of the vortex filaments must be determined from some other source. The three-dimensional potential flow program TEA-230 (Ref. 7) was used to find the vortex strengths for TYPE = 2. rectangular jets. The effect of rectangle aspect ratio on the vortex filament strengths is shown in Figure A1.

Linear interpolation for vortex strengths at aspect ratios other than $a/b = 0.25, 1.0$, and 4.0 was found inadequate. This was not unexpected because linear superposition of solutions is valid only if the geometry is fixed and flow conditions vary. However, an asymptotic equation for vortex strength as a function of a/b provided an excellent fit to the data at all intermediate values.

$$\Gamma = \frac{C_1}{a/b - C_2} + C_3 \quad (16)$$

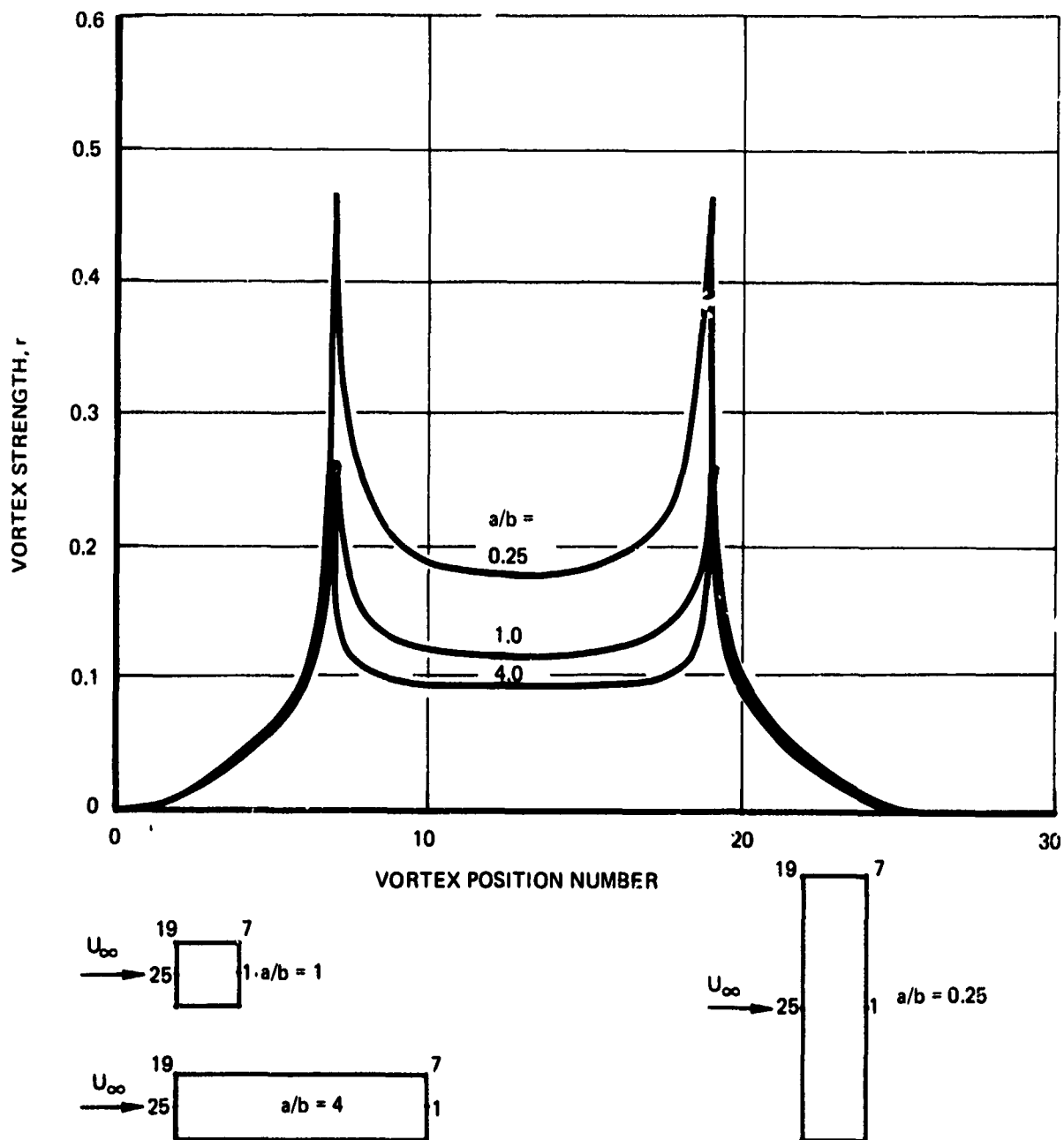


Figure A1: EFFECT OF RECTANGLE ASPECT RATIO ON VORTEX STRENGTH

where the constants C_1 , C_2 , and C_3 are solved for by satisfying equation (16) at $a/b = 0.25, 1.0$ and 4.0 .

$$C_1 = \frac{\Gamma_{0.25} - \Gamma_{1.0}}{\left[\frac{1}{0.25 - C_2} - \frac{1}{1 - C_2} \right]} \quad (17)$$

$$C_2 = \frac{0.25 - 4K}{1 - K} \quad (18)$$

$$C_3 = \Gamma_{1.0} - \frac{C_1}{0.25 - C_2} \quad (19)$$

where

$$K = 0.25 \frac{\Gamma_{1.0} - \Gamma_{4.0}}{\Gamma_{0.25} - \Gamma_{1.0}} \quad (20)$$

The flow direction relative to the cross section has an important effect for rectangular-shaped sections. The effect of wind direction is shown in Figure A2. Solutions for any wind direction can be obtained by linearly combining solutions for 0 and 90 degrees because the geometry is fixed.

$$\Gamma = \Gamma_{0^\circ} \cos \rho + \Gamma_{90^\circ} \sin \rho \quad (21)$$

The vortex strengths for $a/b = 0.25, 1.0$, and 4.0 at relative wind directions of 0 and 90 degrees are tabulated in subroutine RCROSS. Vortex strengths for a particular case are found by asymptotic interpolation (equations 16-20) to account for rectangle aspect ratio and by Equation 21 to account for relative wind direction.

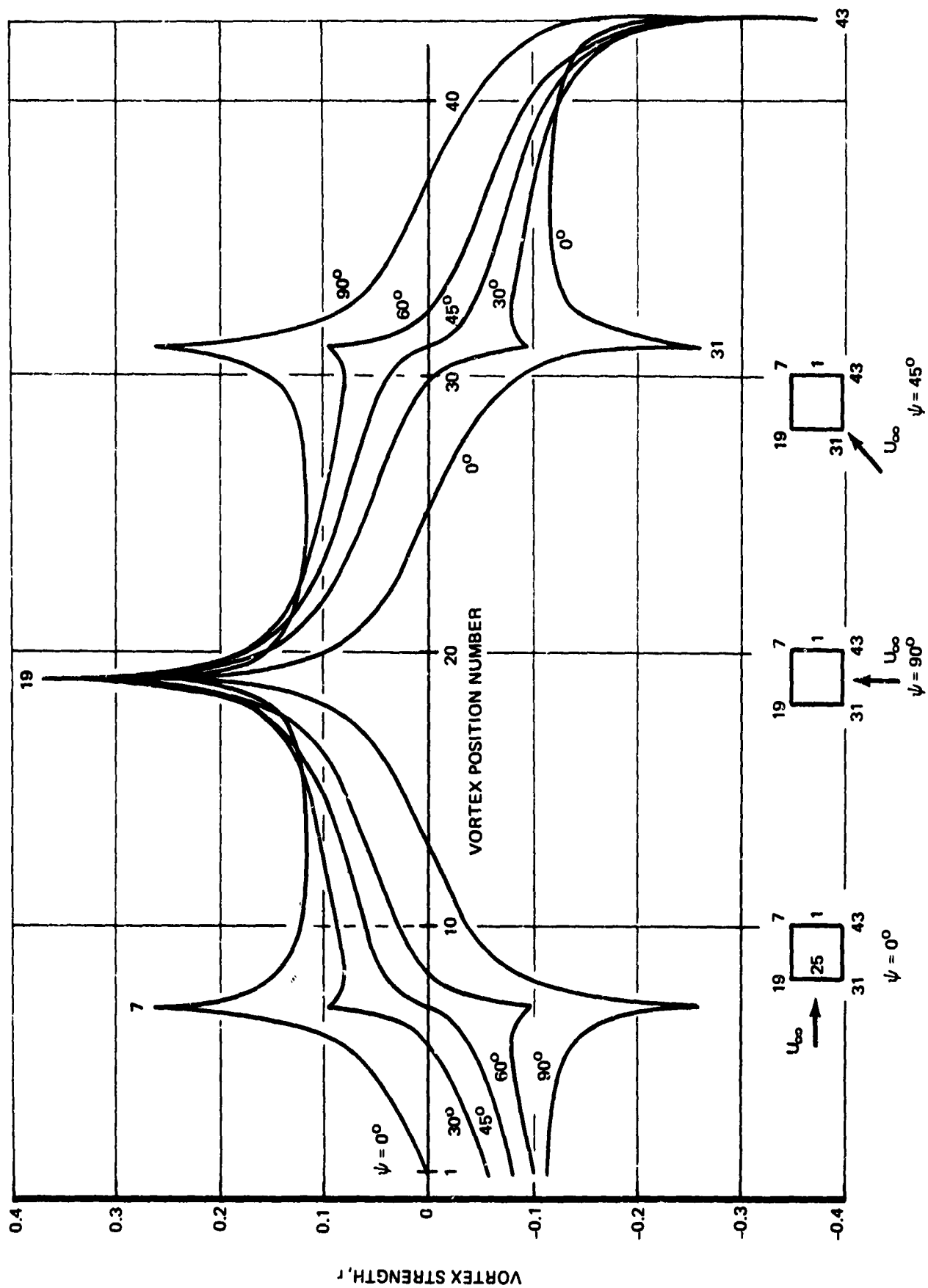


Figure A2: EFFECT OF CROSSWIND ANGLE ON VORTEX STRENGTH

APPENDIX II

Program Sample Cases

This appendix contains card input formats and computer printouts for sample cases computed by programs TEM-356A, TEM-356B, and TEM-357.

Jet Trajectory and Spreading Program TEM-356A

A typical sample case computed by TEM-356A is described below.

TYPE = 1. Input--This sample case is for the circular jet shown in Figure 63. Program inputs are shown in Figure B1. The jet's initial position (x, y, z) is located at the reference coordinate system origin, vector angle is 135 degrees, and dynamic pressure ratio $q_j/q_\infty = 2.78$.

TYPE = 1. Printout--Computer printout is given in Figure D2. Printout includes program inputs, (x, y, z) coordinate output of points on the cross section, and summary data for the jet trajectory, thickness (DEL), and width (H). The (x, y, z) coordinates were punched on cards for computer plotting.

Reingestion Prediction Program TEM-356B

Two sample cases were computed by TEM-356B. Input formats and computer printout for each case are described in the following paragraphs.

Sample Case Number One Input--This sample case is for an early design version of the 747 airplane with long duct nacelles and annular target thrust reversers as sketched in Figure 74. Program inputs are shown in Figure B3. Nacelles are located at 30 and 50 percent span locations. The inboard thrust reverser plume is represented by a TYPE = 4. annular jet defined by MR = 10. arms vectored 120 degrees from the \bar{x} axis. Flow conditions are 70 knots freestream velocity ($U_\infty = 118.16$ ft/sec) and $q_j/q_\infty = 40.96$.

Sample Case Number One Printout--Computer printout is given in Figure B4. Printout includes inlet and jet input data followed by reingestion diagnostic predictions. On page five of the printout, the program predicts far-field fountain reingestion of the fourth jet arm into the outboard inlet. NIP is the number of points intersecting an inlet streamtube at each azimuth angle, α . On page ten, crossflow reingestion is predicted into the outboard inlet. Data summarizing the number of points intersecting the inlet streamtube are printed on page 11. Eight intersection points occur for the third arm. The (x, y, z) coordinates of the inlet streamtube are printed out for clock angles from 0 degrees to 360 degrees.

JET TRAJECTORY AND SPREADING PROGRAM TEM356A

DATE OF RUN APR 22, 1972

TYPE = 1. INDICATES A CIRCULAR JET PLUME
TYPE = 2. INDICATES A SQUARE OR RECTANGULAR JET PLUME
TYPE = 3. INDICATES A TWO-DIMENSIONAL JET PLUME
TYPE = 4. INDICATES AN ANNULAR OR UMBRELLA SHAPED JET PLUME

INPUT CONDITIONS FOR THE FIRST JET FOLLOW ON THE NEXT PAGE

Figure B2: PROGRAM PRINTOUT FOR TYPE = 1 SAMPLE CASE

\$OUT1

TYPE = 0.1E+01,

XYZ0 = 0.0, 0.0, 0.0,

TXYZ = -0.707107E+00, 0.0, -0.707107E+00,

QRATIO = 0.277778E+01,

UINF = 0.5E+02,

ALPHA = 0.0,

PSI = 0.0,

D = 0.2E+01,

DELSO = 0.2E+00,

\$END

Figure B2: PROGRAM PRINTOUT FOR TYPE = 1 SAMPLE CASE (Cont)

COORDINATE OUTPUT OF JET CROSS SECTION NUMBER 1
IS LISTED BELOW

POINT	X	Y	Z	XC	YC
1	.7071	0.0000	-.7071	1.0000	0.0000
2	.7011	-.1305	-.7011	.9914	.1305
3	.6830	-.2588	-.6830	.9659	.2588
4	.6533	-.3827	-.6533	.9239	.3827
5	.6124	-.5000	-.6124	.8660	.5000
6	.5610	-.6088	-.5610	.7934	.6088
7	.5000	-.7071	-.5000	.7071	.7071
8	.4305	-.7934	-.4305	.6088	.7934
9	.3536	-.8660	-.3536	.5000	.8660
10	.2706	-.9239	-.2706	.3827	.9239
11	.1830	-.9659	-.1830	.2588	.9659
12	.0923	-.9914	-.0923	.1305	.9914
13	-.0000	-1.0000	.0000	-.0000	1.0000
14	-.0923	-.9914	.0923	-.1305	.9914
15	-.1830	-.9659	.1830	-.2588	.9659
16	-.2706	-.9239	.2706	-.3827	.9239
17	-.3536	-.8660	.3536	-.5000	.8660
18	-.4305	-.7934	.4305	-.6088	.7934
19	-.5000	-.7071	.5000	-.7071	.7071
20	-.5610	-.6088	.5610	-.7934	.6088
21	-.6124	-.5000	.6124	-.8660	.5000
22	-.6533	-.3827	.6533	-.9239	.3827
23	-.6830	-.2588	.6830	-.9659	.2588
24	-.7011	-.1305	.7011	-.9914	.1305
25	-.7071	.0000	.7071	-1.0000	-.0000
26	-.7011	.1305	.7011	-.9914	-.1305
27	-.6830	.2588	.6830	-.9659	-.2588
28	-.6533	.3827	.6533	-.9239	-.3827
29	-.6124	.5000	.6124	-.8660	-.5000
30	-.5610	.6088	.5610	-.7934	-.6088
31	-.5000	.7071	.5000	-.7071	-.7071
32	-.4305	.7934	.4305	-.6088	-.7934
33	-.3536	.8660	.3536	-.5000	-.8660
34	-.2706	.9239	.2706	-.3827	-.9239
35	-.1830	.9659	.1830	-.2588	-.9659
36	-.0923	.9914	.0923	-.1305	-.9914
37	.0000	1.0000	-.0000	.0000	-1.0000
38	.0923	.9914	-.0923	.1305	-.9914
39	.1830	.9659	-.1830	.2588	-.9659
40	.2706	.9239	-.2706	.3827	-.9239
41	.3536	.8660	-.3536	.5000	-.8660
42	.4305	.7934	-.4305	.6088	-.7934
43	.5000	.7071	-.5000	.7071	-.7071
44	.5610	.6088	-.5610	.7934	-.6088
45	.6124	.5000	-.6124	.8660	-.5000
46	.6533	.3827	-.6533	.9239	-.3827
47	.6830	.2588	-.6830	.9659	-.2588
48	.7011	.1305	-.7011	.9914	-.1305
49	.7071	-.0000	-.7071	1.0000	.0000

FILE B2: PROGRAM PRINTOUT FOR TYPE - 1 SAMPLE CASE (Cont)

IS LISTED BELOW

POINT	X	Y	Z	XC	YC
1	.4307	.0000	-.9850	.8375	.0000
2	.4265	-.1122	-.9809	.8316	.1100
3	.4140	-.2236	-.9686	.8141	.2191
4	.3930	-.3332	-.9479	.7846	.3265
5	.3635	-.4400	-.9189	.7433	.4312
6	.3254	-.5429	-.8814	.6898	.5320
7	.2786	-.6406	-.8353	.6241	.6276
8	.2232	-.7313	-.7808	.5463	.7166
9	.1593	-.8136	-.7179	.4567	.7972
10	.0874	-.8856	-.6472	.3559	.8677
11	.0081	-.9453	-.5692	.2446	.9262
12	-.0777	-.9909	-.4848	.1243	.9709
13	-.1688	-1.0206	-.3951	-.0035	1.0000
14	-.2637	-1.0329	-.3017	-.1368	1.0120
15	-.3608	-1.0264	-.2061	-.2730	1.0057
16	-.4581	-1.0003	-.1104	-.4095	.9801
17	-.5535	-.9541	-.0165	-.5433	.9349
18	-.6447	-.8881	.0732	-.6712	.8701
19	-.7294	-.8028	.1566	-.7901	.7866
20	-.8056	-.6997	.2315	-.8970	.6855
21	-.8710	-.5806	.2959	-.9888	.5688
22	-.9240	-.4479	.3481	-1.0631	.4389
23	-.9630	-.3047	.3864	-1.1178	.2986
24	-.9868	-.1542	.4099	-1.1513	.1511
25	-.9949	.0000	.4178	-1.1625	-.0000
26	-.9868	.1542	.4099	-1.1513	-.1511
27	-.9630	.3047	.3864	-1.1178	-.2986
28	-.9240	.4479	.3481	-1.0631	-.4389
29	-.8710	.5806	.2959	-.9888	-.5688
30	-.8056	.6997	.2315	-.8970	-.6855
31	-.7294	.8028	.1566	-.7901	-.7866
32	-.6447	.8881	.0732	-.6712	-.8701
33	-.5535	.9541	-.0165	-.5433	-.9349
34	-.4581	1.0003	-.1104	-.4095	-.9801
35	-.3608	1.0264	-.2061	-.2730	-1.0057
36	-.2637	1.0329	-.3017	-.1368	-1.0120
37	-.1688	1.0206	-.3951	-.0035	-1.0000
38	-.0777	.9909	-.4848	.1243	-.9709
39	.0081	.9453	-.5692	.2446	-.9262
40	.0874	.8856	-.6472	.3559	-.8677
41	.1593	.8136	-.7179	.4567	-.7972
42	.2232	.7313	-.7808	.5463	-.7166
43	.2786	.6406	-.8353	.6241	-.6276
44	.3254	.5429	-.8814	.6898	-.5320
45	.3635	.4400	-.9189	.7433	-.4312
46	.3930	.3332	-.9479	.7846	-.3265
47	.4140	.2236	-.9686	.8141	-.2191
48	.4265	.1122	-.9809	.8316	-.1100
49	.4307	-.0000	-.9850	.8375	.0000

Figure B2: PROGRAM PRINTOUT FOR TYPE = 1 SAMPLE CASE (Cont)

COORDINATE OUTPUT OF JET CROSS SECTION NUMBER 50
IS LISTED BELOW

POINT	X	Y	Z	XC	YC
1	13.7434	.0000	-10.2242	-4.6797	.0000
2	14.0449	-1.8078	-7.7425	-3.3766	.5040
3	13.8784	-3.0268	-9.1126	-4.0960	.8438
4	14.1111	-3.8819	-7.1977	-3.0906	1.0822
5	14.1370	-3.0114	-6.9842	-2.9785	.8395
6	14.0615	-2.8328	-7.6055	-3.3047	.7897
7	14.0125	-4.0825	-8.0094	-3.5168	1.1381
8	13.9702	-2.7933	-8.3572	-3.6994	.7787
9	13.9550	-1.5421	-8.4823	-3.7650	.4299
10	14.1246	-1.8788	-7.0867	-3.0323	.5238
11	14.2373	-2.2503	-6.1588	-2.5451	.6273
12	14.2823	-3.3581	-5.7885	-2.3506	.9362
13	14.1982	-4.2322	-6.4808	-2.7142	1.1799
14	14.0804	-4.7358	-7.4501	-3.2231	1.3203
15	13.8974	-3.6122	-8.9562	-4.0139	1.0070
16	13.8763	-1.7716	-9.1303	-4.1053	.4939
17	14.0886	-.7856	-7.3828	-3.1878	.2190
18	14.3406	-1.2633	-5.3080	-2.0984	.3522
19	14.4721	-1.7672	-4.2255	-1.5300	.4927
20	14.5562	-2.4072	-3.5334	-1.1666	.6711
21	14.5758	-3.5216	-3.3720	-1.0819	.9818
22	14.5225	-4.3263	-3.8110	-1.3123	1.2061
23	14.4387	-4.3679	-4.5009	-1.6746	1.2177
24	14.3282	-4.8566	-5.4105	-2.1522	1.3539
25	13.7391	.0000	-10.2594	-4.6981	.0000
26	14.3282	4.8566	-5.4105	-2.1522	-1.3539
27	14.4387	4.3679	-4.5009	-1.6746	-1.2177
28	14.5225	4.3263	-3.8110	-1.3123	-1.2061
29	14.5758	3.5216	-3.3720	-1.0819	-.9818
30	14.5562	2.4072	-3.5334	-1.1666	-.6711
31	14.4721	1.7672	-4.2255	-1.5300	-.4927
32	14.3406	1.2633	-5.3080	-2.0984	-.3522
33	14.0886	.7856	-7.3828	-3.1878	-.2190
34	13.8763	1.7716	-9.1303	-4.1053	-.4939
35	13.8974	3.6122	-8.9562	-4.0139	-1.0070
36	14.0804	4.7358	-7.4501	-3.2231	-1.3203
37	14.1982	4.2322	-6.4808	-2.7142	-1.1799
38	14.2823	3.3581	-5.7885	-2.3506	-.9362
39	14.2373	2.2503	-6.1588	-2.5451	-.6273
40	14.1246	1.8788	-7.0867	-3.0323	-.5238
41	13.9550	1.5421	-8.4823	-3.7650	-.4299
42	13.9702	2.7933	-8.3572	-3.6994	-.7787
43	14.0125	4.0825	-8.0094	-3.5168	-1.1381
44	14.0615	2.8328	-7.6055	-3.3047	-.7897
45	14.1370	3.0114	-6.9842	-2.9785	-.8395
46	14.1111	3.8819	-7.1977	-3.0906	-1.0822
47	13.8784	3.0268	-9.1126	-4.0960	-.8438
48	14.0449	1.8078	-7.7425	-3.3766	-.5040
49	13.7434	-.0000	-10.2242	-4.6797	.0000

Figure B2: PROGRAM PRINTOUT FOR TYPE = 1 SAMPLE CASE (Cont)

SUMMARY OF JET CENTERLINE AND SPREADING COEFFICIENT DATA

CROSS SECTION	S/C	X/D	Z/D	XT	YT	ZT	DEL	H
1	0.0000	0.0000	0.0000	0.0000	0.0000	0.0000	2.0000	2.0000
2	.2000	-.1410	.1418	-.2021	0.0000	.2821	2.0000	2.0658
3	.4000	-.2797	.2859	-.5544	0.0000	.5594	2.0000	2.1315
4	.6000	-.4131	.4349	-.8262	0.0000	.8262	2.0000	2.1973
5	.8000	-.5369	.5919	-1.0739	0.0000	1.0739	2.0000	2.2631
6	1.0000	-.6440	.7606	-1.2081	0.0000	1.2881	2.0000	2.3288
7	1.2000	-.7215	.9447	-1.4426	0.0000	1.4426	2.0000	2.3946
8	1.4000	-.7474	1.1421	-1.4947	0.0000	1.4947	2.0000	2.4604
9	1.6000	-.7040	1.3363	-1.4081	0.0000	1.4081	2.0000	2.5261
10	1.8000	-.6005	1.5066	-1.2010	0.0000	1.2010	2.0000	2.5919
11	2.0000	-.4607	1.6492	-.9213	0.0000	.9213	2.0000	2.6577
12	2.2000	-.3012	1.7697	-.6023	0.0000	.6023	2.0000	2.7234
13	2.4000	-.1305	1.8736	-.2610	0.0000	.2610	2.0000	2.7892
14	2.6000	.0471	1.9650	.0441	0.0000	-.0941	2.1873	3.0622
15	2.8000	.2292	2.0465	.4583	0.0000	-.4583	2.4174	3.3844
16	3.0000	.4144	2.1238	.8269	0.0000	-.8289	2.6534	3.7147
17	3.2000	.6020	2.1952	1.2040	0.0000	-1.2040	2.8949	4.0529
18	3.4000	.7913	2.2576	1.5827	0.0000	-1.5827	3.1418	4.3986
19	3.6000	.9820	2.3160	1.9640	0.0000	-1.9640	3.3939	4.7514
20	3.8000	1.1738	2.3742	2.3475	0.0000	-2.3475	3.6506	5.1112
21	4.0000	1.3664	2.4265	2.7328	0.0000	-2.7328	3.9126	5.4777
22	4.2000	1.5598	2.4795	3.1196	0.0000	-3.1196	4.1790	5.8506
23	4.4000	1.7538	2.5262	3.5075	0.0000	-3.5075	4.4499	6.2296
24	4.6000	1.9483	2.5748	3.8965	0.0000	-3.8965	4.7251	6.6151
25	4.8000	2.1432	2.6195	4.2864	0.0000	-4.2864	5.0045	7.0063
26	5.0000	2.3385	2.6625	4.6771	0.0000	-4.6771	5.2880	7.4033
27	5.2000	2.5342	2.7039	5.0684	0.0000	-5.0684	5.5756	7.8058
28	5.4000	2.7302	2.7439	5.4603	0.0000	-5.4603	5.8692	8.2189
29	5.6000	2.9264	2.7826	5.8528	0.0000	-5.8528	5.7680	8.0753
30	5.8000	3.1228	2.8201	6.2457	0.0000	-6.2457	5.8352	8.1693
31	6.0000	3.3195	2.8565	6.6350	0.0000	-6.6390	5.9009	8.2612
32	6.2000	3.5163	2.8919	7.0327	0.0000	-7.0327	5.9651	8.3511
33	6.4000	3.7134	2.9263	7.4267	0.0000	-7.4267	6.0279	8.4391
34	6.6000	3.9105	2.9598	7.8211	0.0000	-7.8211	6.0894	8.5252
35	6.8000	4.1078	2.9925	8.2157	0.0000	-8.2157	6.1497	8.6096
36	7.0000	4.3053	3.0243	8.6106	0.0000	-8.6106	6.2088	8.6923
37	7.2000	4.5029	3.0555	9.0057	0.0000	-9.0057	6.2668	8.7735
38	7.4000	4.7005	3.0859	9.4010	0.0000	-9.4010	6.3237	8.8532
39	7.6000	4.8983	3.1157	9.7966	0.0000	-9.7966	6.3796	8.9315
40	7.8000	5.0962	3.1448	10.1923	0.0000	-10.1923	6.4345	9.0084
41	8.0000	5.2941	3.1734	10.5882	0.0000	-10.5882	6.4885	9.0839
42	8.2000	5.4921	3.2014	10.9843	0.0000	-10.9843	6.5416	9.1583
43	8.4000	5.6902	3.2288	11.3805	0.0000	-11.3805	6.5938	9.2314
44	8.6000	5.8884	3.2557	11.7769	0.0000	-11.7769	6.6452	9.3033
45	8.8000	6.0867	3.2822	12.1733	0.0000	-12.1733	6.6959	9.3742
46	9.0000	6.2850	3.3082	12.5699	0.0000	-12.5699	6.7457	9.4440
47	9.2000	6.4833	3.3337	12.9667	0.0000	-12.9667	6.7948	9.5127
48	9.4000	6.6818	3.3588	13.3635	0.0000	-13.3635	6.8432	9.5805
49	9.6000	6.8802	3.3835	13.7604	0.0000	-13.7604	6.8909	9.6473
50	9.8000	7.0787	3.4079	14.1575	0.0000	-14.1575	6.9380	9.7131

Figure B2: PROGRAM PRINTOUT FOR TYPE = 1 SAMPLE CASE (Concluded)

SEVEN FIELD, TEN DIGIT CRD FORMAT

1	10	11	20	21	30	31	40	41	50	51	60	70	71	72	DEPT	80
2		0.													1	
110.1		-32.3		8.6		8.6			470.						2-1	
133.1		-56.5		10.23		8.6			470.						2-2	
1.															3	
SNEW																
TYPE =		4.														
XYZA =		128.6,		-32.97,		8.6,										
AXYZ =		.999391,		-.0349,		.0,										
T =		1.7,														
R =		.5,														
DELSO =		1.,														
MR =		10.,														
ORATIO =		40.96,														
PSI =		0.,														
XCOWL =		10.8,														
N01 =		1.,														
UIMP =		118.16,														
SEND																
30.		120.														
60.		120.														
90.		120.														
120.		120.														
150.		120.														
180.		120.														
210.		120.														
240.		120.														
270.		120.														
300.		120.														

Figure B3: PROGRAM INPUTS FOR TEM-356B SAMPLE CASE NUMBER ONE

PAGE 1

TEM-356B

THRUST REVERSE REINGESTION PREDICTION PROGRAM

DATE CF RUN APR 14, 1972

INLET INPUT DATA

NI =	2	ZGROUND =	0.000		
AI	"1	ZI	DI	VHI	
110.1000	-22.3.00	0.6500	0.6000	470.0000	
133.1000	-30.50.0	10.2300	0.6000	470.0000	

JET INPUT DATA

NJ = 1

INPUT DATA FOR JET NUMBER 1 FOLLOWS ON NEXT PAGE

Figure B4: PROGRAM PRINTOUT FOR TEM-356B SAMPLE CASE NUMBER ONE

```

SUUT4
TYPE = 0.4E+01,
XYZA = 0.126E+03, -0.3297E+02, 0.86E+01,
XYZI = 0.999991E+00, -0.349E-01, 0.0,
JRAYIO = 0.4C99E+02,
UINF = 0.11816E+03,
PSI = 0.0,
DELSO = 0.1E+01,
T = 0.17E+01,
WR = 10,
R = 0.5E+01,
ACOML = 0.108E+02,
NOI = 1,
END
ADDITIONAL INPUT FOR ANNUAL JET

```

	THETA	BETA
1	30.000	120.000
2	60.000	120.000
3	90.000	120.000
4	120.000	120.000
5	150.000	120.000
6	180.000	120.000
7	210.000	120.000
8	240.000	120.000
9	270.000	120.000
10	300.000	120.000

Figure B4: PROGRAM PRINTOUT FOR TEM-356B SAMPLE CASE NUMBER ONE (Cont)

PAGE 3

```

*****
* REINGESTION DIAGNOSTIC PREDICTIONS *
*****

```

```

REATTACHMENT OF REVERSE FLOW ON COWL WILL NOT
OCCUR, SELF-REINGESTION IS IMPROBABLE
JET = 1
(XC, YO, ZO) = 128.513 -35.468 12.930
THETA = 59.015

```

```

FAR-FIELD FOUNTAIN REINGESTION IS NOT PREDICTED
FOR INLET NUMBER 1, JET NUMBER 1, AND APERTURE NUMBER 1

```

```

FAR-FIELD FOUNTAIN REINGESTION IS NOT PREDICTED
FOR INLET NUMBER 2, JET NUMBER 1, AND APERTURE NUMBER 1

```

```

REATTACHMENT OF REVERSE FLOW ON COWL WILL NOT
OCCUR, SELF-REINGESTION IS IMPROBABLE
JET = 2
(XC, YO, ZO) = 128.449 -37.297 11.100
THETA = 58.273

```

```

FAR-FIELD FOUNTAIN REINGESTION IS NOT PREDICTED
FOR INLET NUMBER 1, JET NUMBER 1, AND APERTURE NUMBER 2

```

```

FAR-FIELD FOUNTAIN REINGESTION IS NOT PREDICTED
FOR INLET NUMBER 2, JET NUMBER 1, AND APERTURE NUMBER 2

```

```

REATTACHMENT OF REVERSE FLOW ON COWL WILL NOT
OCCUR, SELF-REINGESTION IS IMPROBABLE
JET = 3
(XC, YO, ZO) = 128.426 -37.967 8.400
THETA = 58.000

```

Figure B4: PROGRAM PRINTOUT FOR TEM-356B SAMPLE CASE NUMBER ONE (Cont)

PAGE 4

FAR-FIELD FOUNTAIN REINGESTION IS NOT PREDICTED
FOR INLET NUMBER 1, JET NUMBER 1, AND APERTURE NUMBER 3

FAR-FIELD FOUNTAIN REINGESTION IS NOT PREDICTED
FOR INLET NUMBER 2, JET NUMBER 1, AND APERTURE NUMBER 3

REATTACHMENT OF REVERSE FLOW ON COWL WILL NOT
OCCUR, SELF-REINGESTION IS IMPOSSIBLE
JET = 1
XO, YO, ZO = 128.449 -37.277 0.100
THETAO = 58.273

FAR-FIELD FOUNTAIN REINGESTION ANALYSIS USING
THE FOLLOWING JET AND INLET PARAMETERS

JET = 1 APERTURE = 4
(XO,YO,ZO) = 128.449 -37.277 0.100
(TX,TY,TZ) = -.5259 -.7321 -.4330
QRATIO = 40.9600

INLET = 1
(XO,YO,ZO) = 110.1000 -32.3000 8.6000
FREESTREAM VELOCITY = 70.0000 KM/HS

ALPHA	XTOP	YTOP	ZTOP	NIP
30.0	136.64	-55.62	20.78	0
60.0	126.74	-61.28	9.63	0
90.0	123.14	-62.53	6.24	0
120.0	121.34	-64.45	4.80	0
150.0	120.44	-66.05	4.16	0
180.0	120.16	-67.61	3.97	0
210.0	120.44	-69.17	4.16	0
240.0	121.34	-70.73	4.80	0
270.0	123.14	-72.25	6.24	0
300.0	126.74	-73.85	9.60	0
330.0	136.64	-75.46	20.78	0

FAR-FIELD FOUNTAIN REINGESTION IS NOT PREDICTED
FOR INLET NUMBER 1, JET NUMBER 1, AND APERTURE NUMBER 4

FAR-FIELD FOUNTAIN REINGESTION ANALYSIS USING
THE FOLLOWING JET AND INLET PARAMETERS

JET = 1 APERTURE = 4
(XO,YO,ZO) = 128.449 -37.277 0.100
(TX,TY,TZ) = -.5259 -.7321 -.4330
QRATIO = 40.9600

Figure B4: PROGRAM PRINTOUT FOR TEM-356B SAMPLE CASE NUMBER ONE (Cont)

INLET (X1,Y1,Z1) = 2 133.1000 -56.5000 10.2300
FREESTREAM VELOCITY = 70.0000 KNOTS

ALPHA	XTOP	YTOP	ZTOP	NIP
10.0	135.64	-35.82	20.78	0
20.0	124.74	-41.38	9.60	0
30.0	121.14	-42.53	6.24	0
40.0	121.34	-44.45	4.80	0
50.0	120.44	-46.05	4.16	0
60.0	120.16	-47.61	3.97	0
70.0	120.44	-49.17	4.16	0
80.0	121.34	-50.73	4.80	1
90.0	123.14	-52.29	5.24	3
100.0	126.74	-53.85	9.60	4
110.0	130.64	-55.40	20.78	0

FAR-FIELD FOUNTAIN REINGESTION IS PREDICTED FOR THE ABOVE CONDITIONS

REATTACHMENT OF REVERSED FLOW ON COWL WILL NOT OCCUR, SELF-ALIGNMENT IS IMPROVABLE

JET = 1
INLET (X1,Y1,Z1) = 1 128.5128 -35.466 4.270
FREESTREAM VELOCITY = 70.0000 KNOTS
APERTURE = 5
INLET (X1,Y1,Z1) = 1 128.5128 -35.466 4.270
FREESTREAM VELOCITY = 70.0000 KNOTS
APERTURE = 5

FAR-FIELD FOUNTAIN REINGESTION ANALYSIS USING THE FOLLOWING JET AND INLET PARAMETERS

JET = 1
INLET (X1,Y1,Z1) = 1 128.5128 -35.466 4.270
FREESTREAM VELOCITY = 70.0000 KNOTS
APERTURE = 5
INLET (X1,Y1,Z1) = 1 128.5128 -35.466 4.270
FREESTREAM VELOCITY = 70.0000 KNOTS
APERTURE = 5

INLET (X1,Y1,Z1) = 1 128.5128 -35.466 4.270
FREESTREAM VELOCITY = 70.0000 KNOTS
APERTURE = 5

ALPHA	XTOP	YTOP	ZTOP	NIP
10.0	139.38	-30.07	20.78	0
20.0	124.52	-31.42	9.60	0
30.0	125.94	-33.17	6.21	0
40.0	124.14	-34.73	4.78	0
50.0	121.24	-36.28	4.14	0
60.0	122.96	-37.83	3.95	0
70.0	123.24	-39.38	4.14	0
80.0	124.14	-40.94	4.78	0
90.0	125.94	-42.49	6.21	0
100.0	129.52	-44.04	9.60	0
110.0	139.38	-45.60	20.78	0

Figure B4: PROGRAM PRINTOUT FOR TEM-356B SAMPLE CASE NUMBER ONE (Cont)

FAR-FIELD FOUNTAIN REINJECTION IS NOT PREDICTED
FOR INLET NUMBER 1, JET NUMBER 1, AND APERTURE NUMBER 5

FAR-FIELD FOUNTAIN REINJECTION ANALYSIS USING
THE FOLLOWING JET AND INLET PARAMETERS

JET 1
(XG,YO,ZO) = 128.5128 -35.4645 4.2699
(XG,YO,ZO) = -5148 -7500
QKATIO = 40.9600

INLET 2
(XG,YO,ZO) = 133.1000 -56.5000 10.2300
FREESTREAM VELOCITY = 70.0000 KNOTS

ALPHA	XTOP	YTCP	ZTOP	MIP
32.0	139.38	-30.07	20.70	0
60.0	129.52	-31.62	9.56	0
90.0	125.93	-23.17	6.21	0
120.0	124.14	-34.73	4.74	0
150.0	123.24	-36.28	4.14	0
180.0	122.96	-37.83	3.95	0
210.0	123.24	-39.35	4.14	0
240.0	124.14	-40.94	4.70	0
270.0	125.93	-42.45	6.21	0
300.0	129.52	-44.04	9.56	0
330.0	139.38	-45.60	20.70	0

FAR-FIELD FOUNTAIN REINJECTION IS NOT PREDICTED
FOR INLET NUMBER 2, JET NUMBER 1, AND APERTURE NUMBER 5

REATTACHMENT OF REVERSER FLOW ON COWL WILL NOT
OCCUR, SELF-REINJECTION IS IMPROBABLE

JET 1
(XG,YO,ZO) = 128.6000 -32.9700 3.600
APERTURE = 6
THETA0 = 60.020

FAR-FIELD FOUNTAIN REINJECTION ANALYSIS USING
THE FOLLOWING JET AND INLET PARAMETERS

JET 1
(XG,YO,ZO) = 128.6000 -32.9700 3.6000
(XG,YO,ZO) = -4597 -8660
QKATIO = 40.9600

INLET 1
(XG,YO,ZO) = 112.1000 -32.3000 8.6000
FREESTREAM VELOCITY = 70.0000 KNOTS

Figure B4: PROGRAM PRINTOUT FOR TEM-3568 SAMPLE CASE NUMBER ONE (Cont)

ALPHA	XTOP	YTOP	ZTOP	XIP
30.0	140.16	-25.14	20.70	0
60.0	130.30	-26.46	4.56	0
90.0	126.71	-28.24	6.21	0
120.0	124.92	-29.79	4.78	0
150.0	124.02	-31.35	4.14	0
180.0	123.75	-32.50	3.95	0
210.0	124.02	-34.45	4.14	0
240.0	124.92	-36.00	4.78	0
270.0	126.71	-37.55	6.21	0
300.0	130.30	-39.11	9.56	0
330.0	140.16	-40.66	20.70	0

FAR-FIELD FOUNTAIN REINGESTION IS NOT PREDICTED
FOR INLET NUMBER 1, JET NUMBER 1, AND APERTURE NUMBER 6

FAR-FIELD FOUNTAIN REINGESTION ANALYSIS USING
THE FOLLOWING JET AND INLET PARAMETERS

JET
(XO,YO,ZO) = 1 128.6000 APERTURE = 5
(XA,YA,ZA) = -45.97 -32.4700 3.6000
ORATIO = 40.9600 -0176 -0860

INLET
(XI,YI,ZI) = 2 133.1000 -56.5000 10.2300
FREESTREAM VELOCITY = 70.0000 KNOTS

ALPHA	XTOP	YTOP	ZTOP	XIP
30.0	140.16	-25.14	20.70	0
60.0	130.30	-26.46	9.56	0
90.0	126.71	-28.24	6.21	0
120.0	124.92	-29.79	4.78	0
150.0	124.02	-31.35	4.14	0
180.0	123.75	-32.50	3.95	0
210.0	124.02	-34.45	4.14	0
240.0	124.92	-36.00	4.78	0
270.0	126.71	-37.55	6.21	0
300.0	130.30	-39.11	9.56	0
330.0	140.16	-40.66	20.70	0

FAR-FIELD FOUNTAIN REINGESTION IS NOT PREDICTED
FOR INLET NUMBER 2, JET NUMBER 1, AND APERTURE NUMBER 6

REATTACHMENT OF REVERSE FLOW ON COAL WILL NOT
OCCUR, SELF-REINGESTION IS IMPROBABLE

JET
(XO,YO,ZO) = 1 128.6000 APERTURE = 7
ORATIO = 61.615 -30.472 4.270

Figure B4: PROGRAM PRINTOUT FOR TEM-356B SAMPLE CASE NUMBER ONE (Cont)

PAGE 8

FAR-FIELD FOUNTAIN REINGESTION ANALYSIS USING
THE FOLLOWING JET AND INLET PARAMETERS

JET
(X0,Y0,Z0) = 1 128.8872 -30.4715 4.2699
(TX,TY,TZ) = -4846 .4502 -7500
Q/RATIO = 40.9600

INLET
(X1,Y1,Z1) = 1 110.1000 -32.3000 8.6000
PRESTREAM VELOCITY = 70.0000 KNOTS

ALPHA	XTCP	YTOP	ZTCP	NIP
30.0	139.75	-20.14	20.72	0
60.0	129.88	-21.65	9.57	0
90.0	126.29	-23.25	6.22	0
120.0	124.49	-24.80	4.79	0
150.0	123.60	-26.35	4.14	0
180.0	123.12	-27.91	3.94	0
210.0	123.60	-29.46	4.14	0
240.0	124.49	-31.02	4.79	0
270.0	126.29	-32.57	6.22	0
300.0	129.88	-34.13	9.57	0
330.0	139.75	-35.68	20.72	0

FAR-FIELD FOUNTAIN REINGESTION IS NOT PREDICTED
FOR INLET NUMBER 1, JET NUMBER 1, AND APERTURE NUMBER 7

FAR-FIELD FOUNTAIN REINGESTION ANALYSIS USING
THE FOLLOWING JET AND INLET PARAMETERS

JET
(X0,Y0,Z0) = 1 128.8872 -30.4715 4.2699
(TX,TY,TZ) = -4846 .4502 -7500
Q/RATIO = 40.9600

INLET
(X1,Y1,Z1) = 2 113.1000 -36.5000 10.2300
PRESTREAM VELOCITY = 70.0000 KNOTS

ALPHA	XTCP	YTOP	ZTCP	NIP
30.0	139.75	-20.14	20.72	0
60.0	129.88	-21.65	9.57	0
90.0	126.29	-23.25	6.22	0
120.0	124.49	-24.80	4.79	0
150.0	123.60	-26.35	4.14	0
180.0	123.12	-27.91	3.94	0
210.0	123.60	-29.46	4.14	0
240.0	124.49	-31.02	4.79	0
270.0	126.29	-32.57	6.22	0
300.0	129.88	-34.13	9.57	0

Figure B4: PROGRAM PRINTOUT FOR TEM-368B SAMPLE CASE NUMBER ONE (Cont)

330.0 139.75 -15.68 20.72 0
 FAR-FIELD FOUNTAIN REINJECTION IS NOT PREDICTED
 FOR INLET NUMBER 2, JET NUMBER 1, AND APERTURE NUMBER 7

REATTACHMENT OF REVERSE FLOW ON CCHL WILL NOT
 OCCUR, SELF-REINJECTION IS IMPROBABLE
 JET = 1
 (XC,YO,ZO) = 128.751 -28.643 6.100
 THETAO = 61.737

FAR-FIELD FOUNTAIN REINJECTION ANALYSIS USING
 THE FOLLOWING JET AND INLET PARAMETERS

JET = 1 APERTURE = 8
 (XC,YO,ZO) = 128.751 -28.6425 5.1000
 (TX,TY,TZ) = -.4735 -.4330
 GRATIO = 40.9600

INLET = 1
 (XI,YI,ZI) = 110.1000 -32.3000 8.6000
 PRESTREAM VELOCITY = 70.0000 KNOTS

ALPHA	XTOP	YTOP	ZTOP	NIP
30.0	177.83	-10.03	20.82	0
60.0	127.91	-11.45	9.62	0
90.0	124.31	-13.15	6.25	0
120.0	122.50	-14.71	4.81	0
150.0	121.60	-16.28	4.16	0
180.0	121.32	-17.84	3.98	0
210.0	121.60	-19.40	4.16	0
240.0	122.50	-20.96	4.81	0
270.0	124.31	-22.52	6.25	0
300.0	127.91	-24.09	9.62	0
330.0	177.83	-25.65	20.82	0

FAR-FIELD FOUNTAIN REINJECTION IS NOT PREDICTED
 FOR INLET NUMBER 1, JET NUMBER 1, AND APERTURE NUMBER 8

FAR-FIELD FOUNTAIN REINJECTION ANALYSIS USING
 THE FOLLOWING JET AND INLET PARAMETERS

JET = 1 APERTURE = 8
 (XC,YO,ZO) = 126.7511 -28.6425 6.1000
 (TX,TY,TZ) = -.4735 -.4330
 GRATIO = 40.9600

INLET = 2
 (XI,YI,ZI) = 133.1000 -56.5000 10.2300
 PRESTREAM VELOCITY = 70.0000 KNOTS

Figure B4: PROGRAM PRINTOUT FOR TEM-356B SAMPLE CASE NUMBER ONE (Cont)

ALPHA	RTOP	YTOP	ZTOP	MIP
30.0	137.83	-10.03	20.82	0
60.0	127.91	-11.59	9.82	0
90.0	124.31	-13.15	6.25	0
120.0	122.50	-14.71	4.81	0
150.0	121.60	-16.28	3.58	0
180.0	121.32	-17.84	2.58	0
210.0	121.60	-19.40	1.81	0
240.0	122.50	-20.96	1.25	0
270.0	124.31	-22.52	0.82	0
300.0	127.91	-24.08	0.42	0
330.0	137.83	-25.65	0.02	0

FAN-FIELD FOUNTAIN REINGESTION IS NOT PREDICTED
FOR INLET NUMBER 2, JET NUMBER 1, AND APERTURE NUMBER 8

REATTACHMENT OF REVERSER FLOW ON COIL WILL NOT
OCCUR, SELF-REINGESTION IS IMPROBABLE
JET = 1
XO, YO, ZO = 128.776 -27.973 8.600
THETA = 52.000

FAN-FIELD FOUNTAIN REINGESTION IS NOT PREDICTED
FOR INLET NUMBER 1, JET NUMBER 1, AND APERTURE NUMBER 9

FAN-FIELD FOUNTAIN REINGESTION IS NOT PREDICTED
FOR INLET NUMBER 2, JET NUMBER 1, AND APERTURE NUMBER 9

REATTACHMENT OF REVERSER FLOW ON COIL WILL NOT
OCCUR, SELF-REINGESTION IS IMPROBABLE
JET = 1
XO, YO, ZO = 128.751 -28.543 11.100
THETA = 51.337

FAN-FIELD FOUNTAIN REINGESTION IS NOT PREDICTED
FOR INLET NUMBER 1, JET NUMBER 1, AND APERTURE NUMBER 10

FAN-FIELD FOUNTAIN REINGESTION IS NOT PREDICTED
FOR INLET NUMBER 2, JET NUMBER 1, AND APERTURE NUMBER 10

CROSS FLOW REINGESTION IS NOT PREDICTED FOR
JET NUMBER 1 AND INLET NUMBER 1

CROSSFLOW REINGESTION IS PREDICTED FOR
JET NUMBER 1 AND INLET NUMBER 2

Figure B4: PROGRAM PRINTOUT FOR TEM-356B SAMPLE CASE NUMBER ONE (Cont)

PAGE 11

THE FOLLOWING DATA SUMMARIZES THE NUMBER OF
POINTS INTERSECTING THE INLET STREAMTUBE FOR EACH JET STATION

JET STATION INTERSECTIONS

1
2
3
4
5
6
7
8
9
10

THETA EQUALS 0 DEGREES	1	2	3	4	5	6	7	8	9	10
X	18.45508	18.45508	18.45508	18.45508	18.45508	18.45508	18.45508	18.45508	18.45508	18.45508
Y	-56.50000	-56.50000	-56.50000	-56.50000	-56.50000	-56.50000	-56.50000	-56.50000	-56.50000	-56.50000
Z	17.95133	17.95133	17.95133	17.95133	17.95133	17.95133	17.95133	17.95133	17.95133	17.95133
X	103.65360	103.65360	103.65360	103.65360	103.65360	103.65360	103.65360	103.65360	103.65360	103.65360
Y	-56.50000	-56.50000	-56.50000	-56.50000	-56.50000	-56.50000	-56.50000	-56.50000	-56.50000	-56.50000
Z	15.01160	15.01160	15.01160	15.01160	15.01160	15.01160	15.01160	15.01160	15.01160	15.01160
THETA EQUALS 45 DEGREES	1	2	3	4	5	6	7	8	9	10
X	16.07712	16.07712	16.07712	16.07712	16.07712	16.07712	16.07712	16.07712	16.07712	16.07712
Y	-50.65288	-50.65288	-50.65288	-50.65288	-50.65288	-50.65288	-50.65288	-50.65288	-50.65288	-50.65288
Z	15.37440	15.37440	15.37440	15.37440	15.37440	15.37440	15.37440	15.37440	15.37440	15.37440
THETA EQUALS 90 DEGREES	1	2	3	4	5	6	7	8	9	10
X	10.23000	10.23000	10.23000	10.23000	10.23000	10.23000	10.23000	10.23000	10.23000	10.23000
Y	-48.23092	-48.23092	-48.23092	-48.23092	-48.23092	-48.23092	-48.23092	-48.23092	-48.23092	-48.23092
Z	10.23000	10.23000	10.23000	10.23000	10.23000	10.23000	10.23000	10.23000	10.23000	10.23000
THETA EQUALS 135 DEGREES	1	2	3	4	5	6	7	8	9	10
X	4.33263	4.33263	4.33263	4.33263	4.33263	4.33263	4.33263	4.33263	4.33263	4.33263
Y	-50.65288	-50.65288	-50.65288	-50.65288	-50.65288	-50.65288	-50.65288	-50.65288	-50.65288	-50.65288
Z	6.01942	6.01942	6.01942	6.01942	6.01942	6.01942	6.01942	6.01942	6.01942	6.01942
THETA EQUALS 180 DEGREES	1	2	3	4	5	6	7	8	9	10
X	1.74092	1.74092	1.74092	1.74092	1.74092	1.74092	1.74092	1.74092	1.74092	1.74092
Y	-50.50000	-50.50000	-50.50000	-50.50000	-50.50000	-50.50000	-50.50000	-50.50000	-50.50000	-50.50000
Z	1.90000	1.90000	1.90000	1.90000	1.90000	1.90000	1.90000	1.90000	1.90000	1.90000
THETA EQUALS 225 DEGREES	1	2	3	4	5	6	7	8	9	10
X	4.33263	4.33263	4.33263	4.33263	4.33263	4.33263	4.33263	4.33263	4.33263	4.33263
Y	-62.34712	-62.34712	-62.34712	-62.34712	-62.34712	-62.34712	-62.34712	-62.34712	-62.34712	-62.34712
Z	5.00500	5.00500	5.00500	5.00500	5.00500	5.00500	5.00500	5.00500	5.00500	5.00500
THETA EQUALS 270 DEGREES	1	2	3	4	5	6	7	8	9	10
X	10.23000	10.23000	10.23000	10.23000	10.23000	10.23000	10.23000	10.23000	10.23000	10.23000
Y	-64.76908	-64.76908	-64.76908	-64.76908	-64.76908	-64.76908	-64.76908	-64.76908	-64.76908	-64.76908
Z	10.23000	10.23000	10.23000	10.23000	10.23000	10.23000	10.23000	10.23000	10.23000	10.23000
THETA EQUALS 315 DEGREES	1	2	3	4	5	6	7	8	9	10
X	10.23000	10.23000	10.23000	10.23000	10.23000	10.23000	10.23000	10.23000	10.23000	10.23000
Y	-64.76908	-64.76908	-64.76908	-64.76908	-64.76908	-64.76908	-64.76908	-64.76908	-64.76908	-64.76908
Z	10.23000	10.23000	10.23000	10.23000	10.23000	10.23000	10.23000	10.23000	10.23000	10.23000

Figure B4: PROGRAM PRINTOUT FOR TEM-356B SAMPLE CASE NUMBER ONE (Cont)

X	-726.90000	Y	-62.34712	Z	16.07712	X	103.65360	Y	-62.34712	Z	16.07712
	111.01520		-62.34712		16.07712		125.73840		-61.95981		15.69981
	125.41920		-61.04440		15.37540		133.83960		-56.88110		13.61110

THETA EQUALS 360 DEGREES

A	-726.92000	Y	-56.50000	Z	16.45508	X	123.65360	Y	-56.50000	Z	16.45508
	111.01520		-56.50000		16.45508		125.73840		-56.50000		16.45508
	125.41920		-56.50000		17.50528		133.83960		-56.50000		15.72333

NEAR-FIELD FOUNTAIN RELAXATION IS NOT PREDICTED FOR THIS CASE.

INLET INPUT DATA

N1 =	2	ZCGRUND =	0.000
X1	15.0000	Z1	0.000
Y1	15.0000	CI	2.0000
W1	25.0000	470.0000	2.0000

JET INPUT DATA

NJ = 3

INPUT DATA FOR JET NUMBER 1 FOLLOWS ON NEXT PAGE

Figure B4: PROGRAM PRINTOUT FOR TEM-3568 SAMPLE CASE NUMBER TWO (Concluded)

This case demonstrates the need for good arm definition for TYPE = 4. jets. Because the annular surface is represented by discrete arms, they should be placed strategically pointing down and between inlets to ensure that potential intersection points are determined for far-field fountain and crossflow reingestion.

Sample Case Number Two Input--This case was designed to test some of the near-field fountain reingestion criteria. Program inputs are given in Figure B5. Two inlets and three jets were input.

Sample Case Number Two Printout--Computer printout is given in Figure B6. Near-field fountain reingestion is predicted on pages 10 and 11 of the printout.

TR and TV System Performance Program

Thirteen sample cases were computed by TEM-357. Input formats and computer printouts for each case are described in the following paragraphs.

Sample Case Number One for ENGI--Program inputs and printout are shown in Figures B7 and B8. Printout parameters are identified in the following table.

Parameter	Explanation
T	time
AMF	fan nozzle area match
AMP	primary nozzle area match
AMC	common nozzle area match
PCF	thrust level, percent
PCD	duct thrust/total thrust, percent
SMF	fan stability margin, percent
SMC	compressor stability margin, percent
DSMC	compressor stability margin change due to engine acceleration or deceleration, percent
SMCNET	net compressor stability margin, percent
DPF	allowable fan total pressure distortion, percent
DPC	allowable compressor total temperature distortion, percent
DPMAX	allowable engine total pressure distortion, percent
DT	allowable engine total temperature distortion, percent

SEVEN FIELD, TEN DIGIT CRD FORMAT

1	10	11	20	21	30	31	40	41	50	51	60	61	70	71	72	73	74	75	76	77	78	79	80
2		0.																					
10.		10.		10.		2.		470.															
10.		20.		10.		2.		470.															
3																							
\$NEW																							
TYPE =		1.,																					
XYZ0 =		20.,		20.,		5.,																	
XYZ =		0.,		0.,		-1.,																	
D =		2.,																					
DELS0 =		1.,																					
ORATIO =		64.,																					
UINF =		15.,																					
PSI =		0.,																					
XGOWL =		10.,																					
N01 =		2.,																					
SEND																							
\$NEW																							
TYPE =		1.,																					
XYZ0 =		30.,		20.,		20.,																	
XYZ =		-.049325,		-.049325,		-.997564,																	
D =		2.,																					
DELS0 =		1.,																					
ORATIO =		64.,																					
UINF =		15.,																					
PSI =		0.,																					
XGOWL =		10.,																					
N01 =		2.,																					
TITLE	SAMPLE CASE NUMBER TWO FOR TEM-3568										NAME	M. B. SCHOLEY	DATE	4/3/72	PAGE	1	OF	2					

Figure B5: PROGRAM INPUTS FOR TEM-3568 SAMPLE CASE NUMBER TWO

[illegible]

Figure B5: PROGRAM INPUTS FOR TEM-356B SAMPLE CASE NUMBER TWO (Concluded)

PAGE1

TEM-3568

THRUST REVERSER REINGESTION PREDICTION PROGRAM

DATE OF RUN APR 20, 1972

INLET INPUT DATA

NI =	2	ZGROUND =	0.000		
XI		YI	ZI	DI	VHI
10.0000	10.0000	10.0000	10.0000	2.0000	470.0000
10.0000	20.0000	10.0000	10.0000	2.0000	470.0000

JET INPUT DATA

NJ = 3

INPUT DATA FOR JET NUMBER 1 FOLLOWS ON NEXT PAGE

Figure B6: PROGRAM PRINTOUT FOR TEM-3568 SAMPLE CASE NUMBER TWO

PAGE 2

```

JOUT1
TYPE = 0.1E+01,
RYZ0 = 0.2E+02, 0.2E+02, 0.5E+01,
RAYZ = 0.0, 0.0, -0.1E+01,
CRATIO = 0.54E+02,
UINF = 0.15E+02,
PSI = 0.0,
D = 0.2E+01,
DELS0 = 0.1E+01,
XCOML = 0.1E+02,
NDI = 2,
SEND

```

Figure B6: PROGRAM PRINTOUT FOR TEM-356B SAMPLE CASE NUMBER TWO (Cont)

 * REINGESTION DIAGNOSTIC PREDICTIONS *

REATTACHMENT OF REVERSE FLOW ON CUMUL WILL NOT
 OCCUR, SELF-REINGESTION IS IMPROBABLE
 JET = 1
 (X0, Y0, Z0) = 20.000 20.000 5.000
 THETA0 = 90.000

FAR-FIELD FOUNTAIN REINGESTION ANALYSIS USING
 THE FOLLOWING JET AND INLET PARAMETERS
 JET = 1
 (X0, Y0, Z0) = 20.0000 20.0000 5.0000
 (TX, TY, TZ) = 0.0000 0.0000 -1.0000
 J-RATIO = 64.0000
 INLET = 1
 (X1, Y1, Z1) = 10.0000 10.0000 10.0000
 FREESTREAM VELOCITY = 8.0000 KNOTS

ALPHA	ATOP	YTUP	ZTUP	NIP
30.0	24.67	22.56	6.62	0
60.0	21.42	22.05	3.15	0
90.0	20.24	21.53	2.05	0
120.0	17.65	21.07	1.57	0
150.0	19.36	20.51	1.36	0
180.0	19.27	20.00	1.30	0
210.0	19.36	19.49	1.36	0
240.0	19.65	18.98	1.57	0
270.0	20.24	18.47	2.05	0
300.0	21.42	17.95	3.15	0
330.0	24.67	17.44	6.62	0

FAR-FIELD FOUNTAIN REINGESTION IS NOT PREDICTED

Figure B6: PROGRAM PRINTOUT FOR TEM-356B SAMPLE CASE NUMBER TWO (Cont)

PAGE 4

FOR INLET NUMBER 1, JET NUMBER 1

FAR-FIELD FOUNTAIN REINGESTION ANALYSIS USING
THE FOLLOWING JET AND INLET PARAMETERS

JET 1
(XG,YG,ZG) = 20.0000 20.0000 5.0000
(TX,TY,TZ) = 0.0000 0.0000 -1.0000
GRAVITY = 64.0000

INLET 2
(XI,YI,ZI) = 10.0000 20.0000 10.0000
PRESTREAM VELOCITY = 0.0000 KNOTS

ALPHA	XTOP	YTOP	ZTOP	NIP
30.0	24.67	22.56	6.82	0
60.0	21.42	22.05	3.15	0
90.0	20.24	21.53	2.05	0
120.0	19.65	21.02	1.57	0
150.0	19.36	20.51	1.36	0
180.0	19.27	20.00	1.30	0
210.0	19.36	19.49	1.30	0
240.0	19.65	18.98	1.57	0
270.0	20.24	18.47	2.05	0
300.0	21.42	17.95	3.15	0
330.0	24.67	17.44	6.82	0

FAR-FIELD FOUNTAIN REINGESTION IS NOT PREDICTED
FOR INLET NUMBER 2, JET NUMBER 1

CROSS FLOW REINGESTION IS NOT PREDICTED FOR
JET NUMBER 1 AND INLET NUMBER 1

CROSS FLOW REINGESTION IS NOT PREDICTED FOR
JET NUMBER 1 AND INLET NUMBER 2

JET INPUT DATA

NJ = 3

INPUT DATA FOR JET NUMBER 1 FOLLOWS ON NEXT PAGE

Figure B6: PROGRAM PRINTOUT FOR TEM-356B SAMPLE CASE NUMBER TWO (Cont)

PAGE 5

```

$OUT1
TYPE = 0.1E+01,
XYZ0 = 0.3E+02, 0.2E+02, 0.2E+02,
XYZ = -0.49325E-01, 0.49325E-01, -0.49750E+00,
WRATIO = 0.64E+02,
UINP = 0.15E+02,
PSI = 0.0,
J = 0.2E+01,
DELSU = 0.1E+01,
ACCHL = 0.1E+02,
NOI = 2,
$END

```

Figure B6: PROGRAM PRINTOUT FOR TEM-356B SAMPLE CASE NUMBER TWO (Cont)

PAGE 4

FOR INLET NUMBER 1, JET NUMBER 1

FAR-FIELD FOUNTAIN REINGESTION ANALYSIS USING
THE FOLLOWING JET AND INLET PARAMETERS

JET = 1
(XJ,YJ,ZJ) = 20.0000 20.0000 5.0000
(XJ,TJ,ZJ) = 0.0000 0.0000 -1.0000
GRATIO = 64.0000

INLET = 2
(XI,YI,ZI) = 10.0000 20.0000 10.0000
FREESTREAM VELOCITY = 8.8863 KNOTS

ALPHA	XTOP	YTOP	ZTOP	NIP
30.0	24.67	22.56	6.82	0
60.0	21.42	22.05	3.15	0
90.0	20.24	21.53	2.05	0
120.0	19.65	21.02	1.57	0
150.0	19.36	20.51	1.36	0
180.0	19.27	20.00	1.30	0
210.0	19.36	19.49	1.58	0
240.0	19.65	18.98	1.57	0
270.0	20.24	18.47	2.05	0
300.0	21.42	17.95	3.15	0
330.0	24.67	17.44	6.82	0

FAR-FIELD FOUNTAIN REINGESTION IS NOT PREDICTED
FOR INLET NUMBER 2, JET NUMBER 1

CROSS FLOW REINGESTION IS NOT PREDICTED FOR
JET NUMBER 1 AND INLET NUMBER 1

CROSS FLOW REINGESTION IS NOT PREDICTED FOR
JET NUMBER 1 AND INLET NUMBER 2

JET INPUT DATA

NJ = 3

INPUT DATA FOR JET NUMBER 2 FOLLOWS ON NEXT PAGE

Figure B6: PROGRAM PRINTOUT FOR TEM-356B SAMPLE CASE NUMBER TWO (Cont)

PAGE 5

```

ROUTI
TYPE = 0.1E+01,
XYZ0 = 0.3E+02, 0.2E+02, 0.2E+02,
XYZ = -0.49325E-01, 0.49325E-01, -0.49325E+00,
WRATIO = 0.64E+02,
UIMP = 0.15E+02,
PSI = 0.0,
J = 0.2E+01,
DELSO = 0.1E+01,
XCCWL = 0.1E+02,
MOI = 2,
SEND

```

Figure B6: PROGRAM PRINTOUT FOR TEM-356B SAMPLE CASE NUMBER TWO (Cont)

PAGE 6

```

*****
* REINGESTION DIAGNOSTIC PREDICTIONS *
*****

```

```

REATTACHMENT OF REVERSER FLOW UN LUML WILL NOT
OCCUR. SELF-REINGESTION IS IMPROBABLE
JET = 1
(XO, YO, ZO) = 90.000 20.000 5.000
INLETAD = 0

```

```

FAR-FIELD FOUNTAIN REINGESTION ANALYSIS USING
THE FOLLOWING JET AND INLET PARAMETERS

```

```

JET = 1
(XO, YO, ZO) = 20.0000 20.0000 5.0000
(YA, YB, YZ) = 0.0000 0.0000 -1.0000
RATIO = 0.0000
INLET = 1
(XI, YI, ZI) = 10.0000 10.0000 10.0000
PRESTREAM VELOCITY = 0.0003 KNOTS

```

ALPHA	KTOP	YTUP	ZTUP	NIP
30.0	24.67	24.56	6.82	0
60.0	21.42	21.05	3.15	0
90.0	20.24	21.55	2.05	0
120.0	19.65	21.07	1.57	0
150.0	19.36	20.51	1.36	0
180.0	19.27	20.00	1.30	0
210.0	19.36	19.49	1.36	0
240.0	19.65	18.98	1.57	0
270.0	20.24	18.47	2.05	0
300.0	21.42	17.95	3.15	0
330.0	24.67	17.44	6.82	0

FAR-FIELD FOUNTAIN REINGESTION IS NOT PREDICTED

Figure B6: PROGRAM PRINTOUT FOR TEM-356B SAMPLE CASE NUMBER TWO (Cont)

PAGE 7

FUR INLET NUMBER 1, JET NUMBER 2

FAR-FIELD FOUNTAIN REINGESTION ANALYSIS USING
THE FOLLOWING JET AND INLET PARAMETERS

JET = 2
(XO,YO,ZO) = 30.0000 20.0000 20.0000
(IX,IY,IZ) = -0.0493 -0.0493 -0.9976
ORATIO = 04.0000

INLET = 1
(XI,YI,ZI) = 10.0000 20.0000 10.0000
PRESTREAM VELOCITY = 8.8063 KNOTS

ALPHA	XTOP	YTOP	ZTOP	NIP
30.0	37.32	23.56	6.86	0
60.0	34.06	23.05	3.17	0
90.0	32.87	22.53	2.06	0
120.0	32.27	22.02	1.50	0
150.0	31.98	21.50	1.37	0
180.0	31.99	20.95	1.31	0
210.0	31.98	20.47	1.37	0
240.0	32.27	19.96	1.50	0
270.0	32.87	19.45	2.06	0
300.0	34.06	18.93	3.17	0
330.0	37.32	18.42	6.86	0

FAR-FIELD FOUNTAIN REINGESTION IS NOT PREDICTED
FOR INLET NUMBER 2, JET NUMBER 2

CROSS FLOW REINGESTION IS NOT PREDICTED FOR
JET NUMBER 2 AND INLET NUMBER 1

CROSS FLOW REINGESTION IS NOT PREDICTED FOR
JET NUMBER 2 AND INLET NUMBER 2

JET INPUT DATA

NJ = 3

INPUT DATA FOR JET NUMBER 3 FOLLOWS ON NEXT PAGE

Figure B6: PROGRAM PRINTOUT FOR TEM-356B SAMPLE CASE NUMBER TWO (Cont)

PAGE 8

```

SOUT1
TYPE = 0.1E+01,
XYZ0 = 0.3E+02, 0.1E+02, 0.1E+02,
XYZ = -0.139173E+00, 0.C, -0.990204E+03,
ORATIO = 0.64E+02,
UTMF = 0.15E+02,
PSI = 0.0,
D = 0.2E+01,
DELSO = 0.1E+01,
XCOML = 0.1E+02,
MU1 = 1,
SEMO

```

 * REINJECTION DIAGNOSTIC PREDICTIONS *

REATTACHMENT OF REVERSER FLOW ON COWL WILL NOT
 OCCUR, SELF-REINJECTION IS IMPROBABLE
 JET = 3
 (X0, Y0, Z0) = 82.000 10.000 10.000
 THETA0 =

FAR-FIELD FOUNTAIN REINJECTION ANALYSIS USING
 THE FOLLOWING JET AND INLET PARAMETERS

JET = 3
 (X0, Y0, Z0) = 30.0000 10.0000 10.0000
 (X1, Y1, Z1) = -0.1342 0.0000 -0.9903
 QJATIO = 64.0000

INLET = 1
 (X1, Y1, Z1) = 10.0000 10.0000 10.0000
 FREESTREAM VELOCITY = 8.8863 KNOTS

ALPHA	XTOP	YTOP	ZTOP	NIP
30.0	33.96	12.55	6.81	0
60.0	30.71	12.04	3.14	0
90.0	29.54	11.53	2.04	0
120.0	28.95	11.02	1.57	0
150.0	28.05	10.51	1.36	0
180.0	26.56	10.00	1.40	0
210.0	28.65	9.49	1.36	0
240.0	28.95	8.94	1.57	0
270.0	29.54	8.47	2.04	0
300.0	30.71	7.96	3.14	0
330.0	33.96	7.45	6.81	0

FAR-FIELD FOUNTAIN REINJECTION IS NOT PREDICTED

Figure B6: PROGRAM PRINTOUT FOR TEM-356B SAMPLE CASE NUMBER TWO (Cont)

FOR INLET NUMBER 1, JET NUMBER 3

FAR-FIELD FOUNTAIN REINGESTION ANALYSIS USING
THE FOLLOWING JET AND INLET PARAMETERS

JET 2 3
(X0,Y0,Z0) = 30.0000 10.0000 10.0000
(TX,TY,TZ) = -1.342 0.0000 -0.9903
ORATIO = 64.0000

INLET 2
(X1,Y1,Z1) = 10.0000 20.0000 10.0000
FREESTREAM VELOCITY = 4.8863 KNOTS

ALPHA	XTOP	YTOP	ZTOP	NIP
30.0	33.96	12.55	6.81	0
60.0	30.71	12.04	3.14	0
90.0	25.54	11.53	2.04	0
120.0	28.95	11.02	1.57	0
150.0	28.65	10.51	1.36	0
180.0	28.56	10.00	1.30	0
210.0	28.55	9.49	1.36	0
240.0	28.95	8.98	1.57	0
270.0	28.54	8.47	2.04	0
300.0	30.71	7.96	3.14	0
330.0	33.96	7.45	6.81	0

FAR-FIELD FOUNTAIN REINGESTION IS NOT PREDICTED
FOR INLET NUMBER 2, JET NUMBER 3

CROSS FLOW REINGESTION IS NOT PREDICTED FOR
JET NUMBER 3 AND INLET NUMBER 1

CROSS FLOW REINGESTION IS NOT PREDICTED FOR
JET NUMBER 3 AND INLET NUMBER 2

NOZZLE CANT ANGLES IN COMMON PLANE OF JETS ARE
NOT SYMMETRIC FOR THE FOLLOWING PAIR OF JETS
JET1 = 1 JET2 = 2

CANT ANGLE = 0.000 CANT ANGLE = -2.831

NEAR-FIELD FOUNTAIN REINGESTION IS PREDICTED FOR
THE INLET ASSOCIATED WITH THE FIRST JET
JET1 = 1

(X0,Y0,Z0) = 20.000 20.000 5.000 JET2 = 2
(TX,TY,TZ) = 0.000 -1.000 30.000
20.000
-0.049
20.000
-0.998

Figure B6: PROGRAM PRINTOUT FOR TEM-356B SAMPLE CASE NUMBER TWO (Cont)

PAGE 11

NOZZLE CANT ANGLES IN COMMON PLANE OF JETS ARE
NOT SYMMETRIC FOR THE FOLLOWING PAIR OF JETS

JET1 = 1 JET2 = 3
CANT ANGLE = 0.000 CANT ANGLE = -5.675

NEAR-FIELD FOUNTAIN REINGESTION IS PREDICTED FOR
THE INLET ASSOCIATED WITH THE FIRST JET

JET1 = 1 JET2 = 3
(X0,Y0,Z0) = 20.000 20.000 5.000
(TX,TY,TZ) = 0.000 0.000 -1.000
30.000 10.000 10.000
-0.139 0.000 -0.990

NOZZLE CANT ANGLES IN COMMON PLANE OF JETS ARE
NOT SYMMETRIC FOR THE FOLLOWING PAIR OF JETS

JET1 = 2 JET2 = 3
CANT ANGLE = -2.031 CANT ANGLE = -0.000

NEAR-FIELD FOUNTAIN REINGESTION IS PREDICTED FOR
THE INLET ASSOCIATED WITH THE FIRST JET

JET1 = 2 JET2 = 3
(X0,Y0,Z0) = 30.000 20.000 20.000
(TX,TY,TZ) = -0.049 0.049 -0.998
30.000 10.000 10.000
-0.139 0.000 -0.990

Figure B6: PROGRAM PRINTOUT FOR TEM-356B SAMPLE CASE NUMBER TWO (Concluded)

IN FILE, WITH DIGESTORY

[illegible]

Figure B7: PROGRAM INPUTS FOR ENGI SAMPLE CASE NUMBER ONE

CASE NUMBER 1

SAMPLE CASE FOR ENGINE STABILITY MARGIN MODULE

ENGINE STABILITY MARGIN PERFORMANCE MODULE

WPR = 12.0000 IMPIA = 2.0000 IMAN = 1.0000 TITAN = 2.0000 POMEH = 20.0700

T	AMP	AMP	PCF	PLG	SMF	SMC	USMC	SMCNET	DPF	DPC	DPMAX	DT
0.000	1.000	1.000	20.00	93.39	12.70	19.10	0.00	19.10	4.69	14.58	4.69	10.79
.300	1.200	1.000	20.00	93.78	23.90	19.10	0.00	19.10	8.82	14.58	8.82	10.79
.600	1.000	1.000	20.00	93.39	12.70	19.10	0.00	19.10	4.69	14.58	4.69	10.79
.800	.920	1.000	20.00	93.01	7.40	19.10	0.00	19.10	2.73	14.58	2.73	10.79
1.000	1.000	1.000	20.00	93.39	12.70	19.10	0.00	19.10	4.69	14.58	4.69	10.79
1.500	1.100	1.200	20.00	94.26	18.30	19.10	0.00	19.10	6.75	14.58	6.75	10.79
2.000	1.000	.920	20.00	92.97	12.70	19.10	-9.80	9.30	4.69	7.10	4.69	5.25
3.000	1.000	1.000	23.90	93.38	13.64	17.77	-9.32	8.45	5.27	6.47	5.27	4.65
4.000	1.000	1.000	43.50	93.03	16.90	16.03	-6.92	9.11	8.51	7.16	7.16	4.59
5.000	.920	1.000	84.70	91.20	7.14	15.40	-1.87	13.53	6.92	11.96	6.92	6.81

Figure B8: PROGRAM PRINTOUT FOR ENGI SAMPLE CASE FOR ENGINE STABILITY MARGIN MODULE

Sample Case Number Two for CONI--Program inputs and printout are shown in Figures B9 and B10. Skin friction, wetted area (applies only if $D_{he} < 1.0$), underexpansion, and bearing offset losses are listed separately. The Reynolds number scale correction option was used for this case. Nozzle C_V and C_D were corrected to a full scale Reynolds number $Re_{fs} = 10.4 \times 10^6$.

Sample Case Number Three for ANNU--Program inputs and printout for an annular nozzle are given in Figures B9 and B11. Skin friction, underexpansion losses, and annular nozzle ΔC_V increments relative to a standard convergent nozzle are listed separately.

Sample Case Number Four for EQUI--Program inputs and printout appearing in Figures B9 and B12 are similar to those for CONI. The exception is a C_V penalty for increased wetted area due to the D_{he} term.

Sample Case Number Five for TARG--Program inputs and printout for a clamshell target TR are given in Figures B13 and B14. Printout parameters are identified in the following table.

Parameter	Explanation
EBASE	baseline corrected reverser efficiency
DELBYD	reverser efficiency increment due to door length, L/D
DEXBYD	reverser efficiency increment due to setback, X/D
DEHBYD	reverser efficiency increment due to average lip height, LH/D
DESWEP	reverser efficiency increment due to sweep angle, λ
DEARC	reverser efficiency increment due to arc angle, Θ
DECONE	reverser efficiency increment due to cone angle, α
DEBEVL	reverser efficiency increment due to bevel angle, β
ETARC	corrected reverser efficiency, η_{Rc}
ETARG	static reverser efficiency, η_{Rg}
PHI	airflow match,

1960-1969

[illegible]

Figure B9: PROGRAM INPUTS FOR CONI, ANNU, & EQUI

CASE NUMBER 2

SAMPLE CASE FOR CONICAL CRUISE NOZZLE

THROUST REVERSE/VECTRYING NOZZLE INTERNAL PERFORMANCE MODULE

CONICAL CRUISE NOZZLE PERFORMANCE PREDICTIONS

LEVEL 2 PERFORMANCE ESTIMATES

NOZZLE = 0.0000 WALLA = 10.000 DRATIO = 1.0000 DHE = 1.0000 EPS = 1.0000E+07

DT/PI	SKIN FRICTION	WETTED AREA	UNDEXPANSION	BEARING OFFSET	CV	CD
1.1000	.0052	0.0000	0.0000	0.0000	.0049	.0049
1.2000	.0052	0.0000	0.0000	0.0000	.0049	.0049
1.3000	.0050	0.0000	0.0000	0.0000	.0049	.0049
1.4000	.0048	0.0000	0.0000	0.0000	.0052	.0044
1.5000	.0045	0.0000	0.0000	0.0000	.0055	.0042
1.6000	.0042	0.0000	0.0000	0.0000	.0058	.0040
1.7000	.0039	0.0000	0.0000	0.0000	.0064	.0038
1.8000	.0036	0.0000	0.0000	0.0000	.0069	.0036
1.9000	.0033	0.0000	0.0000	0.0000	.0073	.0034
2.0000	.0029	0.0000	0.0000	0.0000	.0077	.0032
2.1000	.0026	0.0000	0.0000	0.0000	.0080	.0030
2.2000	.0023	0.0000	0.0000	0.0000	.0084	.0028
3.0000	.0016	0.0000	.0025	0.0000	.0059	.0055
4.0000	.0016	0.0000	.0120	0.0000	.0064	.0055
5.0000	.0015	0.0000	.0232	0.0000	.0053	.0055

Figure B10: PROGRAM PRINTOUT SAMPLE CASE FOR CONICAL CRUISE NOZZLE

CASE NUMBER 3

SAMPLE CASE FOR ANNULAR CRUISE NOZZLE

THRUST REVERSE/VECTING NOZZLE INTERNAL PERFORMANCE MODULE

ANNULAR CRUISE NOZZLE PERFORMANCE PREDICTIONS

LEVEL 2

DA/L = .6000 WALLA = 5.0000 AM/AE = 1.5625REG = 61.0000HEI = 31.5000

PI/PI	SKIN FRICTION	UNDEREXPANSION	ANNULAR	CV	CD
1.1000	.0048	0.0000	.0027	.9774	.8657
1.2000	.0048	0.0000	.0027	.9777	.8744
1.3000	.0048	0.0000	.0027	.9787	.8830
1.4000	.0048	0.0000	.0027	.9797	.8916
1.5000	.0048	0.0000	.0027	.9802	.9003
1.6000	.0048	0.0000	.0027	.9817	.9090
1.7000	.0048	0.0000	.0027	.9849	.9180
1.8000	.0048	0.0000	.0027	.9867	.9271
1.9000	.0048	0.0000	.0027	.9899	.9361
2.0000	.0048	0.0000	.0027	.9915	.9478
2.1000	.0048	0.0000	.0027	.9932	.9496
2.2000	.0048	0.0000	.0027	.9949	.9527
3.0000	.0048	.0025	.0254	.9943	.9648
4.0000	.0048	.0165	.0725	.9962	.9668
5.0000	.0048	.0260	.0225	.9967	.9668

Figure B11: PROGRAM PRINTOUT SAMPLE CASE FOR ANNULAR CRUISE NOZZLE

CASE NUMBER 4

SAMPLE CASE FOR IRREGULAR (EQUIVALENT) CRUISE NOZZLE

THRUST REVERSE/VECTING NOZZLE INTERNAL PERFORMANCE MODULE
EQUIVALENT CRUISE NOZZLE PERFORMANCE PREDICTIONS

LEVEL 2 PERFORMANCE ESTIMATES

NOZVL = .0030 WALLA = 5.0000 AREA = 1.6000 DME = .2000

PI/PI	SKIN FRICTION	WETTED AREA	UNDEREXPANSION	BEARING OFFSET	CV	CD
1.1000	.0104	.0171	0.0000	.1162	.8562	.8355
1.2000	.0104	.0171	0.0000	.1044	.8441	.8454
1.3000	.0099	.0171	0.0000	.1005	.8724	.8554
1.4000	.0094	.0171	0.0000	.0977	.8808	.8454
1.5000	.0084	.0171	0.0000	.0867	.8875	.8754
1.6000	.0074	.0172	0.0000	.0807	.8942	.8854
1.7000	.0069	.0172	0.0000	.0749	.9011	.8925
1.8000	.0059	.0172	0.0000	.0684	.9081	.9057
1.9000	.0051	.0172	0.0000	.0650	.9126	.9158
2.0000	.0044	.0172	0.0000	.0612	.9171	.9236
2.1000	.0039	.0172	0.0000	.0575	.9214	.9313
2.2000	.0034	.0172	0.0000	.0537	.9257	.9354
2.3000	.0031	.0172	0.0000	.0491	.9303	.9440
2.4000	.0029	.0172	0.0000	.0427	.9238	.9357
2.5000	.0032	.0172	.0244	.0427	.9124	.9357

Figure B12: PROGRAM PRINTOUT SAMPLE CASE FOR NONCIRCULAR NOZZLE

THE FIELD, SEVEN DIGIT OR FORTY

1	2	3	4	5	6	7	8	9	10	11	12	13	14	15	16	17	18	19	20	21	22	IDENT	00
TARGET (CLAMSHELL) THRUST REVERSER																							
1.																						1	
1.2	0.55	0.08	15.	130.	0.	40.																2	
15.																						3C	
																						4	
1.1	1.2	1.2	1.4	1.5	1.8	1.7	1.8	1.9	2.0													5-1	
2.1	2.2	3.0	4.0	5.0																		5-2	
TARGET (ANGULAR) THRUST REVERSER																							
2																						1	
20.	50.	2	1.																			2	
15.																						3A	
																						4	
1.1	1.2	1.3	1.4	1.5	1.6	1.7	1.8	1.9	2.0													5-1	
2.1	2.2	3.0	4.0	5.0																		5-2	
BLOCKER DEFLECTOR THRUST REVERSER																							
0.																						1	
45.																						2	
15.																						3	
																						4	
1.1	1.2	1.3	1.4	1.5	1.6	1.7	1.8	1.9	2.0													5-1	
2.1	2.2	3.0	4.0	5.0																		5-2	

Figure B13: PROGRAM INPUTS FOR TARG, BLOC SAMPLE CASE NUMBER FIVE, SIX, & SEVEN

CASE NUMBER 5

SAMPLE CASE FOR CLAMSHELL TARGET REVERSER

THRUST REVERSER/VECTORIZING NOZZLE INTERNAL PERFORMANCE MODULE
TARGET THRUST REVERSER PERFORMANCE PREDICTIONS

TARG = 1 CLAMSHELL TARGET THRUST REVERSER PERFORMANCE PREDICTIONS

L/D = 1.2000 K/B = .0500 M/U = .0000 SWEEP =15.0000 ARC = 100.0000 CONE = 0.0000 BEVEL =40.0000

PT/P	EMASE	DELAVID	DEANVU	DEHVID	DESHEP	DEARC	DECLINE	DEBEVL	ETARC	ETARG	PHE
1.10	.344	.040	.045	-.070	-.008	.046	-.171	-.160	-.186	.172	.976
1.20	.307	.081	.036	-.075	-.006	.045	-.165	-.149	-.206	.194	.971
1.30	.409	.073	.031	-.079	-.004	.042	-.158	-.137	-.226	.215	.953
1.40	.432	.065	.024	-.084	-.002	.039	-.157	-.126	-.246	.237	.944
1.50	.452	.055	.017	-.087	-.003	.043	-.148	-.116	-.256	.249	.972
1.60	.472	.046	.010	-.090	.001	.078	-.144	-.104	-.267	.261	.979
1.70	.490	.036	.006	-.092	.002	.071	-.140	-.094	-.280	.275	.983
1.80	.509	.027	.003	-.096	.003	.065	-.137	-.087	-.293	.289	.987
1.90	.526	.019	.003	-.099	.002	.057	-.136	-.071	-.297	.294	.990
2.00	.543	.010	-.003	-.105	.001	.049	-.136	-.049	-.300	.297	.992
2.10	.555	.002	-.005	-.110	-.000	.042	-.135	-.049	-.299	.297	.992
2.20	.568	-.006	-.004	-.115	-.001	.034	-.135	-.036	-.299	.294	.992
3.00	.600	-.073	-.030	-.135	-.010	-.028	-.130	-.051	-.224	.222	.992
4.00	.600	-.156	-.058	-.205	-.021	-.106	-.125	-.102	-.091	.090	.992
5.00	.600	-.240	-.096	-.255	-.033	-.106	-.119	.276	-.043	-.042	.992

PROGRAM PRINTOUT SAMPLE CASE FOR CLAMSHELL TARGET REVERSER

Sample Case Number Six for TARG-- Program inputs and printout for an annular target TR are given in Figures B13 and B15.

Sample Case Number Seven for BLOC--Program inputs and printout for a blocker external deflector TR are given in Figures B13 and B16. Printout parameters are identified in the following table.

Parameter	Explanation
ERBASE	baseline static reverser efficiency
DERBASE	increment due to blocker door angle
ETARG	static reverser efficiency, η_{Rg}
ETARC	corrected reverser efficiency, η_{Rc}
PHIBASE	baseline airflow match
DPHI	increment due to blocker door angle
PHI	airflow match, \bar{I}

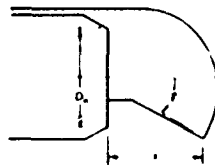
Sample Case Number Eight for SING--Program inputs and printout for a single bearing nozzle are given in Figures B17 and B18. Theoretical thrust components for this nozzle were given in Figure 29.

Sample Case Number Nine for THRE--Program inputs and printout for three bearing nozzle configuration number eight are contained in Figures B17 and B19.

Sample Case Number Ten for SPHE--Program inputs and printout for a spherical eyeball nozzle are given in Figures B17 and B20.

Sample Case Number Eleven for LOBS--Program inputs and printout are given in Figures B21 and B22 for a lobstertail nozzle.

Sample Case Number Twelve for EXTE--Program inputs and printout are given in Figures B21 and B23 for a hinged external deflector. Correlations for hinged deflectors were developed during Part IC and are discussed in Volume II of this report. Special geometric inputs required are X/D_n , D_n/D , and γ as defined in the following sketch:



CASE NUMBER 6
 SAMPLE CASE FOR ANNULAR TARGET THRUST REVERSER
 THRUST REVERSER/VECTURING NOZZLE INTERNAL PERFORMANCE MODULE
 TARGET THRUST REVERSE PERFORMANCE PREDICTIONS
 TARG = 2.0 ANNULAR TARGET THRUST REVERSE PERFORMANCE PREDICTIONS
 PHI = 80.0000 THETA = 50.0000 C/H = 2.0000 AR/AC = 1.0000

PT/P	ETARC	ETARG	PHI
1.10	.575	.477	.830
1.20	.575	.466	.845
1.30	.575	.492	.850
1.40	.575	.499	.860
1.50	.575	.503	.875
1.60	.575	.508	.884
1.70	.575	.510	.887
1.80	.575	.512	.891
1.90	.575	.514	.893
2.00	.575	.515	.895
2.10	.575	.515	.895
2.20	.575	.515	.895
3.00	.575	.515	.895
4.00	.575	.515	.895
5.00	.575	.515	.895

Figure B15: PROGRAM PRINTOUT SAMPLE CASE FOR ANNULAR TARGET THRUST REVERSER

CASE NUMBER 7

SAMPLE CASE FOR BLOCKER DEFLECTUM THRUST REVERSER

THRUST REVERSE/VECTING NOZZLE INTERNAL PERFORMANCE MODULE

BLOCKER DEFLECTION THRUST REVERSE PERFORMANCE PREDICTIONS

BFLAG = 0. INDICATING BLOCKER-INTERNAL DEFLECTOR THRUST REVERSE CONFIGURATION

BLOCKER DCMR ANGLE = 45.00 DEGREES

BASELINE BLOCKER DCMR ANGLE = 45.00 DEGREES

PTYPE	PRBASE	DERBASE	ETANG	ETARC	PMIDASE	DPHI	PM
1.10	.390	0.000	.390	.400	.977	0.000	.977
1.20	.404	0.000	.404	.417	.978	0.000	.978
1.30	.417	0.000	.417	.426	.980	0.000	.980
1.40	.431	0.000	.431	.439	.981	0.000	.981
1.50	.444	0.000	.444	.452	.983	0.000	.983
1.60	.455	0.000	.455	.463	.984	0.000	.984
1.70	.466	0.000	.466	.474	.985	0.000	.985
1.80	.478	0.000	.478	.485	.985	0.000	.985
1.90	.489	0.000	.489	.496	.986	0.000	.986
2.00	.500	0.000	.500	.507	.987	0.000	.987
2.10	.505	0.000	.505	.512	.987	0.000	.987
2.20	.510	0.000	.510	.517	.987	0.000	.987
3.00	.530	0.000	.530	.537	.987	0.000	.987
4.00	.517	0.000	.517	.528	.979	0.000	.979
5.00	.503	0.000	.503	.516	.974	0.000	.974

Figure B16: PROGRAM PRINTOUT SAMPLE CASE FOR BLOCKER DEFLECTOR THRUST REVERSER

[illegible]

Figure B17: PROGRAM INPUTS FOR SING, THIRE, SPHE SAMPLES CASES NUMBER EIGHT, NINE, & TEN

CASE NUMBER A

SAMPLE CASE FOR SINGLE BEARING MUZZLE

THRUST REVERSE/VECTURING MUZZLE INTERNAL PERFORMANCE MODULE

SINGLE BEARING MUZZLE CALCULATIONS

ALPHA = 45.00 BETA = 50.00 PHI = 120.00 OMEGA = -0.00 DMU/L = .4500

COMPONENT THRUST RATIO $F_x/F_R = -.0780$ $F_y/F_R = -.0427$ $F_z/F_R = -.9960$

COMPUTED FLOW TURNING ANGLE = 44.52 DEGREES

COMPUTED VECTOR ANGLE = 85.48 DEGREES

PT/PI	CV	CO
1.1000	.9033	.9145
1.2000	.9049	.9211
1.3000	.9064	.9257
1.4000	.9079	.9303
1.5000	.9114	.9370
1.6000	.9148	.9438
1.7000	.9182	.9505
1.8000	.9216	.9573
1.9000	.9260	.9618
2.0000	.9304	.9683
2.1000	.9347	.9708
2.2000	.9391	.9753
3.0000	.9422	.9824
4.0000	.9422	.9824
5.0000	.9422	.9824

Figure B18: PROGRAM PRINTOUT SAMPLE CASE FOR SINGLE BEARING MUZZLE

CASE NUMBER 9

SAMPLE CASE FOR THREE BEARING NOZZLE

THRUST REVERSE/VECTING NOZZLE INTERNAL PERFORMANCE MODULE

THREE BEARING NOZZLE CALCULATIONS

PHI = 60.000 AD/AE = 1.3450 SIGMA = 90.0000 A = 3.555 L = 12.974 D = 4.770

PT/PI	CV	CD	EI/AVG	PHI
1.1000	.9970	.9197	.9380	.9260
1.2000	.9790	.9225	.9420	.9250
1.3000	.9768	.9285	.9460	.9253
1.4000	.9745	.9365	.9500	.9255
1.5000	.9768	.9405	.9540	.9280
1.6000	.9790	.9465	.9580	.9305
1.7000	.9790	.9527	.9615	.9328
1.8000	.9790	.9590	.9650	.9350
1.9000	.9790	.9645	.9675	.9370
2.0000	.9790	.9700	.9700	.9390
2.1000	.9790	.9730	.9718	.9407
2.2000	.9790	.9760	.9732	.9424
3.0000	.9790	.9805	.9800	.9460
4.0000	.9875	.9805	.9800	.9460
5.0000	.9960	.9805	.9800	.9460

Figure B12: PROGRAM PRINTOUT SAMPLE CASE FOR THREE BEARING NOZZLE

CASE NUMBER 10

SAMPLE CASE FOR SPHERICAL EYEBALL NOZZLE

THUS/ REVERSE/VECTING NOZZLE INTERNAL PERFORMANCE MODULE

SPHERICAL EYEBALL NOZZLE CALCULATIONS

THETA MECHANICAL 90.0 DEGREES MAXIMUM

THETA ACTUAL 99.5 DEGREES

PI/PI	CV	CU	RTAVG	PHI
1.1000	.9465	.7130	.9636	1.0000
1.2000	.9480	.7270	.9634	1.0000
1.3000	.9495	.7410	.9642	1.0000
1.4000	.9510	.7550	.9649	1.0000
1.5000	.9515	.7675	.9642	1.0000
1.6000	.9520	.7800	.9638	1.0000
1.7000	.9525	.7925	.9635	1.0000
1.8000	.9530	.8050	.9631	1.0000
1.9000	.9525	.8135	.9620	1.0000
2.0000	.9520	.8220	.9609	1.0000
2.1000	.9515	.8305	.9598	1.0000
2.2000	.9510	.8390	.9587	1.0000
3.0000	.9440	.8720	.9497	1.0000
4.0000	.9322	.8852	.9417	1.0000
5.0000	.9185	.8870	.9325	1.0000

Figure B20: PROGRAM PRINTOUT SAMPLE CASE FOR SPHERICAL EYEBALL NOZZLE

W. J. Egan, Inc., 2251 Ditch Creek Road

[illegible]

Figure B21: PROGRAM INPUTS FOR LOBS, EXTE, CASC SAMPLE CASES NUMBER ELEVEN, TWELVE, & THIRTEEN

CASE NUMBER 11

SAMPLE CASE FOR LOBSTERTAIL NOZZLE

THRUST REVERSER/VECTING NOZZLE INTERNAL PERFORMANCE MODULE

LOBSTERTAIL OR AFT-NOOD DEFLECTOR NOZZLE CALCULATIONS

VECTOR ANGLE = 95.00 DEGREES

PI/PI	CV	CD	EIANG	PHI
1.10	.9477	.8725	.9525	.9528
1.20	.9513	.8807	.9561	.9558
1.30	.9549	.8890	.9597	.9588
1.40	.9585	.8973	.9634	.9615
1.50	.9621	.9056	.9670	.9641
1.60	.9645	.9140	.9694	.9668
1.70	.9669	.9227	.9718	.9691
1.80	.9693	.9315	.9742	.9715
1.90	.9717	.9403	.9766	.9738
2.00	.9737	.9467	.9789	.9760
2.10	.9749	.9531	.9802	.9782
2.20	.9761	.9562	.9816	.9794
3.00	.9719	.9687	.9843	.9885
4.00	.9490	.9687	.9739	.9885
5.00	.9232	.9687	.9601	.9885

Figure B22: PROGRAM PRINTOUT SAMPLE CASE FOR LOBSTERTAIL NOZZLE

CASE NUMBER 12

Y4 SAMPLE CASE FOR HINGED EXTERNAL DEFLECTOR NOZZLE

THRUST REVERSER/VECTORIZING NOZZLE INTERNAL PERFORMANCE MODULE

EXTERNAL DEFLECTOR VECTORIZING NOZZLE PERFORMANCE PREDICTIONS

CFLAG = 2.0 THETA = 0.00 XDN = .40 DND = 1.150 GAMMA = 30.00

CFLAG = 2.0 INDICATES HINGED EXTERNAL DEFLECTOR CALCULATIONS

PT/PI	CV	CD	ETA VG	ETA VC	PHI	SIGMA
1.0000	.0357	.6931	.8647	.8660	.9985	68.0000
1.2000	.8443	.7014	.8647	.8650	.9985	69.0000
1.4000	.8495	.7215	.8745	.8610	1.0157	70.5000
1.6000	.8403	.7273	.8843	.8483	1.0554	71.8333
2.0000	.8349	.7955	.9053	.8420	1.0752	72.5000
10.0000	.8120	.7967	.9053	.8420	1.0752	72.5000

Figure B23: PROGRAM PRINTOUT SAMPLE CASE FOR EXTERNAL DEFLECTOR NOZZLE

Sample Case Number Thirteen for CASC--Program inputs and printout
are given in Figures B21 and B24 for a cascade lattice with
blade entrance angle of 15 degrees and solidity $c/s = 1.5$.
Output parameters include exit Mach number M_2 , outlet flow
angle α_2 , total pressure loss $\Delta P_T/P_\infty$, C_v , and C_D .

CASE NUMBER 1

SAMPLE CASE FOR CASCADE LOSSES

THRUST REVERSER/VECTORIZING NOZZLE INTERNAL PERFORMANCE MODULE

CASCADE LOSS PREDICTIONS

BETAL = 15.00 ALPHA = 0.00 SIGMA = 1.5000 O/S = .7060 S/E = .0576

T/C = .1162 TE/S = .0376 TTN = 519.00 GAM = 1.4000

LEV = .0010 CMD = .0333 ARHVB = 1.4740

PT/PI	M2	ALPHA2	DELPT/PI	CV	CD
1.1000	.3477	-37.8252	.0116	.9682	.9579
1.2000	.4954	-38.2820	.0209	.9713	.9618
2.3000	.5871	-38.7235	.0286	.9744	.9648
1.4000	.6699	-39.1826	.0350	.9767	.9675
1.5000	.7403	-39.6255	.0406	.9787	.9700
1.6000	.8013	-40.0764	.0455	.9805	.9725
1.7000	.8567	-40.5221	.0499	.9823	.9750
1.8000	.9054	-40.9673	.0538	.9840	.9768
1.9000	1.0000	-41.3814	.0661	.9854	.9793
2.0000	1.0000	-41.3906	.0657	.9853	.9795
2.1000	1.0000	-41.3958	.0654	.9853	.9797
2.2000	1.0000	-41.4050	.0650	.9852	.9799
3.0000	1.0000	-41.4825	.0622	.9790	.9911
4.0000	1.0000	-41.5744	.0589	.9659	.9822
5.0000	1.0000	-41.6453	.0553	.9566	.9830

Figure B24: PROGRAM PRINTOUT SAMPLE CASE FOR CASCADE LOSSES

REFERENCES

1. Petit, J. E. and Scholey, M. B., Thrust Reverser and Thrust Vectoring Literature Review, AFAPL-TR-72-11, April 1972
2. McClung, C. D., Test Data Report - Parametric Test of Conical Convergent Nozzles, Volume I, T6-5614-1, The Boeing Company, 1970
3. Bragg, S. L., "Effect of Compressibility on the Discharge Coefficient of Orifices and Convergent Nozzles," Journal of Mechanical Engineering Science, Vol. 2, No. 1, 1960
4. Postlewaite, J. E., "Thrust Performance of Suppressor Nozzles," Journal of Aircraft, Vol. 3, No. 6, 1966
5. Neal, B. and Hurlbert, C. F., Static and Wind Tunnel Tests of Target Thrust Reversers for the 737 Airplane, D6-32035TN (Proprietary), The Boeing Company, 1968
6. Brazier, M. E., Thrust Reverser Model Tests for the C-5A Airplane, D6-10687, The Boeing Company, 1965
7. Nordstrom, D. C., Thrust Reverser Model Test - - 3/4 Long Duct Nacelle, Boeing Coordination Sheet ME-PI-84, 1965
8. Background and Related Experience in Exhaust Nozzle Reverser and Deflector Systems, 70-2602, Pratt & Whitney Aircraft, 1970
9. Mullin, R. J., Static Model Tests of an In-Flight Thrust Control Unit for the F-11A, AD 8778321, 1970
10. Barrott, W. J., Investigation of the Performance Characteristics of a Dual Exit Thrust Vectoring Nozzle, D6-9083, The Boeing Company, 1963
11. Kentfield, J. A. C., "Nozzles for Jet Lift V/Stol Aircraft," Journal of Aircraft, Vol. 4, No. 4, pp 283-291, July-August 1967
12. Thrust Deflection Doors for Lift Turbojet Engines, D6-11473, The Boeing Company

REFERENCES (Cont.)

13. Siao, T. T. and Hubbard, P. G., "Deflection of Jets, I. Symmetrically Placed V-Shaped Obstacles"
14. Ambrose, H. H., "Head Losses in Mitre Bends"
15. Finley, D. G. and Mathieson, G. C. R., "An Examination of the Flow and Pressure Losses Blade Rows of Axial Flow Turbines, R and M No. 2891, 1951"
16. Stewart, W. L. et al, "A Study of Boundary Layer Characteristics of Turbomachine Blade Rows and Their Relation to Over-All Blade Loss," Journal of Basic Engineering, 1960
17. Abramovich, G. N., The Theory of Turbulent Jets, MIT Press, Cambridge, Mass., 1963
18. Shandorov, G. J., Calculation of a Jet Axis in a Drifting Flow, NASA TT-F-10, 638, 1966
19. Callaghan, E. E. and Ruggeri, R. S., Investigation of the Penetration of Air Jet Directed Perpendicularly to an Air Stream, NACA TN 1615, 1948
20. Jordinson, R., Flow in a Jet Directed Normal to the Wind, ARCR&M No. 3074, 1956
21. Storms, K. R., Low-Speed Wind Tunnel Investigation of a Jet Directed Normal to the Wind, University of Washington Aeronautical Lab Report 885, 1965
22. Pratte, B. D. and Baines, W. D., "Profiles of the Round Turbulent Jet in a Crossflow," ASCE, Journal of the Hydraulics Division, 1967
23. Vizel, Ya. M. and Mostinskii, I. L., "Deflection of a Jet Injected into a Stream," J. Eng. Physics, Vol. 8, Nov. 2, 1965
24. Margason, R. J., The Path of a Jet Directed at Large Angles to a Subsonic Freestream, NASA TN D-4919, 1968
25. Filler, L., Survey and Study of the Penetration and Deflection of a Jet Injected at an Angle into a Uniform Stream, D6-20380TN, The Boeing Company, 1968

REFERENCES (Cont.)

26. Cooper, M. A., Temperature Field of the Two Dimensional Transverse Hot Air Jet in a Freestream Flow, Vanderbilt University Department of Mechanical Engineering, 1971
27. Platten, J. L. and Keffer, J. F., Entrainment in Deflected Axisymmetric Jets at Various Angles to the Stream, University of Toronto Mechanical Engineering Report UTME-TP6808, 1968
28. Gerend, R. P., Penetration of a Jet into a Nonuniform Stream, M. S. Thesis, School of Mech. Eng., Seattle University, 1968
29. Wooler, P. T., "Development of an Analytical Model for the Flow of a Jet Into a Subsonic Crossover," NASA SP-318, 1969
30. Chang-Lu, Hsiu-Chen, Aufrollung eines zylindrischen strahles Durch Querwind (Rollup of a Cylindrical Jet in a Crosswind), Doctorial Dissertation, University of Gottingen, 1942
31. Soukup, S. M., Potential Flow Aspects of the Cross-Sectional Deformation of Jet Configurations in Cross-Flow, Masters Thesis, University of Tennessee, 1968
32. Braun, G. W. and McAllister, J. D., "Cross Wind Effects on Trajectory and Cross Section of Turbulent Jets," NASA SP-218, pp 141-164, 1969
33. Hackett, J. E. and Miller, H. R., "The Aerodynamics of the Lifting Jet in a Cross Flowing Stream," NASA SP-218, pp 37-48, 1969
34. Colehour, J. L. and Gilbert, R. F., A RELaxation Solution for Two-Dimensional and Axisymmetric Compressible Potential Flow Problems, D6-20364, Volume I, The Boeing Company, 1963
35. Tatom, J. W., A Study of Jet Impingement on Curved Surfaces Followed by Oblique Introduction Into a Freestream Flow, Vanderbilt University Department of Mechanical Engineering, 1971
36. McClung, C. D., 747 Reverser Exhaust Flow Field Test, T6-336, The Boeing Company, 1967

REFERENCES (Cont.)

37. Bourque, C. and Newman, B. G., "Reattachment of a Two Dimensional Incompressible Jet to an Adjacent Flat Plate," Aeronautical Quarterly, Vol. XI, 1960
38. von Glahn, U. H., The Coanda Effect for Jet Deflection and Vertical Lift with Multiple-Flat-Plate and Curved-Plate Deflection Surfaces, NACA TN 4377, 1958
39. Hall, G. R. and Rogers, K. H., Recirculation Effects Produced by a Pair of Heated Jets Impinging on a Ground Plane, NASA CR-1307, 1969
40. Abbott, W. A., Studies of Flow Fields Created by Vertical and Inclined Jets When Stationary or Moving over a Horizontal Surface, ARC C.P. No. 911, 1965
41. Colin, P. E. et al, The Impingement of a Circular Jet Normal to a Flat Surface with and without Cross Flow, von Karman Institute for Fluid Dynamics, Rhode St. Genese, Belgium, 1969
42. Ryan, P. E. and Cosgrove, W. J., Empirically Determined Wind and Scale Effects on Hot Gas Recirculation Characteristics of Jet V/STOL Aircraft, NASA CR-1445, 1969
43. Binion, T. W., Investiagion of the Recirculation Region of a Flow Field Caused by a Jet in Ground Effect with Crossflow, AEDC-TR-70-192, 1970
44. Poland, D. T., The Aerodynamics of Thrust Reversers for High Bypass Turbofans, AIAA Paper No. 67-418, 1967
45. Kozlowski, H. STOL Transport Thrust Reverser/Vectoring Technology Program, PWA-4588, 1972
46. Petit, J. E. and Scholey, M. B., STOL Transport Thrust Reverser/Vectoring Program Supplemental Test Plan, D180-14140-1, The Boeing Company, 1971
47. Petit, J. E., STOL Transport Thrust Reverser/Vectoring Program Supplemental Test Report, D180-14801-1, The Boeing Company, 1972
48. Rubbert, P. E., Saaris, G. R., et al, A General Method for Determining the Aerodynamic Characteristics of Fan-in-Wing Configurations, Vol. 1 - - Theory and Application, D6-15047-1, 1967